UNRAVELING THE INTERACTIONS BETWEEN LEUKOCYTES AND PLATELET-DERIVED EXTRACELLULAR VESICLES IN ATHEROSCLEROSIS

By

Aigli Evryviadou

A thesis submitted to the University of Birmingham for the degree of DOCTOR OF PHILOSOPHY

Institute of Cardiovascular Sciences
College of Medical and Dental Sciences
University of Birmingham
December 2018

Abstract

Atherosclerosis is a progressive inflammatory disease, characterized by accumulation of fatty deposits and degenerative material in the wall of arteries forming a growing atheromatous plaque that upon rupture may cause thrombosis. An essential step in atherosclerosis progression is monocyte recruitment to the inflamed vessel wall and subsequent uptake of fats that upon apoptosis contribute to further inflammation. Increased levels of PEV have been reported to circulate in atherosclerosis patients, suggesting that they possibly contribute to disease development.

We demonstrated that PEV are released from platelets upon activation through various routes. PEV contain adhesion receptors such as GPIb and GPIIb and may also contain a mitochondrion. *In vitro* platelet activation in the blood results in PEV release that preferentially form aggregates with monocytes. Monocytes can internalize PEV through various endocytic mechanisms. PEV aggregation with monocytes was functional as monocytes that had aggregated with PEV exhibited increased recruitment to the carotid endothelium in mice with established atherosclerosis *in vivo*. We also generated and characterized a new mouse model, which is athero-prone and inducible of platelet clearance. This mouse will help elucidate the acute and chronic effects of injected PEV in atherosclerosis, independently of platelets.

Our observations are important because they have identified a novel thrombo-inflammatory pathway of leukocyte recruitment to the vessel wall, that may be relevant in atherosclerosis.

Acknowledgements

First I would like to thank my supervisor Ed Rainger for trusting me with this project, for having his door open to give me advice, guidance and support at any time and for always dealing with any mistakes with humour! I would also like to thank my second supervisor Gerard Nash for additional advice, guidance and support and for an extra dose of humour!

Many thanks go to past and present members of the Leukocyte Trafficking Group; Myriam Chimen for general advice throughout and IVM training, Lozan Sheriff and Lea Dibb for general advice and psychological support whenever needed, Sahithi Kuravi for NTA training and general advice, Matt Harrison for genotyping and animal work advice and training and Lewis Clarke mainly for his lab pranks. Also thanks to Bonita, Hafsa, Mohammed and the rest people in the NG15 office.

Special thanks go to Yotis Senis for acting as an informal mentor to me. Also thanks to Paul Harrison for additional guidance and advice, Dean Kavanagh for IVM training, Adam Lokman for cryostat training, Steve Thomas for help with Storm imaging, Carol Murphy for advice on endocytosis experiments, Trish Lalor for support with liver experiments, Rob Shaw for microscopy training, June, Mitch, Timo, Zoltan, Silke, Alex M, Pushpa and Steph W for support with various platelet experiments and Dave Westwood for general lab support. Also thanks to BMSU staff for their help with animal work especially Ian, Diane, Claire, James, Sharon and Julie. Lastly, thanks to all the volunteers who donated blood for my experiments.

I would also like to acknowledge the British Heart Foundation that funded my project and Steve Watson who is a co-holder on the project grant.

I would like to extend my thanks to my non-university friends in Birmingham for filling the past years with lovely memories.

Finally, my warmest thanks go to my family and friends in Cyprus for all their love, support and faith in me and for putting up with me studying and living abroad for 7.5 years. I dedicate this thesis to you!

Table of Contents

List of Figures

List of Tables

Abbreviations

α2A: 2A-Adrenergic receptor

ADP: Adenosine Diphosphate

AFM: Atomic Force Microscopy

AMPK: AMP-Activated Protein Kinase

ANOVA: Analysis of Variance

APC: Antigen Presenting Cells

Apo: Apolipoprotein

ATP: Adenosine Triphosphate

BAX: BCL2-Associated X Protein

CAMs: Cell Adhesion Molecules

CCL5: C-C Motif Ligand 5

CD: Cluster of Differentiation

C.D: Cytochalasin D

CETP: Cholesteyl Ester Transfer Protein

CIRT: Cardiovascular Inflammation Reduction Trial

CLEC-2: C-type Lectin-like Receptor 2

COLCOT: Colchicine Cardiovascular Outcomes Trial

COX: Cyclooxygenase

CPDA: Citrate Phosphate Dextrose Adenine

CRP-XL: Cross-linked Collagen-related Peptide

CVD: Cardiovascular Disease

CXCL4: C-X-C Motif Ligand 4

CXCR4: C-X-C Receptor Type 4

DAMP: Damage-Associated Molecular Patterns

DMSO: Dimethyl Sulfoxide

EBV: Epstein-Barr Virus

EC: Endothelial Cells

ECM: Extracellular Matrix

EDTA: Ethylenediaminetetraacetic Acid

EIPA: 5-(N-ethyl-N-isopropyl)-amiloride

ESCRT: Endosomal Sorting Complexes Required For Transport

EV: Extracellular Vesicles

FACS: Fluorescence-Activated Cell Sorting

FCR: Fc Receptor

GP: Glycoprotein

GTP: Guanosine Triphosphate

HDL: High Density Lipoprotein

H&E: Haematoxylin and Eosin

HSP: Heat Shock Protein

ICAM: Intercellular Adhesion Molecule

IFN: Interferon

Ig: Immunoglobulin

IL: Interleukin

ITP: Autoimmune Thrombocytopenic Purpura

KI: Knock In

KO: Knock Out

LDL: Low Density Lipoprotein

LDLR: Low Density Lipoprotein Receptor

LDM: Low Dose Methotrexate

LMP-1: Latent Membrane Protein

Lp-PLA2: Lipoprotein-associated Phospholipase A2

LPS: Lipopolysaccharide

mAb: Monoclonal Antibody

M-CSF: Macrophage Colony-Stimulating Factor

MFI: Mean/Median Fluorescence Intensity

MHC: Major Histocompatibility Complex

miRNA: Micro-RNA

mitoRNA: Mitochondrial RNA

MITP: Microsomal Triglyceride Transfer Protein

MKK4/JNK2: Mitogen-activated Protein Kinase Kinase 4/c-Jun N-Terminal Kinase 2

MMP: Metalloproteinase

MP: Microparticles

mt: Mitochondrial

MT: MitoTracker

mRNA: Messenger RNA

MV: Microvesicles

MVB: Multivesicular Body

MVE: Multivesicular Endosome

NETs: Neutrophil Extracellular Traps

NO: Nitric Oxide

NS: No Significance

NTA: NanoSight Tracking Analysis

OCT: Optimal Cutting Temperature

ORO: Oil Red O

PAF: Platelet-Activating Factor

PAR: Protease-activated Receptor

PBMCs: Peripheral Blood Mononuclear Cells

PBS: Phosphate-Buffered Saline

PCSK: Proprotein Convertase Subtilisin/Kexin

PCR: Polymerase Chain Reaction

PDGF: Platelet-derived Growth Factor

PEV: Platelet-derived Extracellular Vesicles

PFA: Formaldehyde in PBS

PG12: Prostacyclin

PKC: Protein Kinase C

PLT: Platelet

PMV: Platelet-derived Microvesicles

PI3K: Phosphoinositide 3-Kinase

PPAR: Peroxisome Proliferator-Activated Receptor

PPL: Project Licence

PS: Phosphatidylserine

PSGL: P-Selectin Glycoprotein Ligand

RA: Rheumatoid Arthritis

RES: Reticuloendothelial System

ROS: Reactive Oxygen Species

RPS: Resistive Pulse Sensing

rRNA: Ribosomal RNA

RT: Room Temperature

SDS: Sodium Dodecyl Sulfate

SEM: Standard Error of the Mean

SMC: Smooth Muscle Cells

sPLA2: Extracellular Group IIa Phospholipase A2

STORM: Stochastic Optical Reconstruction Microscopy

TC: Tissue Culture

TEM: Transmission Electron Microscopy

TF: Tissue Factor

Tg: Transgene

TGFβ: Transforming Growth Factor beta

TNFα: Tumour Necrosis Factor alpha

TLR: Toll-Like Receptor

TP: Thromboxane A2 Receptor

tRNA: Transfer RNA

TSG: Tumour Susceptibility Gene

TRAP: Thrombin-receptor Activating Peptide

TxA_2: Thromboxane

ULBP1: UL16 Binding Protein 1

VCAM: Vascular Cell Adhesion Molecule

VEGF: Vascular Endothelial Growth Factor

VLDL: Very Low Density Lipoprotein

vWF: von Willebrand Factor

WBC: White Blood Cells

WT: Wild Type

1. GENERAL INTRODUCTION

1.1 Atherosclerosis

Atherosclerosis is a progressive inflammatory disease, characterised by accumulation of fatty deposits and degenerative material in the wall of arteries forming a growing atheromatous plaque that upon rupture may cause thrombosis (Libby et al., 2011). It constitutes the primary cause of heart disease and stroke, accounting for 50 % of all deaths in the western world (Lusis, 2000).

Development of Atherosclerosis

Healthy artery walls consist of three layers. The innermost layer, the tunica intima, is lined by a monolayer of endothelial cells that is in direct contact with the blood and a sheet of elastic fibres, the internal elastic lamina underneath that contains extracellular connective tissue matrix. The middle layer, the tunica media, consists of smooth muscle cells (SMCs) in a complex extracellular matrix. The outermost layer, the adventitia, contains connective tissue, mast cells, nerve ending and microvessels.

Atherosclerosis is initiated by lipoprotein accumulation and aggregation with matrix and collagen fibrils in the subendothelial matrix of the intima. The next step in atherosclerosis progression involves monocyte recruitment at the inflammatory site.

Leukocyte recruitment is a physiological response in the event of infection and inflammation. Leukocytes are recruited at the site of inflammation by traversing the endothelium (**Fig.1.1**). In atherosclerosis, the endothelial cells get activated and upregulate expression of L-, P- and E-selectins and intercellular adhesion molecules (ICAMs), such as ICAM-1 (Borregaard, 2010; Galkina and Ley, 2007; Johnson-Tidey et al., 1994). These adhesion molecules are recognised by the P-selectin glycoprotein ligand-1 (PSGL-1) and L-selectin on the surface of leukocytes that mediate capture from flow. Sequential formation and dissolution of these bonds under the shear forces

generated by blood flow results in rolling adhesion along the luminal endothelial cells (Kansas 1996; McEver and Cummings, 1997). This initial interaction results in the activation of the β2 integrins lymphocyte function-associated antigen 1 (LFA-1) and Macrophage-1 antigen (Mac-1) on the leukocyte which then bind to the ICAM-1 immunoglobulin receptors of the endothelium; leading to arrest of rolling and "firm adhesion" (Woollard and Geissmann, 2010; Yago et al., 2010; Mueller et al., 2010; Ley et al., 2007; Campbell et al., 1998). After firmly adhering, the leukocyte then crawls on the endothelial surface until it finds an endothelial cell junction, which it uses to transmigrate in a process depending on β2 integrins and ICAM molecules (Ley et al., 2007; Phillipson et al., 2006). Having crossed the endothelial barrier, the leukocyte continues its journey towards invading pathogens by following chemotactic gradients.

Following recruitment in the artery wall, monocytes mature into macrophage with the aim to clear the accumulated lipoprotein in atherosclerosis. Upon uptake of fats, macrophages become foam cells. With time, foam cells die liberating their contents into the necrotic core of the lesion (**Fig. 1.2**). The lesion progresses with the migration of SMCs from the media to the intima and secretion of fibrous elements such as collagen, elastin and proteoglycans that contribute to plaque build up. SMC may also die like foam cells further increasing the size of the lesion, which initially expands towards the adventitia but as the lesion advances it starts to expand into the lumen of the vessel, occluding blood flow (**Fig. 1.3**). Advanced lesions also contain cholesterol crystals and microvessels. Monocytes keep getting recruited in the vessel wall at all stages in atheroma formation in order to clear the degenerative material but instead they keep dying further worsening the plaque. (Libby et al., 2011) In the event of a physical disruption that breaks the plaque's fibrous cap, coagulation factors and platelets in the

blood may come into contact with tissue factor and other pro-thrombogenic agents in the lesion, triggering thrombosis (**Fig. 1.4**).

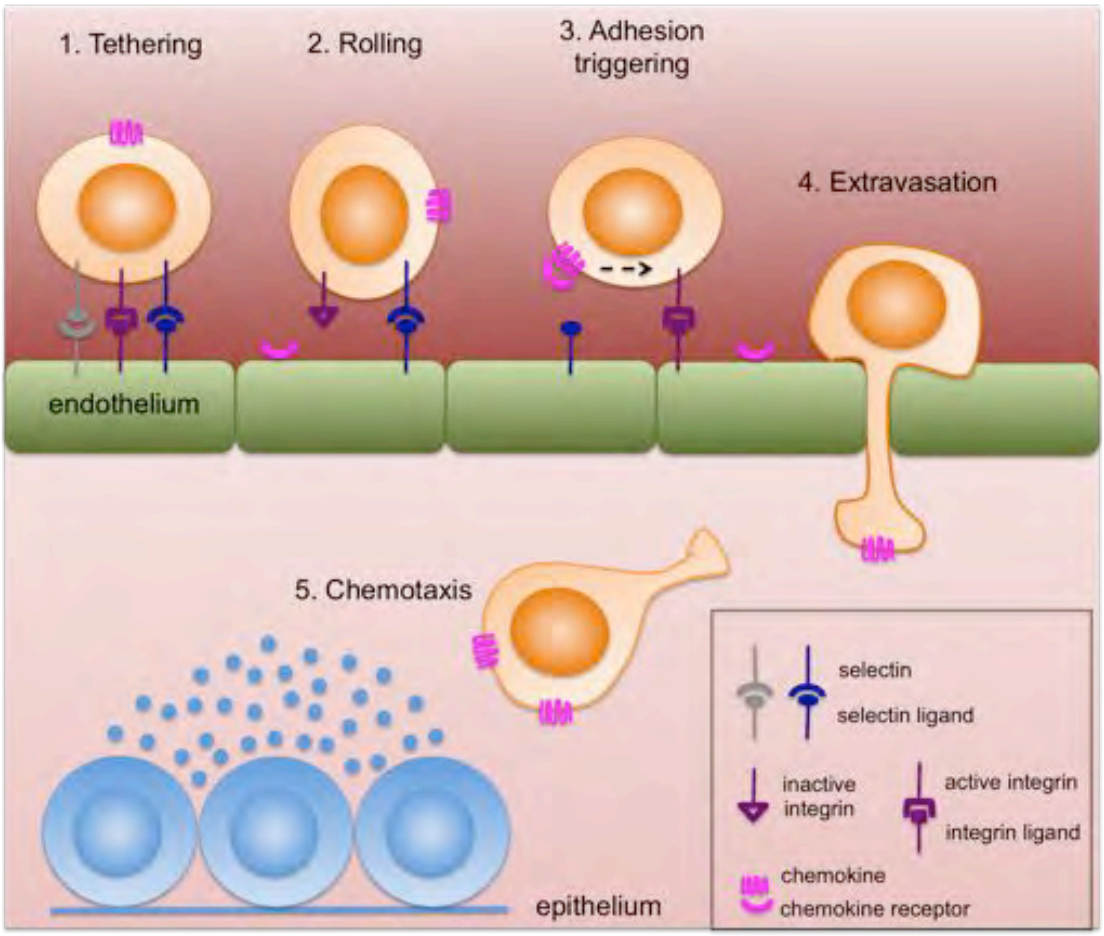

Figure 1.1. The Leukocyte recruitment cascade.

Leukocytes from blood are recruited at the sites of inflammation by traversing the endothelium in a process that involves tethering to the endothelium, followed by rolling along the surface, leukocyte firm adhesion and activation, mediated by different selectins and integrins such as p-selectin, PSGL-1, ICAM-1, Mac-1 and LFA-1. Upon transendothelial migration, leukocytes are attracted towards invading pathogens by chemotaxis.

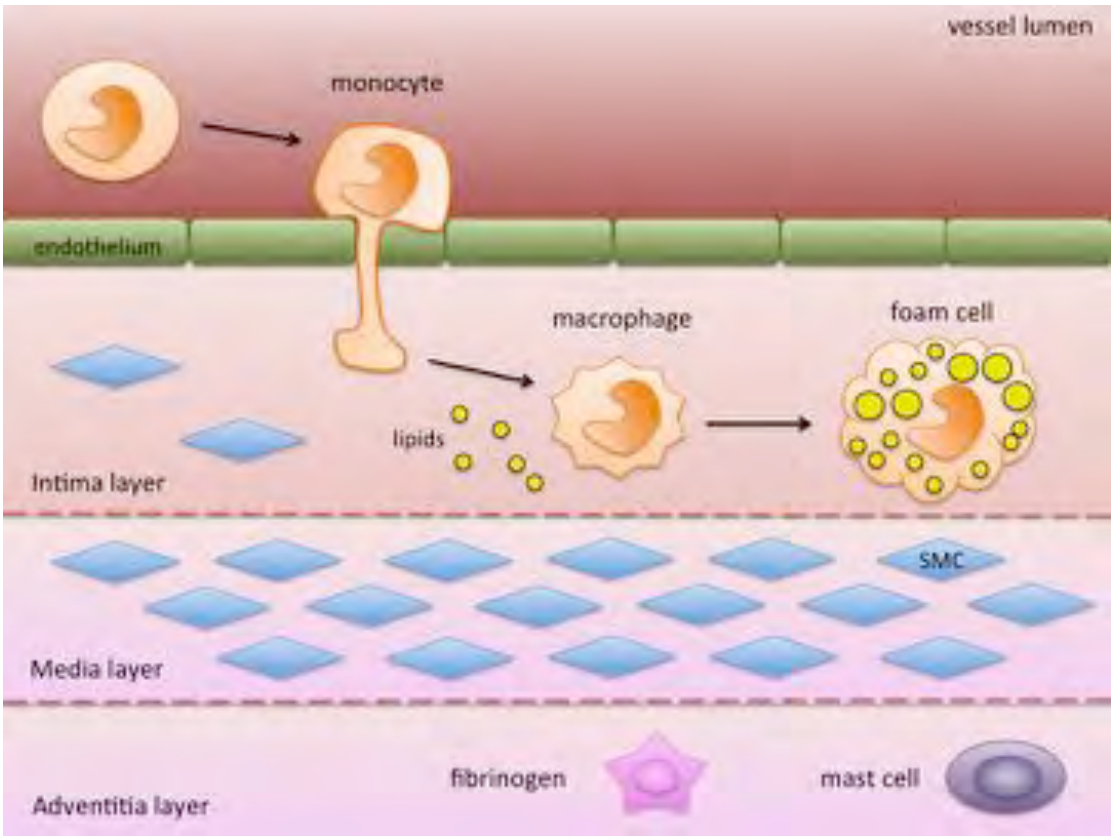

Figure 1.2. Monocyte recruitment in atherosclerosis and foam cell formation

Atherosclerosis is initiated by accumulation of lipids in the innermost layer of the artery wall, the tunica intima, causing inflammation. The monocyte is recruited at the inflammatory site by traversing the endothelium, it differentiates into a macrophage and then, with the uptake of lipid it becomes a foam cell.

Atherosclerosis occurs near bifurcations or in curvatures of arteries where there is oscillatory or low wall shear stress i.e. bidirectional or low frictional force imposed on the endothelium by the flowing blood (Pedersen et al., 1999; Chiu et al., 2011; Chatzizisis et al., 2007; Andreou et al., 2015). The risk factors for cardiovascular disease, as defined by the American Heart Association, include smoking, obesity, lack of exercise, poor diet, high blood cholesterol, high blood pressure and high blood glucose.

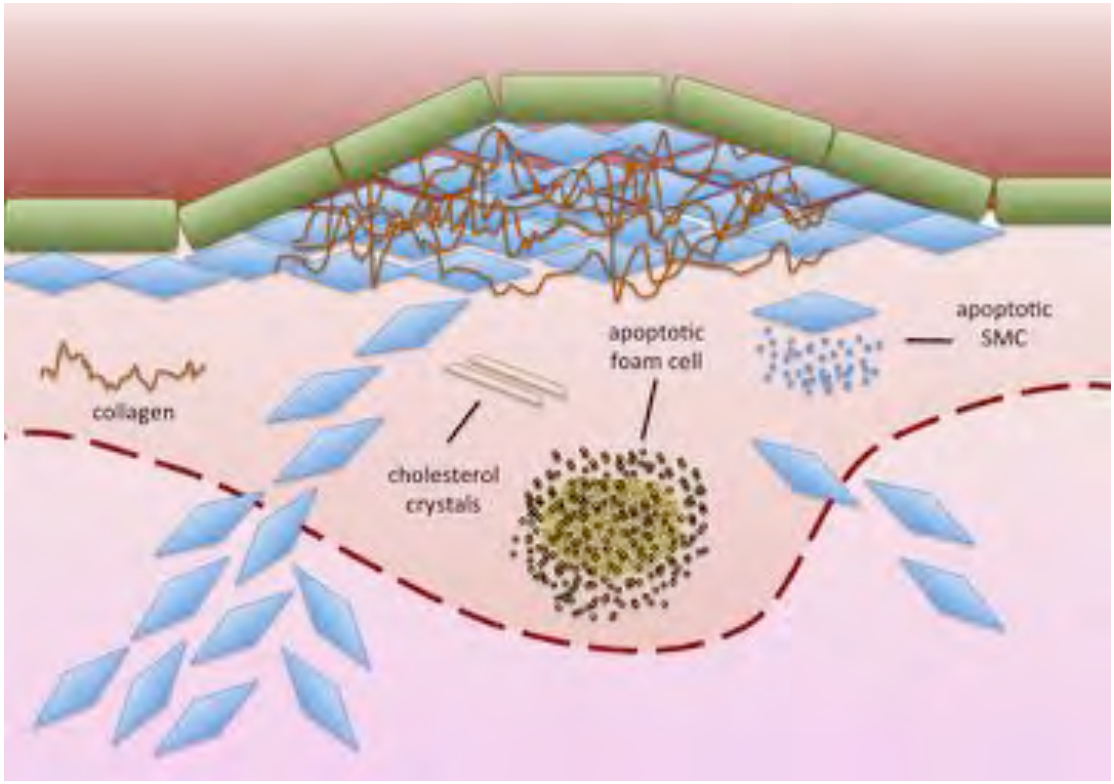

Figure 1.3. SMC migration and proliferation in atherosclerosis

Lesion progresses with the migration of smooth muscle cells from the media layer to the intima and increased synthesis of collagen and other ECM macromolecules, in order to provide extra support to the vessel wall. With time, foam cells die bursting their contents out, contributing to inflammation. SMC can die as well, further inflaming the artery wall. Advancing lesions also contain crystalised cholesterol. The size of the plaque increases and starts to extend into the lumen of the artery, limiting blood flow.

Once blood endothelial cells encounter oscillatory or low shear stress, they up-regulate expression of cellular adhesion molecules on their surface such as monocyte chemotactic protein-1 (MCP-1), also called chemokine (C-C motif) ligand 2 (CCL2) which causes monocyte recruitment in the arterial wall (Chien, 2003; Chien, 2007; Hsai et al., 2001; Hsai et al., 2003; Hwang et al., 2003a; Li et al., 2005; Shyy et al., 1994; Shyy et al., 1995) and platelet-derived growth factors (PDGFs) that promote endothelial cell growth and migration of smooth muscle cells into the sub-intimal space (Kraiss et al., 1996; Malek et al., 1993; Wilcox et al., 1988). On the contrary, at the straight parts of the arteries where there is sustained laminar blood flow and high shear stress, the above

genes are down- regulated and endothelial growth-arrest genes are favored instead (Berk, 2008; Chien, 2003; Chien, 2007; Hsai et al., 2003; Hwang et al., 2003b; Li et al., 2005; Malek et al.; 1993; Traub et al., 1998).

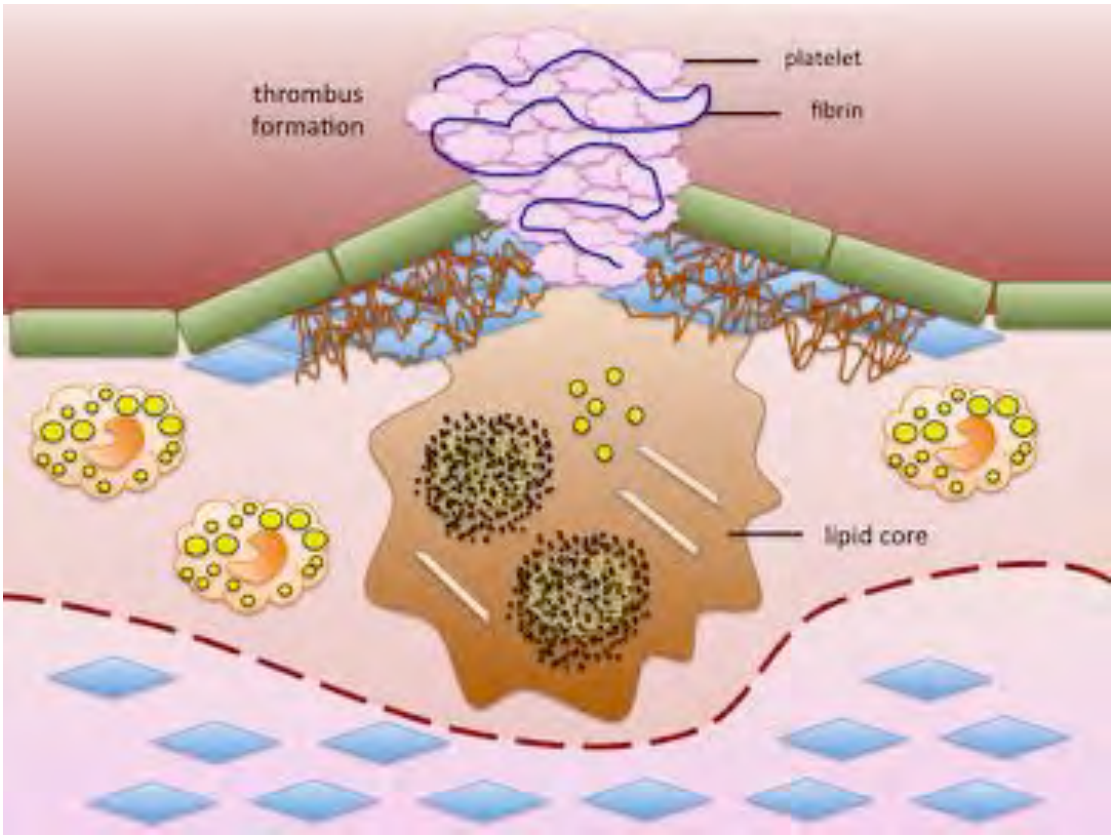

Figure 1.4. Pathological thrombosis upon atherosclerotic plaque rupture

A physical rupture of the plaque's fibrous cap, brings the blood coagulation components in contact with tissue factors in the plaque's interior which triggers the formation of a thrombus that may occlude blood flow completely.

Low endothelial shear stress results in the development and progression of atherosclerosis through a variety of mechanisms; a) by attenuating nitric-oxide (NO)-dependent atheroprotection, b) by promoting LDL uptake, synthesis and permeability, c) by promoting oxidative stress, d) by promoting inflammation, e) by promoting vascular smooth muscle cell migration, differentiation, and proliferation, f) by ECM degradation in vascular wall and plaque fibrous cap, g) by attenuating ECM synthesis in

vascular wall and plaque fibrous cap, h) by increasing plaque thrombogenecity and i) by affecting atherosclerotic wall structure. These mechanisms are described below.

Attenuation of Nitric-oxide (NO)-dependent atheroprotection

Nitric oxide, a major regulator of vascular tone (Palmer et al., 1987), possesses major anti-atherosclerotic properties. It down-regulates expression of both the monocyte chemoattractant peptide-1 (MCP1) and the vascular cell adhesion molecule-1 (VCAM1), inhibits lipid oxidation, inhibits vascular smooth muscle proliferation, prevents platelet aggregation and inhibits expression and action of matrix metalloproteinases (MMPs) (Cai and Harrison, 2000; Wang et al., 2005; Chen and Wang, 2004; Upchurch et al., 2001; Akool et al., 2003).

Physiologic shear stress continuously stimulates NO production by the blood endothelial cells (Lam et al., 2006; Go et al., 2001). However, in conditions of disturbed flow, low shear stress results in the decrease of NO available by limiting eNOS mRNA and protein expression, ultimately leading to decreased atheroprotection (Gambillara et al., 2006; Cheng et al., 2005).

Low-density lipoprotein (LDL) uptake, synthesis and permeability

Low shear stress results in sustained activation of sterol regulatory element-binding proteins (SREBPs) in endothelial cells in a beta (1)-integrin-dependent manner. SREBPs cause up-regulation of low-density lipoprotein receptor (LDLR), cholesterol synthase and fatty acid synthase (Liu et al., 2007), resulting in uptake and synthesis of LDL by endothelial cells, ultimately contributing to sub-endothelial accumulation of LDL (Chien, 2003).

Low shear stress also enables endothelial cells to change shape from fusiform to polygon, resulting in wider junctions between adjacent cells (Malek et al., 1999; Chien, 2003). This low shear stress-associated gap formation makes endothelial cells more permeable to LDL, contributing to further sub-endothelial accumulation of LDL (Traub and Berk, 1998; Himburg et al., 2004).

Oxidative stress

Once LDL particles get access to the subendothelium, they associate with intimal proteoglycans and undergo oxidative modification (Ross, 1999; Hansson, 2005). Low shear stress results in reactive oxygen species (ROS) production in the artery wall that then oxidise LDL, by endothelial upregulation of gene expression of major oxidative enzymes such as NADPH oxidase (Harrison et al., 2006; Hwang et al., 2003; McNally et al., 2003). In addition, animal studies have shown that the extracellular group IIa phospholipase A2 (sPLA2) can also contribute to LDL oxidation and atherosclerosis progression (Ivandic et al., 1999).

Inflammation

Another consequence of low shear stress is increased recruitment of circulating inflammatory cells (monocytes, T-lymphocytes, mast cells, eosinophils, dendritic cells) into the arterial wall. Increased infiltration of these cells is mainly due to activation of nuclear factor-kappa β (NF-κB), which leads to the up-regulation of various endothelial genes downstream of it. These genes encode adhesion proteins e.g. vascular cell adhesion molecule (VCAM-1), intercellular adhesion molecule (ICAM)-1 and E-selectin; chemotactic proteins e.g. monocyte chemoattractant protein (MCP)-1, pro-inflammatory cytokines e.g. tumor necrosis factor (TNF)-α, interleukin (IL)-1 and interferon (IFN)-γ and growth factors such as the macrophage colony-stimulating factor

(M-CSF) that stimulates macrophage proliferation, differentiation and scavenger receptor expression (Watson et al., 1997).

Oxidised LDL also modulates inflammation by inhibiting endothelial synthesis of nitric oxide (Wang et al., 2011). Oxidized LDL is rapidly taken up by macrophages to form foam cells. LDL modified by myeloperoxidase binds to macrophage scavenger receptors such as CD36 and SR-A (Podrez et al., 2000; Suzuki et al., 1997; Febbraio et al., 2000). Absence of these receptors results in a reduction in the size of atherosclerotic plaques. Activity of these receptors is controlled by the transcription factor PPARγ and by various cytokines such as TNFα and IFNγ (Tontonoz et al., 1998). Sphingomyelinase on the other hand hydrolyzes the sphingomyelin of LDL and promotes LDL retention and aggregation, this way enhancing macrophage uptake (Marathe et al., 1999).

Vascular smooth muscle cell (VSMC) migration, differentiation and proliferation

Under conditions of disturbed flow, endothelial cells over-express various growth factors such as platelet-derived growth factor (PDGF) and vascular endothelial growth factor (VEGF) (Malek et al., 1999; Palumbo et al., 2002) that attract VSMC from the media to the intima layer and stimulate their proliferation (Jones et al., 2005; Ross, 1999). Once in the intima layer, VSMC start producing extracellular matrix (ECM) components, such as collagen (Ross, 1999). By time, VSMC and fibroblasts produce a fibrous cap over the thrombogenic lipid core to keep it away from flowing platelets. The lipid core along with the associated fibrous cap is what makes up the atherosclerotic plaques (Stary et al., 1995; Virmani et al., 2000).

ECM degradation and synthesis in vascular wall and plaque fibrous cap

The pro-inflammatory cytokines (TNF-α, IL-1, IFN-γ) that are upregulated under low shear stress conditions, stimulate the secretion of matrix metalloproteinases

(MMPs) from macrophages, VSMC, T-lymphocytes and mast cells, that degrade the ECM in the atherosclerotic plaques (Dollery and Libby, 2006).

Apart from increased ECM degradation, there is also decreased ECM synthesis in vascular wall and plaque fibrous cap in low shear stress conditions, due to inhibition of collagen production by VSMC, by the IFN-γ (Xu et al., 2003).

The fibrous cap is maintained by continuous matrix synthesis and breakdown that are regulated by inflammatory cells. T lymphocytes secrete gamma interferon that inhibits matrix production by SMC (Armento et al., 1991). In addition, macrophages secrete ECM degradative enzymes such as interstitial collagenase, gelatinases and stromolysin (Henney et al., 1991; Galis et al., 1994; Nikkari et al., 1995).

An important player in fibrous plaque formation is the interaction between the costimulatory protein CD40 and its ligand CD40L (CD154). These proteins are found on endothelial cells, SMC, macrophages and T cells and CD40 ligation stimulates synthesis of cytokines, matrix metalloproteinases and adhesion molecules. Disruption of CD40 engagement with its ligand has lesion progression limiting consequences due to decreased macrophage recruitment and associated lipid deposition but increased SMC accumulation and associated ECM on the other hand (Schonbeck et al., 2000).

Plaque Thrombogenicity

During the atherogenic process, the plaque's core becomes more thrombogenic with increased expression of TF that triggers coagulation by the endothelium and macrophages. Synthesis of TF is promoted by the CD40/CD40L signalling pathway and the oxidization of LDL (Schonbeck et al., 2000). Furthermore, disturbed flow and underlying low shear stress downregulate the expression of anti-thrombotic agents such as eNOS and prostacyclin (Ziegler et al., 1998; Qiu and Tarbell, 2000).

Severe atherosclerosis may lead to thrombosis and associated complications upon plaque rupture. Whether a lesion will lead to the formation of thrombus depends primarily on how stable the plaque is, which further depends on the plaque's composition. A vulnerable plaque is typically characterised by a thin fibrous cap and a large number of recruited inflammatory cells.

The vulnerability of the plaque is further affected by the level of calcification and neovascularization. Calcification in the intima occurs when cytokines such as TGFβ1 and oxysteroles stimulate vascular cells that start to express osteoblastic features (Watson et al., 1994).

1.1.1 The Role of Platelets

Platelets are the smallest of blood cells, having a diameter of just 2-3μm (Paulus, 1975). They originate from fragmentation of the megakaryocytes of the bone marrow and as a result they are anucleate (Machlus et al., 2014). They exist only in the mammalian blood and their life span in the human is up to 10 days (Leeksma and Cohen, 1955). Platelet activation, coagulation and resulting thrombus formation are essential to prevent haemorrhage upon tissue injury, however; in pathological conditions, these processes may cause thrombotic vessel occlusion such as in myocardial infarction or ischaemic stroke which may have detrimental effects or even be fatal (Savage et al., 1998).

The Response of Platelets to Vascular Injury

Any damage to the vascular endothelium that exposes the subendothelial extracellular matrix (ECM) triggers platelet recruitment at the injured site. Circulating platelets initially decelerate over the compromised site due to transient interactions

with the extracellular matrix. These initial interactions trigger platelet activation, which results in the expression of specialized integrins that then enable firm adhesion of platelets to the ECM. Activated platelets release agonists that activate more platelets and start platelet aggregation that seals the wound and prevent further haemorrhage until wound healing takes place (**see Fig. 1.5**).

Initial interaction between platelets and the subendothelium is influenced by the rheological conditions of the blood. In veins and microvessels, where there is low shear stress, platelets bind directly to exposed collagen, fibronectin and laminin. However under conditions of high shear stress, such as those in the large arteries, platelet binding to the subendothelium is achieved indirectly, through binding plasma VWF that itself rapidly binds exposed collagen (Savage et al., 1998; Jackson et al., 2003).

Platelets initially bind VWF through the platelet receptor GPIba (Sakariassen et al., 1986). This binding has a fast dissociation rate; hence it is incapable of mediating stable adhesion and indeed functions in the same manner as selectins during leukocyte recruitment, supporting platelet rolling. However, this interaction keeps platelets in close proximity with the vessel surface, with rolling along the VWF in the direction of blood flow. The resulting deceleration or “rolling” enables another platelet receptor, called glycoprotein-VI (GPVI), to interact with exposed collagen. GP VI binds collagen with low affinity; therefore it is incapable of mediating stable adhesion either. However, it induces intracellular signaling that activates platelets and transforms platelet integrins to a high-affinity state. Platelet activation, results in the activation of integrin receptor αIIbβ3 (glycoprotein IIbIIIα, GPIIbIIIa), forming a stable bond with VWF (Savage et al., 1998; Jackson et al., 2003).

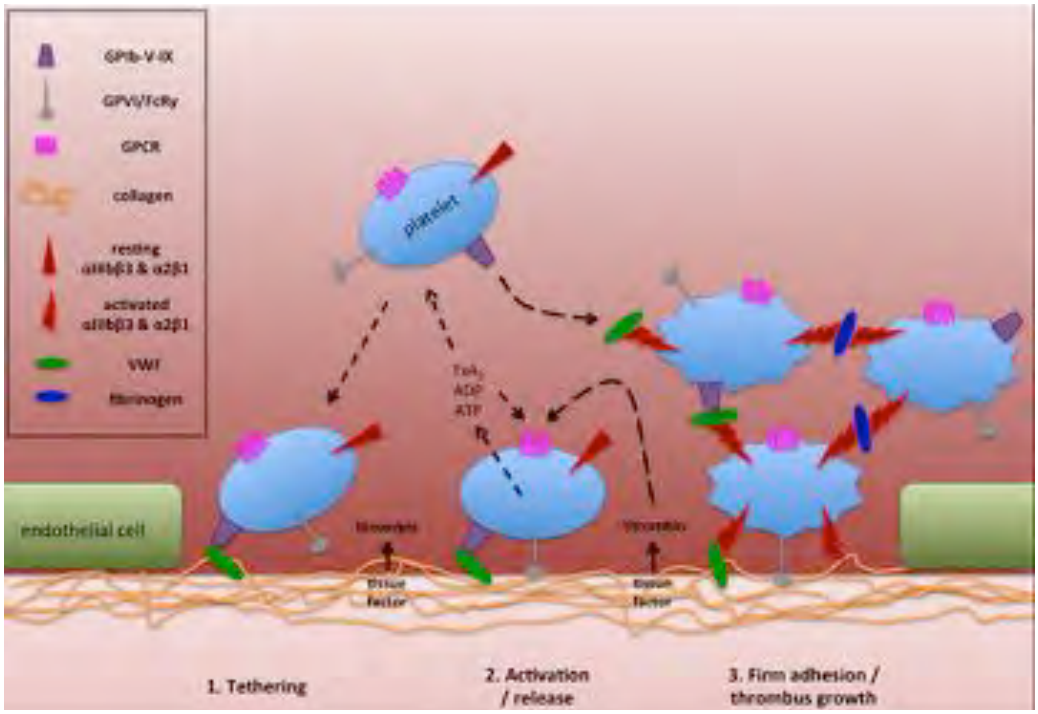

Figure.1.5. Platelet Recruitment at sites of Vascular Injury

Platelets initially bind to the exposed ECM (collagen) indirectly, through binding with their GPIb to VWF adhered to collagen. Next, platelet GPVI binding to collagen initiates platelet activation that causes platelet integrin shift to a high-affinity state. Platelet activation also leads to extracellular release of soluble agonists such as ADP, ATP and TxA_2 that activate additional platelets. Exposed tissue factor stimulates the formation of thrombin, which contributes to platelet activation. Finally, platelets adhere firmly to collagen directly through activated $\alpha_2\beta_1$ and indirectly through $\alpha IIb\beta_3$ binding to VWF and ensure sustained GPVI signaling and initiation of thrombus growth.

Platelet activation induces the production of various eicosanoids (signalling molecules made by oxidation of 20-carbon fatty acids) from the arachidonic acid. These reactions are brought about by the action of the enzyme cyclooxygenase. The various eicosanoids produced such as thromboxane A2 and different prostaglandins can act as vasoconstriction agents, contributing to haemostasis. The lipid mediator thromboxane A2 (TxA_2) is also a potent secondary activation signal for platelets reinforcing the initial GPVI-mediated activation and stimulating adjacent cells through cognate receptors on the platelet surface (Paul et al., 1999). Platelet activation also contributes to coagulation by exposure of phosphatidylserine (PS) on the plasma membrane to which coagulation

factors bind and through which interaction their enzymatic activity is potentiated (Heemskerk et al., 2005).

Upon coverage of the total injured vessel wall area with a monolayer of platelets, the next step in thrombus formation is the recruitment of additional platelets which subsequently aggregate. The different soluble agonists that are produced or secreted from activated platelets attached to collagen (or to VWF attached to collagen) such as ADP, thromboxane, epinephrine and thrombin cause passing circulating platelets to activate as well and then aggregate. These soluble agonists activate platelet GP IIbIIIα through a series of signalling events causing a conformational change which enables it to bind fibrinogen and free VWF, forming stable bridges between platelets (Savage et al., 1998).

Platelet activation and aggregation (primary haemostasis) leading to clot formation is linked to activation of the coagulation cascade (secondary haemostasis) that leads to fibrin formation from fibrinogen by the proteolytic activity of thrombin. Fibrin fibrils further strengthen the clot (Furie and Furie, 2005), preventing premature disaggregation and ensuring effective thrombus formation.

Pathological thrombosis upon atherosclerotic plaque rupture

Platelets were initially thought to have a role in atherosclerosis only in the final event, which is pathological thrombosis upon atherosclerotic plaque rupture. A physical rupture of the plaque's fibrous cap, brings the blood coagulation components in contact with tissue factors in the plaque's interior which triggers the formation of a thrombus that may occlude blood flow completely. However, there is now accumulating evidence to suggest that platelets are also involved in the initial steps of atherosclerosis a) by

acting as an adhesive substrate that leads to the recruitment of monocytes to the surface of the vessel wall, and b) by releasing chemokines that stimulate monocyte activation and support transendothelial migration. Some examples are given below.

Both granulocytic and mononuclear leukocytes were shown to be able to bind immobilised, activated platelets from flow via p-selectin (Buttrum et al., 1993; Lalor et al., 1995; Bahra and Nash, 1998).

In an *in vitro* flow-based adhesion assay where secretory smooth arterial smooth muscle cells (SMCs) were cocultured with endothelial cells, simulating inflammatory conditions, flowing platelets were able to bind to the activated endothelium and get activated themselves (platelets do not ordinarily bind to endothelium). P-selectin expression on the activated platelet was able to preferentially capture flowing monocytes, this way recruiting them to the endothelium as well. In addition, platelet factor 4 (CXCL4) release from the activated platelet supported monocyte activation on the endothelial surface, followed by transendothelial migration (Kuckleburg et al., 2011).

In the blood of healthy individuals, platelets naturally form aggregates with leukocytes at low levels (Yip et al., 2013). However in different inflammatory diseases such as diabetes, rheumatoid arthritis, inflammatory bowel disease, atherosclerosis and athero-thrombotic disease, the incidence of these aggregates is higher and correlates with the severity of disease (Harding et al., 2004; Joseph et al., 2001; Tekelioglu et al., 2013; Wrigley et al., 2013; Furman et al., 1998). Indeed, circulating activated platelets were found to preferentially bind monocytes in whole blood, forming heterotypic aggregates that exacerbate atherosclerosis in apolipoprotein-E-deficient mice. These

activated platelets secreted the chemokines CCL5 (RANTES) and CXCL4 that activate monocytes and endothelial cells, leading to monocyte recruitment (Huo et al., 2003).

1.1.2 The role of Extracellular Vesicles

Extracellular vesicles are membranous vesicles released from activated cells. They are present in various biological fluids such as blood (Nieuwland and Sturk, 2007; Yuana et al., 2010), urine (Miranda et al., 2010; Royo et al., 2016), saliva (Xiao and Wong, 2012), semen (Vojtech et al., 2014), breast milk (Admyre et al., 2007), amniotic fluid (Asea et al., 2008), ascites fluid (Peng et al., 2011), cerebrospinal fluid (Street et al., 2012) and bile (Li et al., 2014). EV present proteins indicative of their cellular origin and may also contain different types of genetic material (Valadi et al., 2007). High levels of EV have been reported in patients with cardiovascular risk factors and after cardiovascular events (Rautou et al., 2011).

EV are a heterogeneous population in terms of size, density, morphology, cell origin, organelle origin and composition. Taking these differential characteristics into account, van der Pol et al., (2012) divided EV into three main types: (a) exosomes, (b) microvesicles (MV) or microparticles (MP) and (c) apoptotic vesicles (**Fig. 1.6**). The classification of these three EV types is shown in **Table 1.1**.

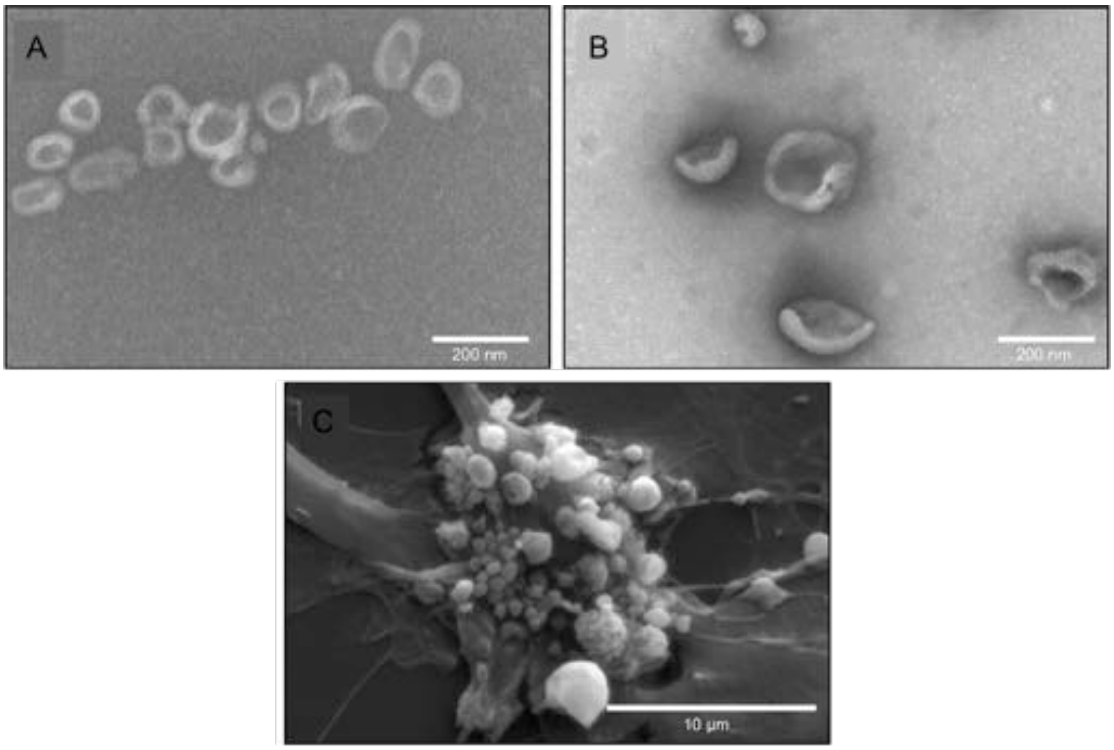

Figure 1.6. The three main types of EV.

Transmission electron micrographs of human plasma (A) exosomes, urine (B) microvesicles and a scanning electron micrograph of (C) apoptotic vesicles released from human umbilical vein endothelial cells. Edwin van der Pol et al., 2012.

Exosomes are cell-derived vesicles that originate from the endosome (Booth et al., 2006; Fang et al., 2007; Harding et al., 1983; Lenassi et al., 2010; Pan et al., 1985). They are released by most cell types and tend to have a diameter of 30-100nm (Escola et al., 1998; Heijnen et al., 1999; Raposo et al., 1996; Trams et al., 1981), a density between 1.13 and 1.19 g/ml (Escola et al., 1998; Heijnen et al., 1999; Raposo et al., 1996), they have a "cup" shape (Escola et al., 1998; Heijnen et al., 1999; Raposo et al., 1996; Andre' et al., 2004). Based on biochemical studies it was found that exosomes are made of high levels of cholesterol, sphingomyelin, ceramide and glycerophospholipids with long and saturated fatty acyl-chains (Subra et al., 2007; Trajkovic et al., 2008; Wubbolts et al., 2003). Regarding their protein content, exosomes are enriched in proteins that have a role in membrane transport and fusion such as Rab, GTPases,

Annexins and flotillin, vesicular trafficking mediators such as Alix and tumour susceptibility gene 101 (TSG101), stress proteins (hsp70 and hsp90), integrins (e.g. α4) and tetraspanins such as CD9 and CD63 (Simons and Raposo, 2009; Thery et al., 2009; Beyer and Pisetsky, 2010; Mathivanan et al., 2010; Bombrie et al., 2011; Chaput and Thery, 2011; Record et al., 2011; Wubbolts et al., 2003).

	Apoptotic bodies	**Microvesicles**	**Exosomes**
Size	0.5-2 μm	100-1000 nm	20-100 nm
Density (g/ml)	1.16-1.28	1.04-1.07	1.13-1.19
Formation	cell surface, outward blebbing of apoptotic cell membrane	cell surface, outward blebbing of cell membrane	endolysosomal pathway, inward endosomal membrane budding, and multivesicular bodies fusion with cell membrane
Contents	nuclear fractions, DNA, RNA, miRNA, protein, cell organelles	RNA, miRNA, other non-coding RNA, cytoplasmic protein and membrane protein, cell organelles, lipids	RNA, miRNA, other non-coding RNA, cytoplasmic protein and membrane protein, major histocompatibility complex (MHC)
Markers	Annexin V	Annexin V, origin cell-specific markers	integrins (α3, α4, β1, β2), lactadherin, Tetraspanins (CD81, CD82, CD9, CD63), ESCRT proteins (alix, TSG101), actin, flotillin, clathrin

Table 1.1. EV classification

Adapted from Yin et al., 2015.

Microvesicles (MV) or microparticles (MP) are the vesicles released from the plasma membrane as a result of cell stress or upon cell activation. They can be as small as the smallest exosomes (Wolf, 1967) but can reach up to 1.0 μm (Thery et al., 2009). The density of MV is unknown. MV often expose phosphatidylserine (PS), the main phospholipid component of the cell membrane (Thery et al., 2009; Beyer and Pisetsky, 2010) and they also express transmembrane proteins and receptors and enclose cytosolic molecules such as enzymes, transcription factors and RNA obtained from their parent cell (VanWijk et al., 2003).

MV are released from the plasma membrane by shedding/budding that requires membrane remodeling. When cells are at rest, lipids are unevenly distributed, with phosphatidylcholine and sphingomyelin concentrated on the outer leaflet of the membrane and PS and phosphatidylethanolamine located on the inner leaflet (Manno et al., 2002; Seigneuret et al., 1984). This lipid order is maintained by the action of phospholipid transporters; flippases that transport lipids from the outer leaflet to the inner, and floppases that move PS from the interior to the exterior leaflet (Daleke, 2003). When cells are activated, this lipid asymmetry is disrupted because PS is transferred to the external leaflet due to increased floppase action (Bevers et al., 1999; van Helvoort, 1996). In addition a bidirectional non-specific lipid transporter gets activated by an influx of Ca^{2+} during cell activation and starts transporting all phospholipids down their concentration gradient, leading to random distribution (Bevers and Williamson, 2010). Furthermore, the increase in calcium ions inhibits flippase activity (Daleke, 2003). Eventually, the random distribution of phospholipids causes a temporary imbalance between the two leaflets that results in the shedding of MVs (Freyssinet and Toti, 2010) (**Fig. 1.7** & **Fig. 1.8**).

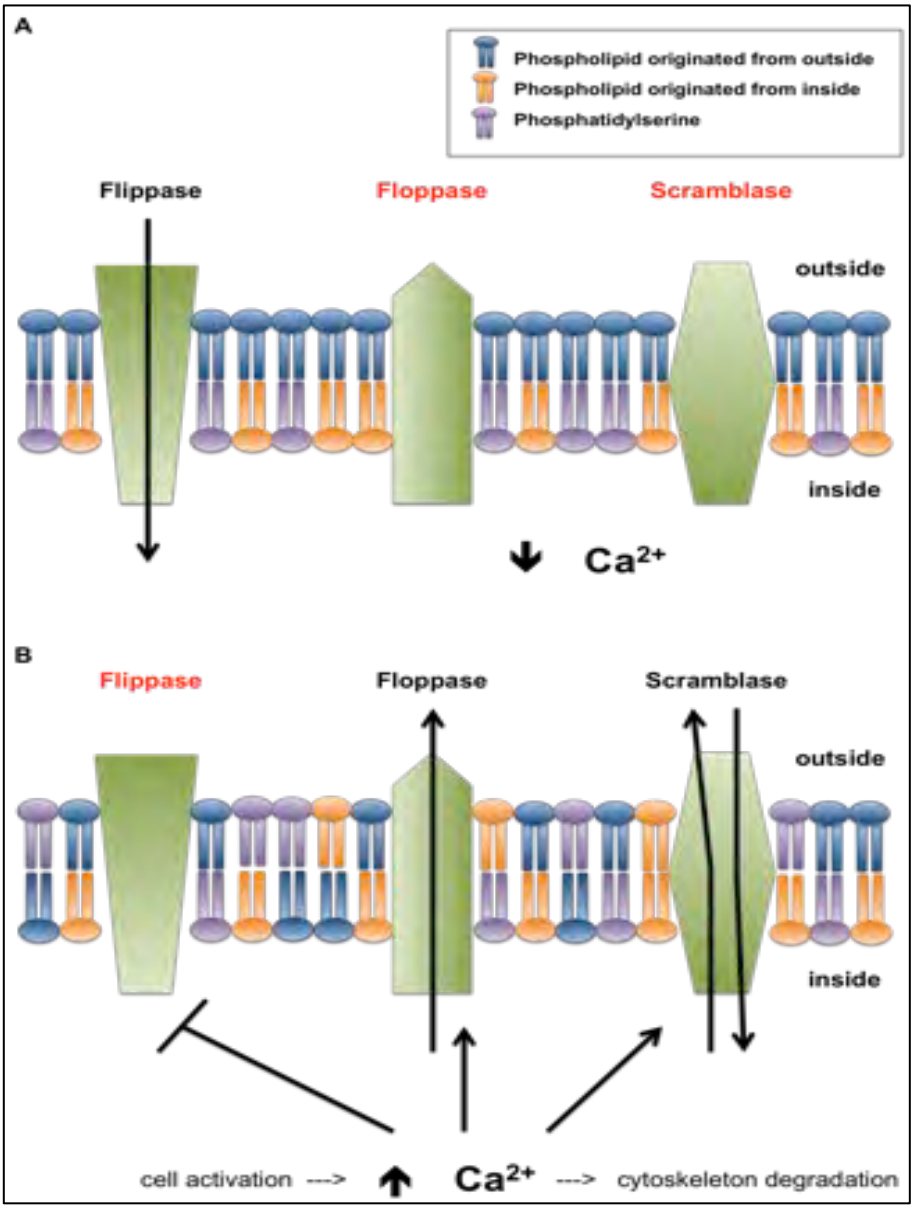

Figure 1.7. Change in phospholipid distribution leading to MV formation

(A) Maintenance of the asymmetric distribution of phospholipids in the membrane of a resting cell, by low cytoplasmic calcium concentration and active flippase enzymatic activity **(B)** Loss of the asymmetric distribution of phospholipids in the cell membrane due to cell activation and associated rise in cytoplasmic calcium level that activates the floppase and scramblase enzymes, leading to exposure at the outside surface of phosphatidylserine.

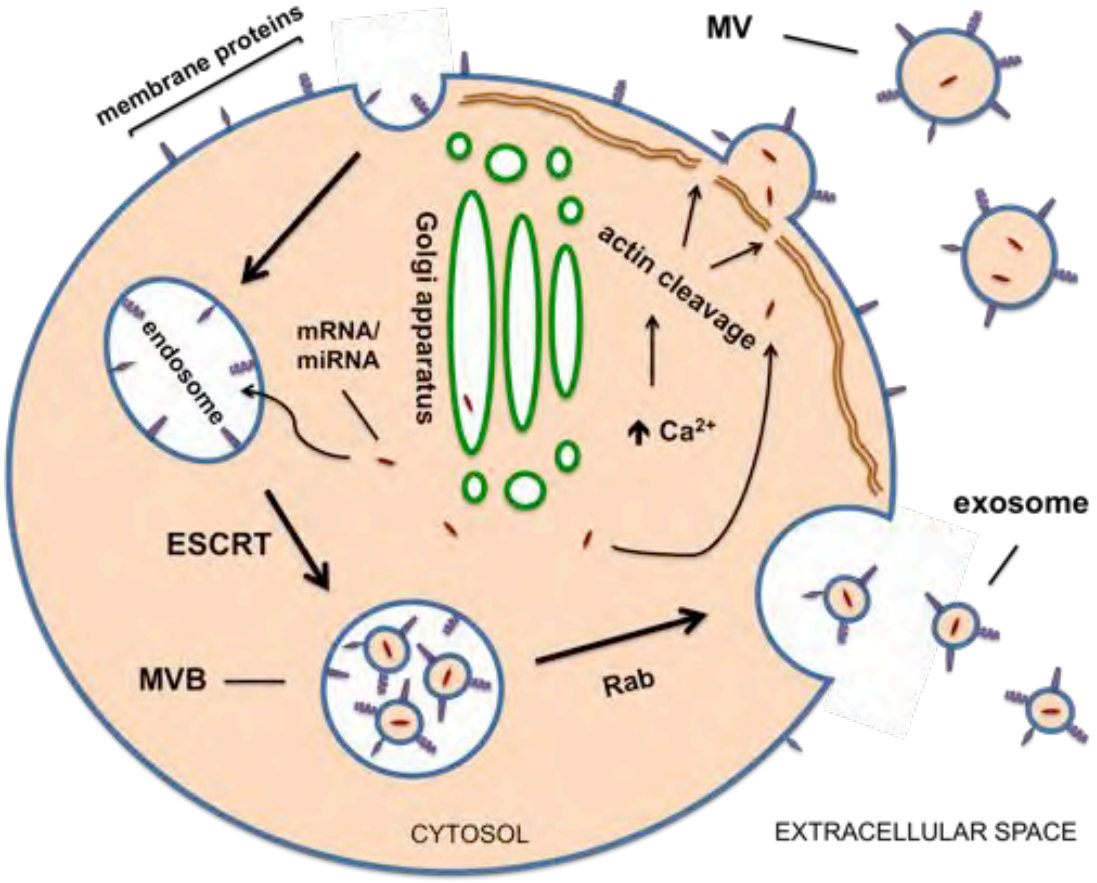

Figure 1.8. Exosome and MV Formation

Exosomes are generated by the budding of endosomal membranes inwardly. Once the membranes accummulate, they form multivesicular bodies that travel to the plasma membrane where they fuse with and secrete the exosomes to the extracellular space. The transport, fusion and secretion of exosomes is facilitated by ESCRT and Rab proteins. MV on the other hand, are formed by structural rearrangement of the cytoskeleton, due to cleavage of actin filaments by enzymes activated by the rise in cytoplasmic calcium level. The associated loss of the asymmetric distribution of phospholipids, causes the membrane to budd off and form MV.

EV and cholesterol metabolism

Removal of excess cholesterol from cells is paramount in atherosclerosis, as cholesterol overload in monocytes/macrophages results in foam cell formation, a key event in atherosclerosis (Reiss and Cronstein, 2012; Cochain and Zernecke, 2017). Excess cholesterol is primarily removed by the efflux of apolipoprotein A1 (ApoA1), which is regulated by the ATP-binding cassette transporter A1 (ABCA1) at the plasma

membrane (Ikonen, 2008; Maxfield and Meer, 2010). There is evidence that ABCA1 mediates MV formation during the production of high-density lipoprotein (HDL) (Nandi et al., 2009) and more recently it has been shown that these EV contribute to approximately 1/3 of ABCA1- and ApoA1-mediated cholesterol efflux (Hafiane and Genest, 2017). In addition, overexpression of ABCA1 is associated with incresed release of cholesterol-rich EV from THP-1 macrophages and other cell lines (Liu et al., 2007).

On the contrary, EV may promote foam cell formation and atherosclerosis progression. T cell-derived exosomes have been shown to induce cholesterol accumulation in human monocytes by enriching cholesterol and exposing PS at their outer membrane leaflet (Zakharova et al., 2007).

EV and Vascular Endothelial Cells

EV from various sources exert a variety of effects on the vascular endothelium. T-cell-derived MV can decrease endothelial production of NO and increase oxidative stress (Mostefai et al., 2008). MV secreted from monocytes might contain caspase leading to EC apoptosis (Hezel et al., 2017). In addition, MV derived from human atheromatous plaques have been found to upregulate endothelial expression of ICAM-1 facilitating monocyte adhesion and transendothelial migration (Raoutou et al., 2011).

On the other hand, EV may also exert endothelial-protective effects. MV released from activated HUVECs have been shown to prevent lipid-induced endothelial damage by reducing oxidative stress through Akt/eNOS signaling (Mahmoud et al., 2017). Endothelial-derived MV may contain activated protein C

(APC) and protein C receptor (CD201), preventing cell death in a PAR-1-dependent manner (Perez-Casal, 2011).

EV and Vascular Smooth Muscle Cells

Communication between EC and VSMC is important in maintaining vessel wall homeostasis. VSMC themselves release EV in response to endoplasmic reticulum (ER) stress that cause endothelial dysfunction (Jia et al., 2017). VSMC-derived EV can also transfer miR-150 to EC, triggering EC migration (Zhao et al., 2016). In atherosclerosis, VSMC EV promote extracellular mineralization (Kapustin et al., 2015).

EV released from other cells can also modulate VSMC function. Leukocyte-derived EV from atherosclerotic blood was found to promote the adhesion and migration of VSMC (Vanhaverbeke and et al., 2017), through the transfer of miRNA-223 (Shan et al., 2015) or by activating ERK and Akt (Niu et al., 2016).

EV and Vascular Inflammation

EV can directly induce inflammation by stimulating secretion of inflammatory cytokines e.g. monocyte chemotactic protein-1 (MCP-1) and IL-6, by stimulating the upregulation of adhesion receptors on EC and leukocytese.g. ICAM-1, VCAM-1, P-selectin and E-selectin and by activating the coagulation cascade (Yin et al., 2015). Myeloid cell-derived EV were shown to contribute to inflammation through their phospholipid content that activates toll-like receptor TLR-4 on macrophages (Thomas and Salter, 2010). Macrophage- and dendritic

cell-derived exosomes were found to contain enzymes associated with leukotriene synthesis, thus further promoting granulocyte migration (Esser et al., 2010).

Various cells release EV that carry inflammatory mediators such as IL-1β that cause inflammation directly. They may also carry lipid mediators such as phospholipids and arachidonic acid that can activate cells and induce them to produce and release different chemokines and cytokines such as IL-6/8 and MCPs (Wang et al., 2011; Qu et al., 2007; Pizzirani et al., 2007; Thomas and Salter, 2010; Esser et al., 2010; Berckmans et al., 2005; Distler et al., 2005; Beyer and Pisetsky, 2010; Distler and Distler, 2010; Jungel et al., 2007; Rautou et al., 2011).

However, other studies have identified anti-inflammatory actions for EV. Neutrophil-derived EV can inhibit monocyte/ macrophage activation in a TGFβ1-dependent mechanism (Gasser and Schifferli, 2004), or by binding monoclonal antibodies immunoglobulin M (IgM) that binds oxidized epitopes (Tsiantoulas et al., 2015).

EV and Angiogenesis and Vasculogenesis

MV from human atherosclerotic plaques were found to mediate endothelial proliferation and angiogenesis, a potential mechanism for the transition from stable to unstable lesions. This effect was achieved by VEFG expression and CD40 ligation (Leroyer et al., 2008). In addition, endothelial cells, released EV *in vitro* that contained the metalloproteinases MMMP-2 and MMP-9, which are known to degrade matrix, thus facilitating neovascularization (Taraboletti et al., 2002). Endothelial- and leukocyte-

derived MV can also have angiogenesis-inhibitory effects by inducing increased ROS and decreased NO production (Burger and Kipps, 2006; Mostefai et al., 2008).

EV and Coagulation

EV shed from atherosclerotic plaques are highly pro-coagulant (Mallat et al., 1999). EV-mediated coagulation is usually through the exposure of PS or TF on the EV membrane (Nomura and Shimizu, 2015, Tesselaar et al., 2007). On the other hand, MV from EC and leukocytes can serve as a circulating source for fibrinolysis by the generation of plasmin on their surface through the active surface tissue plasminogen activator (Lacroix et al., 2012).

1.1.3 The role of Platelet-derived Extracellular Vesicles (PEV)

Overview of PEV

PEV constitute about 30% of EVs in the plasma, as reviewed in 2014 (Arraud et al. 2014). The number of PEV released from platelets and their protein concentration depend on the platelet activation pathway (Aatonen et al., 2014). In terms of size, the large majority of PEV (90%) are smaller than 500 nm (Arraud et al., 2014; Yuana et al., 2010; Gabriel and Giordano, 2010; Aatonen et al., 2014).

Platelets release PEV upon activation. Platelet activation *in vivo* or *in vitro* is achieved by stimulation with different agonists that interact with various platelet membrane receptors. Such stimulants include collagen and cross-linked collagen-related peptide (CRP) that bind platelet glycoprotein VI, thrombin and thrombin-receptor activating peptide (TRAP) which bind and cleave protease-activated receptors (PAR), heat-aggregated immunoglobulin G that binds to the FcγRII receptor and

adenine di-phosphate (ADP) that binds to purinergic receptors (Boudreau et al., 2014; Heijnen et al., 1999; Aatonen et al., 2014). In addition, PEV are released from platelets when the levels of second messengers such as Ca^{2+}**a**re increased directly, by addition of compounds such as calcium ionophors and phorbol esters (Aatonen et al., 2014; Boudreau et al., 2014). Cytosolic rise in calcium levels is a prerequisite for PEV release upon platelet activation. Other methods to generate PEV from activated platelets include high shear (Miyazaki et al., 1996; Holme et al., 1998), contact with artificial surfaces (Gemmell et al., 1995), complement proteins (Sims et al., 1988) and low temperature (Bode and Knupp, 1994). PEV can be also formed by platelet activation-independent ways such as by integrin-mediated destabilization of actin cytoskeleton (Cauwenberghs et al., 2006) during *in vitro* aging of platelets (Bode et al., 1991), upon platelet destruction (Wiedmer et al., 1993) or directly from megakaryocytes rather than from platelets (Cramer et al., 1997).

Depending on the platelet activation pathway involved, PEV carry numerous proteins (>500), known to be involved in various cellular responses, to have different molecular functions and to be located at distinct sites within the platelet (Garcia et al., 2005; Milioli et al., 2015). For example, activation of platelets by calcium ionophore A23187, leads to PEV formation that bear many proteins characteristic of α granules (such as thrombospondin, platelet factor 4 and β-thromboglobulin) (Horstman and Ahn, 1999; Holme et al., 1998), whereas activation by thrombin results in PEV high in signaling regulatory proteins (such as Dok-2) (Shai et al., 2012). Most identified PEV-born proteins are known to be involved in signal transduction and cell communication and to be found in the cytoplasm of platelets; however a significant portion (21%) have unknown or unclassified molecular functions. Of particular interest, PEV express more

than 40 platelet membrane surface receptors such as glycoproteins Ib (CD42), IIb (CD41), IIIa, IV (CD36), V (CD42d), IX (CD42a), p-selectin (CD62), as well as different chemokines such as CXCL4, pro-platelet basic protein (CXCL7) and CCL5 (Garcia et al., 2005; Aatonen et al., 2014). PMV and platelet-derived exosomes express largely distinct proteins with only 28% of PMV proteins and 45% of platelet exosomal proteins in common (Aatonen et al., 2014).

PEV are also rich deposits of mRNA and miRNA species as discovered by recent transcriptomic studies (Pienimaeki-Roemer et al., 2017). As platelets do not contain a nucleus, their RNA content derives from megakaryocytes during platelet biogenesis. Comparison of regulated miRNAs from PEV versus senescent platelets revealed 70 regulated miRNAs with approximately one third being up-regulated. Upregulated PEV-derived miRNAs are known to target mRNAs that have roles in lipid metabolism (such as ABCB1), inflammation and vascular disease (such as complement factors and interleukins), platelet adhesion and activation (such as GPVI), coagulation (eg. fibrinogen and collagen), endocytosis and vesicle trafficking (e.g. Rab proteins), autophagy (e.g. ATG12), and generation and binding of small RNA (e.g. DICER1). The microRNA profile of PEV is also agonist specific (Ambrose et al., 2018).

The life span of PEV in the human circulation is unknown. Mouse studies of PEV injection into peripheral blood observed clearance within 30 minutes (unpublished observation from Flaumenhaft, 2006). The phosphatidylserine (PS) on PEV surface can trigger opsonization by the complement component C3b. Opsonized PEV are then bound to CR1 on erythrocytes and delivered to endothelial phagocytes in the liver and spleen for receptor-mediated endocytosis.

PEV in Atherosclerosis

Increased levels of PEV have been reported to circulate in atherosclerosis patients (Michelsen et al., 2009), suggesting that they possibly contribute to disease development. There is also an accumulation of studies correlating the level of plasma EV with the occurrence of a number of cardiovascular and other diseases (**Table 1.2.**). In addition, studies on certain atherosclerosis medications, such as statins, have attributed, at least part of their cardioprotective effect, on the associated reduction in (P)EV concentration (Suades et al., 2013). Below there is evidence to suggest that PEV are also involved in many aspects of atherosclerosis, such as, adhesion, inflammation, procoagulation, angiogenesis and lipid deposition.

PEV contain various adhesion receptors on their surface as stated previously, such as glycoproteins Ia/Ib/IIa/IIb/IIIa (Aatonen et al., 2014; Garcia et al., 2005). Lukasik et al. (2013), found a correlation between increased PEV release from platelets and atherosclerotic thickening of carotid artery wall and plaque formation. These platelets expressed decreased levels of active GPIIb/IIIa, suggesting that this receptor was transferred into the PEV.

PEV have been found to promote adhesion of monocytes to activated endothelial cells. PEV-derived arachidonic acid and/or GPIb mediated this effect. PEV also increased expression of lymphocyte function-associated antigen-1 (CD11a) and macrophage antigen-1 (CD11b) by monocytes (Chimen et al., unpublished; Barry et al., 1998). PEV can also activate the intercellular adhesion molecule 1 (ICAM-1) that mediates transendothelial migration of leukocytes (Forlow et al., 2000; Lukasik et al., 2013). In addition, PEV can release chemotactic gradients that recruit leukocytes to the vascular endothelium. Specifically, PEV induced chemotaxis of U-937 cells in a protein kinase C

(PKC)- dependent way (Barry et al., 1998). In addition, PEV were reported to have transferred CD41 to cancer cells that enhanced their adhesion to fibrinogen and endothelium (Janowska-Wieczorek et al., 2004). Moreover, PMV may bind hematopoietic stem-progenitor cells and transfer to them various platelet membrane receptors such as CD41, CD62, CXCR4 and PAR-1, thus enhancing their adhesion to the endothelium (Janowska-Wieczorek et al., 2001).

Clinical Disorders Associated with Elevated PEV levels	**References**
Acute coronary syndrome	Sun et al., 2016; Bernal-Mizrachi et al., 2003
Hypertension	Preston et al., 2003; Nomura et al., 2002
Diabetes Type 1	Sabatier et al., 2002
Diabetes Type 2	Tan et al., 2005; Koga et al., 2006; Sabatier et al., 2002
Peripheral artery disease	van der Zee et al., 2006
Preeclampsia	VanWijk et al., 2002;
Pulmonary or venous embolism	Inami et al., 2003
Sepsis	Nieuwland et al., 2000; Joop et al., 2001
Immune thrombocytopenic purpura	Sewify et al., 2013
Thrombotic thrombocytopenic purpura	Galli et al., 1996; Kelton et al., 1992
Heparin-induced thrombocytopenia	Hughes et al., 2000;
Drug-induced thrombocytopenia	Thushara et al., 2014
Transient ischemic attack	Lee et al., 1993
Multiple sclerosis	Marcos-Ramiro et al., 2014
Alzheimer disease	Goncalves et al., 2016
Cardiopulmonary bypass	Nieuwland et al., 1997
Scott syndrome	Sims et al., 1989
Polycystic ovary syndrome	Willis et al., 2014; Koiou et al., 2011
Systemic lupus erythematosus	Lood et al., 2017
Obstructive sleep apnea syndrome	Maruyama et al., 2012
Psoriasis	Tamagawa-Mineoka et al., 2010
Uremia	Ando et al., 2002

Table 1.2. Clinical disorders associated with elevated PEV levels

PEV also induce SMC recruitment to the inflamed vessel wall. PEV release various mitogens such as platelet-derived growth factor (PDGF), platelet-derived

endothelial cell growth factor, endothelin, thrombospodin and endothelial growth factor that promote recruitment and multiplication of SMC in the arterial walls (Diehl et al., 2010).

As already described in this chapter, the inner leaflet of the lipid bilayer membrane of platelets is composed of different aminophospholipids such as phosphatidylserine (PS) that gets exposed to the extracellular space only when platelets get activated (Thiagarajan and Tait, 1991). PS-expressing platelet-derived microvesicles (PMV) promote coagulation in the presence of calcium (Zwaal and Schroit, 1997). Notably, the membrane of PMV was found to be 50-100 times more procoagulant than the surface of activated platelets (Sinauridze et al., 2007) and EV-depleted plasma was found to be incapable of clotting (Nieuwland and Sturk, 2007). The role of PMV in haemostasis is pathologically confirmed from the bleeding phenotype in PMV deficiency conditions such as Scott Syndrome and Castaman syndrome (Piccin et al., 2007; Castaman et al., 1996).

In addition, PMV express surface receptors for coagulation factor VIII, factor Va and activated coagulation factor IX (Gilbert et al., 1991; Comfurius et al., 1990; Hoffman et al., 1992). Factor VIII is a cofactor in the tenase enzyme complex which forms on the membrane of activated platelets. Factor Va combines with factor Xa and form the prothrombinase complex. Each PMV was able to bind as much factor VIII as a stimulated platelet (Gilbert et al., 1991). PEV can also bind to subendothelial matrix (fibrinogen, fibronectin and collagen) *in vitro* and *in vivo* via glycoprotein IIbIIIa (GPIIbIIIa) and to act as a substrate for platelet adhesion (Merten et al., 1999). These findings suggest that the procoagulant effect can take place at distant sites and for longer periods than that for activated platelets.

The role of platelets in thrombotic inflammation is now well documented (Wagner and Burger, 2003). PEV play a role in inflammation accordingly by delivery of proinflammatory mediators, such as the chemokine CXCR4 (Rozmyslowicz et al., 2003) and IL-1 (Boilard et al., 2010).

When PMV get exposed to phospholipase A2, they release arachidonic acid. The platelets then metabolize it to thromboxane A2, resulting in their activation (Barry et al., 1997). PMV-released arachidonic acid also transactivates monocytes and endothelial cells leading to increased monocyte adhesion to endothelial cells through intracellular cell adhesion molecule-1 (ICAM-1) binding and elevated chemotaxis of monocytoid cells (Barry et al., 1998). The arachidonic acid also induces synthesis of cyclooxygenase-2 (COX-2)-derived prostacyclin (PGI2) (Barry et al., 1999; Barry et al., 1997). PEV can also activate cells through exposure of platelet activating factor (Iwamoto et al., 1996). Furthermore, PEV can bind leukocytes through p-selectin – PSGL-1 interaction and enhance indirect leukocyte-leukocyte aggregation in flow and increase neutrophil phagocytic activity (Forlow et al., 2000; Jy et al., 1995). Laffont et al. (2016) have discovered that PEV are internalised by primary human macrophages and deliver microRNAs that reprogram macrophage gene expression towards a phagocytic function.

Notably, circulating microparticles from patients with myocardial infarction could hinder the nitric oxide-dependent vasodilation (Boulanger et al., 2001) and PMV-derived cyclooxygenase from a rabbit artery model was found to convert arachidonic acid produced by endothelial cells into the vasoconstrictor thromboxane A_2 (Pfister, 2004), suggesting that PEV can mediate vascular tone.

Activated platelets release PEV containing mitochondria (Laffont et al., 2016) and by hydrolysis of the mitochondrial membrane, different inflammatory stimuli are produced that activate neutrophils (Boudreau et al., 2014). These PEV-derived mitochondria are functional and can be internalized by leukocytes and can serve as a substrate for phospholipase A2 (PLA2 IIA) that leads to the formation of inflammatory mediators e.g. lysophospholipids and fatty acids (Boudreau et al., 2014). Such mediators are known to activate leukocytes and promote the progression of atherosclerosis.

There is now sufficient evidence to suggest that PEV are important mediators between oxidative stress and platelet activation. Oxidized LDL can trigger the formation of PEV that then promote platelet activation. However, platelets that lacked the scavenger receptor CD36 could not get activated in this setting, suggesting a possible role for platelet- derived CD36 in atherosclerosis. The action of the PEV-CD36 complex was mediated by the MKK4/JNK2 (mitogen-activated protein kinase kinase 4/c-Jun N-terminal kinase 2) signaling pathway. In addition, PEV also induced the formation of 8-iso-prostaglandin-F2α, a marker of oxidative stress, from platelets, that triggered procoagulant effects (Wang et al., 2012).

PEV are heavily involved in angiogenesis. They can induce proliferation, survival, migration and tube formation of endothelial cells *in vitro* mainly through the action of lipid growth factors (Kim et al., 2004) and by inducing phosphorylation of MAPK p42/44 and serine/threonine kinase (Janowska-Wieczorek et al., 2004). PEV were also found to promote angiogenesis *in vivo* in a transplantation model of ischaemia (Brill et al., 2005). PEV can also contribute to neovascularization by stimulation of metalloproteinase production (Dashevsky et al., 2009; Janowska-Wieczorek et al., 2004). Another example includes PEV delivery of miR-24 to tumor cells *in vivo* targeting

mt-Nd2 mRNA, regulating mitochondrial function and inhibiting angiogenesis (Michael et al., 2016).

Further dissection of the roles of PEV in adhesion, inflammation, procoagulation, angiogenesis and lipid deposition, might identify targets for development of future pharmacological agents in order to prevent and treat atherosclerotic cardiovascular diseases.

1.2 Project Hypothesis and Aims

Our hypothesis is that PEV play a role in the progression of atherosclerosis through a) facilitating the recruitment of monocytes to the inflamed endothelium and b) through the transfer of agents that render monocytes or monocyte components such as mitochondria or lysosomes dysfunctional.

Hence, our overall aims are to investigate a) PEV-mediated recruitment of monocytes in atherosclerosis and b) potential adoption of PEV components such as mitochondria from PEV that can potentially affect monocyte behaviour in atherosclerosis.

2 METHODS

2.1 Ethics

2.1.1 Human

Peripheral blood was collected from healthy volunteers with written informed consent and approval from the University of Birmingham Local Ethical Review Committee (ERN-07-058).

2.1.2 Mouse

All procedures were performed in accordance with Home Office regulations and approval from a local ethics committee. Procedures were conducted under Home Office Project License PPL 40 3659.

2.2 Sources, Housing and Diet of Mice

C57BL/6 mice and apolipoprotein E-null ($ApoE^{-/-}$) mice on a C57BL/6 background were obtained from Charles River UK and were further bred and maintained at the Biomedical Services Unit.

hiL4R/GPIbα-$Tg^{+/+}$ mice on a C57BL/6 background were generated by Ware and colleagues (2002) and were obtained from Wolfgang Bergmeier (University of North Carolina) and were further bred and maintained at the Biomedical Services Unit.

$ApoE^{-/-}$ hiL4R/GPIbα-$Tg^{+/+}$ mice were generated by crossing $ApoE^{-/-}$ with IL4R/GPIbα-$Tg^{+/+}$ mice to first generate heterozygous $ApoE^{+/-}$ hiL4R/GPIbα-$Tg^{+/-}$mice. Heterozygous mice were crossed among themselves to generate different genotype combinations of which only the $ApoE^{-/-}$ hiL4R/GPIbα-$Tg^{+/+}$ and $ApoE^{-/-}$ hiL4R/GPIbα-$Tg^{+/-}$ mice were used in experiments and for further breeding.

All mice were fed on Chow diet upon weaning. Where induction of atherosclerosis was required, mice were switched to Western RD diet (0.15% cholesterol, Special Diet Services) at 10-12 weeks of age and were maintained on this high fat diet for 6 or 14 weeks, before culling.

2.3 Blood Collection

2.3.1 Human

Blood was withdrawn by venepuncture into tubes containing anticoagulant; either in 10 % citrate-phosphate-dextrose solution with adenine (CPDA) (Sigma-Aldrich) for platelet extraction or for whole blood use, or in 1.6 mg/ml ethylenediaminetetraacetic acid (EDTA)-coated tubes (Sarstedt) for WBC extraction. Anti-coagulated blood was mixed by inversion. Blood samples were stored at room temperature and processing started within 30 minutes of collection for platelet extraction or for whole blood use or within 1hour for white blood cell extraction.

2.3.2 Mouse

2.3.2.1 Cardiac Bleeds

When total peripheral blood or large volumes of blood were required i.e. to extract a particular cell type, blood was collected by cardiac puncture using 25-gauge needle from animals under anaesthesia induced by inhalation of 4% isofluorane. Collected blood was immediately inserted into tubes containing anticoagulant where needed; either in 10 % CPDA for platelet extraction, as its platelet activation inhibition is reversible or in 1.6 mg/ml EDTA-coated tubes which best preserves cellular components and cell morphology (Banfi et al., 2007) for WBC extraction or whole blood analysis, as recommended by the NCCLS (National Committee for Clinical Laboratory

Standards). Blood was mixed by inversion or left untreated in order to clot where necessary. Blood samples were stored at room temperature and processing started within 30 minutes of collection for platelet extraction or within 1hour for white blood cell extraction or whole blood use.

Citrate acts as an anticoagulant by chelating free calcium and so reducing the activity of coagulation pathway components such as platelet activation. However, its inhibitory action on platelets is reversible. Upon platelet stimulation with agonists, calcium ions get released from platelets and overcome the ionic equilibrium promoted by the citrate as a chelator. Hence, the shedding of PEV can occur. However, EDTA is a stronger calcium chelator that does not allow platelets to recover efficiently; hence platelet stimulation in EDTA-anticoagulated blood may result in lower levels of leukocyte-platelet/PEV aggregates.

2.3.2.2 Saphenous Vein Bleeds

When repeated blood collections in small volumes were required i.e. to perform haematological or biochemical tests, blood was collected through the saphenous vein on the lower leg. Mice were restrained by scruffing and placed in a 50ml falcon tube, face down. One of the back legs was hung outside of the tube and was shaved close to the foot to reveal the saphenous vein. The vein was punctured once using 26-gauge needle to cause minor bleeding. Blood droplets were collected using EDTA dipotassium salt coated or clot activator-coated Microvette® CB300 capillary tubes (Sarstedt), (for haematological tests or serum isolation respectively). Upon blood collection, the site of puncture was pressed using paper for a few seconds to stop haemorrhage.

2.4 Genotyping

2.4.1 ApoE Gene

DNA was extracted from ear tissue using the ISOLATE II Genomic kit (Bioline) according to manufacturer's instructions. DNA samples were amplified for the wild type ApoE gene and the recombinant ApoE-deficient gene by PCR (see **Table 2.1.**). The master mix was prepared using 1.1x Reddy Mix PCR Master Mix (Thermo Scientific) (see **Table 2.2.**). The amplified DNA samples (see **Table 2.3.**) were run on a 1.5% agarose gel containing SYBR Safe stain (Thermo Fisher) at 120 volts in 1x Tris-Borate-EDTA buffer (Sigma) for approximately 60 minutes. A 1 KbPlus DNA ladder (Invitrogen) was also loaded on the gel. The gel was visualized under UV light. The presence of the wild type ApoE gene was denoted by a 155-bp fragment (Primer 1 + Primer 2) and the recombinant, ApoE deficient gene by a 245-bp fragment (Primer 2 + Primer 3). Heterozygous mice were identified by exhibiting both bands (see **Fig. 2.1**).

Primer 1	5'- GCC TAG CCG AGG GAG AGC CG -3'
Primer 2	5'- TGT GAC TTG GGA GCT CTG CAG C -3'
Primer 3	5'- GCC GCC CCG ACT GCA TCT -3'

Table 2.1. The sequences of primers for WT and genetically modified ApoE gene.

Reagent	Per reaction
Reddy Mix PCR Master Mix (1.1x)	45µl
Primer 1 (10pmoles/µl)	2µl
Primer 2 (10pmoles/µl)	2µl
Primer 3 (10pmoles/µl)	2µl
DNA	5µl

Table 2.2.. The components of the PCR reaction for the ApoE gene.

95°C – 3 minutes	1 cycle
94°C – 20 seconds	35 cycles
68°C – 40 seconds	
72°C – 120 seconds	
72°C – 10 minutes	1 cycle
4°C – hold	

Table 2.3. The PCR settings for the ApoE gene.

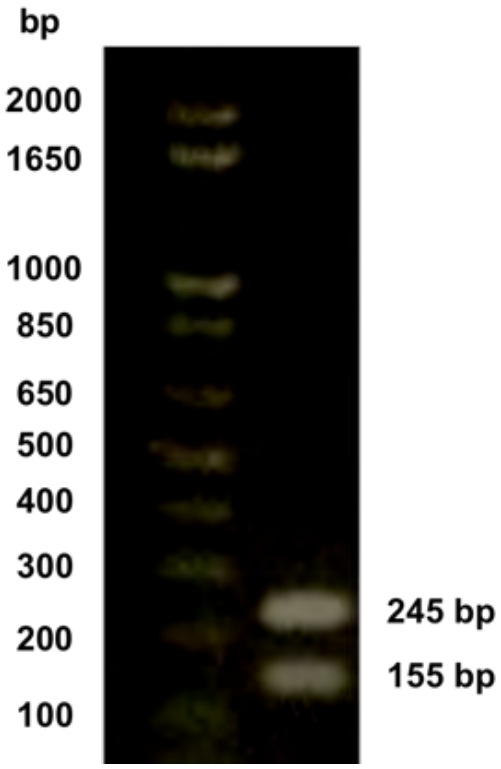

Figure 2.1. Representative gel showing ApoE WT and ApoE KO DNA bands

$ApoE^{+/-}$ animals exhibit two bands at 245bp and 155bp, $ApoE^{-/-}$ animals only exhibit the 245bp band and $ApoE^{+/+}$ animals only exhibit the 155bp band. The TrackItTM 1 Kb Plus DNA ladder is shown for band size determination.

2.4.2 hiL4Rα Gene

Presence of the hiL4Rα gene was assessed by expression of hiL4Rα protein on the platelets, as detected by FACS (Accuri C6, BD Biosciences) (see **Fig. 2.2**). Anticoagulated blood samples were diluted 10x in PBS and stained with 1:10 mouse anti-human CD124 PE/ mouse IgG1PE (BD Biosciences) for 30 minutes.

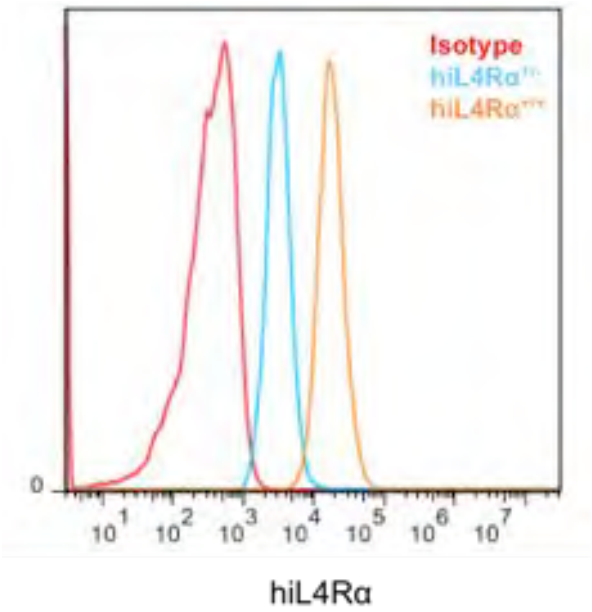

Figure 2.2. Representative FACS histogram showing hiL4Rα trace of ApoE KO-hiL4Rα/GPIbα Tg mice

hiL4Rα homozygous KI mice exhibit higher hiL4Rα fluorescence than hiL4Rα heterozygous mice.

2.5 Cell Extraction from Blood

2.5.1 Human

2.5.1.1 Platelets

Whole blood was collected in 10 % citrate-phosphate-dextrose solution with adenine (Sigma-Aldrich) and centrifuged at 250 x g for 15 minutes in the presence of 10 % Theophylline solution (60mM theophylline anhydrous, 4.8mM D-glucose anhydrous, phosphate buffered saline without Ca^{2+}/Mg^{2+}) (0.2µm pore-filtered) (Sigma-Aldrich), in order to prevent phosphodiesterase-mediated breakdown of cAMP into AMP and thereby platelet activation (Moake et al., 1977; Feinstein et al., 1975; Salzman et al., 1972; Mills and Smith, 1971). Platelet-rich plasma was collected and washed in Theophylline-Albumin solution (6mM theophylline anhydrous, 0.48mM D-glucose anhydrous, 0.15 % bovine albumin fraction V solution, phosphate buffered saline

without Ca^{2+}/Mg^{2+}) (0.2 µm pore-filtered) by centrifugation at 800 x g for 15 minutes. The pellet containing platelets was resuspended in 100 µl of Theophylline-Albumin solution per 5 ml of whole blood.

2.5.1.2 Monocytes

Blood was collected in 1.6 mg/ml ethylenediaminetetraacetic acid (EDTA)-coated tubes (Sarstedt). In order to separate the different components of the blood, 2.5 ml of Histopaque 1199 (Sigma) was added to 10 ml tubes, 2.5 ml of Histopaque 1077 (Sigma) was layered on top of Histopaque 1199. Following addition of 5 ml anti-coagulated blood, the tubes were centrifuged for 30 minutes at 700 x g. The top cloudy layer between the plasma and the Histopaque 1199, that contains the mononuclear cells (PBMCs), was collected using a Pasteur pipette and transferred to a fresh falcon tube. The cells were washed twice in 10 ml MACS buffer (2 mM EDTA-Sigma, 0.5 % bovine albumin fraction V from ThermoFisher Scientific in PBS) at 400 x g for 6 minutes. The cells were pelleted and resuspended in 80 µl MACS buffer per 1 x 10^7 cells. 20 µl of CD14 magnetic microbeads were added and the cells were incubated on ice for 20 minutes. The suspension was washed in MACS buffer by centrifugation at 400 x g for 6 minutes. Pellet was resuspended in 500 µl MACS buffer. Suspensions were passed through an MS column (Miltenyi Biotec) that was attached to a MiniMACS magnetic separator (Miltenyi Biotec). The flow-through was discarded and the column was washed twice in 500 µl MACS buffer. The column was removed from the magnetic separator, 1 ml of MACS buffer was added and the fluid was forced through the column using the column plunger into an eppendorf tube to collect the purified monocytes.

2.5.2 Mouse

2.5.2.1 Platelets

Whole blood was collected in 10 % citrate-phosphate-dextrose solution with adenine (Sigma-Aldrich) and centrifuged at 150 x g for 6 minutes in the presence of 10 % Theophylline solution (60mM theophylline anhydrous, 4.8mM D-glucose anhydrous, phosphate buffered saline without Ca^{2+}/Mg^{2+}) (0.2µm pore-filtered) (Sigma-Aldrich). Platelet-rich plasma and the top half of the red blood cell layer was transferred to a fresh eppendorf. 0.150 ml of Theophylline solution was added to the remaining red blood cell layer and 100 µl of Theophylline solution was added to the tube containing platelet-rich plasma (PRP) and the top half of the red blood cell layer and resuspended. Both tubes were centrifuged at 200 x g for 6 minutes. PRP was collected from both tubes and pooled together in fresh eppendorf. PRP was centrifuged at 1000 x g for 6 minutes to pellet platelets. Supernatant was removed and the platelets were resuspended in required medium.

2.6 PEV Generation and Detection

2.6.1 Human and Mouse PEV Generation

3 x 10^8 platelets were resuspended in 1ml PBS-Albumin solution (0.15% bovine albumin fraction V solution, phosphate buffered saline with Ca2+/Mg2+) (0.2µm pore-filtered) and stimulated with 1 µg/ml (for human) or 10 µg/ml (for mouse) CRP-XL (Prof. Farndale Group, Department of Biochemistry, University of Cambridge) or 0.5 U /ml thrombin (Sigma) at 37 ˚C for 30 minutes to generate extracellular vesicles. Samples were spun at 2000 x g for 20 minutes to pellet platelets. The supernatants containing the vesicles were transferred in fresh tubes leaving behind ~100 µl in order to prevent contamination with the platelet pellet and were further spun at 13 000 x g

for 2 minutes to pellet any platelet remnants. The supernatants containing pure vesicles were transferred to fresh tubes leaving behind ~100 µl in order to prevent contamination with the pellet.

2.6.2 PEV Detection

Samples were run on a BD Accuri C6 flow cytometer to assess successful generation, contamination with platelets and staining levels. Threshold levels were set at 6700 for the forward scatter and 7500 for the side scatter in order to eliminate noise. APC, Mitotracker deep red and PKH26 staining were observed in channel FL4. FITC and PKH67 staining were observed in the FL1 channel. PEV gating was determined by running microspheres of < 1 µm in size and is shown in **Fig. 2.3**.

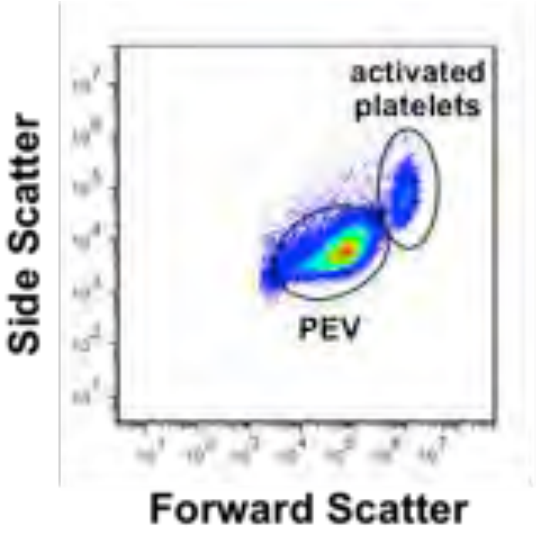

Figure 2.3. Gating strategy for detecting PEV

Platelet gating is determined by size and granularity. The PEV gate was determined by running microspheres of < 1 µm in size and exhibits smaller size and lower granularity than activated platelets.

2.7 Cell and Particle Counting

2.7.1 Platelets

The number of human or mouse purified platelets was counted using a Beckman Coulter Z2 cell and particle counter according to manufacturer's instructions. Briefly, the counter was washed in ISOTON II Diluent (Beckman Coulter). The platelet

suspension was diluted by a factor of 20 in ISOTON II Diluent in Beckman Coulter counter cuvettes.

2.7.2 PBMC and Monocytes

PBMCs and monocytes were counted using a Nexcelom Cellometer K2 Image Cytometer according to manufacturer's instructions. Briefly, PBMC suspension (PBMC suspended in 1ml MACS buffer) was diluted by a factor of 20 in MACS buffer, whereas monocyte suspension (monocytes suspended in 100µl MACS buffer) was diluted by a factor of 10. 20µl of the diluted cells were injected in a Nexcelom Cellometer K2 slide and placed in the machine. The image was focused manually.

2.7.3 PEV

The concentration and size distribution of PEV (including both PMV and platelet exosomes) were determined by nanoparticle tracking analysis that can detect particles from as small as 10 nm, using a Nanosight NS300 (Malvern Panalytical) (Pikramenou group, Chemistry Department, University of Birmingham) using NTA software 3.0. Diluted samples (1:50 in 0.2 µm pore-filtered milli Q water) were loaded into the counting chamber manually using 1ml plastic syringes. milli Q water was further loaded through the syringe pump to ensure sample flow during imaging. Focus was set manually. Data acquisition was undertaken at ambient temperature (23.1 – 23.5°C). Settings for data acquisition were: detect threshold 50, 15 runs, FPS 25.0, automatic camera level/ slider shutter/ slider gain, blur size/ max jump distance, viscosity 0.9. The chamber was washed with 70% ethanol in between samples. Samples were measured three times each.

2.7.4 Mouse Whole Blood

Diluted mouse peripheral blood was analysed for total cell counts and haematological parameters using the Pentra 60 haematocytometer (ABX Diagnostics).

2.8 Staining of Washed Platelets

2.8.1 Antibodies

3 x 10^8 platelets were resuspended in 100µl of Theophylline-Albumin solution (6mM theophylline anhydrous, 0.48mM D-glucose anhydrous, 0.15 % bovine albumin fraction V solution, phosphate buffered saline without Ca^{2+}/Mg^{2+}) (0.2 µm pore-filtered) and stained with APC anti-CD42b (GPIbα) antibody (BioLegend) (1:6); APC isotype (BioLegend) (1:6); FITC anti-CD41a (GPIIb) (Dako) (1:10); FITC isotype (Dako) (1:10) by 30-minute incubation at 4 ˚C in the dark. Following incubation stained platelets were washed in Theophylline-Albumin solution to remove excess antibody.

2.8.2 Dyes

The membrane of the platelets was stained using the PKH67 Green Fluorescent Cell Linker Kit (Sigma-Aldrich) or the PKH26 Red Fluorescent Cell Linker Kit (Sigma-Aldrich) as follows: Platelet pellets containing 3 x 10^8 platelets each, were resuspended in 750 µl Diluent C. In a fresh tube 15 µl of dye was diluted in 750 µl of Diluent C. The dye solution was added to the cell solution and left to incubate at RT in the dark for 5 minutes with periodic mixing. An equal volume of 1.5 % Bovine Albumin Fraction V solution (7.5 %, Life Technologies) in diluted theophylline solution was added to the stained cells and left to incubate for 1 minute to neutralize free dye. Cells were then washed by centrifugation at 800 x g for 10 minutes at 20-25 ˚C. The pellet was rewashed twice in 10 ml of the same solution.

Platelets were alternatively stained with MitoTracker Deep Red, Orange, or Green to label their mitochondria as follows: 3 x 10^8 platelets were resuspended in 1 ml Theophylline-Albumin solution and stained with 0.2 µM / ml MitoTracker for 15 minutes at RT in the dark. Platelets were washed twice to remove excess dye.

Double staining of platelets for their mitochondria and membrane was achieved by consecutive staining. Platelets were first stained using MitoTracker dye and then with PKH- dye as indicated above.

2.9 *In vitro* Leukocyte-PEV Aggregation Assays

2.9.1 Aggregation between Leukocytes and PEV in Whole Blood

CPDA-anticoagulated whole blood was treated with 1µg/ml CRP-XL or 100nM TRAP (Alta Bioscience, Birmingham, UK) and incubated at 37˚ on a roller mixer to apply low shear stress in order to mimic the flow conditions in the circulation. Alternatively, CPDA-anticoagulated whole blood was treated with purified and stained PEV prepared in advance and incubated at 37˚ on a roller mixer.

At the end of incubation, samples were fixed in 1 % formaldehyde solution (Sigma) at RT for 10 minutes. Following fixation, cells were washed in Dulbeco's phosphate buffered saline (PBS) (Sigma) without Ca^{2+}/Mg^{2+} by centrifugation at 400 x g for 5 minutes. Pellet was resuspended in 200 µl PBS and cells were stained with FITC anti-CD16; FITC isotype antibody (1:50) (BioLegend) or PE-Cy7 anti-CD16; PE-Cy7 isotype (1:50) (eBioscience) and PE anti-CD14; PE isotype (1:100) (ImmunoTools) by 30-minute incubation at 4˚C. Following staining, cells were washed in PBS by centrifugation to remove excess antibody. Pellets were resuspended in ACK Lysing buffer (Life Technologies) and left to incubate at RT for 10 minutes in order to lyse red

blood cells. Lysing buffer was neutralised in 10 x by volume PBS and samples were centrifuged to remove lysed red blood cells. Pellets were resuspended in 300 µl PBS, transferred into FACS (fluorescence-activated cell sorting) tubes and stored in the fridge until analysis by flow cytometry.

2.9.2 PEV Aggregation with Washed Monocytes and Internalisation

1 x 10^6 unstained monocytes were incubated with unstained PEV generated from 3 x 10^8 platelets at 37˚C on a roller mixer to impose low shear for 30 minutes or for a 60-minute time course. For endocytosis investigations, monocytes were pre-treated with various endocytosis inhibitors; 10µM Cytochalasin D (Sigma-Aldrich), 100 µM Ly294002 (Abcam), 200µM EIPA (Sigma-Aldrich) or 80 µg/ml Dynasore (Abcam) diluted in DMSO for 30 minutes before introducing PEV. For mitochondria transfer studies, monocytes unstained or MitoTracker-stained were incubated with MitoTracker-stained PEV/platelets or PEV/platelet filtrate (filtration through 0.2µm pore filters). Following incubation, free PEV were removed by centrifugation at 400 x g for 5 minutes.

To prepare for flow cytometry analysis, pelleted monocytes were resuspended in 100 µl MACS buffer and stained with anti-GPIbα-APC or APC isotype (1:10), anti-CD14-PE (1:50), anti-CD16-FITC (1:50) or with anti-GPIIb-FITC isotype (1:10), anti-CD14-PE, anti-CD16-PE-Cy7 (1:50) by incubation at 4˚C for 30 minutes where required (antibody concentrations were determined by dose-response experiments). Alternatively, for PEV internalisation investigation, half of the monocytes pre-incubated with PEV were a) first stained with anti-GPIbα antibody for 30 minutes and then fixed and permeabilised using the Foxp3 kit (eBioscience) according to manufacturer's instructions (to stain only surface PEV), and the rest monocytes were b) first fixed and permeabilised and secondly stained with anti-GPIbα antibody (to stain both surface and internalized PEV).

Lastly, washed cells were resuspended in 300 µl PBS, transferred into FACS tubes and saved in the fridge until analysis by flow cytometry.

2.9.3 Detection of Aggregates by Flow Cytometry

Samples were run on a Dako CYAN ADP flow cytometer (acquisition parameters are listed in **Table 2.5**). PKH67 staining was observed in the FITC channel and Mitotracker deep red was observed in the APC channel. Since PEV are at least 10-50 times smaller than leukocytes, any PEV bound to leukocytes cannot be distinguished as individual entities, separate from leukocytes, hence the machine records any aggregates as being leukocytes (based on forward versus side scatter). In brief, leukocyte-PEV aggregates are identified as the leukocytes (identified by size/granularity/expression of leukocyte markers) that also express PEV markers. (Gating strategy adapted from Shantsila et al., 2011). The software FlowJo version 7.6 was used to analyse flow cytometry data.

Name	Voltage	Gain
Forward Scatter	N/A	6.5
Side Scatter	490	1.4
FITC	530	1.0
PE	560	1.0
PE-Cy7	820	1.0
APC	830	1.0

Table 2.4. Acquisition Parameters set on the CYAN ADP flow cytometer

2.9.3.1 Gating Strategy for Monocyte-platelet/ PEV Aggregates

The monocyte population is defined by CD14 expression and granularity. The two main monocyte subsets are differentiated by expression levels of CD14 and CD16: high expression of CD14 and no expression of CD16 define CD14+veCD16-ve monocytes

whereas high CD16 expression and variable expression of CD14 defines CD14+veCD16+ve monocytes (see **Figure 2.2.**). CD14+veCD16-ve monocytes-PEV aggregates are defined by having high expression of CD14, no expression of CD16 and express a platelet/ PEV marker. CD14+veCD16+ve monocyte-PEV aggregates are defined by having high CD16 expression and also express platelet/ PEV markers (see figure 2.1).

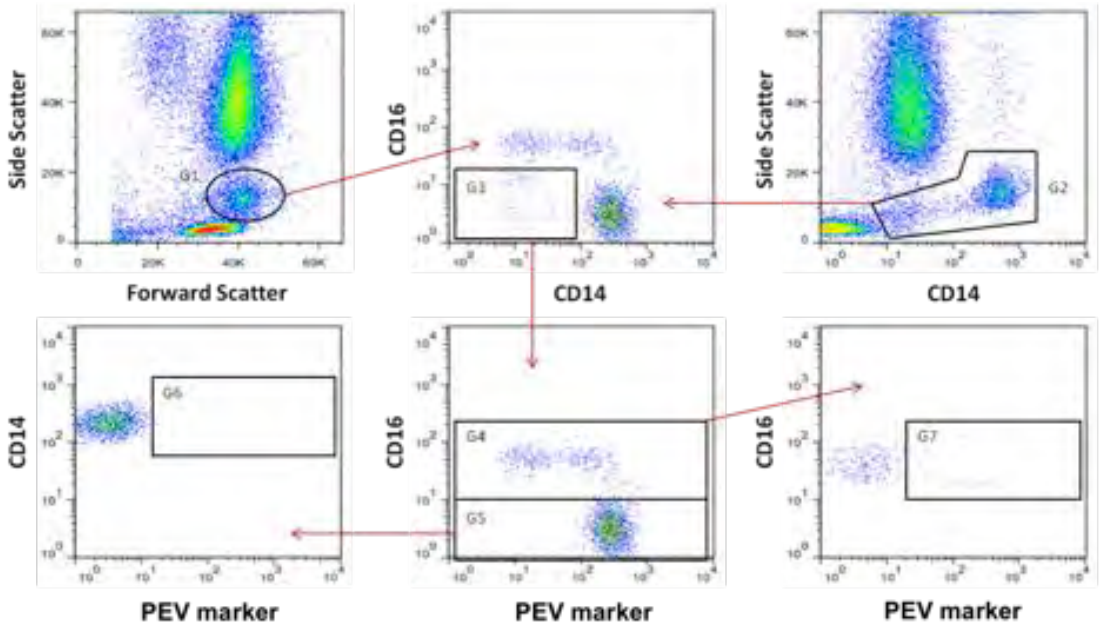

Figure 2.4. Gating strategy for detecting monocyte-platelet/ PEV aggregates

The monocyte population is defined by size and granularity (gate #1) and by CD14 expression (gate #2). Gates #1 and #2 are then applied to a CD14 versus CD16 plot. A gate (#3) is set to remove any events low for both CD14 and CD16. The new plot is then used to split the population into two subsets. Gate #4 is set to include only cells that express high levels of CD16, representing the CD14+CD16+ subset. Gate #5 is set to include only cells that express high levels of CD14 and low levels of CD16, representing the CD14+CD16- subset. Then gate #6 is applied to a PEV marker plot and double expression of the two markers defines a CD14+CD16+monocyte-platelet/PEV aggregate. Similarly, gate #4 is applied to a PEV marker plot and double expression of the two markers defines a CD14+CD16-monocyte-PEV aggregate (gate #7).

2.9.3.2 Gating Strategy for Lymphocyte-PEV Aggregates

The lymphocyte population is defined by size and granularity. Lymphocyte-PEV aggregates are defined by having the lymphocyte size and granularity and also being positive for platelet/ PEV markers (see **Figure 2.3**.).

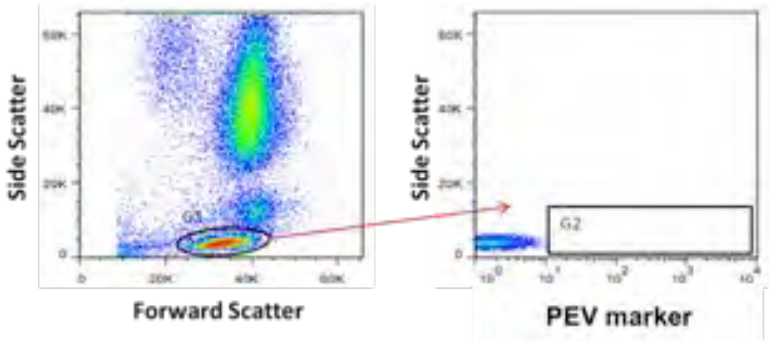

Figure 2.5. Gating strategy for detecting lymphocyte-PEV aggregates
The lymphocyte population is defined by size and granularity (gate#1). Gate #1 is then applied to a platelet/ PEV marker versus Side Scatter plot and any events that fall in gate#2 exhibiting expression of a PEV marker are defined as lymphocyte-platelet/ PEV markers.

2.9.3.3 Gating Strategy for Neutrophil-PEV Aggregates

The neutrophil population is defined by size, granularity and CD16 expression. Neutrophil-platelet/ PEV aggregates are defined by size, granularity and CD16 expression and positivity for a platelet/ PEV marker (see **Figure 2.4**).

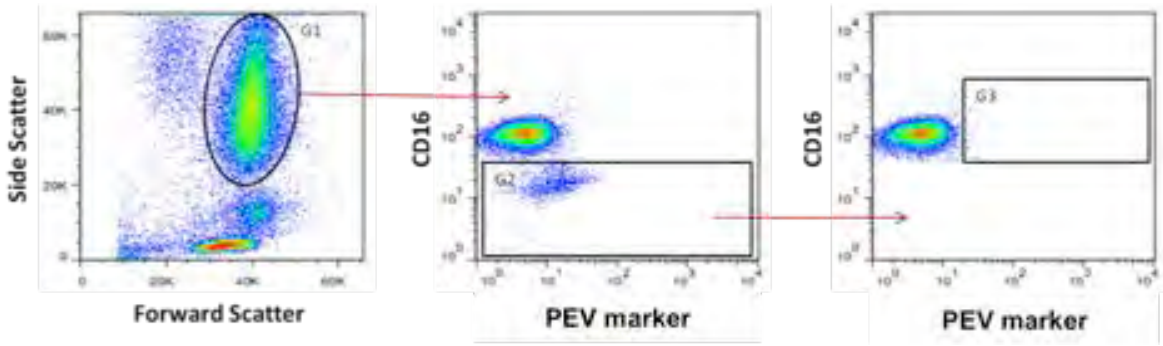

Figure 2.6. Gating strategy for detecting neutrophil-platelet/ PEV aggregates

The neutrophil population is defined by size and granularity (gate#1). Gate #1 is then applied to a PEV marker versus CD16 plot. A gate (#2) is set to remove any events low for both CD14 and CD16. A gate (#3) is set in the new plot to include any events that are both high in CD16 expression and positive for the platelet/ PEV marker that defines the neutrophil-platelet/ PEV aggregates.

2.9.4 Detection of Aggregates by Microscopy

Pelleted monocyte-platelet extracellular vesicle aggregates were resuspended in medium 199, no phenol red (Thermo Fisher Scientific). 1.5 x 10^5 monocytes were plated on glass microwell plates (MatTek Corporation) that were coated in advance with poly-l-lysine solution (Sigma) for 5 minutes at RT, washed with tissue culture grade water and left to dry for 2-3 hours before introducing cells and medium. Alternatively, 1.5 x 10^5 monocytes were plated in 8-well µ-slides T/C treated (Thistle Scientific). Plated cells were incubated at 37°C for 30 minutes or as indicated in a CO_2 incubator (NU-5510, NuAire). The cells were then fixed in 2% formaldehyde solution (Sigma) for 10 minutes. Following fixation, the culture surface was blocked with Bovine Albumin Fraction V solution 6.7% (Thermo Fisher Scientific), 10% goat serum (Sigma-Aldrich) and FcR blocking reagent (1:100, Miltenyi Biotec) for 30 minutes. The culture surface was washed with Dulbeco's phosphate buffered saline (Sigma). Cells were incubated with anti-CD14-alexa fluor 647 (1:200, abcam) or rabbit anti-LAMP-1 (1:50) (abcam), and either GPIb alpha/ IgG1 isotype-alexa fluor 488 (1:200, Novus Biologicals) for 1

hour at 4°C. Wells were washed in Dulbeco's phosphate buffered saline and further stained with goat anti-rabbit-alexa fluor 647 (secondary antibody for LAMP-1) for 1 hour. Wells were washed in PBS and saved at 4°C in Vectashield antifade mounting medium with DAPI (Vector Laboratories) until imaging.

Alternatively, cells were stained live with MitoTracker Deep Red (1:10000)/Orange (1:5000)/Green (1:1000) and washed extensively before plating.

Fixed monocyte-PEV aggregates (and monocyte-platelet/filtrate incubates) were imaged by confocal microscopy, either using an N-Storm Super Resolution Microscope (Nikon) or an Axioscan 780 (Zeiss). Z-stacks of 0.2μm depth (in all colour channels) were produced spanning the whole monocytes from top surface to bottom surface using the 100x lens.

Live mitotracker-stained monocytes were imaged in real time by STORM (Stochastic Optical Reconstruction Microscopy) using a Nikon N-Storm Super Resolution Microscope. The same monocytes were imaged every second for 50 seconds using a 100x lens at approximately the middle depth inside the cells to determine mitochondria motion.

2.9.4.1 Image Processing

Fluorescent images produced by confocal microscopy were processed using the ImageJ/FIJI software. Z-stacks produced, were used to create composite images (max projection for GPIb, DAPI, PKH67, PKH26, LAMP1 and MitoTracker and average projection for CD14) to show the total PEV signal by individual monocytes. Automatic background subtraction was performed. The mean PEV fluorescence intensity was measured individually for each monocyte from the composite images.

The path of individual mitochondria in monocytes was tracked over the course of 50 seconds using the Trackmate plugin on FIJI software and a projection image was created with all individual trajectories .

2.10 Murine Tissue Preparation and Histochemistry

Peripheral blood was removed by cardiac puncture as previously described and mice were culled by intra-peritoneal injection of euthatal. 20 ml of PBS was injected in the left ventricle of the heart in order to wash organs post mordem. Aorta, heart, lungs, liver, kidneys, stomach and intestine were extracted and weighed.

2.10.1 Aortas

Mouse aortas were fixed in 2 % PFA for 10 minutes and washed in PBS. They were stained with Oil Red O according to manufacturer's guidelines in order to remove external fat and connective tissue. Aortas were cut longitudinally and re-stained with Oil Red O to stain atheromatous plaques. Aortas were mounted flat using double-sided sticky tape onto slides and imaged using a digital camera (Canon EOS) using the P-mode. Photoshop was used to select aorta from the background. Percentage of plaque coverage was measured on ImageJ by auto threshold analysis.

2.10.2 Livers

Mouse livers were fixed in 2 % PFA immediately upon extraction. They were embedded in paraffin and sectioned using a microtome. Sections were stained with haematoxylin & eosin and imaged by brightfield microscopy using an AxioScan microscope (Zeiss) using a 20x lens.

2.11 Serum Lipid Measurements

Peripheral blood was left untreated at room temperature for 2-4 hours to clot. Clotted blood was centrifuged at 15 000 x g for 10 min to collect serum. Serum was stored at -20°C. Serum triglycerides (Randox), total cholesterol, high-density lipoprotein and low-density lipoprotein were determined by colourimetric assays according to manufacturer's guidelines.

2.12 Platelet Depletion

Endogenous platelets in the ApoE$^{-/-}$ hiL4R/GPIbα-Tg$^{+/+}$ mouse were depleted by intra-venous injection of 2.5 μg or 5μg / g body weight of anti-hiL4Rα (R & D Systems).

2.13 Intravital Microscopy in the Mouse

2.13.1 Mice Preparation and Surgical Procedure

ApoE-/- mice were fed a high fat diet for six weeks from 10 weeks of age. Mice were then anaesthetized by intra-peritoneal injection with 10 μl / g body weight of medetomidine-ketamine. The upper front side of the mice was shaved. The shaved area was disinfected using chlorhexidine (Sigma-Aldrich). The mice were placed on a heated mat with their chest facing upwards. An incision was made on top of the throat area to expose the trachea. The membrane tissue around the trachea was cleared away. The trachea was cannulated to aid mouse breathing. The left common carotid artery was then exposed and detached from surrounding tissue. The left common carotid artery was then cannulated and the cannula was used to attach a syringe for cell injection into the circulation. The right common carotid artery was then exposed and the cleared from surrounding fat close to the bifurcation site. A small piece of thin black nylon plastic was placed underneath the artery.

2.13.2 Preparation of Cells to be Injected

PEV were generated from 3 x 10^8 purified mouse platelets as described in section 2.6.1., and were incubated with 1.5 x 10^6 human monocytes for 30 minutes at 37°C. The cells were stained with 25μM cell tracker orange (Thermo Fisher Scientific) during the incubation with PEV. Stained monocytes were spun twice at 400 x g for 6 minutes to remove free dye and free PEV. Pelleted monocytes were resuspended in 500μl PBS-Albumin solution (0.15% bovine albumin fraction V solution, phosphate buffered saline with Ca^{2+}/Mg^{2+}) and kept on ice until injection. Stained monocytes without PEV were injected as a control.

2.13.3 Imaging and Imaging Analysis

Interaction of injected cells with the vessel wall was monitored by fluorescent video-microscopy using an Olympus BX61WI Upright Confocal microscope in the 561 channel using a 4x objective in the right common carotid artery at the athero-prone fork site for six minutes following cell introduction. The number of stable and unstable monocyte adhesion was manually counted using the Slidebook 6 Reader Software. The speed and the duration of the adhesion interactions were also calculated manually using data from the Slidebook 6 Reader Software. Briefly, rolling velocity was calculated by dividing the measured distance travelled by each cell (cell trace) as seen on a single frame by the time during which the imaging of one frame lasts.

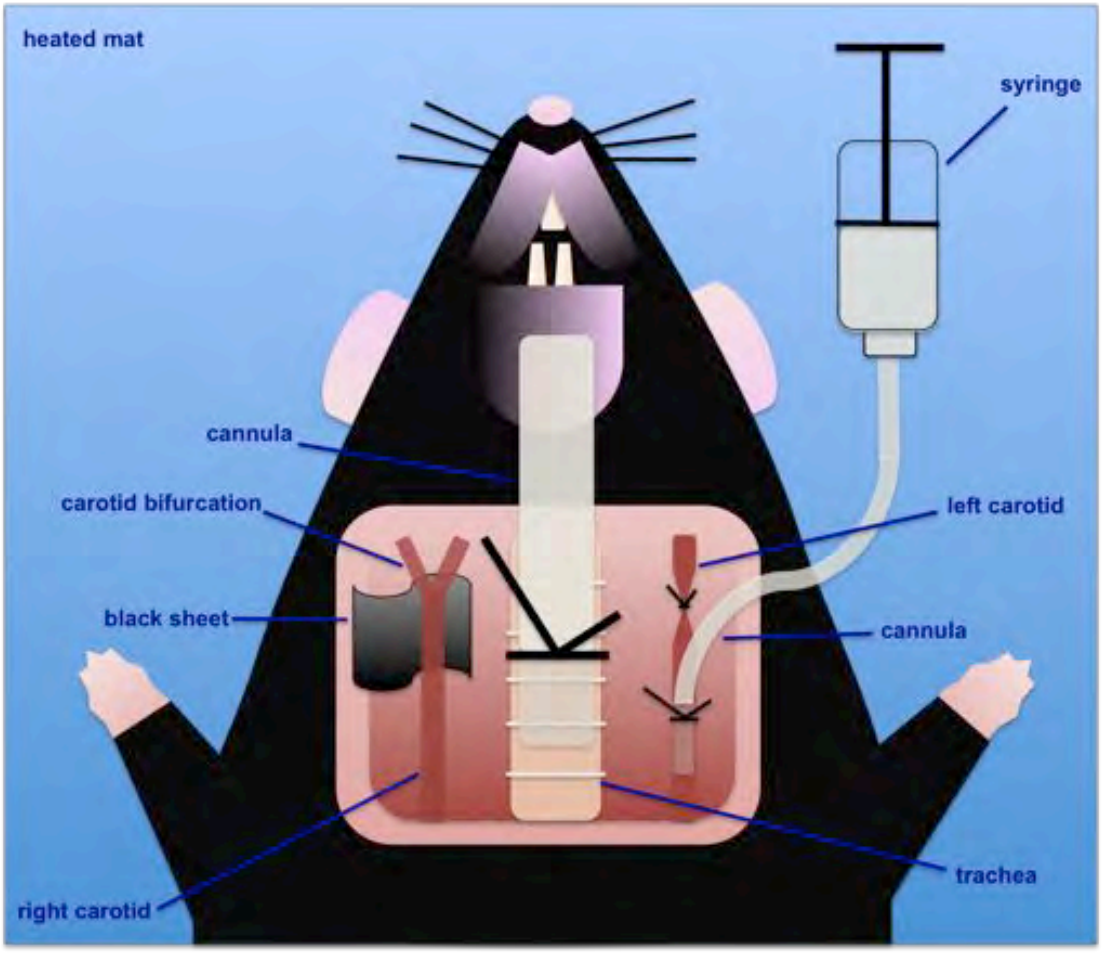

Figure 2.5. Mouse surgical preparation for injecting cells in the left carotid artery and imaging interactions in the right carotid artery

2.14 Graphical and Statistical Analysis

Graphical and statistical analysis was performed using the software GraphPad Prism 4. Data are shown as mean +/- standard error of the mean. The tests used for each experiment and their outcomes are detailed in the figure legends and the text of the results sections of individual chapters.

3 CHARACTERISATION OF INDUCED PEV

3.1 Introduction

Platelets release PEV upon activation. Physiological platelet activation occurs upon vascular injury, when platelets attach to the exposed extracellular matrix. The most thrombogenic component of the exposed extracellular matrix is collagen (Baumgartner and Haudenschild, 1972). Collagen, apart from acting as a substrate for platelet adhesion, also induces platelet activation (Cowan et al., 1981; Morton et al., 1989; Poole and Watson, 1995). There are two platelet receptors that interact with collagen; firstly collagen binds integrin $\alpha_2\beta_1$ to anchor platelets on collagen, then enabling binding to the lower affinity receptor glycoprotein VI (GPVI) that induces the activation of platelets (Morton et al., 1989; Santoro et al., 1991).

Activated platelets then release soluble agonists that induce activation of new platelets. Released thrombin activates platelets by binding and cleaving protease-activated receptors PAR-1 and PAR-4. There is some evidence to suggest that cleavage of PAR-1 by thrombin is facilitated by the adherence of thrombin to receptor GPIbα of the GPIb/IX/V complex (Brass, 2003). Adenine di-Phosphate (ADP) from the dense granules of platelets binds to purinergic receptors $P2Y_1$ and $P2Y_{12,}$ and the lipid mediator thromboxane A2 (TxA_2) binds to TxA_2 receptor (TP), both contribute to further platelet activation (George, 2000; Grette, 1962; Zucker and Borrelli, 1962; Hovig, 1963; Hugues and Lapiere, 1964; Mills et al., 1968; Murugappan et al., 2004). Circulating epinephrine also contributes to platelet activation through the 2A-adrenergic receptor ($\alpha 2_A$) (Lanza et al., 1988) (**Fig. 3.1.**).

In addition to these physiological agonists, synthetic peptides such as thrombin receptor-activating peptide (TRAP) and cross-linked collagen-related peptide (CRP-XL)

that mimic thrombin and collagen respectively are also used to induce platelet activation *in vitro*.

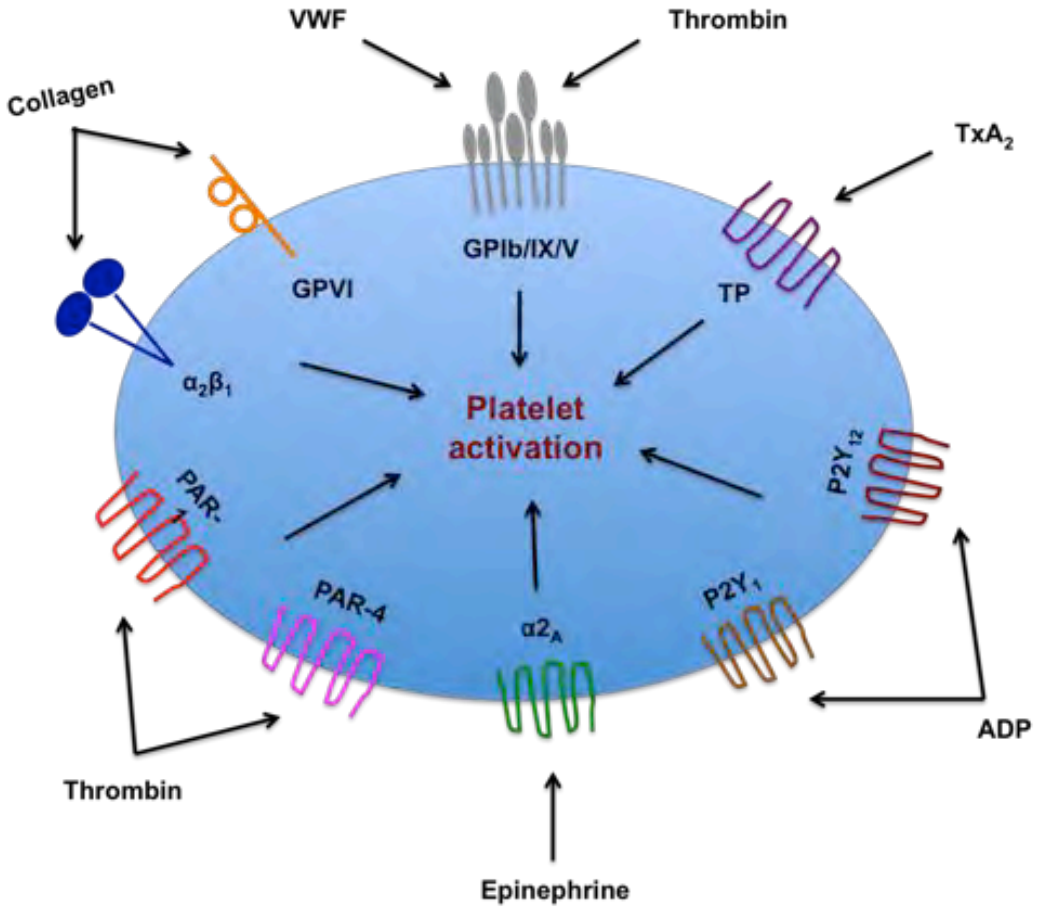

Figure 3.1. Major platelet receptor-ligand interactions leading to primary or secondary cell activation

The number of PEV released from platelets and their protein concentration depend on the platelet activation pathway (Aatonen et al., 2014). In terms of size, the large majority of PEV (90%) are smaller than 500 nm (Arraud et al., 2014; Yuana et al., 2010; Gabriel et al., 2010; Aatonen et al., 2014).

Depending on the platelet activation pathway involved, PEV carry different assemblages of proteins. These are known to be involved in various cellular responses, to have different molecular functions and to be located at distinct sites within the platelet

(Garcia et al., 2005). PEV express more than 40 platelet membrane surface receptors such as glycoproteins GPIb (CD42), GPIIb (CD41), GPIIIa, GPIV (CD36), GPV (CD42d), GPIX (CD42a) and P-selectin (CD62) (Garcia et al., 2005). The identity of the proteins found in PMV or platelet-derived exosomes is largely distinct, with only 28% of PMV proteins and 45% of platelet exosomal proteins in common (Aatonen et al., 2014).

The aims for this chapter were to:

1) Investigate the potential of different agonists to induce the *in vitro* formation of PEV by platelets.
2) Assess purity of PEV and optimise purification technique .
3) Assess PEV detection techniques.
4) Identify different PEV components that can serve as PEV markers.

3.2 Methodology

Platelets were isolated from CPDA-anticoagulated blood and were stimulated with different agonists (1 μg/ml CRP-XL and 0.5 U/ml thrombin) in the presence of Ca_{2+} for 30 minutes at 37˚C to induce the formation and release of PEV. Prior to generation of PEV, platelets were labelled with antibodies against GPIbα or GPIIb coupled to fluorescent probes or with appropriate isotype controls, or with the lipophilic dye PKH67 (cell membrane dye), or were left unstained. PEV were purified by two-step sequential centrifugation; 2000 x g for 20 minutes followed by 13000 x g for 2 minutes to pellet and remove platelets. PEV were stained at the platelet stage instead at after platelet stimulation in order to avoid using an ultracentrifugation wash step to pellet PEV, as this would result in PEV loss from incomplete sedimentation and aggregation in the pellet (Weber and Clayton, 2013). PEV were quantified and characterized by FACS

(Accuri C6) and Nanoparticle tracking analysis (NanoSight). Statistical analysis was performed using Graph Pad Prism 6. (For further detail see methods section 2).

3.3 Results

Our first aim was to induce EV formation and release from platelets, to purify the resulting PEV suspension and to characterize them in terms of numbers, size, granularity and molecular and lipid composition. Two potent platelet agonists that act in different ways were used to activate platelets; CRP-XL that binds and activates through GPVI, and thrombin that binds and cleaves PAR receptors. Both agonists were used at a concentration known to induce robust, but not excessive platelet activation; 1 μg/ml CRP-XL and 0.5 U/ml thrombin. Upon stimulation, PEV were purified by double centrifugation and the supernatant was analysed on a flow cytometer (Accuri C6) and a nanoparticle tracking analyser (NanoSight).

Both agonists were capable of inducing platelets to shed EV. The number of PEV generated in response to CRP-XL stimulation or with thrombin stimulation using flow cytometric quantification was not significantly different; therefore both agonists generated the same number of PEV (**Fig. 3.2A**). Next, we compared the number of PEV formed from CRP-XL stimulation, as detected by flow cytometry versus nanoparticle tracking analysis quantification. The number of PEV detected by FACS was significantly smaller than the number of PEV detected by NanoSight (**Fig. 3.2B**). Specifically, the number of particles detected by NanoSight was >1000 times greater than the number of particles detected by Accuri.

In order to determine whether PEV were effectively purified by the double centrifugation, stimulated platelets were run on the flow cytometer before and after

centrifugation and the percentage of events in the platelet gate was recorded (**Fig. 3.3A**). Double centrifugation significantly reduced the number of platelets in the PEV suspension. Upon stimulation, there is almost 10% contamination with platelets in the PEV suspension. This number falls below 1% upon double centrifugation (**Fig. 3.3B**).

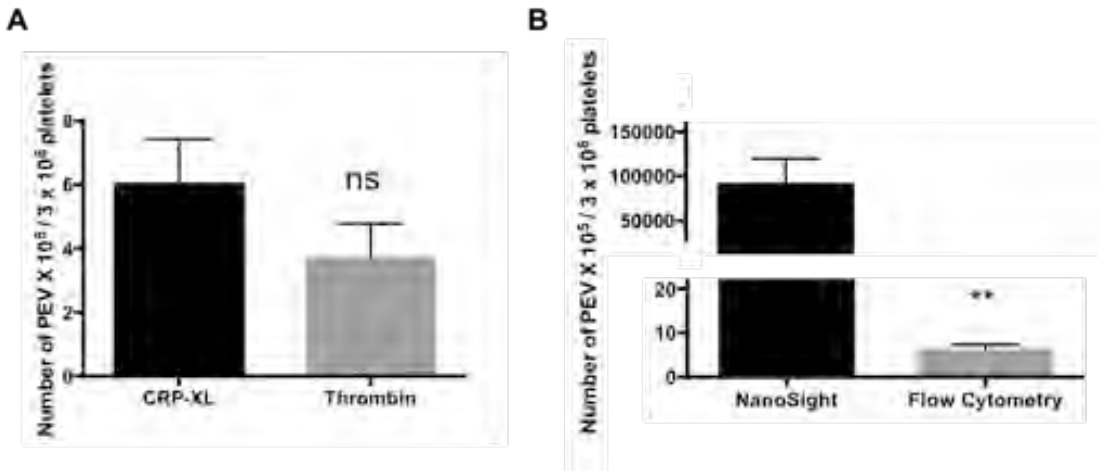

Figure 3.2. PEV Quantification

(A) Number of PEV produced from 3 x 10^8 platelets stimulated with CRP-XL or thrombin, as quantified by flow cytometry. Data are represented as mean +/- SEM of 3-10 experiments. **(B)** Number of PEV produced from 3 x 10^8 platelets stimulated with CRP-XL, quantified by flow cytometry or nanoparticle tracking analysis. Data are represented as mean +/- SEM of 3-10 experiments. **(**All data were analysed by unpaired t-test. * indicates $P<0.05$, ** indicates $P<0.01$.

Having generated PEV successfully and quantified them, the next objective was to determine their size and granularity characteristics. Unpurified PEV (with platelet contamination) were analysed by flow cytometry and the trace of forward scatter (a measure of size), as well as the side scatter (a measure of granularity) were observed. The forward scatter histogram (ungated) indicated the presence of two distinct populations as evident by the presence of two distinct peaks (**Fig. 3.4A**). The two peaks corresponded to the platelet and PEV gate (not shown). The platelet peak was narrower than the PEV peak, showing that the size of platelets was less variable than the size of

PEV. Upon quantification, PEV were found to be significantly smaller than platelets, specifically >10 times smaller based on forward scatter measurements (**Fig. 3.4B**). Hence, PEV and platelets do not form a continuum of size, but they are two distinct entities in terms of size.

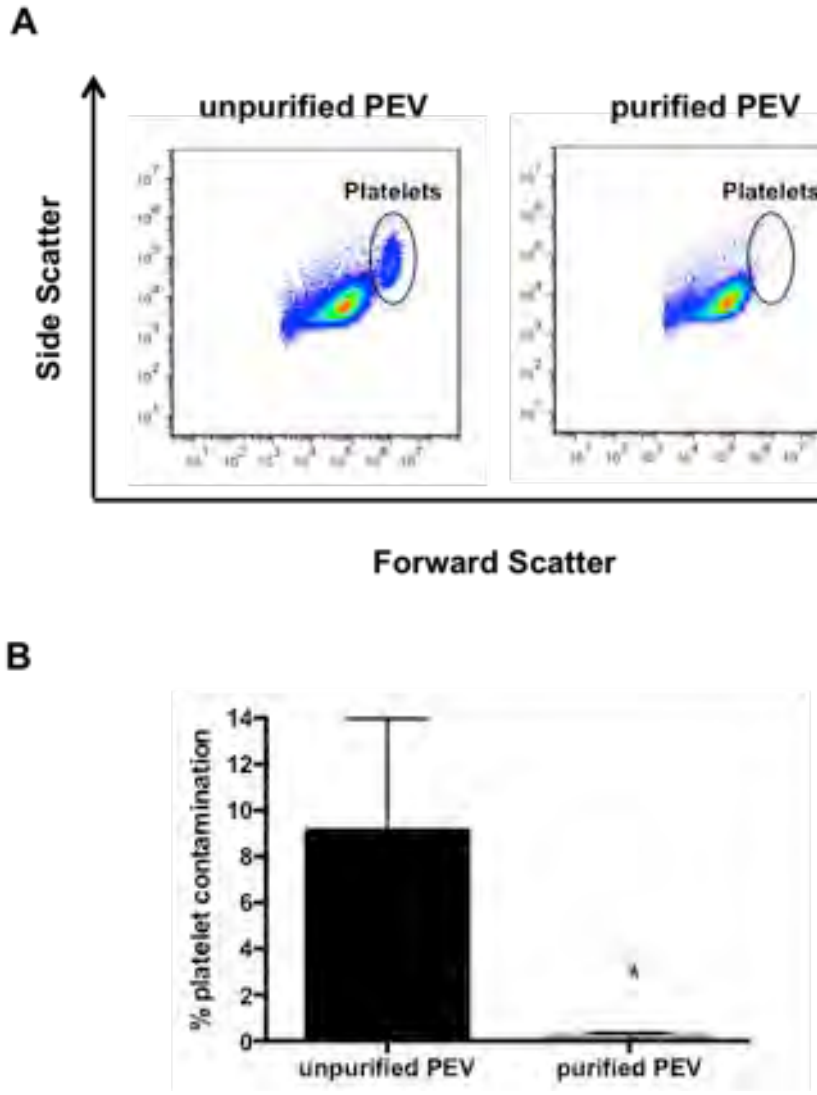

Figure 3.3. PEV Purification

(A) Representative FACS dot-plots showing the number of events in a platelet gate before and after purification of PEV by centrifugation. **(B)** Contamination of PEV with platelets before vs after purification of PEV by centrifugation. Data are represented as mean +/- SEM of 5-8 experiments. Data were analysed by t-test. * indicates $P<0.05$, ** indicates $P<0.01$.

PEV were also analysed on a NanoSight in order to get real size measurements in non-arbitrary units. The size distribution profile of a representative PEV sample was automatically produced by the NTA software version NTA 3.0 0068 and is shown in **Fig. 3.4C**. The diameter of PEV spans from 0-650nm. Four peaks can be seen; an extremely small peak at 35nm, a large peak at 145nm and two peaks of intermediate height at 339nm and 591nm. The majority of PEV are 100-250nm in size.

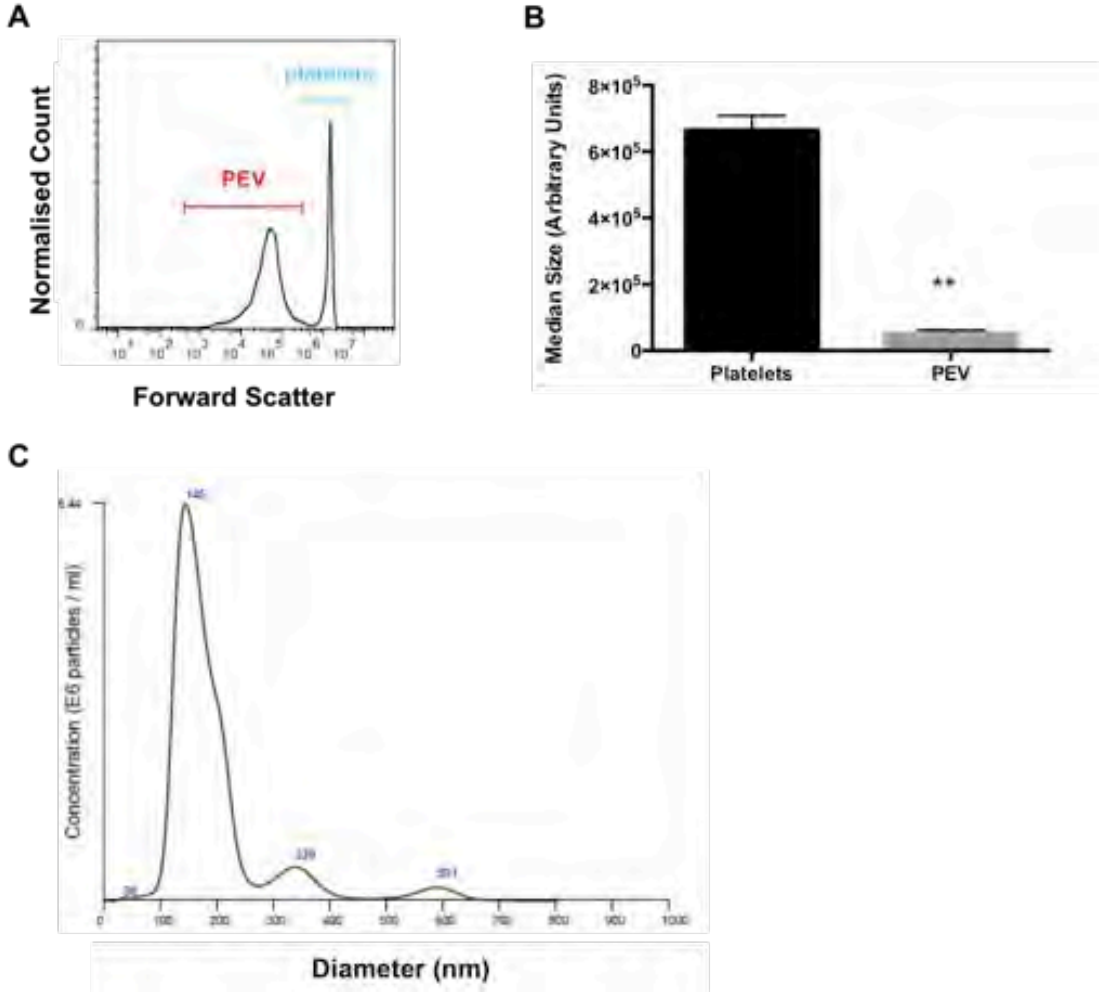

Figure 3.4. Size distribution of Platelets and PEV

(A) Representative histogram of size trace (forward scatter) of PEV vs platelets upon CRP-XL stimulation, as detected by flow cytometry. **(B)** Median size of platelets vs PEV, as detected by flow cytometry. Data are represented as mean +/- SEM of 6 experiments. **(C)** Representative histogram of size distribution of purified PEV released upon platelet

stimulation with CRP-XL, as measured by nanoparticle tracking analysis. Data were analysed by t-test. * indicates P<0.05, ** indicates P<0.01.

The side scatter histogram (ungated) also indicated the presence of two populations as evident by the presence of two distinct peaks (**Fig. 3.5A**). The two peaks corresponded to the platelet and PEV gate (not shown). Upon quantification, PEV were found to be significantly less granular than platelets (**Fig. 3.5B**). Hence, PEV and platelets do not form a continuum of increased granularity, but they are two distinct entities characterised by different granularity.

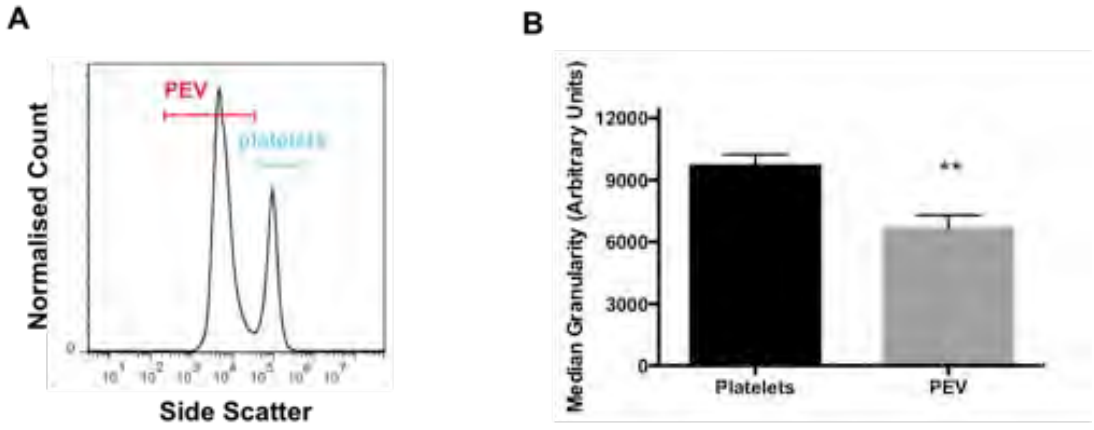

Figure 3.5. Granularity of Platelets and PEV

(A) Representative histogram of granularity trace (side scatter) of PEV and platelets upon CRP-XL stimulation, as detected by flow cytometry. **(B)** Median granularity of platelets and PEV. Data are represented as mean +/- SEM of 3-10 experiments. All data were analysed by t-test, ** indicates P<0.01.

Having characterised PEV in terms of size and granularity, the next objective was to assess their molecular content to identify molecules that could serve as PEV markers in experiments with leukocytes. The first molecule investigated was GPIb, which is a highly abundant adhesion receptor on the platelet surface. Washed platelets were stained with an anti-GPIbα antibody coupled to fluorescent tag before stimulation with agonists so that both whole platelets and PEV get stained. Unpurified PEV were analysed by FACS upon platelet stimulation and the GPIbα expression trace for both

platelets and PEV was observed. Platelets/PEV were also stained with an isotype antibody as a control. **Figure 3.6A** shows overlay histograms of GPIbα expression of isotype and GPIbα-stained platelets and PEV. The gate of positive events is set based on the expression profile of the isotype sample. The large shift to the right of GPIbα expression on platelets shows that the whole platelet population is strongly positive for GPIbα. The smaller shift to the right on the GPIbα scale for PEV shows that not all PEV express GPIb on their surface. Upon quantification, 100% of platelets expressed GPIbα on their surface, whereas only ~75% of PEV expressed GPIbα (**Fig. 3.6B**). In addition, PEV were found to express significantly less GPIbα in quantity than platelets. (**Fig. 3.6C**).

In order to determine whether this expression pattern was valid for other platelet markers, we also investigated expression of another highly abundant surface platelet integrin; GPIIb. Washed platelets were stained with an anti-GPIIb antibody coupled to fluorescent tag before stimulation with agonists so that both whole platelets and PEV were stained. Unpurified PEV were analysed by FACS upon platelet stimulation and the GPIIb expression trace for both platelets and PEV was observed. Platelets/PEV were also stained with an isotype antibody as a control. **Figure 3.7A** shows overlay histograms of GPIIb expression of isotype and GPIIb-stained platelets and PEV. The gate of positive events is set based on the expression profile of the isotype sample. The large shift to the right of GPIIb expression on the platelets shows that the whole platelet population is strongly positive for GPIIb. The smaller shift to the right on the GPIIb scale for PEV shows that not all PEV express GPIIb on their surface. Upon quantification, 100% of platelets expressed GPIIb on their surface, whereas only 75% of PEV expressed

it (**Fig. 3.7B**). In addition, PEV were found to express significantly less GPIIb in quantity than platelets, specifically >20 times less (**Fig. 3.7C**).

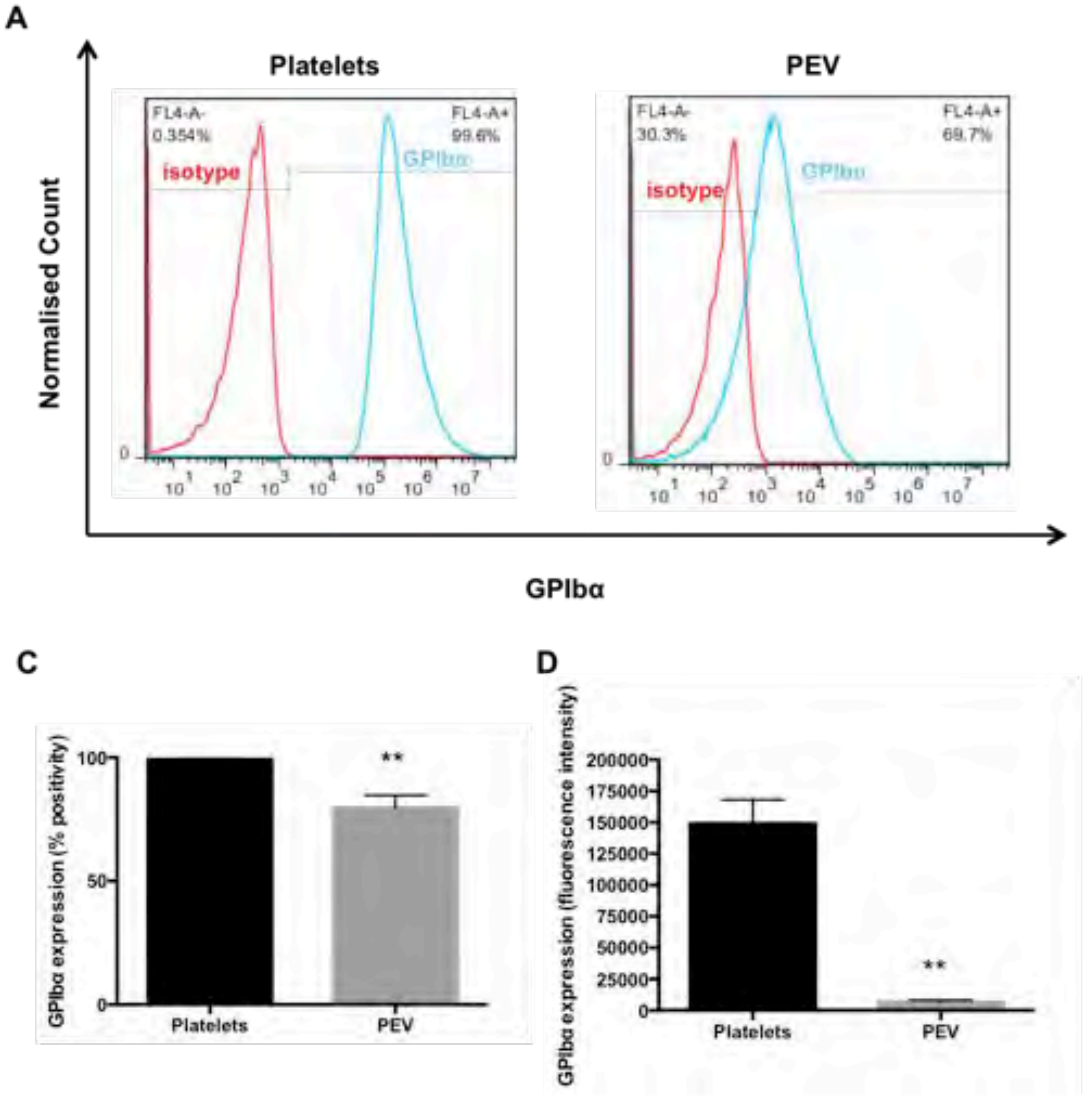

Figure 3.6. Expression of GPIbα on platelets and PEV

(A) Representative histograms of GPIbα expression of platelets and PEV, as detected by flow cytometry. **(B)** Percentage of platelets and PEV, positive for GPIbα, as detected by flow cytometry. Data are represented as mean +/- SEM of 4 experiments. **(C)** Median GPIbα expression of platelets versus PEV, as detected by flow cytometry. Data are represented as mean +/- SEM of 4 experiments. All data were analysed by t-test. ** indicates $P<0.01$.

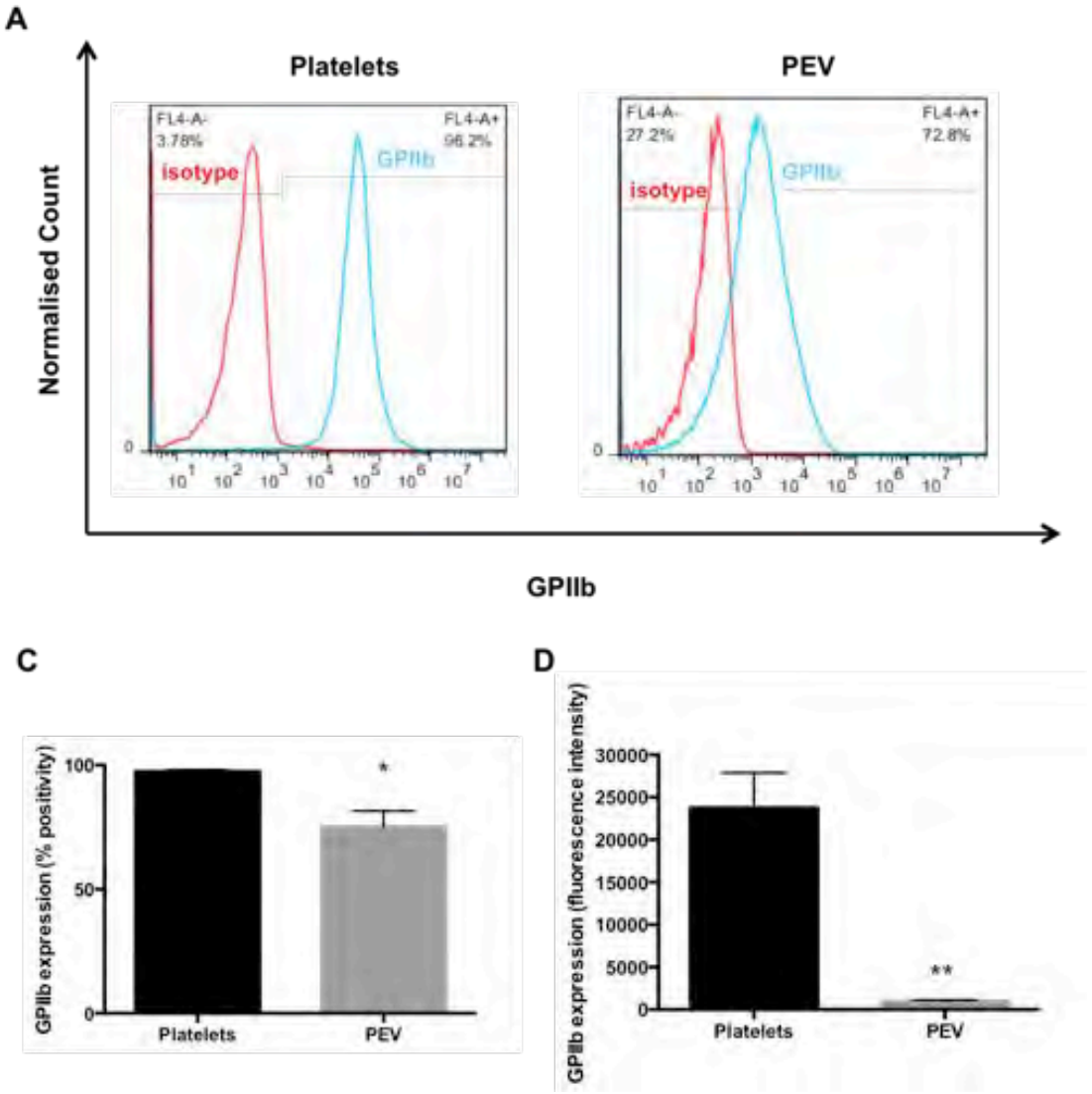

Figure 3.7. Expression of GPIIb on platelets and PEV

(A) Representative histograms of GPIIb expression of platelets and PEV, as detected by flow cytometry. **(B)** Percentage of platelets and PEV, positive for GPIIb, as detected by flow cytometry. Data are represented as mean +/- SEM of 4 experiments. **(C)** Median GPIIb expression of platelets and PEV, as detected by flow cytometry. Data are represented as mean +/- SEM of 4 experiments. All data were analysed by t-test. * indicates $P<0.05$, ** indicates $P<0.01$.

Since not 100% of PEV were positive for GPIb and GPIIb, we hypothesised that unstained vesicles did not bear the receptors. However, to exclude the possibility that

the negatively stained vesicles were an artefact of the preparation and staining process, washed platelets were stained with the lipophilic dye PKH67 that fluorescently stains the cell membrane by incorporating aliphatic reporter molecules into the cell membrane lipid bilayer by selective partitioning. Platelets were stained before stimulation with agonists so that both whole platelets and PEV were stained. Unpurified PEV were analysed by FACS upon platelet stimulation and the PKH67 expression trace for both platelets and PEV was observed. Platelets/PEV were also analysed with unstained cells as a control. **Figure 3.8A** shows overlay histograms of PKH67 expression of unstained and PKH67-stained platelets and PEV. The gate of positive events is set based on the expression profile of the unstained sample.

The large shift to the right of PKH67 expression of the whole platelet population and the whole PEV population shows that both are positive for PKH67. Upon quantification, 100% of both platelets and PEV expressed PKH67 (**Fig. 3.8B**). In addition, PEV were found to express significantly less PKH67 in quantity than platelets, specifically about 10 times less (**Fig. 3.8C**).

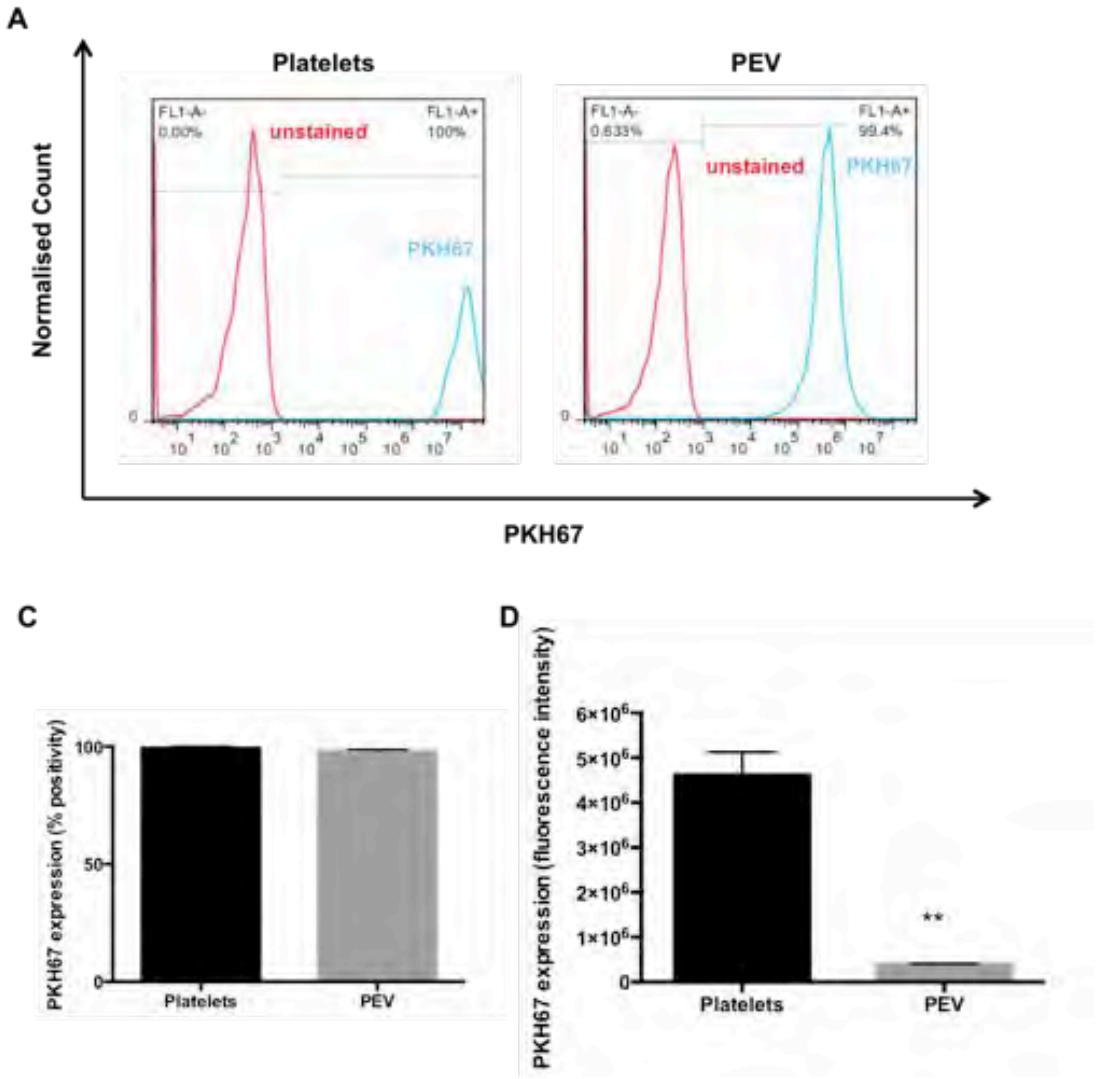

Figure 3.8. Membrane lipids of Platelets and PEV

(A) Representative histograms of PKH67 (membrane marker) expression of platelets and PEV, as detected by flow cytometry. **(B)** Percentage of platelets and PEV, positive for PKH67, as detected by flow cytometry. Data are represented as mean +/- SEM of 3 experiments. **(C)** Median PKH67 expression of platelets vs PEV, as detected by flow cytometry. Data are represented as mean +/- SEM of 3 experiments. All data were analysed by t-test. ** indicates $P<0.01$.

3.4 Discussion

PEV were successfully generated by platelet stimulation with two different agonists that activate in different ways; CRP-XL that binds and activates through GPVI, and thrombin that binds and cleaves PAR receptors. Both agonists were used at a high concentration known to induce robust platelet activation; 1 μg/ml CRP-XL and 0.5 U/ml

thrombin. The number of PEV generated was statistically the same for both agents so thrombin and CRP-XL are equally powerful and efficient in inducing PEV release from platelets. The literature is contradictory as to which stimulant(s) is/are the most potent in generating PEV. Collagen and CRP-XL have been considered by some more powerful in inducing PEV shedding than thrombin, TRAP and ADP (Heemskerk et al., 1999; Sims et al., 1989). However, more recent observations found thrombin to be a stronger stimulant than collagen and CRP-XL (Aatonen et al., 2014).

Quantification of PEV was attempted using Flow Cytometry (FC) and Nanoparticle Tracking analysis (NTA). Nanoparticle Tracking technology was able to count >1000 times more PEV than Flow Cytometry. Our data on PEV quantification by conventional flow cytometry agree with those of others (Aatonen et al., 2014; van der Pol et al., 2014). According to manufacturer's specifications, an Accuri C6 flow cytometer cannot detect particles smaller of 500nm, hence the large discrepancy between the two instruments is logical. Accuri C6 can only detect the larger PMV so caution must be taken when interpreting PEV data from such flow cytometers, as it is unknown whether these are representative of the whole PEV population. However, this method provides a good indicator of platelet contamination in PMV-preparations. PEV were purified using a two-step centrifugation strategy. This resulted from 10% initial platelet contamination to <1% platelet contamination. Perhaps a repeat centrifugation step at 13 000 x g could minimize platelet contamination more. More sensitive techniques to count PMV include nanosight tracking analysis (NTA), resistive pulse sensing (RPS), transmission electron microscopy (TEM), atomic force microscopy (AFM) and flow cytometers dedicated to detecting submicrometer particles (van der Pol et al., 2014, Nieuwland et al., 2013). However these techniques (excluding dedicated

flow cytometry) do not allow fluorescence detection, hence the most beneficial and relevant technique for clinical research is perhaps dedicated flow cytometry.

We therefore argue that a flow cytometer such as an Accuri C6 should be mainly used to check platelet contamination and to test for the expression of markers that are known to be present on large MV. For exosome detection or when whole EV population data are required, a more sophisticated instrument should be used such as a NanoSight that has a fluorescent mode. On average, in our experiments each platelet generates 10-40 PEV (based on the initial platelet count stimulated and the yield in PEV, as count by NanoSight), which agrees with past research (Aatonen et al., 2014).

PEV were found to be significantly smaller and less granular than platelets. PEV span from 0 to 650 nm in size, the majority being between 100-250nm. Our results are in accordance with independent observations made in other labs (Arraud et al., 2014; Yuana et al., 2010; Gabriel et al., 2010; Aatonen et al., 2014). Independent observations made by Brisson and colleagues (2017) suggest that platelet stimulation with thrombin, TRAP or CRP-XL produces EV with similar size distribution. In our studies, the size distribution of PEV was multimodal, suggesting the presence of more than two PEV subpopulations so PEV may not be simply divided in exosomes and PMV, but may be further differentiated in terms of composition and the contents they may carry. With regards to protein cargo, the majority of the larger PMV were confirmed to express the adhesion receptors GPIb and GPIIb, a pattern of expression also found by many other labs (Garcia et al., 2005; Aatonen et al., 2014; Brisson et al., 2017). Hence these receptors can be used as good PMV markers. The expression level of GPIb and GPIIb of PMV was significantly lower than the expression level of platelets, therefore we hypothesised that the expression level of GPIb or GPIIb can be perhaps used in other

experiments to differentiate between platelet or PMV binding, if any, to the surface of monocytes and other leukocytes.

By definition, EV are membranous vesicles, hence a good marker for EV would be a stained membrane. The lipophilic dye PKH67 has proven to be very efficient in staining the PMV membrane as all detected PMV in our experiments. In summary, PMV expressed lower levels of cellular proteins compared to their parent cell, smaller amounts of plasma membrane and had lower granularity. This is not surprising bearing in mind that PEV are of much smaller size compared to their parent cell.

4 CHARACTERISATION OF PEV-LEUKOCYTE AGGREGATES IN ACTIVATED WHOLE BLOOD

4.1 Introduction

Increased levels of circulating PEV have been detected in atherosclerosis patients (Michelsen et al., 2009). In addition, elevated levels of monocyte-platelet aggregates have been reported to circulate in atherosclerosis (Shantsila and Lip, 2009). Hence, there is a possibility that PEV also form aggregates with monocytes in atherosclerosis and that the formation of these aggregates contributes to disease development. Since PEV possess various adhesion receptors on their surface such as GPIb, GPIIb and P-selectin, there is a possibility that upon binding, monocytes use the bound PEV as a bridge for recruitment them to the vessel wall. In addition, binding of PEV to monocytes, could be followed by transfer of proinflammatory mediators from PEV, such as arachidonic acid, tissue factor or scavenger receptors such as CD36 that could activate leukocytes and shift them towards an inflammatory phenotype. Both of these mechanisms could contribute to progression of atherosclerosis.

The monocyte population is divided into two main subsets; those that express CD16 on their surface, simply termed CD16+ve monocytes, and those that do not express CD16 on their surface, simply termed CD16-ve monocytes and often delineated by CD14 expression. According to proteomics analysis more than 200 proteins are differentially expressed between CD16+ve and CD16-ve monocytes, resulting in functional differences between them (Zhao et al., 2009). Hence, there could be differences between the two-monocyte subsets and their interactions with PEV.

The aims for this chapter were to:

1) Investigate the potential of PEV to form aggregates with monocytes and other leukocytes in activated blood

2) Detect differences if any between CD16+ve and CD16-ve monocytes in their capacity to form aggregates with PEV

4.2 Methodology

Platelet agonist TRAP (100 μM) was added to CPDA-anticoagulated peripheral blood or blood was left untreated over the course of 30 minutes at 37˚C under shear stress induced by roller mixer. Heterotypic aggregation was detected by FACS (Cyan ADP) by the presence of platelet/PEV markers (GPIbα and GPIIb) on the leukocytes. Statistical analysis was performed using Graph Pad Prism 6. (For further detail see methods section 2).

4.3 Results

4.3.1 Detection of PEV-Leukocyte Aggrgates using GPIb as the PEV marker

Upon confirmation that activation of platelets through GPVI and PAR receptors successfully results in the release of PEV (see Chapter 3), we then wanted to test whether PEV released into the blood formed aggregates with monocytes or other leukocytes. Peripheral blood was treated with a high concentration of TRAP (100μM) or left untreated over the course of 30 minutes at 37˚C on a roller mixer. At the end of treatment, samples were fixed and stained for monocyte/leukocyte markers (CD14 and CD16) and for the platelet/PEV marker GPIb. Samples were analysed on a Cyan ADP flow cytometer and the different leukocyte populations were analysed for presence of GPIbα, which serves as evidence of heterotypic aggregation.

4.3.1.1 Formation of Aggregates between PEV and CD16-ve Monocytes

Representative flow cytometry dot-plots show acquisition of PEV-borne GPIbα by the CD16-ve monocyte subset over the course of 30 minutes (**Fig. 4.1**). There is a

very small percentage of cells that are positive for GPIbα in the control samples. There is clearly a higher number of events in the GPIbα+ve gate for the 10-, 15-, 20-, 25- and 30-min treatment samples compared to the 0- and 30-min control samples, suggesting that CD16-ve monocytes form aggregates with platelets and/or PEV upon TRAP treatment in the blood. However, there is no clear trend in the acquisition rate of GPIbα, so we cannot conclude that PEV binding to CD16-ve monocytes is proportional to time of stimulation with TRAP.

We then looked at the GPIbα expression profiles of the CD16-ve monocytes in order to get deeper insights on the interaction with platelets and/ or PEV. **Figure 4.2** displays a representative histogram for the CD16-ve monocytes with traces from each time point and controls overlaid. The GPIbα expression trace of platelets is also overlaid to enable us to determine whether CD16-ve monocytes bind platelets or PEV. Since our experiments in Chapter 3 revealed that PEV show significantly lower expression of GPIbα than platelets, we speculated that we could differentiate whether leukocytes bind PEV or platelets (if at all) from their GPIbα expression level.

The distribution curve of GPIbα for the CD16-ve monocytes is shown in **Figure 4.2**. The curve is shifted towards higher expression of GPIbα at all time points compared to the 0-min and 30-min controls, implying that CD16-ve monocytes form aggregates with GPIbα+ve entities. The expression curve is almost identical at all time points of treatment, suggesting that time of incubation with TRAP does not have a major effect on aggregation levels. However, expression peak of GPIbα is lower than the expression on platelets, implying that CD16-ve monocytes bind PEV. However, the right tail of the curve extends into the platelet expression levels and higher, suggesting that a

small percentage of cells might have bound to whole platelets or that they have bound to many PEV and the sum of their GPIbα cargo reaches the GPIbα cargo of a platelet.

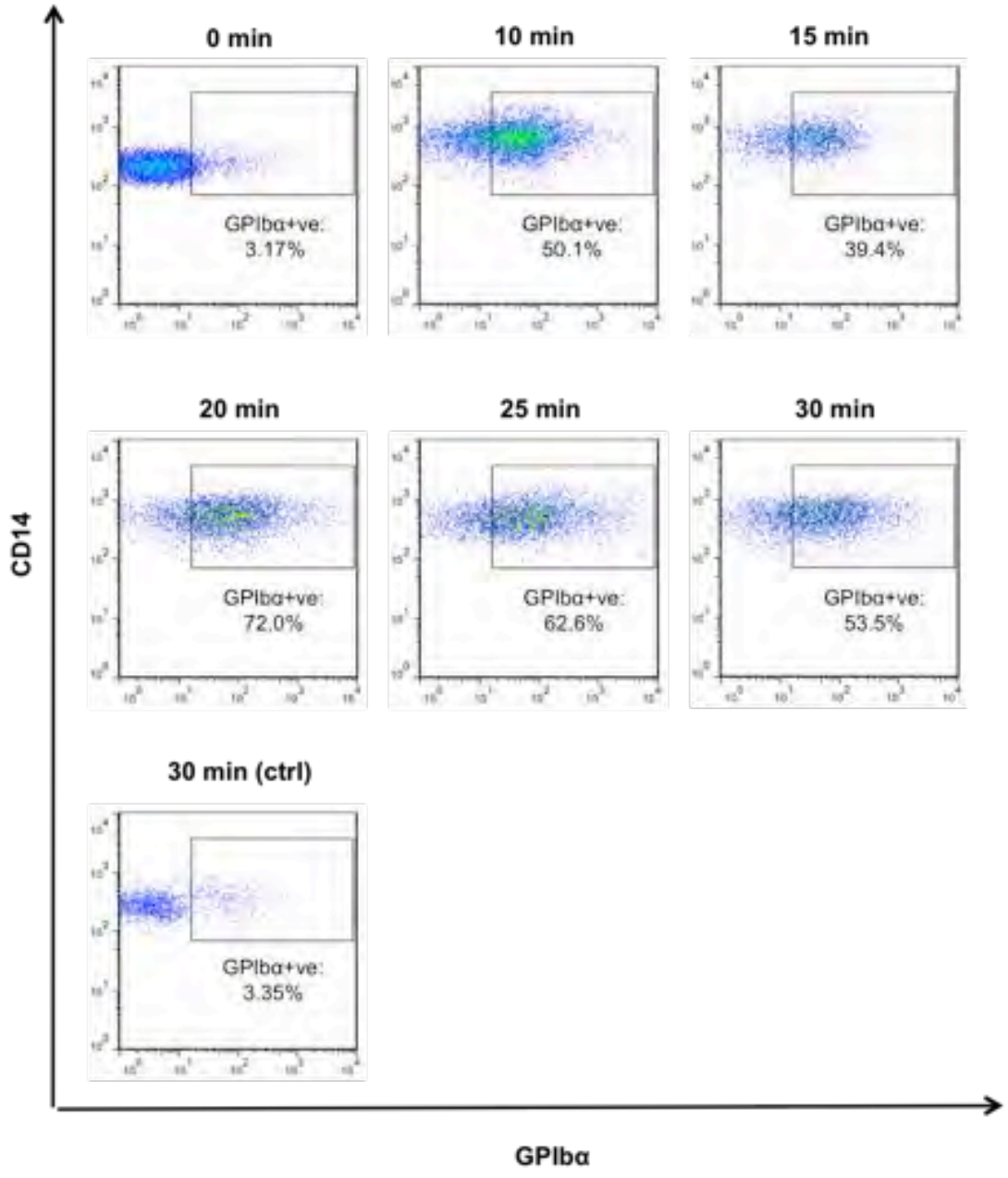

Figure 4.1. Formation of aggregates between CD16-ve monocytes and platelets and/or PEV in whole blood over time in response to 100µM TRAP

Representative FACS dotplots demonstrating percentage of GPIbα+ve CD16-ve monocytes over time up to 30 minutes in response to stimulation with 100µm TRAP under roller mixing. Gate of positive events was set by isotype sample (not shown). A 0-min control (immediate fixation) and a 30-min control (no TRAP, roller mixing) were included.

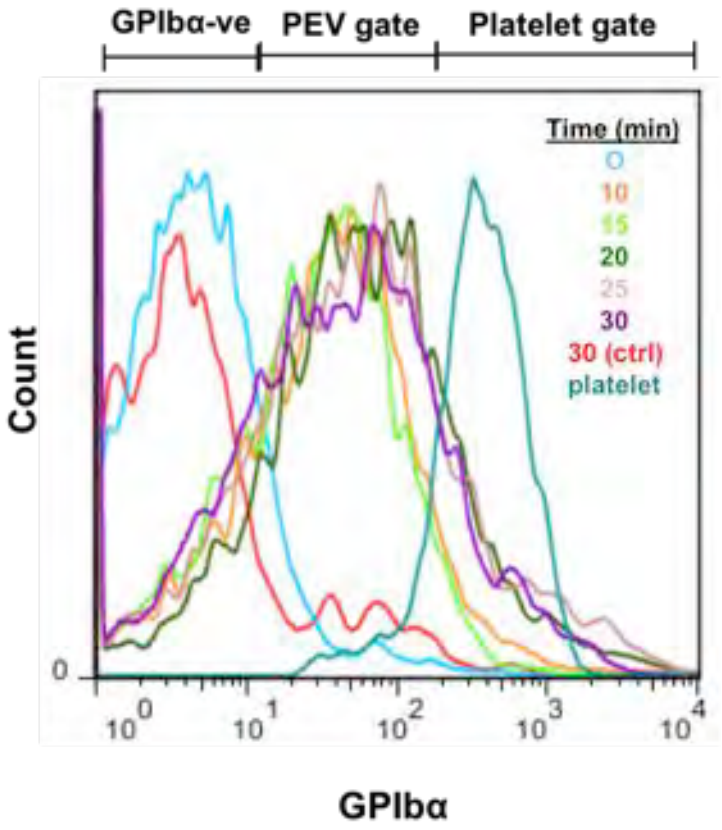

Figure 4.2. GPIbα expression of CD16-ve monocytes over time in whole blood in response to stimulation with 100µM TRAP

Representative FACS overlay histograms demonstrating GPIbα expression on CD16-ve monocytes over time up to 30 minutes in response to stimulation with 100µm TRAP under roller mixing. A 0-min control (immediate fixation) and a 30-min control (no TRAP, roller mixing) were included. The GPIbα expression trace of resting platelets is also shown.

The expression of GPIbα on CD16-ve monocytes was analyzed graphically and statistically from a number of experiments. The percentage of CD16-ve monocytes expressing GPIbα at 30-min with TRAP vs 30-min no TRAP is statistically higher and the percentage increases significantly by increasing incubation time with TRAP (**Fig. 4.3A**).

The graph of median GPIbα expression of CD16-ve monocytes is shown in **Figure 4.3D**. The median GPIbα expression of CD16-ve monocytes at 30-min incubation with TRAP vs 30-min no TRAP is significantly higher, so TRAP increases the median

GPIbα expression on CD16-ve monocytes. The median GPIbα expression on CD16-ve monocytes increases significantly with increasing incubation time with TRAP.

The data from the overlay histogram clearly showed that CD16-ve monocytes formed aggregates with PEV, however, since there was an indication that a small percentage of monocytes formed aggregates with platelets, we decided to also perform statistical analysis separately in the “PEV gate” and “Platelet gate”.

The percentage of CD16-ve monocytes binding to GPIbα+ve entities in the PEV gate (**Fig. 4.3B**) increased significantly with time whereas the percentage in the platelet gate did not change through the experiment (**Fig. 4.3C**). The percentage of CD16-ve monocytes expressing GPIbα upon 30-minute incubation with TRAP was significantly higher than the no TRAP control in both the PEV and platelet gate. However, the GPIbα expression intensity was not affected by incubation time in either gate (**Fig. 4.3E** and **F**). The fluorescence intensity at 30 minutes incubation with TRAP was also not significantly higher than the control in both gates.

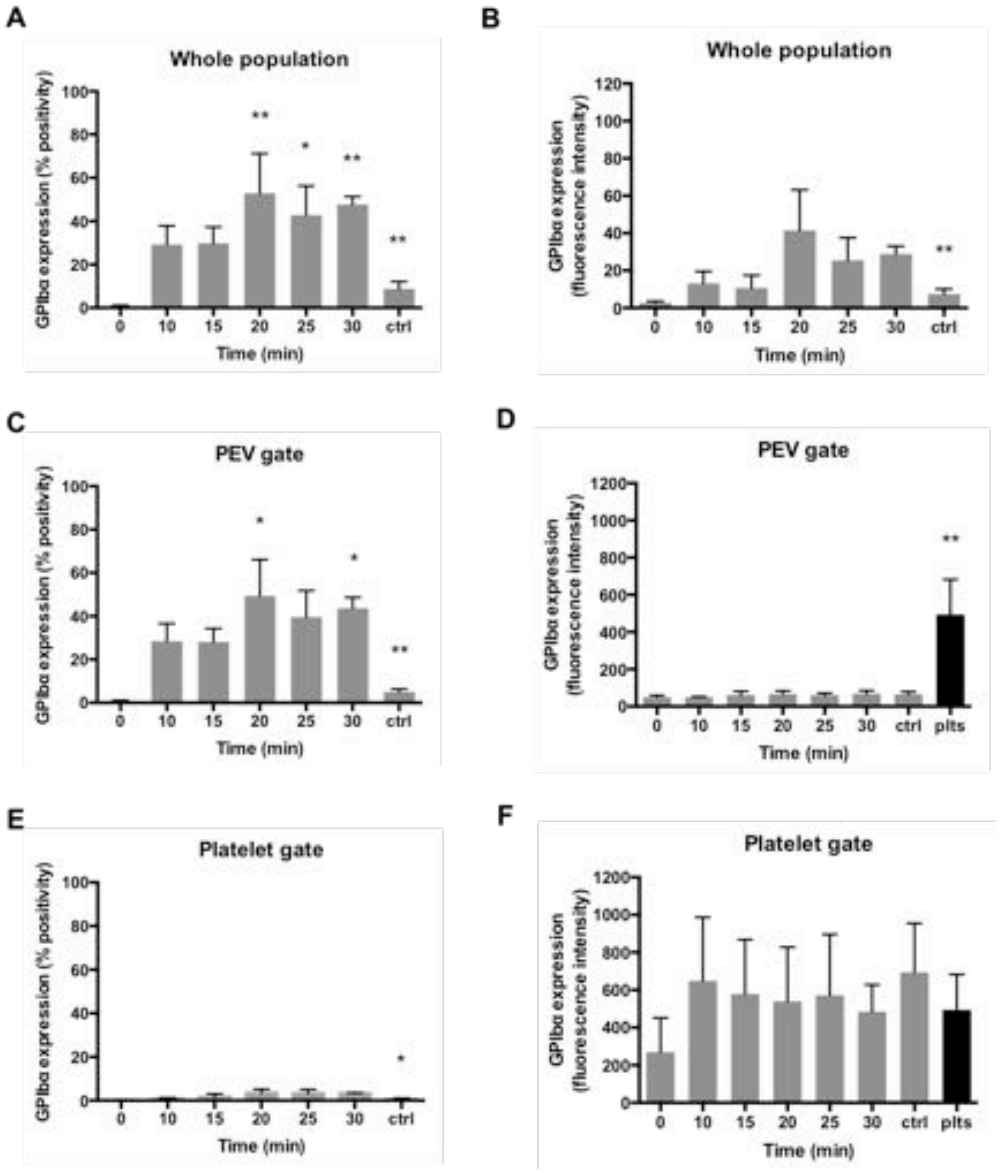

Figure 4.3. Formation of aggregates between CD16-ve monocytes and platelets and/or PEV in whole blood over time in response to 100µM TRAP

Percentage of GPIbα+ve CD16-ve monocytes as a whole **(A)**, in the PEV gate **(B)** and in the Platelet gate **(C)** over time up to 30 minutes in response to stimulation with 100µm TRAP under roller mixing. Median GPIbα expression on CD16-ve monocytes as a whole **(D)**, in the PEV gate **(E)** and in the Platelet gate **(F)**. A 0-min control (immediate fixation) and a 30-min control (no TRAP, roller mixing) are also shown. Data are represented as mean +/- SEM of 3-4 experiments. All data were analysed by One-way ANOVA to determine effect of time, and where applicable data were also analysed by Dunnett's multiple comparisons test. T-tests were performed between 30-min TRAP vs 30-min control **(A, B, C, D, E, F)** and between mean GPIbα expression of 30-min TRAP vs platelet GPIbα expression **(E, F)**. * indicates $P<0.05$, ** indicates $P<0.01$.

4.3.1.2 Formation of Aggregates between PEV and CD16+ve Monocytes

We also investigated the behaviour of CD16+ve monocytes. A similar behaviour is observed with the CD16+ve monocytes, with a higher number of events in the GPIbα+ve gate of representative flow cytometry dot-plots for the 10-, 15-, 20-, 25- and 30-min samples compared to the 0- and 30-min control samples (**Fig. 4.4**). Hence, CD16+ve monocytes also form aggregates with platelets and/or PEV upon TRAP treatment in the blood. Again, there is no clear trend in the acquisition rate of GPIbα, so we cannot conclude that PEV binding to CD16+ve monocytes is proportional to time of incubation with TRAP. However, we can observe distinct populations of GPIbα+ve events, one with low and one with high expression. The population highlighted inside the red rectangle in the 10-min sample is an example. Interestingly as time passes the number of cells in this population diminishes. It is probable that population represents monocytes that have bound whole platelets, however, over time these detach from the monocytes so that by 30 minutes few remain.

The GPIbα expression profile of the CD16+ve monocytes was also analyzed. **Figure 4.5** displays a representative histogram for the CD16+ve monocytes with traces from each time point and controls overlaid. The GPIbα expression trace of platelets is also overlaid to enable us determine whether CD16+ve monocytes bind platelets or PEV.

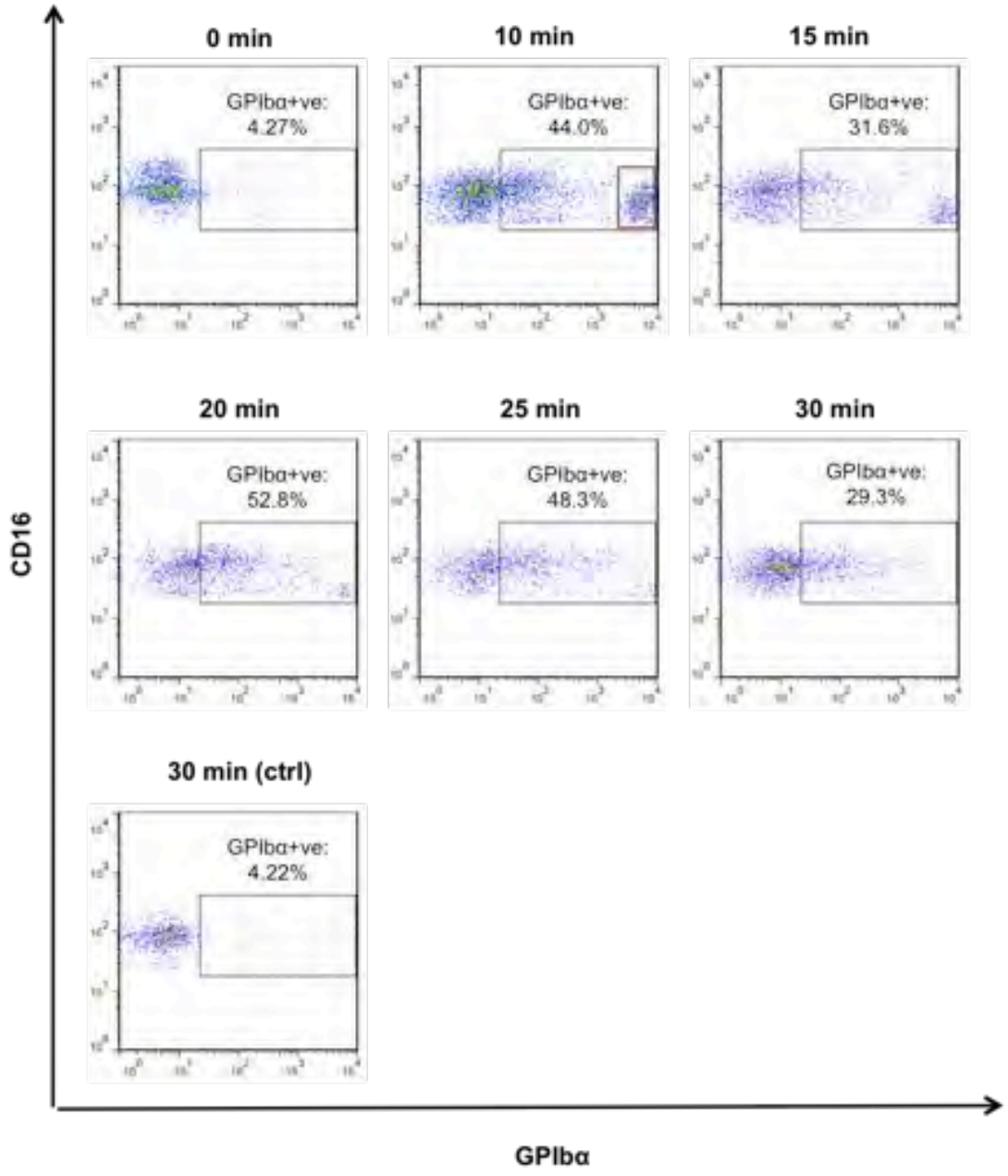

Figure 4.4. Formation of aggregates between CD16+ve monocytes and platelets and/or PEV in whole blood over time in response to 100μM TRAP

Representative FACS dotplots demonstrating percentage of GPIbα+ve CD16+ve monocytes over time up to 30 minutes in response to stimulation with 100μm TRAP under roller mixing. Gate of positive events was set by isotype sample (not shown). A 0-min control (immediate fixation) and a 30-min control (no TRAP, roller mixing) were included.

CD16+ve monocytes show a different pattern of staining compared to CD16-ve monocytes. This distribution is bimodal, with a GPIbα "low" and "high" population. The

GPIbα high cells show expression greater than platelets. This indicates that a percentage of this population is binding whole platelets. The GPIbα "low" population shows staining below the intensity of platelets, indicating PEV acquisition. Hence, the GPIbα+ve section was separated into two subsections; a GPIbα+ve section of lower expression than the platelet expression in order to enable us to detect interactions with PEV ("PEV gate") and a GPIbα+ve section of higher expression than the platelet expression in order to enable us to detect interactions with platelets ("Platelet gate").

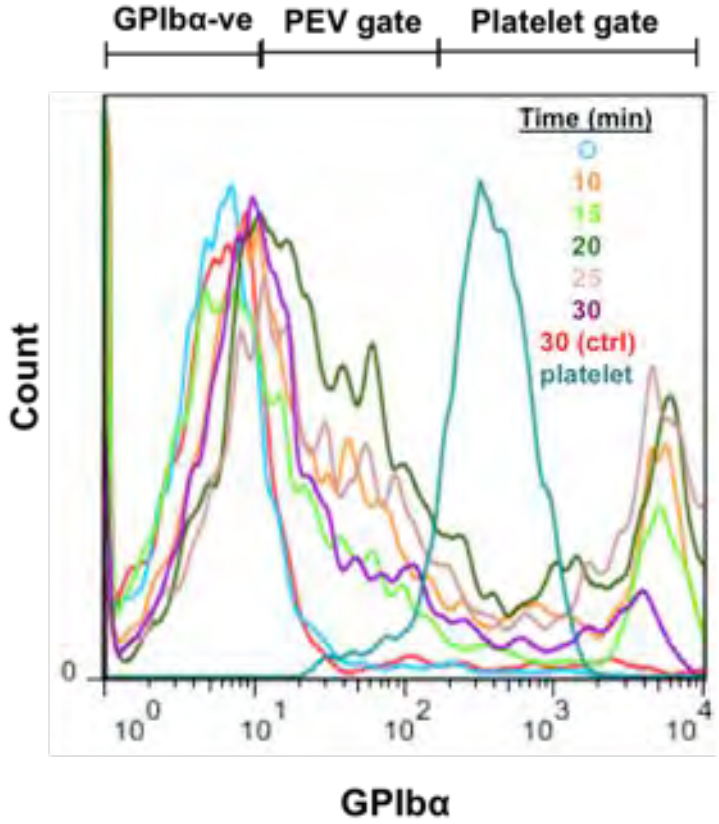

Figure 4.5. GPIbα expression of CD16+ve monocytes over time in whole blood in response to whole blood stimulation with 100μM TRAP

Representative FACS overlay histograms demonstrating GPIbα expression on CD16+ve monocytes over time up to 30 minutes in response to stimulation with 100μm TRAP under roller mixing. A 0-min control (immediate fixation) and a 30-min control (no TRAP, roller mixing) were included. The GPIbα expression trace of resting platelets is also shown.

The percentage of CD16+ve monocytes expressing GPIbα at 30-min with TRAP vs 30-min no TRAP is statistically higher. The percentage of CD16+ve monocytes acquiring GPIbα increases significantly with time (**Fig. 4.6A**).

The graph of median GPIbα expression of CD16+ve monocytes is shown in **Figure 4.6D**. The mean GPIbα expression of CD16+ve monocytes at 30-min incubation with TRAP vs 30-min no TRAP is statistically higher. The median GPIbα expression on CD16+ve monocytes is proportional to time of incubation.

Upon observing that CD16+ve monocytes form aggregates distinctively with platelets and PEV, statistical analysis was also performed separately in the "PEV gate" and "Platelet gate". Time of incubation does not affect the percentage of CD16+ve monocytes binding to PEV (**Fig. 4.6B**) or platelets (**Fig. 4.6C**) significantly, even though we can observe a decreasing trend for platelet binding and increasing trend for PEV binding. The GPIbα expression intensity on monocytes in the "platelet gate" is statistically the same as the GPIbα expression of platelets, suggesting that several platelets bind to monocytes (**Fig. 4.6F**). The GPIbα expression intensity on monocytes in the "PEV gate" is significantly lower than the GPIbα expression of platelets, suggesting that those monocytes bind PEV instead (**Fig. 4.6E**).

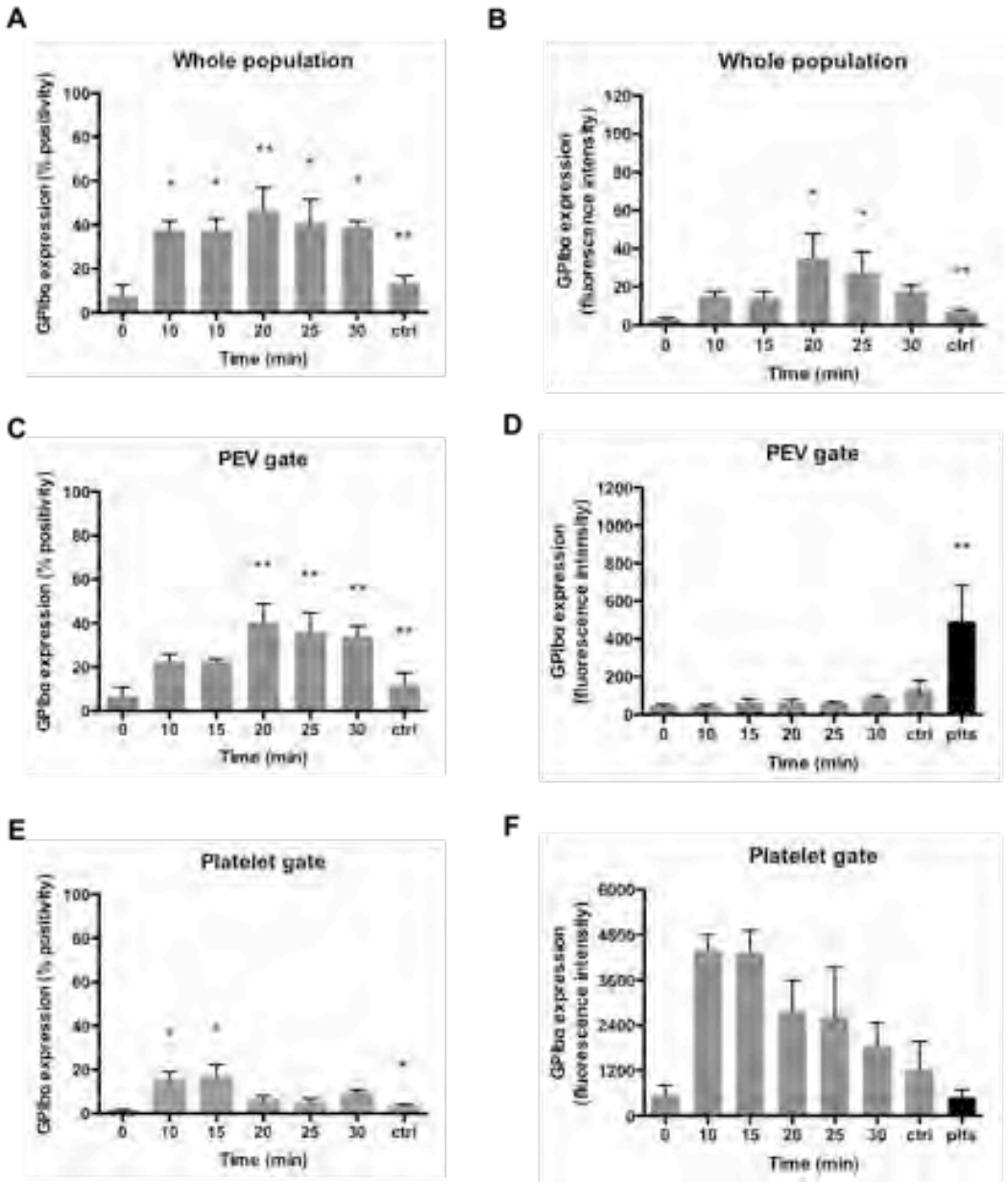

Fig. 4.6. Formation of aggregates between CD16+ve monocytes and platelets and/or PEV in whole blood over time in response to 100μM TRAP

Percentage of GPIbα+ve CD16+ve monocytes as a whole **(A)**, in the PEV gate **(B)** and in the Platelet gate **(C)** over time up to 30 minutes in response to stimulation with 100μm TRAP under roller mixing. Median GPIbα expression on CD16+ve monocytes as a whole **(D)**, in the PEV gate **(E)** and in the Platelet gate **(F)**. A 0-min control (immediate fixation) and a 30-min control (no TRAP, roller mixing) are also shown. Data are represented as mean +/- SEM of 3-4 experiments. All data were analysed by One-way ANOVA to determine effect of time, and where applicable data were also analysed by Dunnett's multiple comparisons test. T-tests were performed between 30-min TRAP vs 30-min control **(A, B, C, D, E, F)** and between mean GPIbα expression of 30-min TRAP vs platelet GPIbα expression **(E, F)**. * indicates $P<0.05$, ** indicates $P<0.01$.

4.3.1.3 Formation of Aggregates between PEV and Neutrophils

We then investigated the behaviour of neutrophils in order to determine whether the affinity for PEV was monocyte-specific or also true for other leukocytes. We analysed the acquisition of PEV-borne GPIbα by neutrophils over the course of 30 minutes (**Fig. 4.7**). There is a very small percentage of cells that are positive for GPIbα in the control samples. There is clearly a higher number of events in the GPIbα+ve gate for the 10-, 15-, 20-, 25- and 30-min treatment samples compared to the 0- and 30-min control samples, showing that neutrophils also form aggregates with platelets and/or PEV upon TRAP treatment in the blood. However, there is no clear trend in the acquisition rate of GPIbα, so PEV binding to neutrophils does not increase with time.

Analysis of the GPIbα expression histogram of neutrophils indicates that the main body of the curve shifts very little towards higher expression compared to the controls. However, the right tail extends towards noticeable higher expression and reaches the expression of platelet (**Fig. 4.8A**).

Graphical and statistical analysis is shown in **Fig. 4.9**. Incubation with TRAP increases the percentage of GPIbα+ve neutrophils significantly (**Fig. 4.9A**). The percentage of neutrophils expressing GPIbα at 30-min with TRAP vs 30-min no TRAP is statistically higher.

The graph of median GPIbα expression of the total neutrophil population is shown in **Figure 4.9D**. Incubation with TRAP significantly increases the median GPIbα expression on neutrophils. The median GPIbα expression of neutrophils at 30-min incubation with TRAP vs 30-min no TRAP is statistically higher, so TRAP increases the median GPIbα expression on neutrophils.

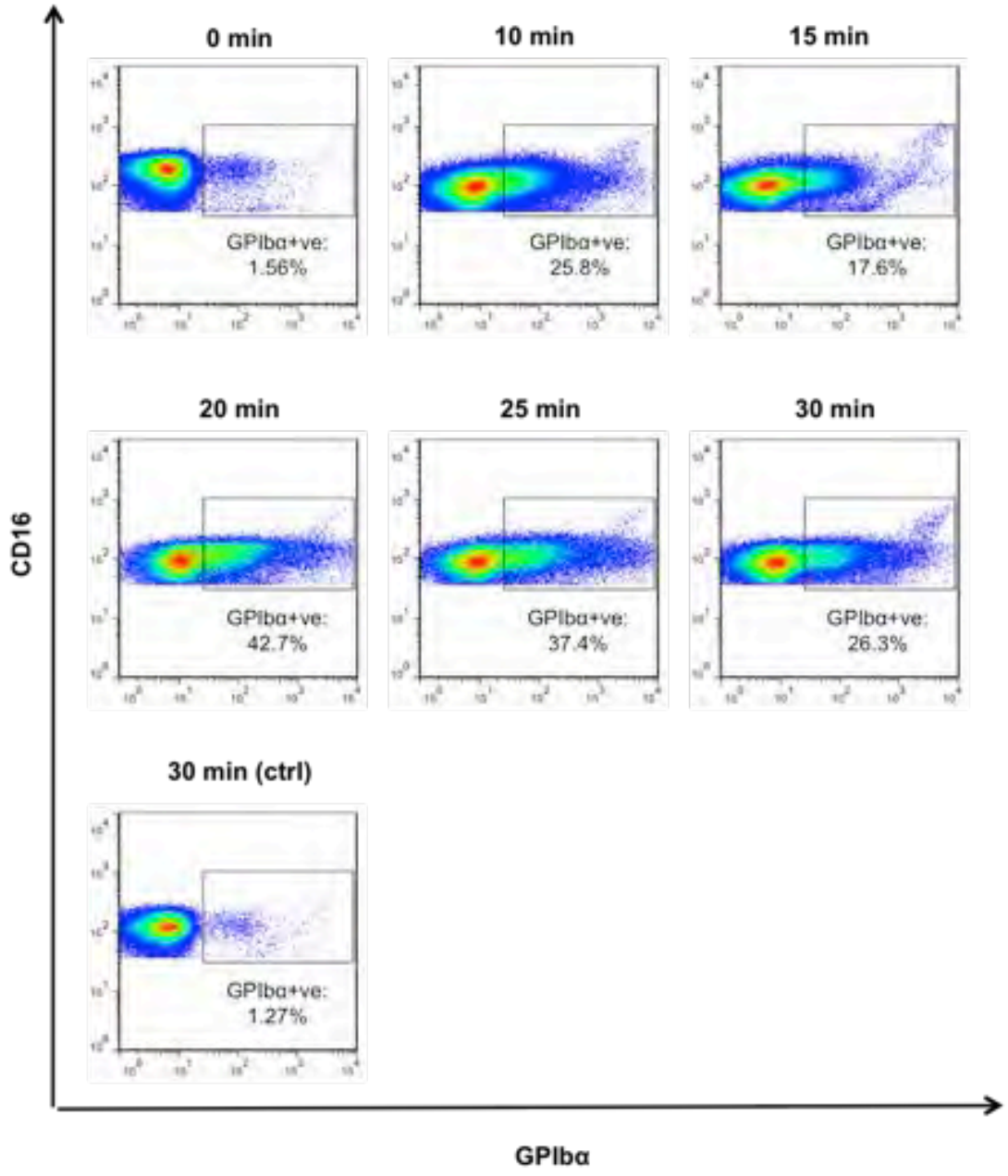

Figure 4.7. Formation of aggregates between Neutrophils and Platelets and/or PEV in whole blood over time in response to 100μM TRAP

Representative FACS dotplots demonstrating percentage of GPIbα+ve neutrophils over time up to 30 minutes in response to stimulation with 100μm TRAP under roller mixing. Gate of positive events was set by isotype sample (not shown). A 0-min control (immediate fixation) and a 30-min control (no TRAP, roller mixing) were included.

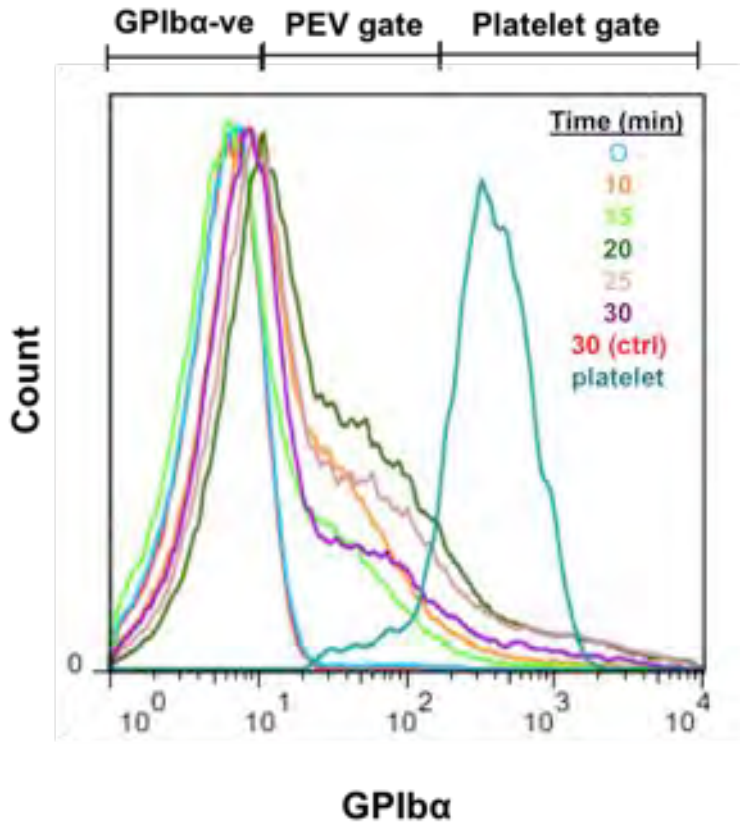

Figure 4.8. GPIbα expression of neutrophils over time in whole blood in response to whole blood stimulation with 100μM TRAP

Representative FACS overlay histograms demonstrating GPIbα expression on neutrophils over time up to 30 minutes in response to stimulation with 100μm TRAP under roller mixing. A 0-min control (immediate fixation) and a 30-min control (no TRAP, roller mixing) were included. The GPIbα expression trace of resting platelets is also shown.

The percentage of GPIbα+ve neutrophils was also measured separately in the platelet gate and in the PEV gate and was analyzed statistically over the course of 30 minutes. The percentage of neutrophils binding to PEV increases significantly by time (**Fig. 4.9B**), however the expression intensity in the PEV gate does not increase significantly by time (**Fig. 4.9E**).

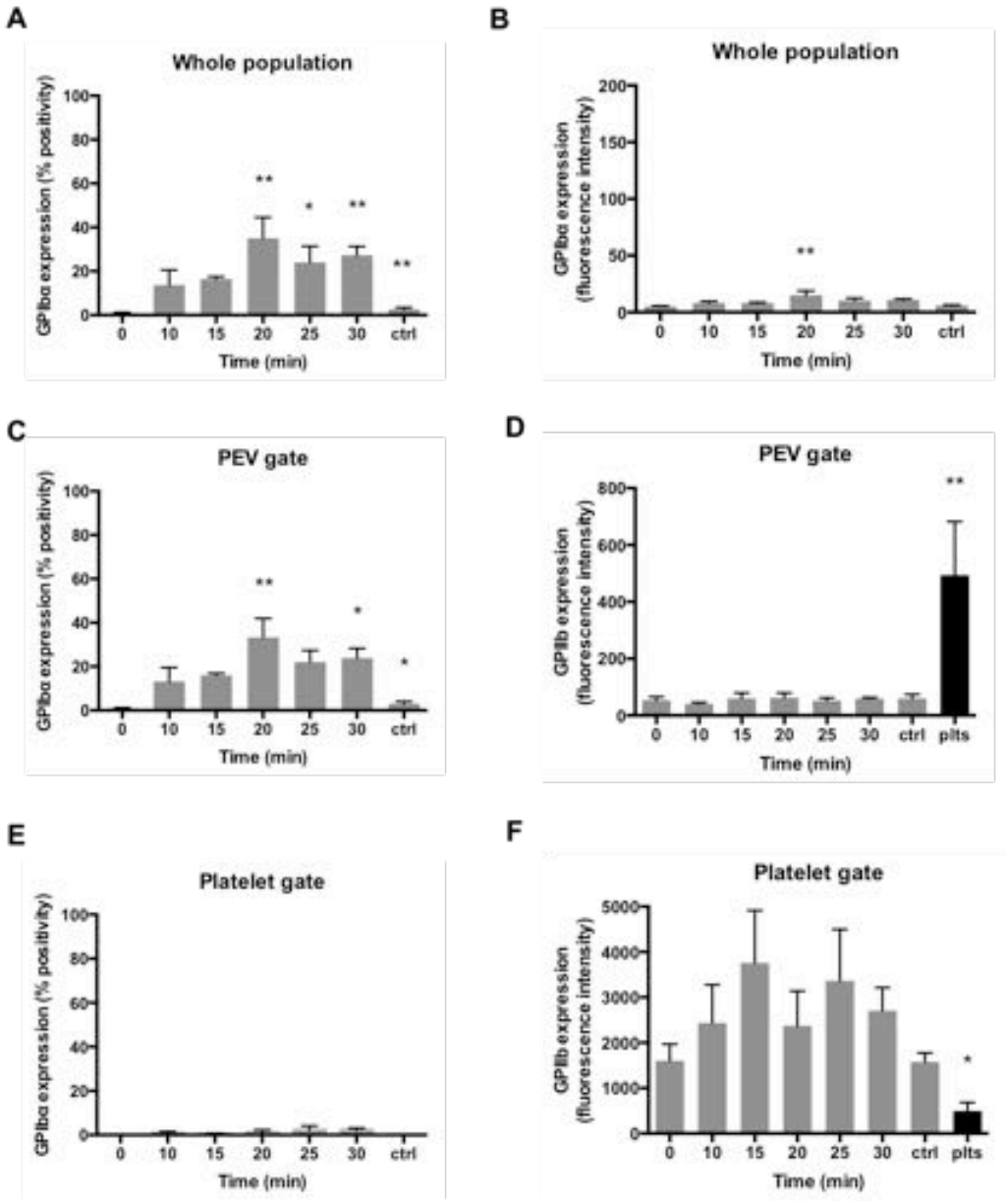

Fig. 4.9. Formation of aggregates between neutrophils and platelets and/or PEV in whole blood over time in response to 100μM TRAP

Percentage of GPIbα+ve neutrophils as a whole **(A)**, in the PEV gate **(B)** and in the Platelet gate **(C)** over time up to 30 minutes in response to stimulation with 100μm TRAP under roller mixing. Median GPIbα expression on neutrophils as a whole **(D)**, in the PEV gate **(E)** and in the Platelet gate **(F)**. A 0-min control (immediate fixation) and a 30-min control (no TRAP, roller mixing) are also shown. Data are represented as mean +/- SEM of 3-4 experiments. All data were analysed by One-way ANOVA to determine effect of time, and where applicable data were also analysed by Dunnett's multiple comparisons test. T-tests were performed between 30-min TRAP vs 30-min control **(A, B, C, D, E, F)** and between mean GPIbα expression of 30-min TRAP vs platelet GPIbα expression **(E, F)**. * indicates P<0.05, ** indicates P<0.01.

The percentage of neutrophils binding to platelets (**Fig. 4.9C**) and the expression intensity in the platelet gate (**Fig. 4.9F**) do not change significantly with time. The GPIbα expression on neutrophils in the "platelet gate" is significantly higher than the GPIbα expression of platelets, suggesting that neutrophils bind to >1 platelets (**Fig. 4.9F**).

4.3.1.4 Formation of Aggregates between PEV and Lymphocytes

We also investigated the behaviour of lymphocytes. The acquisition of PEV-borne GPIbα by lymphocytes over the course of 30 minutes can be seen on the representative flow cytometry dotplots of **Fig. 4.10**. The gate for GPIbα+ve events is set according to expression level upon staining with an appropriate isotype antibody (not shown). There is a small percentage of cells that are positive for GPIbα in the control samples. This increases to some degree at later time points, suggesting that some lymphocytes form aggregates with platelets and/or PEV upon TRAP treatment in the blood. However, there is no clear trend in the acquisition rate of GPIbα.

Analysis of the expression histogram of lymphocytes indicates that a subpopulation of the cells acquire low levels of GPIbα and the intensity of staining does not approach that of platelets, indicating acquisition of PEV (**Fig. 4.11A**).

The percentage of lymphocytes expressing GPIbα at 30-min no TRAP vs 30-min TRAP is statistically the same, suggesting that PEV do not form aggregates with lymphocytes. As a consequence, time of incubation with TRAP does not have an effect on the percentage of lymphocyte-PEV aggregates (**Fig. 4.12A**).

The graph of median GPIbα expression of lymphocytes is shown in **Figure 4.12D**. There is no statistical difference between the 0-min and 30-min control sample

or between the 30-min no TRAP and the 30-min TRAP sample, so lymphocytes do not form aggregates with PEV or platelets in response to TRAP treatment.

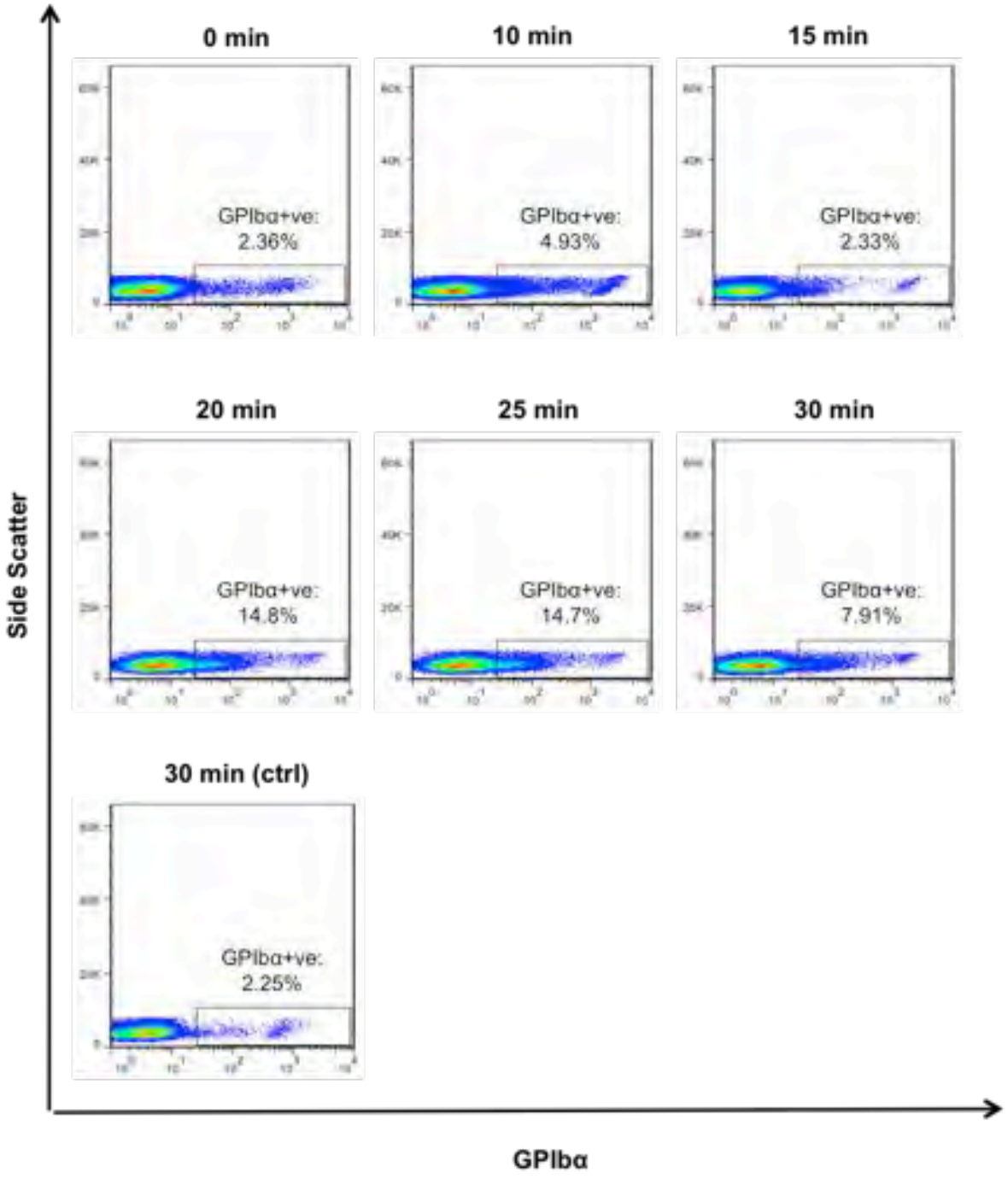

Figure 4.10. Formation of aggregates between lymphocytes and platelets and/or PEV in whole blood over time in response to 100µM TRAP

Representative FACS dotplots demonstrating percentage of GPIbα+ve lymphocytes over time up to 30 minutes in response to stimulation with 100µm TRAP under roller mixing.

Gate of positive events was set by isotype sample (not shown). A 0-min control (immediate fixation) and a 30-min control (no TRAP, roller mixing) were included.

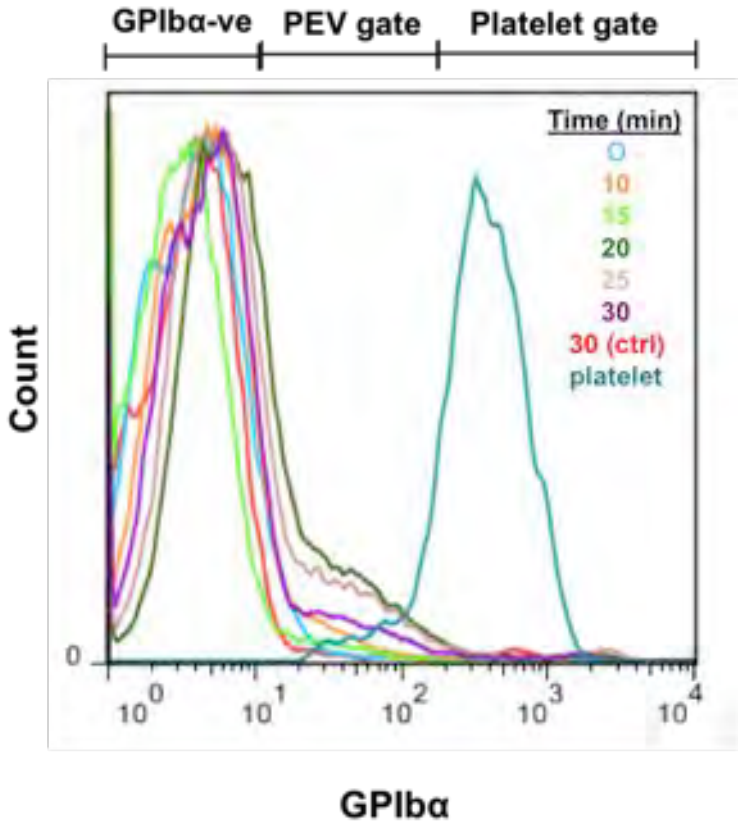

Figure 4.11. GPIbα expression of lymphocytes over time in whole blood in response to whole blood stimulation with 100μM TRAP

Representative FACS overlay histograms demonstrating GPIbα expression on lymphocytes over time up to 30 minutes in response to stimulation with 100μm TRAP under roller mixing. A 0-min control (immediate fixation) and a 30-min control (no TRAP, roller mixing) were included. The GPIbα expression trace of resting platelets is also shown.

The percentage of GPIbα+ve lymphocytes and the GPIbα expression intensity were also measured separately in the platelet gate and in the PEV gate and they did not change upon TRAP treatment (**Fig. 4.12B, C, E, F**).

The results of section 4.3.1 are summarized in Tables 12.1 and 12.2 of the Supplementary Material.

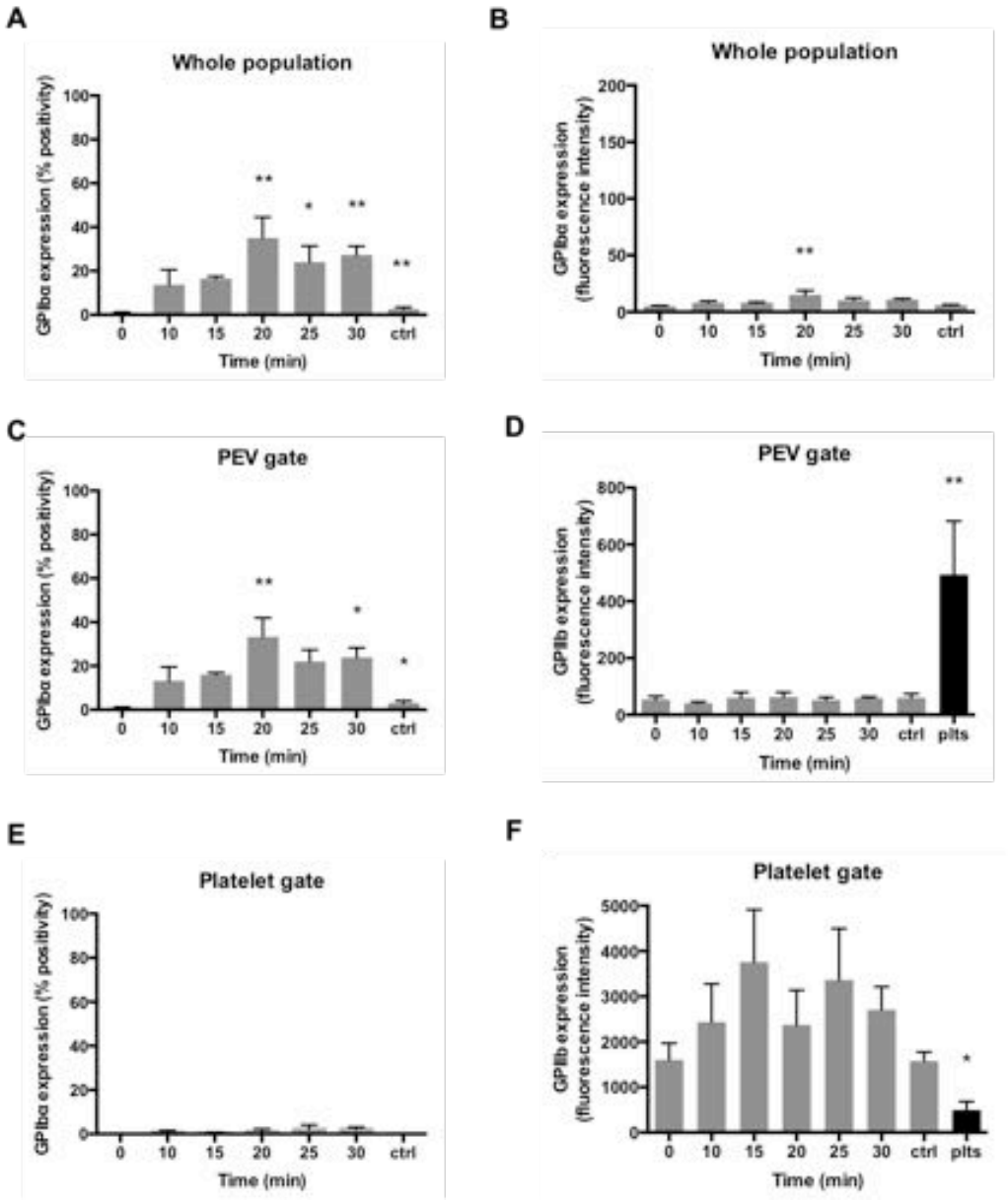

Fig. 4.12. Formation of aggregates between lymphocytes and platelets and/or PEV in whole blood over time in response to 100μM TRAP

Percentage of GPIbα+ve lymphocytes as a whole **(A)**, in the PEV gate **(B)** and in the Platelet gate **(C)** over time up to 30 minutes in response to stimulation with 100μm TRAP under roller mixing. Median GPIbα expression on lymphocytes as a whole **(D)**, in the PEV gate **(E)** and in the Platelet gate **(F)**. A 0-min control (immediate fixation) and a 30-min control (no TRAP, roller mixing) are also shown. Data are represented as mean +/- SEM of 3-4 experiments. All data were analysed by One-way ANOVA to determine effect of time, and where applicable data were also analysed by Dunnett's multiple comparisons test. T-tests were performed between 30-min TRAP vs 30-min control **(A, B, C, D, E, F)** and between mean GPIbα expression of 30-min TRAP vs platelet GPIbα expression **(E, F)**. * indicates P<0.05, ** indicates P<0.01.

4.3.2 Detection of PEV-Leukocyte Aggrgates using GPIIb as the PEV marker

Formation of leukocyte-PEV aggregates upon whole blood stimulation with TRAP was also assessed by labelling PEV for a different marker; GPIIb; in order to detect whether marker choice affects level of aggregation. GPIIb was also largely expressed on PMV in our pevious experiments (see Chapter 3). It gets upregulated on the platelet surface upon activation in contrast to GPIb that does not.

4.3.2.1 Formation of Aggregates between PEV and CD16-ve Monocytes

Representative flow cytometry dotplots show acquisition of PEV-borne GPIIb by the CD16-ve monocyte subset after 30-min of incubation with TRAP under shear (**Fig. 4.13A**). There is minimal percentage of cells that are positive for GPIIb in the 0-min sample. There is a high number of events in the GPIIb+ve gate for the 30-min sample, suggesting that CD16-ve monocytes form aggregates with platelets and/or PEV upon TRAP treatment in the blood.

A representative GPIIb expression histogram of the CD16-ve monocytes was analyzed in order to get deeper insights on the interaction between leukocytes and platelets and/ or PEV (**Fig. 4.13B)** The GPIIb expression trace of platelets is also overlaid on each histogram to enable us determine whether leukocytes bind platelets or PEV. The TRAP-treated sample shows higher expression of GPIIb compared to the control. There is bimodal expression, one peak of lower and one of higher expression than the platelet expression. This result suggests that a subpopulation of CD16-ve monocytes binds preferentially to PEV, and another subpopulation binds to platelets.

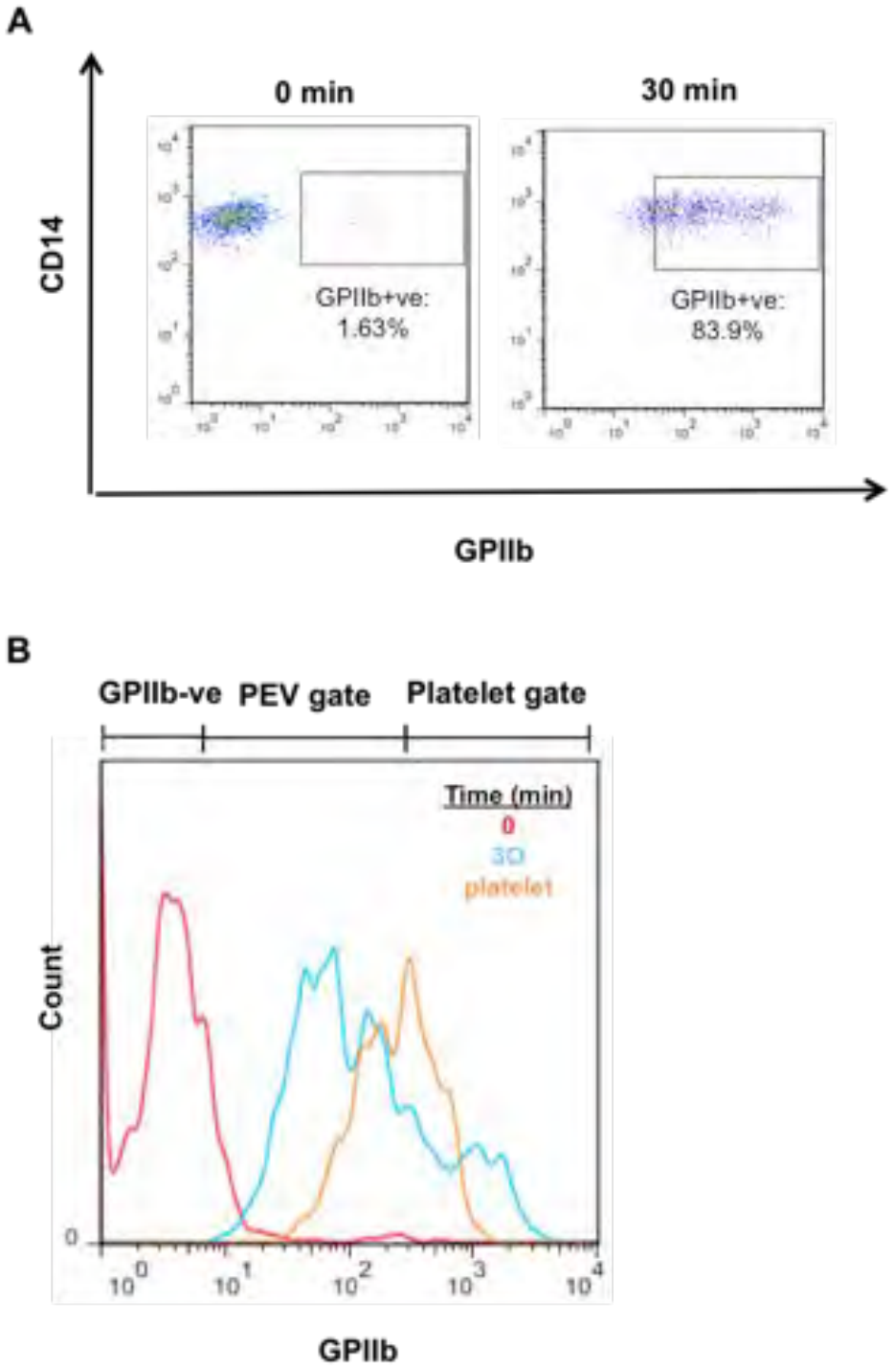

Figure 4.13. Formation of aggregates between CD16-ve monocytes and platelets and/or PEV in whole blood in response to treatment with 100µM TRAP

(A) Representative FACS dotplots demonstrating percentage of GPIIb+ve CD16-ve monocytes and **(B)** representative FACS overlay histograms demonstrating GPIIb expression on CD16-ve monocytes before and after 30 minutes stimulation with 100µm TRAP under roller mixing. Gate of positive events was set by isotype sample (not shown).

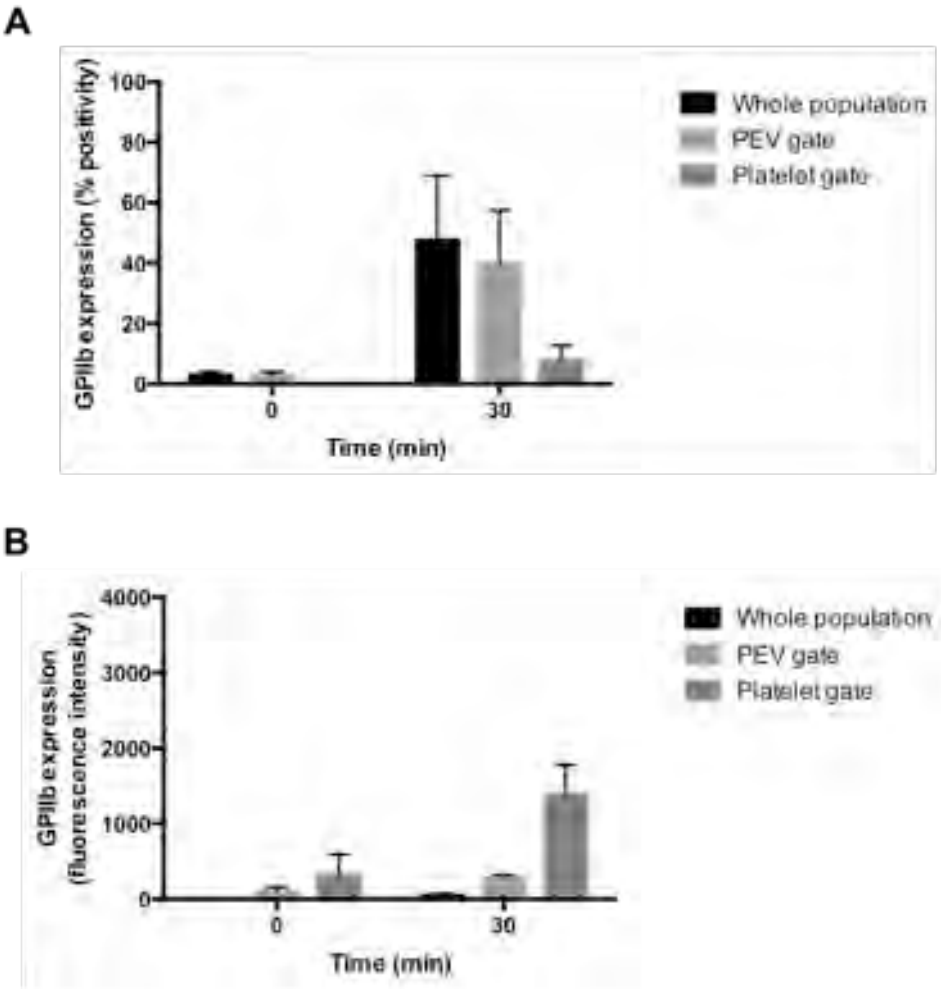

Figure 4.14. Formation of aggregates between CD16-ve monocytes and platelets and/or PEV in whole blood over time in response to 100µM TRAP

(A) Percentage of GPIIb+ve CD16-ve monocytes as a whole, in the PEV gate and in the Platelet gate after treatment with TRAP. **(B)** Median GPIIb expression on CD16-ve monocytes as a whole, in the PEV gate and in the Platelet gate. Data are represented as mean +/- SEM of 3 experiments. All data were analysed by T-tests to determine difference between 0-min and 30-min samples.

Upon graphical analysis of a number of experiments, we observed that the percentage of the whole CD16-ve monocyte population and the CD16-ve monocyte population in the PEV gate increased upon treatment with TRAP (**Fig. 4.14A**). However, the median GPIIb expression of CD16-ve monocytes after 30-min incubation with TRAP did not increase significantly (**Fig. 4.14B**).

4.3.2.2 Formation of Aggregates between PEV and CD16+ve Monocytes

A similar behaviour is also observed with the CD16+ve monocytes. There is minimal percentage of cells that are positive for GPIIb before TRAP treatment and there is a high number of events in the GPIIb+ve gate for the 30-min sample, suggesting that CD16+ve monocytes form aggregates with platelets and/or PEV upon TRAP treatment in the blood (**Fig. 4.15A**). The TRAP-treated sample also shows higher expression of GPIIb compared to the control. There is bimodal expression, one peak of lower and one of higher expression than the platelet expression. This result suggests that a subpopulation of CD16+ve monocytes binds preferentially to PEV, and another subpopulation binds to platelets (**Fig. 4.15B**).

Upon graphical analysis of a number of experiments, we observed that the percentage of the whole CD16+ve monocyte population and the CD16+ve monocyte population in the PEV gate significantly increased upon treatment with TRAP (**Fig. 4.16A**). However, the median GPIIb expression of CD16+ve monocytes after 30-min incubation with TRAP did not increase significantly (**Fig. 4.16B**).

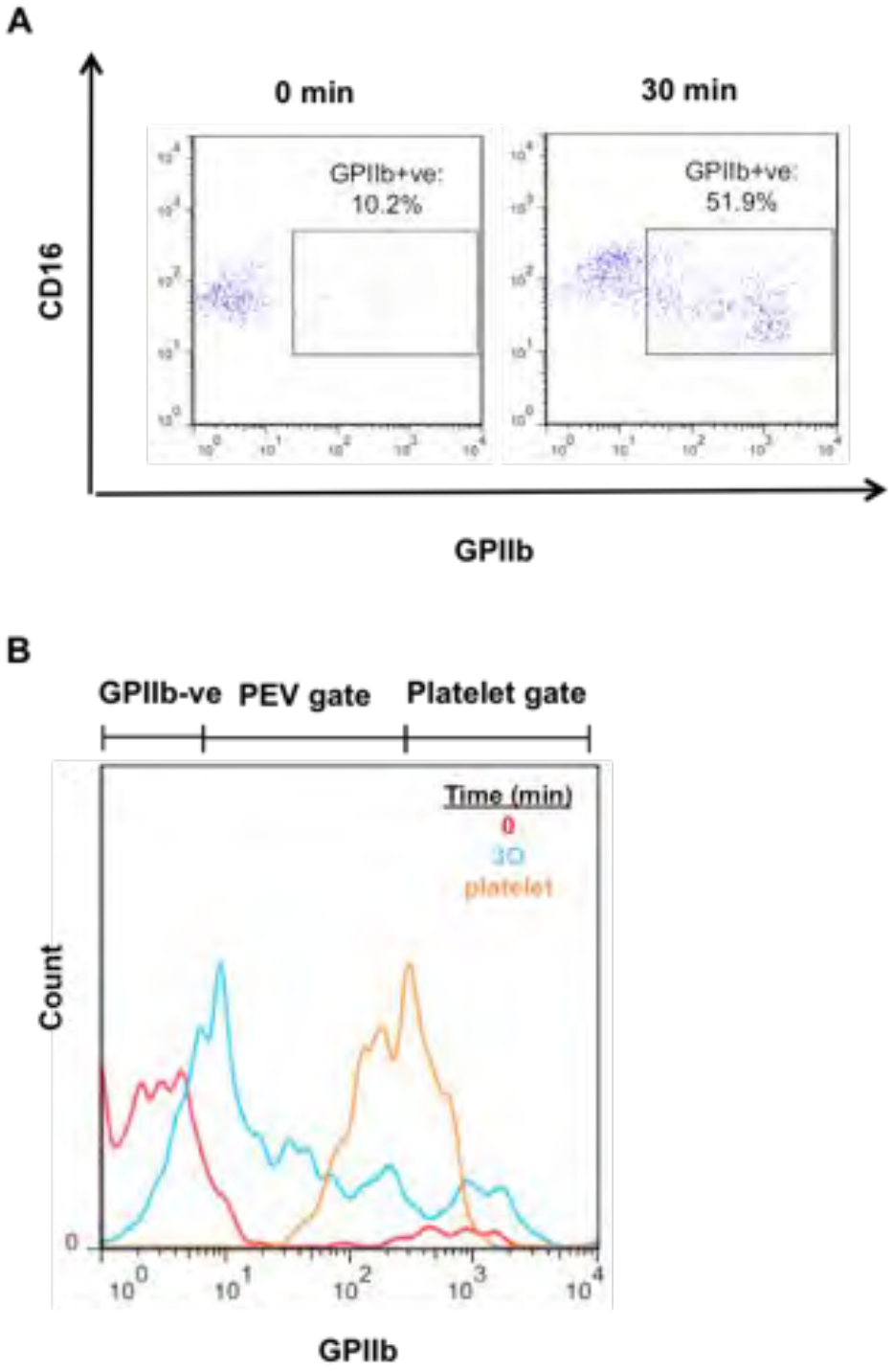

Figure 4.15. Formation of aggregates between CD16+ve monocytes and platelets and/or PEV in whole blood in response to treatment with 100µM TRAP

(A) Representative FACS dotplots demonstrating percentage of GPIIb+ve CD16+ve monocytes and **(B)** representative FACS overlay histograms demonstrating GPIIb expression on CD16-ve monocytes before and after 30 minutes stimulation with 100µm TRAP under roller mixing. Gate of positive events was set by isotype sample (not shown).

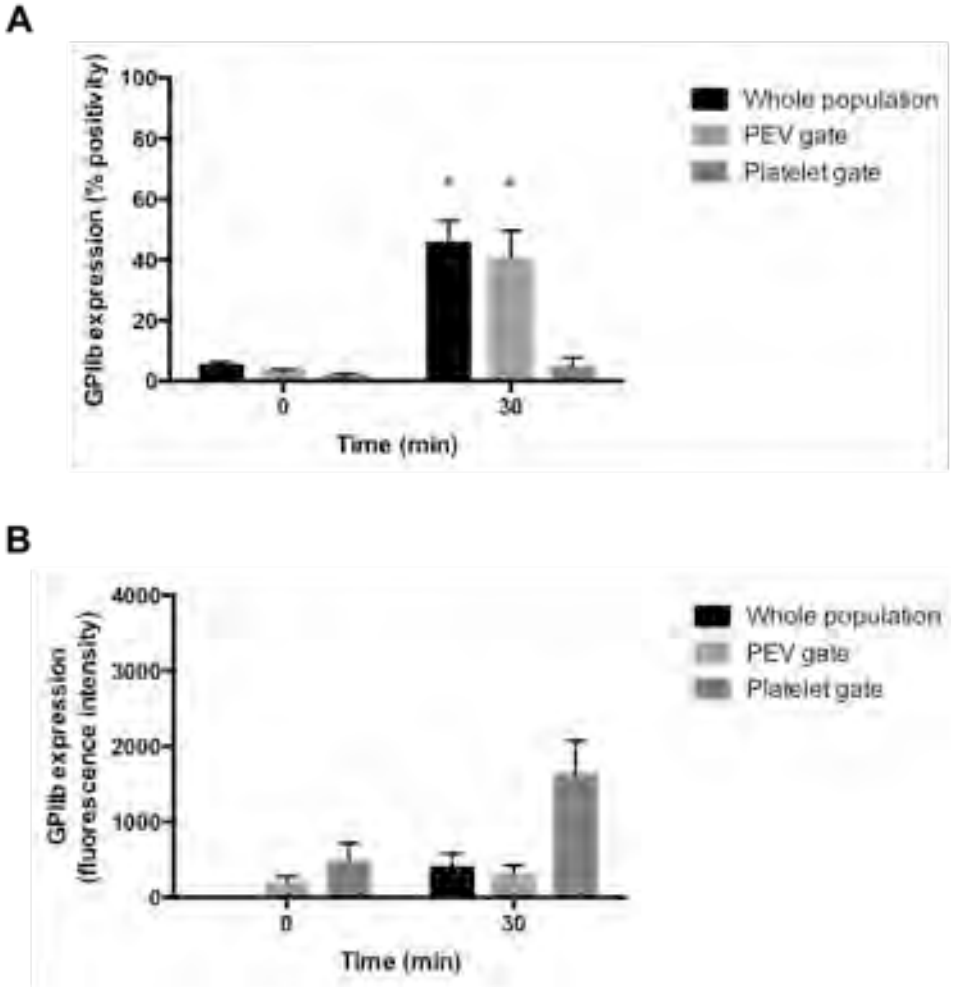

Figure 4.16. Formation of aggregates between CD16+ve monocytes and platelets and/or PEV in whole blood over time in response to 100µM TRAP

(A) Percentage of GPIIb+ve CD16+ve monocytes as a whole, in the PEV gate and in the Platelet gate after treatment with TRAP. **(B)** Median GPIIb expression on CD16-ve monocytes as a whole, in the PEV gate and in the Platelet gate. Data are represented as mean +/- SEM of 3 experiments. All data were analysed by T-tests to determine difference between 0-min and 30-min samples. * indicates $P < 0.05$.

4.3.2.3 Formation of Aggregates between PEV and Neutrophils

We also investigated the acquisition of PEV-borne GPIIb by the neutrophil population. There is minimal percentage of cells that are positive for GPIIb before TRAP treatment and there is a high number of events in the GPIIb+ve gate for the 30-min sample, suggesting that neutrophils form aggregates with platelets and/or PEV upon TRAP treatment in the blood (**Fig. 4.17A**). The TRAP-treated sample also shows higher

expression of GPIIb compared to the control. There is bimodal expression, one peak of lower and one of higher expression than the platelet expression. This result suggests that a subpopulation of neutrophils binds preferentially to PEV, and another subpopulation binds to platelets (**Fig. 4.17B**).

Upon graphical analysis of a number of experiments, we observed that the percentage of the whole neutrophil population, the neutrophil population in the PEV gate and in the platelets gate, all significantly increased upon treatment with TRAP (**Fig. 4.18A**). However, the median GPIIb expression of neutrophils after 30-min incubation with TRAP did not increase significantly (**Fig. 4.18B**).

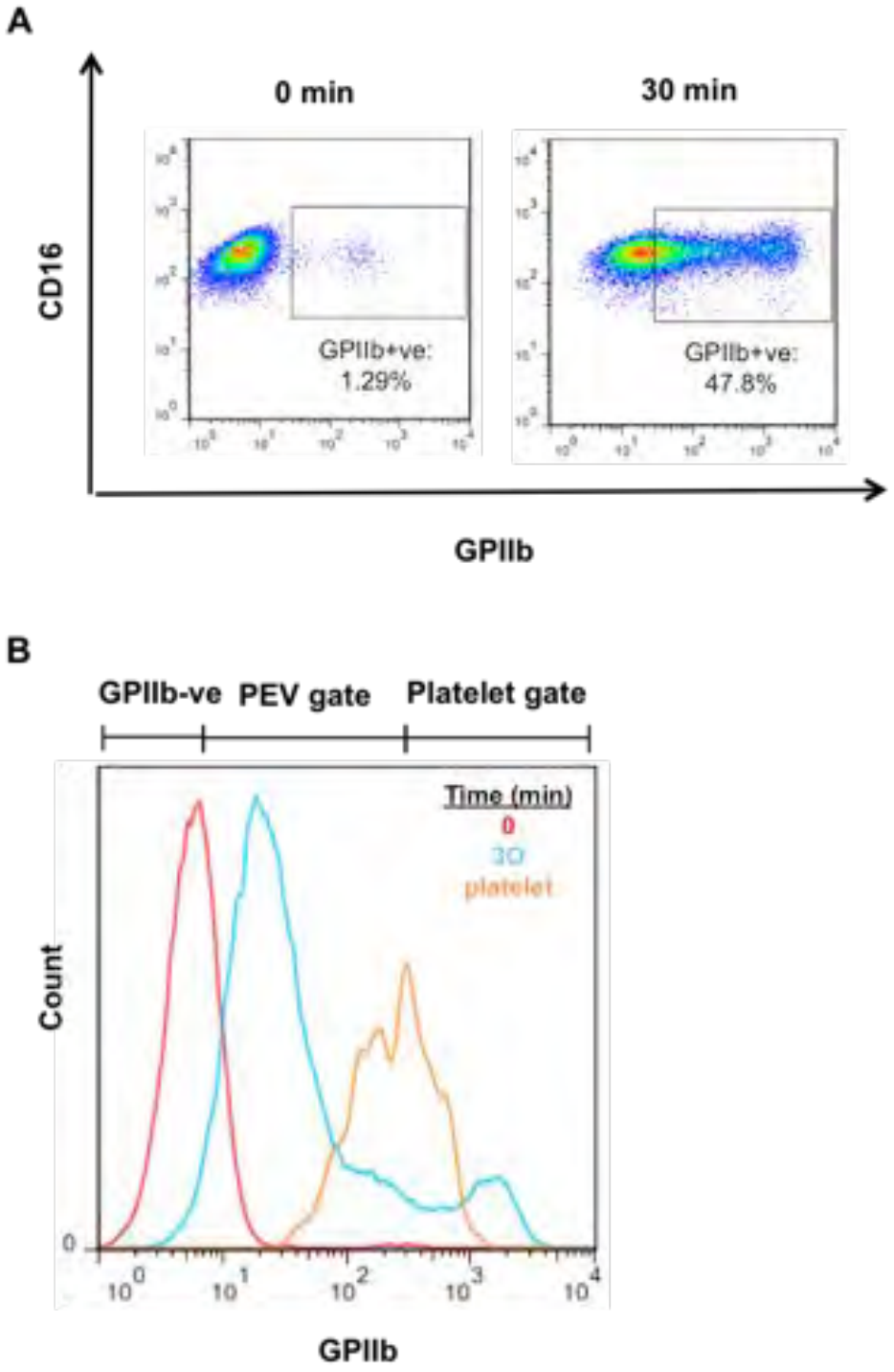

Figure 4.17. Formation of aggregates between neutrophils and platelets and/or PEV in whole blood in response to treatment with 100µM TRAP

(A) Representative FACS dotplots demonstrating percentage of GPIIb+ve neutrophils and **(B)** representative FACS overlay histograms demonstrating GPIIb expression on neutrophils before and after 30 minutes stimulation with 100µm TRAP under roller mixing. Gate of positive events was set by isotype sample (not shown).

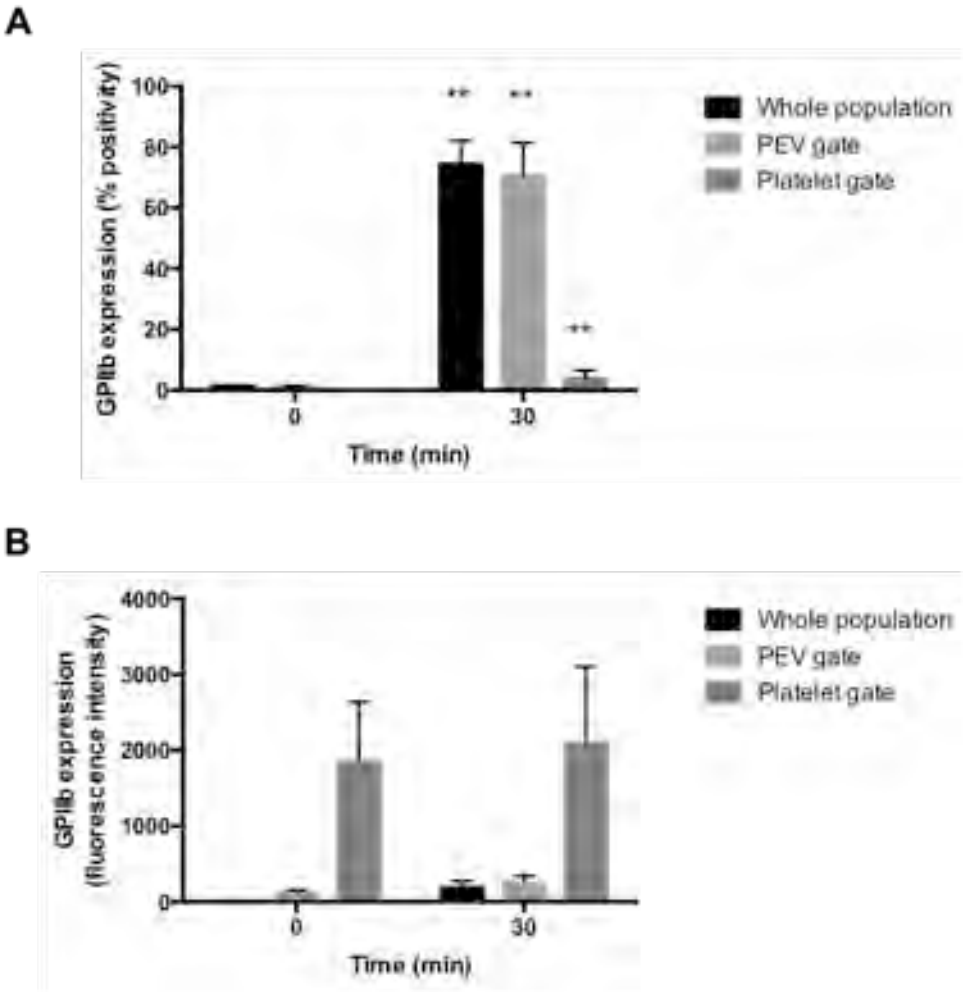

Figure 4.18. Formation of aggregates between neutrophils and platelets and/or PEV in whole blood over time in response to 100µM TRAP

(A) Percentage of GPIIb+ve neutrophils as a whole, in the PEV gate and in the Platelet gate after treatment with TRAP. **(B)** Median GPIIb expression on neutrophils as a whole, in the PEV gate and in the Platelet gate. Data are represented as mean +/- SEM of 3 experiments. All data were analysed by T-tests to determine difference between 0-min and 30-min samples. ** indicates $P < 0.01$.

4.3.2.4 Formation of Aggregates between PEV and Lymphocytes

The acquisition of PEV-borne GPIIb by the lymphocyte population was also investigated. There is minimal percentage of cells that are positive for GPIIb before TRAP treatment and there is a little higher number of events in the GPIIb+ve gate for the 30-min sample, suggesting that lymphocytes form aggregates with platelets and/or PEV upon TRAP treatment in the blood to a small extent (**Fig. 4.19A**). The TRAP-treated sample shows a little higher expression of GPIIb compared to the control. There is bimodal expression, one peak of lower and one of higher expression than the platelet expression. This result suggests that a small subpopulation of neutrophils binds preferentially to PEV, and another small subpopulation binds to platelets (**Fig. 4.19B**).

Upon graphical analysis of a number of experiments, we observed that the percentage of the whole neutrophil population and the neutrophil population in the PEV gate significantly increased upon treatment with TRAP (**Fig. 4.20A**). However, the median GPIIb expression of neutrophils after 30-min incubation with TRAP did not increase significantly (**Fig. 4.20B**).

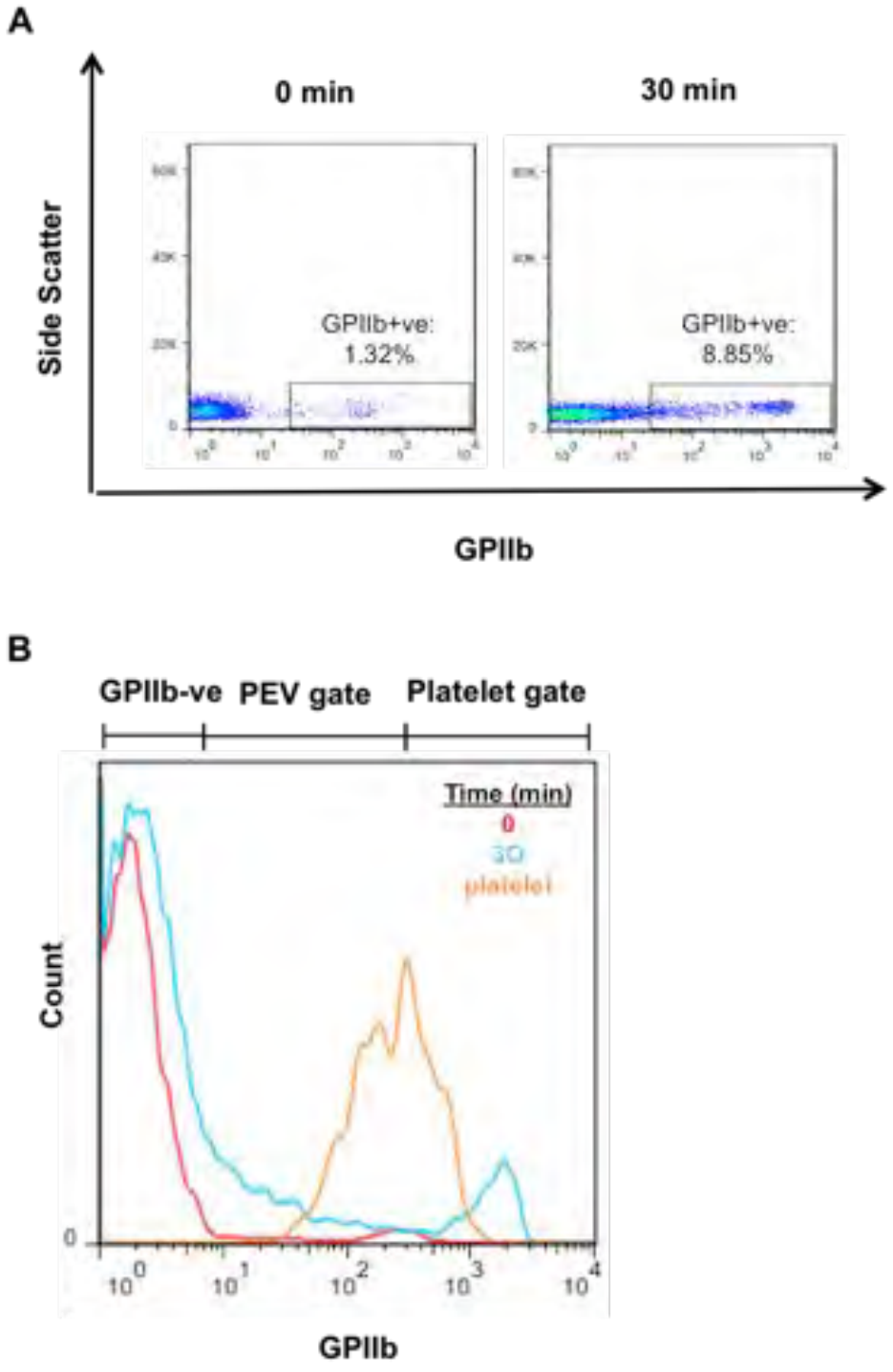

Figure 4.19. Formation of aggregates between lymphocytes and platelets and/or PEV in whole blood in response to treatment with 100µM TRAP

(A) Representative FACS dotplots demonstrating percentage of GPIIb+ve lymphocytes and **(B)** representative FACS overlay histograms demonstrating GPIIb expression on lymphocytes before and after 30 minutes stimulation with 100µm TRAP under roller mixing. Gate of positive events was set by isotype sample (not shown).

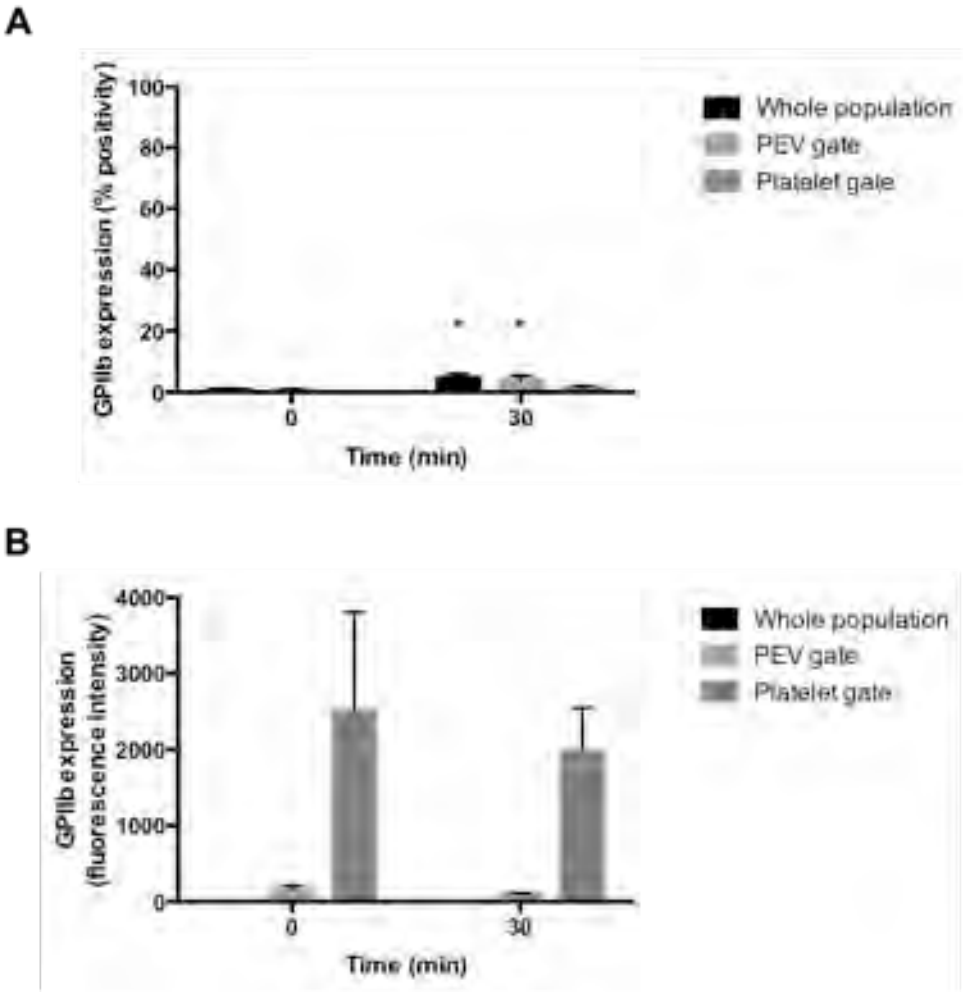

Fig. 4.20. Formation of aggregates between neutrophils and platelets and/or PEV in whole blood over time in response to 100μM TRAP

(A) Percentage of GPIIb+ve lymphocytes as a whole, in the PEV gate and in the Platelet gate after treatment with TRAP. **(B)** Median GPIIb expression on lymphocytes as a whole, in the PEV gate and in the Platelet gate. Data are represented as mean +/- SEM of 3 experiments. All data were analysed by T-tests to determine difference between 0-min and 30-min samples. * indicates $P < 0.05$.

4.4 Discussion

The potential of PEV released from activated platelets in stimulated whole blood to form aggregates with leukocytes was investigated. CPDA-anticoagulated blood was incubated under conditions of roller mixing at 37°C in the presence of the platelet stimulant TRAP in order to cause PEV shedding and to investigate the binding of these

PEV, if any, to leukocytes. Heterotypic aggregation was detected by FACS, based on presence of platelet/PEV-borne GPIb or GPIIb on the leukocytes.

It has been shown that the anticoagulant used critically affects measurement of circulating platelet-leukocyte aggregates (Bournazos et al., 2008). Citrate acts as an anticoagulant by chelating free calcium and so inhibiting platelet activation. However, its inhibitory action on platelets is reversible. Upon platelet stimulation with agonists, calcium ions get released from platelets and overcome the ionic equilibrium promoted by the citrate as a chelator. However, EDTA is a stronger calcium chelator that does not allow platelets to recover efficiently; hence platelet activation and associated PEV release would be inhibited. Heparin on the other hand has a different mechanism of action; it binds and enhances the inhibitory activity of plasma antithrombin against several serine proteases of the coagulation system such as thrombin and factor Xa. Heparin-anticoagulated blood was found to contain the highest level of platelet-leukocyte complexes at basal levels (Basavaraj et al., 2012). Hence, CPDA seemed to be the best choice.

The percentage of leukocytes acquiring GPIb or GPIIb in the blood increased significantly with addition of TRAP. Based on fluorescence intensity readings, we discovered that leukocytes acquired GPIb / GPIIb in quanta that are significantly smaller than whole platelets at resting conditions. This suggested that leukocytes bound PEV. This result agrees with our data from Chapter 3, where it was shown that PEV carry significantly lower GPIbα and GPIIb cargo than platelets. It has already been shown that platelet activation causes the release of GPIb+ve PEV (Flaumenhaft et al., 2009). GPIb release from activated platelets (Michelson, 1994; Schmitz et al., 1998; Hourdillé et al., 1992; Hourdillé et al., 1990) and GPIIb release (Chen et al., 2015) would

result in decreased platelet GP signal, hence one could argue that the low signal on the leukocytes does not come from PEV, but from whole platelets that have lost a portion of these molecules. However this cannot be true as platelet activation with TRAP in the blood resulted not in a single but in two GPIb/GPIIb+ve expression curves on the leukocytes, with the higher expression curve being at the levels of resting platelets or even higher, and the lower expression curve lying at significantly lower expression levels than resting platelets. This suggested the presence of two distinct GPIb- or GPIIb+ve populations i.e. platelets and PEV.

Leukocyte-platelet/PEV aggregation before any treatment upon immediate fixation after venepuncture was minimal in our experiments. Overall, PEV exhibited a preferential affinity for binding monocytes. Lymphocytes exhibited the lowest affinity for forming heterotypic aggregates with PEV and neutrophils exhibited an intermediate affinity.

The two main monocyte subsets exhibited similar but not identical patterns of PEV acquisition. Both subsets were able to form aggregates with whole platelets to some extent. CD16+ve monocytes exhibit a greater propensity for binding platelets than CD16-ve monocytes, however, both monocyte subsets exhibit a higher affinity for PEV rather than platelets. According to proteomics analysis > 200 proteins are differentially expressed between CD16+ and CD16- monocytes, resulting in functional differences between them (Zhao et al., 2009), hence their differential interaction with PEV at times could be the result of differential expression of surface receptors.

Other laboratories that investigated platelet-leukocyte interactions found high levels of whole platelets bound to leukocytes (Nagasawa et al., 2013; Xiao and Theroux, 2004; Jensen et al., 2001) and did not mention anything about PEV binding. We argue

that in these experiments whole platelets bound to leukocytes because the experiment was performed in static conditions without any shear imposed, hence their result is an artefact of their experimental procedure. In our laboratory we could detect high levels of whole platelets bound to leukocytes (mainly monocytes) even without activation with a stimulant if blood was left under static conditions. However when shear is imposed on the previously static blood, the platelet unbind from leukocytes. Indeed, in our experiments with TRAP we detected low levels of whole platelets bound to leukocytes and the signal from these platelets decreased with time of incubation under low shear stress conditions.

In this study, we used a combination of CD14 and CD16 expression as well as forward scatter and side scatter characteristics to differentiate between leukocyte types. Another study used pan-leukocyte marker CD45 gating combined with side scatter to measure platelet-leukocyte aggregates by flow cytometry (Nagasawa et al., 2013). Both gating strategies appear to be able to differentiate leukocyte types adequately. However, CD45 staining alone cannot differentiate between monocyte subsets.

The number of PEV bound per monocyte/leukocyte could not be determined precisely in these experiments as we used a Cyan ADP to analyse leukocytes in lysed blood. A Cyan ADP cannot detect vesicles hence we could not compare fluorescence intensity of GPIb/GPIIb on a single PEV with fluorescence intensity of one of these markers on leukocytes in the blood to get an idea on how many PEV bound leukocytes.

Previous studies in our lab assessed the level of platelet/PEV-leukocyte aggregates in the blood in response to platelet activation using the thromboxane mimetic U46619, rhodocytin, ADP, CRP-XL and calf thymous histones (Box CL et al.,

2014). Rhodocytin, which is found in snake venom and activates platelets through binding the surface receptor CLEC-2 (Suzuki-Inoue et al., 2006), appeared to be the most potent agonist, resulting in the highest number of monocyte-platelet/PEV aggregates. On the other hand, ADP, U46619 and CRP-XL exhibited a much lower maximum response. A lower level of heterotypic aggregates was expected with ADP and the thromboxane mimetic as these are known to be weak activators (secondary, released from the platelets).

In this study we assumed that the presence of the platelet receptors GPIb and GPIIb on leukocytes is evidence of PEV binding. However there is a possibility that these receptors were shed from platelets independently of vesicles. We tried to answer this question in the next chapters (Chapters 5 and 6).

Conclusions

PEV exhibit a high affinity for forming heterotypic aggregates preferentially with monocytes in activated whole blood. The binding is time-dependent and non-monocyte subset dependent. PEV showed lower affinity for binding other leukocyte types, such as lymphocytes and neutrophils.

5 CHARACTERISATION OF PEV-LEUKOCYTE AGGREGATES USING EXOGENOUS PEV

5.1 Introduction

As suggested from our experiments in Chapter 4, activation of whole blood with TRAP results in the release of PEV from platelets that preferentially form heterotypic aggregates with monocytes. Preferential affinity for monocytes by PEV has been also recently observed in anti-coagulated whole blood that was stored for 3 hours upon collection (Weiss et al., 2018). However, formation of PEV-leukocyte aggregates upon exogenous PEV administration has not been exclusively investigated to date.

Eitan et al., 2017 showed that incubation of plasma-derived EV with washed PBMCs resulted in the formation of aggregates between EV and monocytes and between EV and B cells. T cells did not form aggregates with the EV. A higher percentage of monocytes aggregated with the plasma EV than B cells. The percentage of monocytes and B cells that aggregated with the plasma EV was dose-dependent and time-responsive in the assay. In these experiments, plasma EVs activated monocytes and B cells. Other studies have found that EV from RBC units bound to purified monocytes but not T-cells when incubated together in culture and induced pro-inflammatory cytokine secretion (Danesh et al., 2013). In addition, EV from the blood of diabetes patients formed preferential aggregates with monocytes than with the rest blood cells and also increased monocyte cytokine levels when incubated together *in vitro* (Freeman et al., 2018). In all these studies the authors did not investigate the cell origin of the EV. The effects noted on the monocytes might have arisen at least partly from PEV.

The presence of PEV on the leukocytes in Chapter 4 was judged by the presence of the platelet receptors GPIb and GPIIb in quanta that were significantly smaller than whole platelets. However there is a possibility that these receptors were shed from platelets independently of vesicles. One way to answer this question would be to label a

different component of PEV than proteins, i.e. the surrounding membrane. However, trying to label the PEV membrane in whole blood would result in labelling the plasma membrane of all blood cells. Hence, there is need for PEV purification in order to stain their membrane independently of blood. Labelled PEV can subsequently be incubated with whole blood to determine any aggregation.

Provision of exogenous PEV changes the dynamics of PEV-leukocyte aggregation seen in Chapter 4. With exogenous PEV there is a constant number of PEV available to interact with leukocytes, which are all available upon addition. When inducing PEV release in the blood with agonists or during prolonged storage, there is continuous shedding of PEV in the blood hence the number of PEV available to interact with leukocytes increases with time. In addition, incubation of exogenous PEV with leukocytes allows investigation of PEV binding independently of platelets. Only PEV are labeled in theory (given that purification of PEV from whole platelets is efficient), hence any signal on the leukocytes is PEV-derived since endogenous platelets remain unstained and should be undetected.

The aims for this chapter were to:

1) Investigate the potential of exogenous PEV to form aggregates with monocytes and other leukocytes.
2) Investigate the dynamics of leukocyte-PEV aggregation.
3) Detect differences if any between CD16+ve and CD16-ve monocytes in their capacity to form aggregates with exogenous PEV.

5.2 Methodology

5.2.1 Formation of Aggregates between Leukocytes in Blood and exogenously provided PEV

Purified PEV (produced from platelet stimulation with CRP-XL), stained with anti-GPIbα antibody or PKH67 dye were incubated with CPDA-anticoagulated blood at 37˚C on a roller mixer, either over the course of 20 minutes or for 10 minutes at different concentrations of PEV (from 2 x 10^7 PEV to 2 x 10^{10} PEV incubated with 200µl of blood) in order to generate PEV-leukocyte aggregates and investigate the dynamics of the interaction. Heterotypic aggregation was detected by FACS (Cyan ADP). Statistical analysis was performed using Graph Pad Prism 6. (For further detail see methods section 2).

5.2.2 Formation of Aggregates between Washed Monocytes in Blood and PEV

Purified PEV were incubated with washed monocytes in phosphate buffered saline with Ca2+/Mg2+ (0.2µm pore-filtered) over the course of 65 minutes at 37˚C on a roller mixer in order to investigate the dynamics of heterotypic aggregation. Heterotypic aggregation was detected by FACS (Cyan ADP). Statistical analysis was performed using Graph Pad Prism 6. (For further detail see methods section 2).

5.3 Results

5.3.1 Formation of Aggregates between Leukocytes in Blood and GPIb-labeled PEV over a Time-Course

Upon observing that platelet activation in the blood resulted in the release of PEV that form aggregates with leukocytes, preferentially monocytes, we wanted to

investigate this interaction in more detail. In this case, we generated purified PEV, stained for GPIbα, and incubated them with blood, under shear over a 20-minute time-course. We incubated 2 x 10^9 PEV with 200µl of blood as 2 x 10^9 PEV is the average number of PEV we get from 6 x 10^7 platelets which is the number of platelets there is on average in 200 µl of blood.

5.3.1.1 Formation of Aggregates between PEV and CD16-ve Monocytes

Representative flow cytometry dot-plots show acquisition of PEV by CD16-ve monocytes over the course of 20 minutes (**Fig. 5.1**). There is negligible background signal for GPIbα expression before PEV addition to the blood (0-min sample). There is clearly a higher percentage of cells positive for GPIbα at all time points compared to the 0-min control, hence exogenously-provided PEV are forming heterotypic aggregates with the CD16-ve monocytes. The percentage of GPIbα-ve CD16-ve monocytes increases with time.

We also analysed the GPIbα histograms of the CD16-ve monocytes. The traces from each time point and controls were overlaid. The GPIbα expression trace of platelets was also overlaid on each histogram. The distribution curve is at all time points greatly shifted towards higher expression compared to the 0-min control. The shift becomes larger with time (**Fig. 5.2A**). The expression at all times is significantly lower than the platelet expression indicating that CD16-ve monocytes are only binding PEV.

The percentage of CD16-ve monocytes expressing GPIbα was analysed statistically. The percentage expressing GPIbα increases significantly by time of

incubation with PEV, hence formation of CD16-ve monocyte-PEV aggregates is time-dependent (one-way anova) (**Fig. 5.2B**).

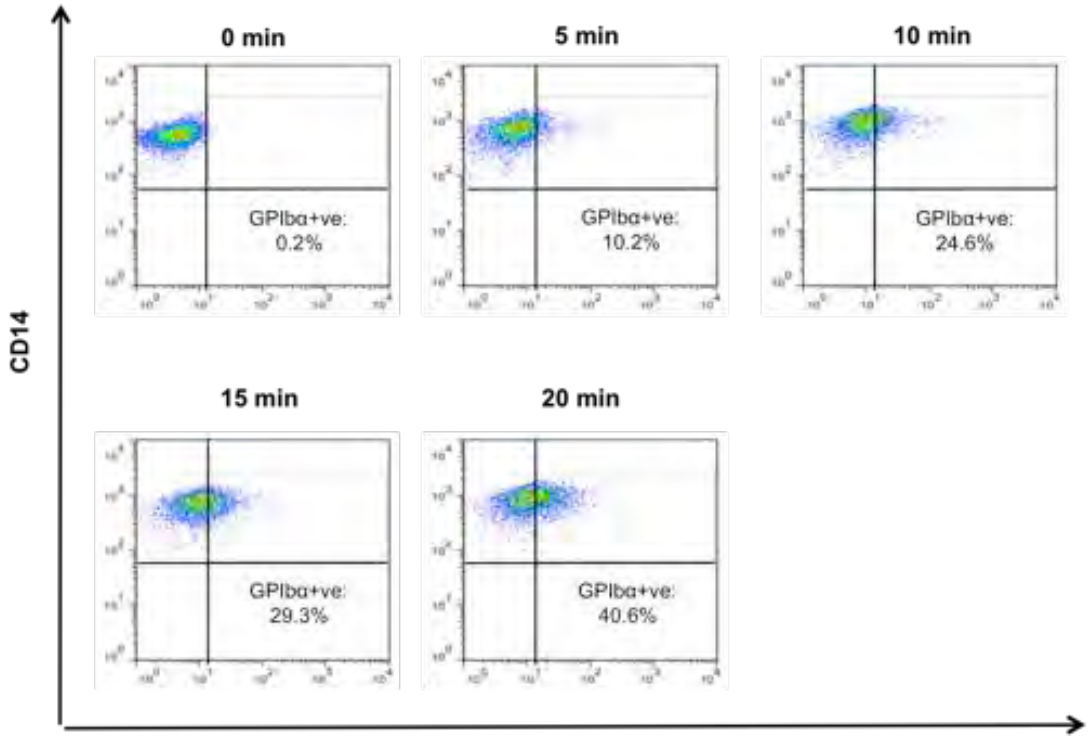

Figure 5.1. Formation of aggregates between CD16-ve Monocytes in blood and added PEV over time

Representative FACS dotplots demonstrating percentage of CD16-ve monocytes positive for GPIbα over time. Gate of positive events was set by isotype sample (not shown).

The median fluorescence intensity of GPIbα expression on CD16-ve monocytes was also analysed statistically and found to increase significantly with time of incubation with PEV. Hence, formation of CD16-ve monocyte-PEV aggregates is time-dependent (**Fig. 5.2C**).

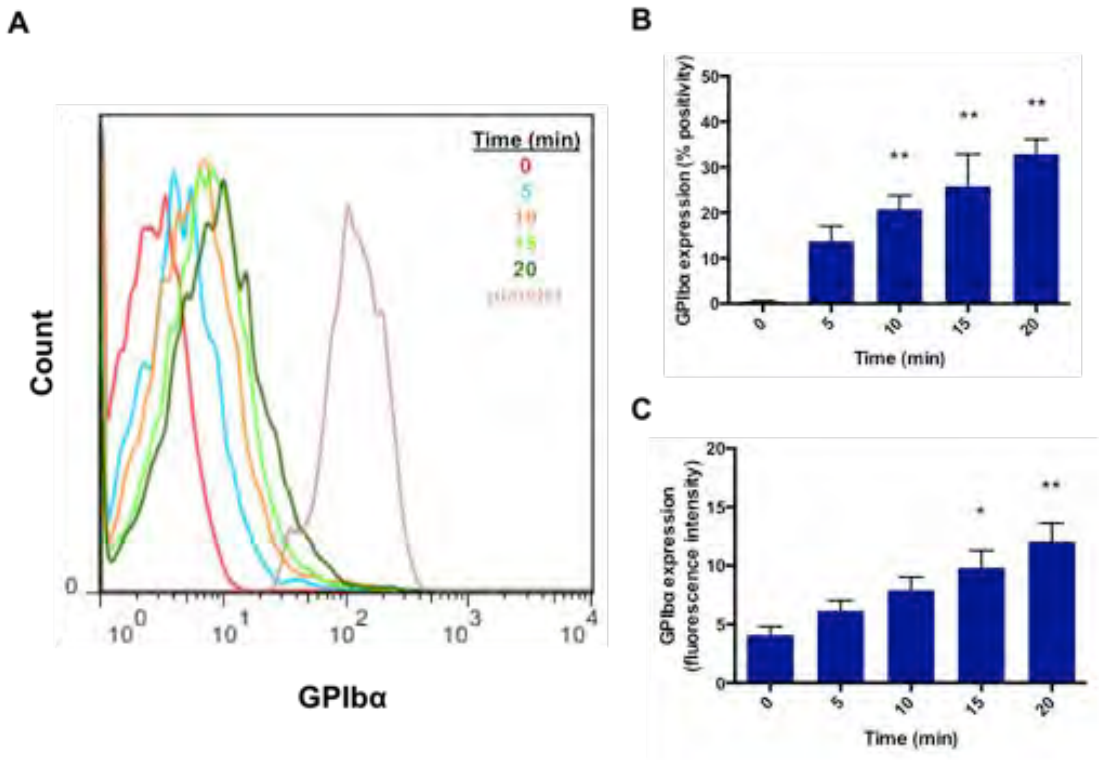

Figure 5.2. Formation of aggregates between CD16-ve monocytes in blood and added PEV over time

(A) Representative FACS overlay histograms demonstrating GPIbα expression on CD16-ve monocytes over time. The trace of platelets is overlaid. **(B)** Percentage of GPIIb+ve CD16-ve monocytes over time. **(C)** Median GPIbα expression on CD16-ve monocytes and. Data are represented as mean +/- SEM of 3-4 experiments. Data were analysed by One-way ANOVA to determine effect of time. All data were analysed by One-way ANOVA to determine effect of time, and by Dunnett's multiple comparisons test. ** indicates $P<0.01$.

5.3.1.2 Formation of Aggregates between PEV and CD16+ve Monocytes

Acquisition of PEV-borne GPIbα by the CD16+ve monocyte subset over the course of 20 minutes is shown in representative flow cytometry dotplots of **Figure 5.3**. There is negligible background signal for GPIbα expression before PEV addition to the blood (0-min sample). There is clearly a higher percentage of cells positive for GPIbα at all time points compared to the 0-min control, hence exogenously-provided PEV are

forming heterotypic aggregates with the CD16+ve monocytes. The percentage of GPIbα-ve CD16+ve monocytes seems to increase by time.

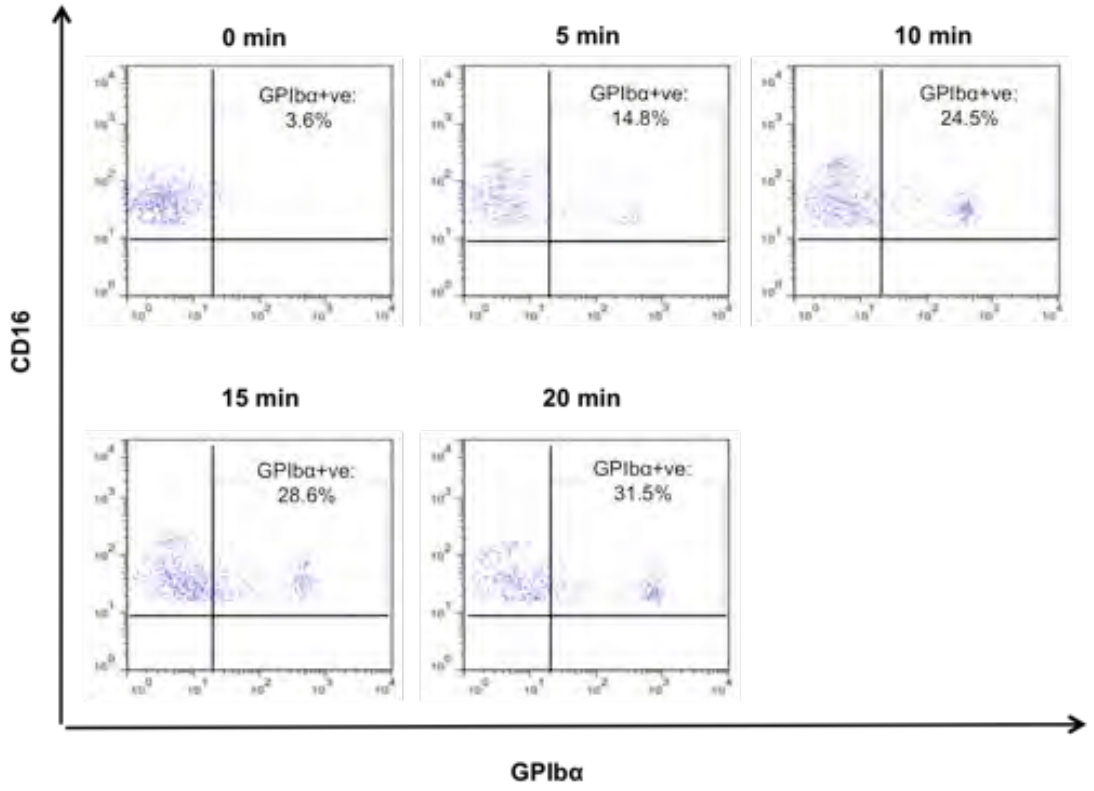

Figure 5.3. Formation of aggregates between CD16+ve monocytes in blood and added PEV over time

Representative FACS dotplots demonstrating percentage of GPIbα+ve CD16+ve monocytes over time. Gate of positive events was set by isotype sample (not shown).

The histogram of GPIbα expression is different for the CD16+ve monocytes compared to CD16-ve (**Fig. 5.4A**). This distribution seems to be bimodal, having two peaks, even though the peak of higher expression is relatively small. This peak falls at the levels of staining found on platelets. This means that the majority of CD16+ve monocytes form aggregates with PEV and a very low percentage of the cells may bind to the platelets that were not removed during the PEV purification step.

The percentage of CD16+ve monocytes expressing GPIbα and the median GPIbα expression in the PEV gate was analysed statistically. Both parameters increased significantly with time of incubation with PEV, hence formation of CD16+ve monocyte-PEV aggregates is time-dependent (**Fig. 5.4B** and **C**).

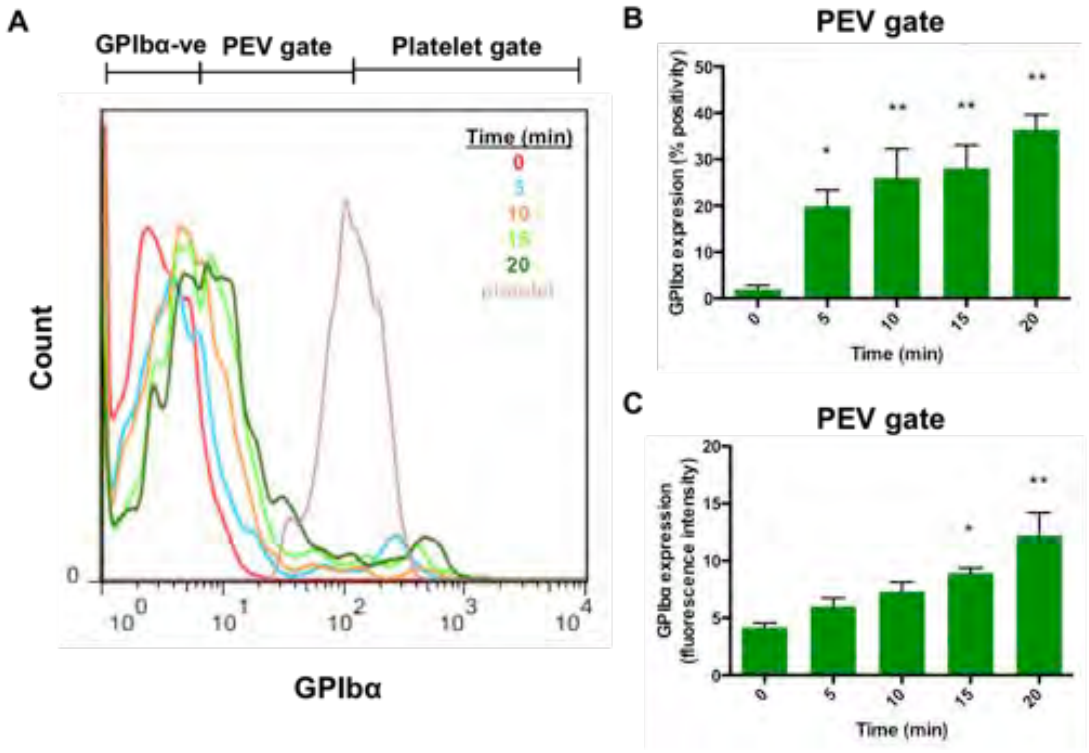

Figure 5.4. Formation of aggregates between CD16+ve monocytes in blood and added PEV over time

(A) Representative FACS overlay histograms demonstrating GPIbα expression on CD16+ve monocytes over time. The trace of platelets is overlaid. **(B)** Percentage of GPIIb+ve CD16+ve monocytes over time. **(C)** Median GPIbα expression on CD16+ve monocytes and. Data are represented as mean +/- SEM of 3-4 experiments. Data were analysed by One-way ANOVA to determine effect of time, and by Dunnett's multiple comparisons test. ** indicates P<0.01.

5.3.1.3 Formation of Aggregates between PEV and other Leukocyte Populations

Interestingly, in this format of the PEV binding assay, we could not observe significant acquisition of GPIb on neutrophils (**Fig. 5.5** and **5.6**). Although a small

population (<5% showed some positive staining, this was extremely low fluorescent intensity and was not significantly different from untreated control samples).

Lymphocytes showed a similar response, with a small population (1-2%) showing low levels of staining, again this was not significantly different from control samples (**Fig. 5.7** and **5.8**).

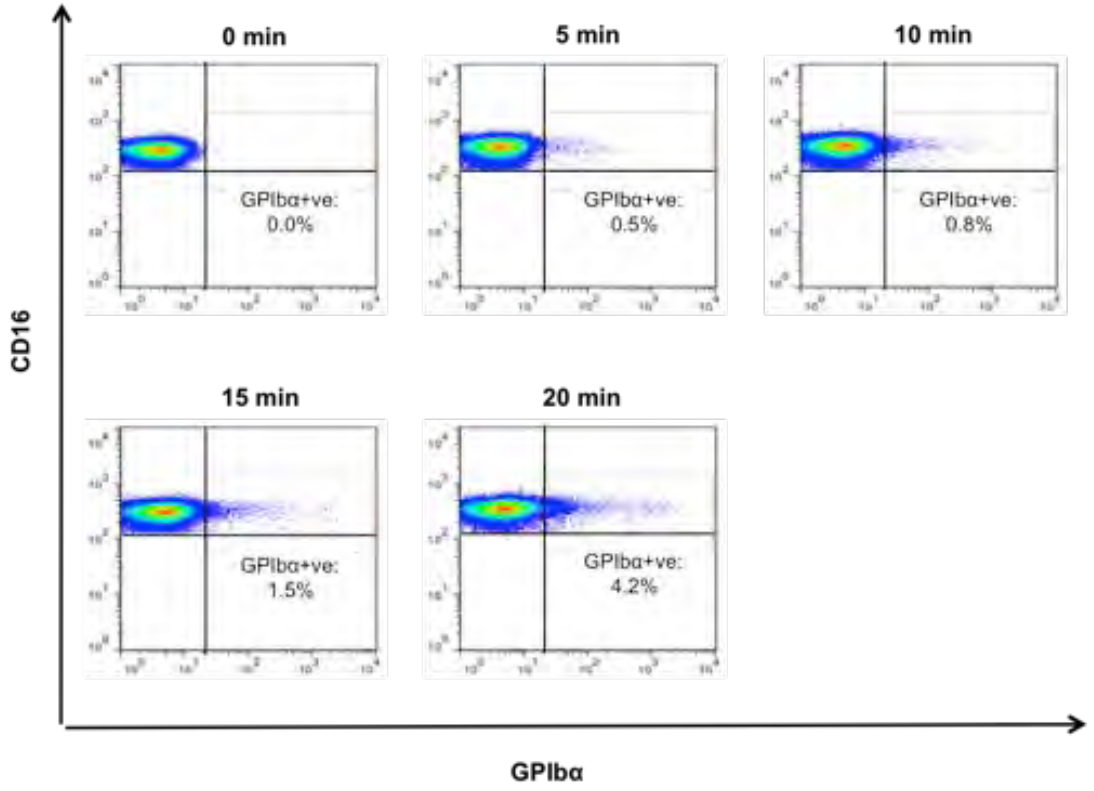

Figure 5.5. Formation of aggregates between Neutrophils in blood and added PEV over time

Representative FACS dotplots demonstrating percentage of GPIbα+ve neutrophils over time. Gate of positive events was set by isotype sample (not shown).

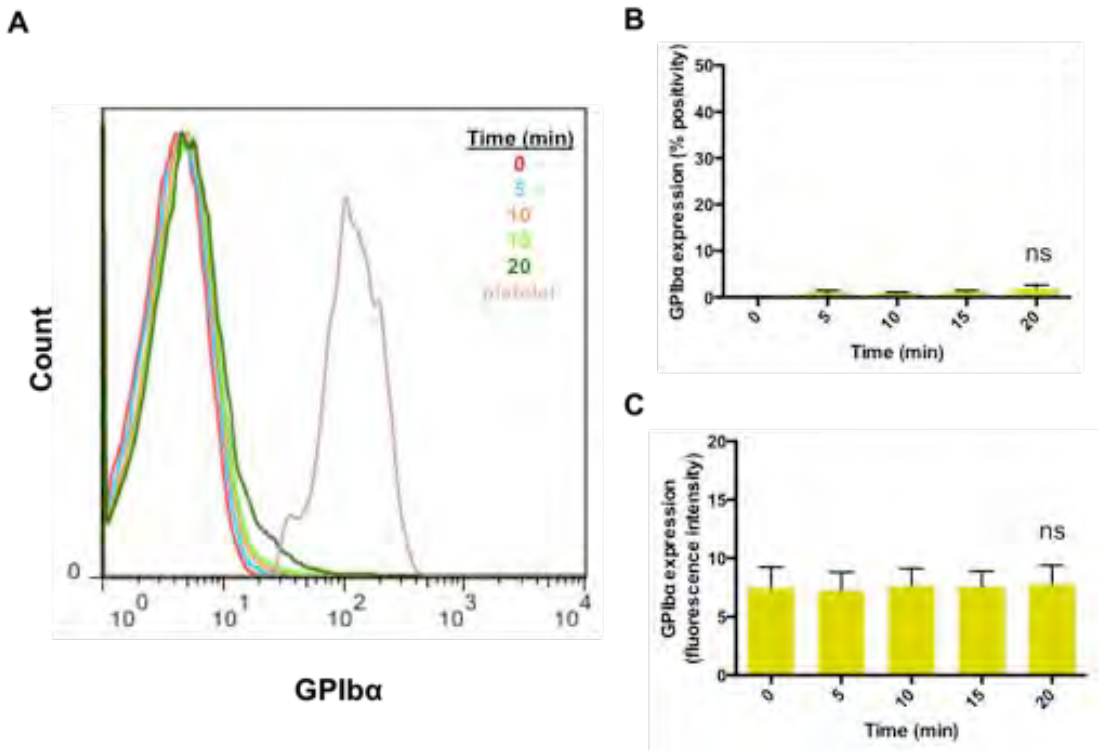

Figure 5.6. Formation of aggregates between Neutrophils in blood and added PEV over time

(A) Representative FACS overlay histograms demonstrating GPIbα expression on neutrophils over time. The trace of platelets is overlaid. **(B)** Percentage of GPIIb+ve neutrophils over time. **(C)** Median GPIbα expression on neutrophils. Data are represented as mean +/- SEM of 3-4 experiments. Data were analysed by One-way ANOVA to determine effect of time. ns indicates P>0.05.

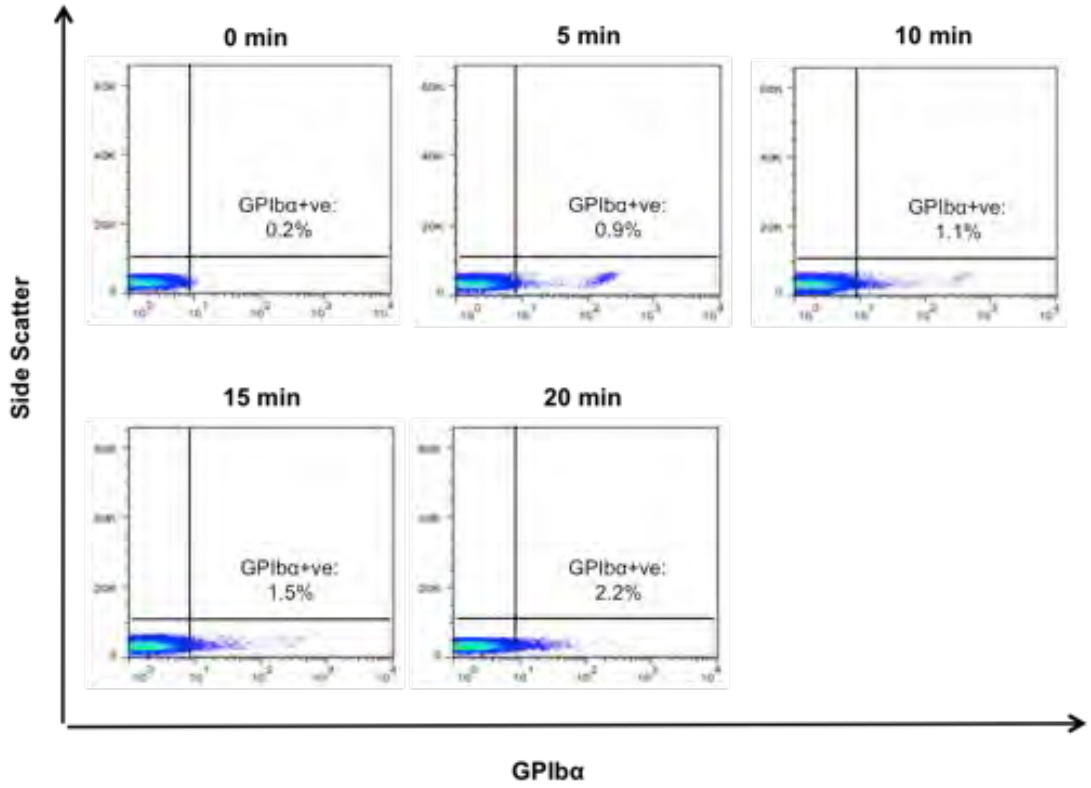

Figure 5.7. Formation of aggregates between Lymphocytes in blood and added PEV over time

Representative FACS dotplots demonstrating percentage of GPIbα+ve neutrophils over time. Gate of positive events was set by isotype sample (not shown).

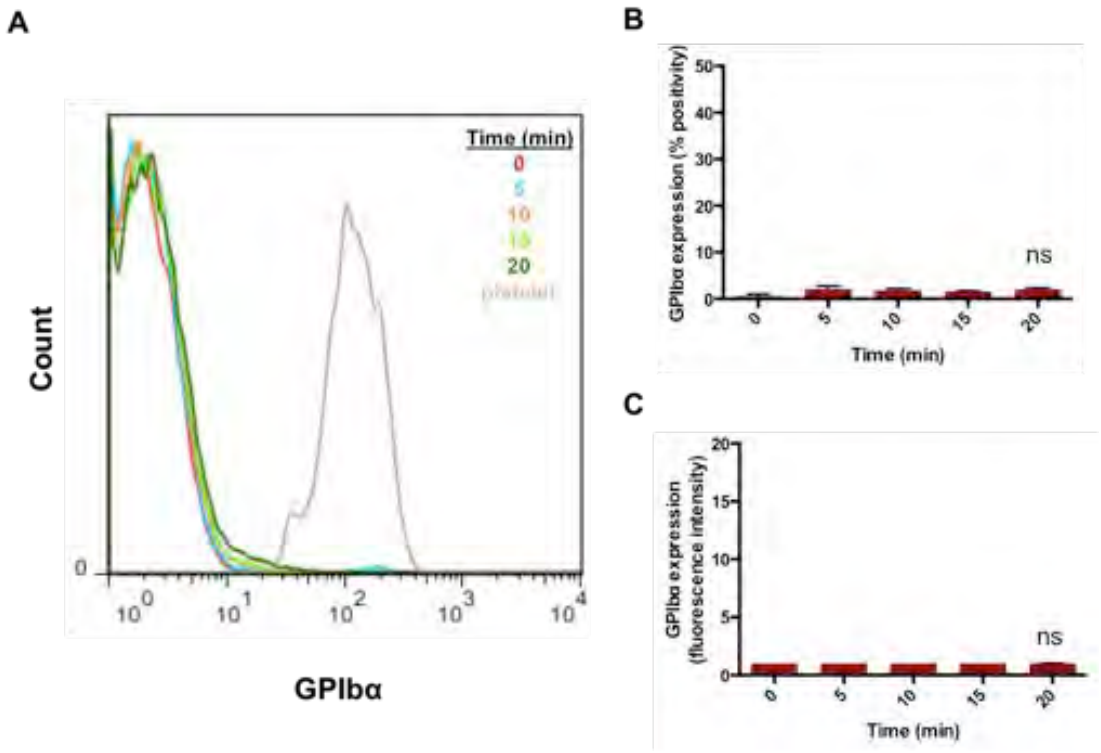

Figure 5.8. Formation of aggregates between Lymphocytes in blood and exogenously provided PEV over time

(A) Representative FACS overlay histograms demonstrating GPIbα expression on lymphocytes over time. The trace of platelets is overlaid. **(B)** Percentage of GPIIb+ve lymphocytes over time. **(C)** Median GPIbα expression on lymphocytes. Data are represented as mean +/- SEM of 3-4 experiments. Data were analysed by One-way ANOVA to determine effect of time. ns indicates P>0.05.

5.3.2 Formation of Aggregates between Leukocytes in Blood and GPIb-labeled PEV over a Concentration Gradient

Upon observation that PEV added into blood form aggregates preferentially with monocytes in a time-dependent manner, we hypothesized that the formation of these heterotypic aggregates depends on the number of PEV incubated with blood and that there is a threshold beyond which, monocytes can no longer aggregate with any more PEV. Hence, we added GPIbα-stained purified PEV into blood over a concentration gradient; from subphysiological numbers (2 x 10^8), to physiological numbers (2 x 10^{10}) and incubated for 10 minutes at 37°C under shear. At the end of incubation, we

measured the percentage of GPIbα+ve leukocytes and the median fluorescence intensity of GPIbα on the leukocytes by FACS.

Representative flow cytometry dot-plots and histograms can be found in Supplementary Material (**Fig. 12.1 – 12.5**). The percentage of leukocytes expressing GPIbα and the median fluorescence intensity of GPIbα from a number of experiments on the different leukocyte populations is shown in **Fig. 5.10**. The percentage of CD16-ve and CD16+ve monocytes and that of neutrophils expressing GPIbα increases significantly by increasing the number of PEV incubated with blood (**Fig. 5.10A**), whereas the percentage of lymphocytes expressing GPIbα does not. The median GPIbα expression of CD16-ve and CD16+ve monocytes was also found to increase significantly by increased PEV concentration, whereas that of neutrophils and lymphocytes does not (**Fig. 5.10B**).

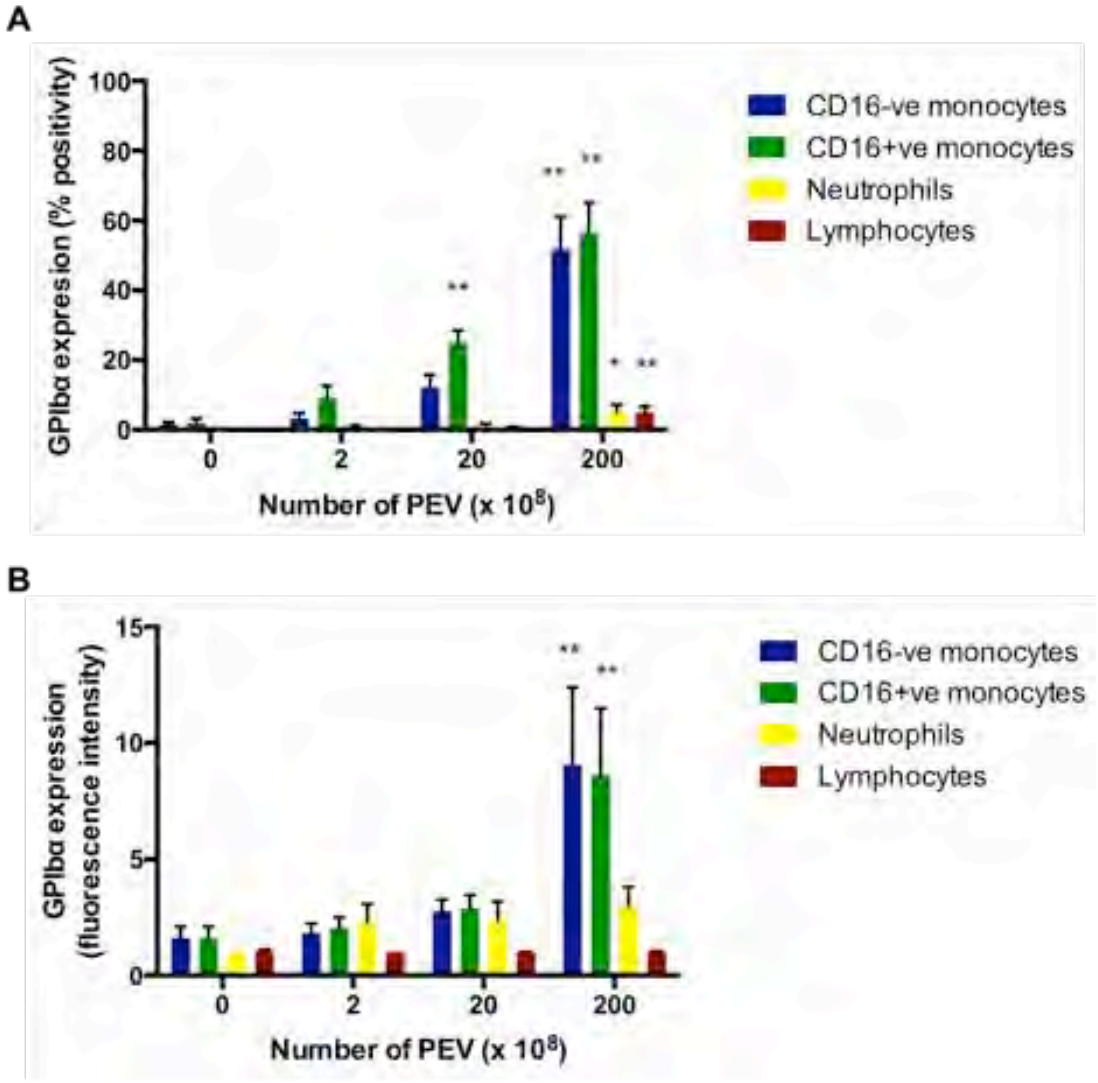

Figure 5.9. Formation of aggregates between leukocytes in blood and exogenously provided PEV over a PEV concentration gradient

(A) Percentage of GPIbα+ve leukocytes over time. **(B)** Median GPIbα expression on the different leukocyte populations. Data are represented as mean +/- SEM of 3-4 experiments. Data were analysed by One-way ANOVA to determine effect of PEV concentration, and by Dunnett's multiple comparison test. * indicates $P<0.05$, ** indicates $P<0.01$.

5.3.3 Formation of Aggregates between Leukocytes in Blood and PKH67-labeled PEV over a Time-Course

There was a possibility that labelling PEV with antibodies physically obstructed the formation of aggregates with leukocytes due to the comparable size of antibodies with the smallest of exosomes. In addition, PEV were about 75% positive for GPIbα as judged by FACS, whereas PKH67 lipophilic dye was found to label 100% of PEV (see section 3.3.1). Hence, we decided to repeat incubation of blood with washed PEV, this time by staining with PKH67 that marks the PEV membrane, over the same 20-min time-course. The PKH67 dye was used because it does not leak and it does not get transferred from cell to cell.

Representative flow cytometry dot-plots and histograms can be found in the Supplementary Material (**Fig. 12.6 – 12.10**). The percentage of the different leukocytes expressing PKH67 and their respective fluorescence intensity is shown in **Figure 5.10**. The percentage of CD16-ve and CD16+ve monocytes expressing PKH67 increases significantly with time of incubation with PEV, whereas that of neutrophils and lymphocytes does not (**Fig. 5.10A**). The median PKH67 expression of all leukocytes did not increase significantly with time (**Fig. 5.10B**).

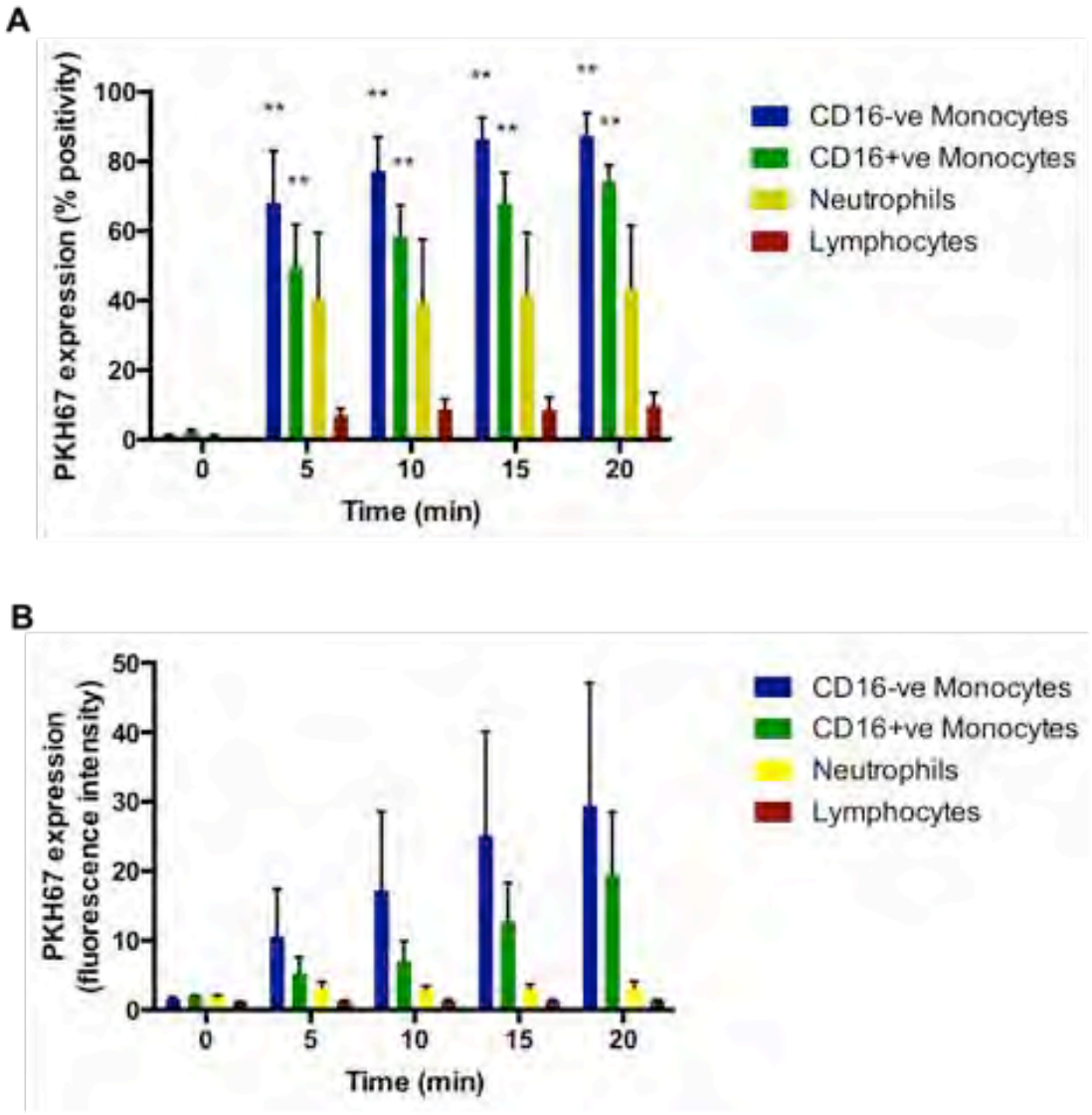

Figure 5.10. Formation of aggregates between leukocytes in blood and exogenously provided PEV over time

(A) Percentage of PKH67+ve leukocytes over time. **(C)** Median PKH67 expression on the different leukocyte populations. Data are represented as mean +/- SEM of 3-4 experiments. Data were analysed by One-way ANOVA to determine effect of time and by Dunnett's multiple comparison test. ** indicates $P<0.01$.

5.3.4 Formation of Aggregates between PEV and Washed Monocytes over a Time-Course

Upon observation that PEV show a preferential affinity for binding monocytes, we wanted to isolate the interaction between PEV and monocytes, to observe its dynamics in more detail. Washed monocytes were incubated with PEV at a physiological ratio at 37°C and under roller mixing over the course of 60 minutes.

5.3.4.1 Formation of Aggregates between PEV and CD16-ve Monocytes

Representative flow cytometry dot-plots can be found in the Supplementary Material (**Fig. 12.11**). The GPIbα expression histograms for CD16-ve at all time points are shown in **Figure 5.11A**. The expression profile for platelets is also overlaid. CD16-ve monocytes exhibit one peaks of positive GPIbα expression; Lower than that of platelets. Hence, CD16-ve monocytes aggregated with PEV. The expression profile of monocytes from 10 minutes of incubation onwards is about the same. The expression profile of monocytes at 5 minutes of incubation is lower. Hence, heterotypic aggregation is time-dependent, but after10 minutes of incubation, monocytes reach a point of saturation.

Upon statistical analysis, the percentage of CD16-ve monocytes was found to increase significantly with time (**Fig. 5.11B**). However, the median GPIbα expression does not change significantly with time (**Fig. 5.11C**). However, there seems to be a clear trend with CD16-ve monocytes acquiring GPIbα at an increasing trend up to 20 minutes of incubation, reaching a maximum, and subsequently the amount of GPIbα on them starts decreasing.

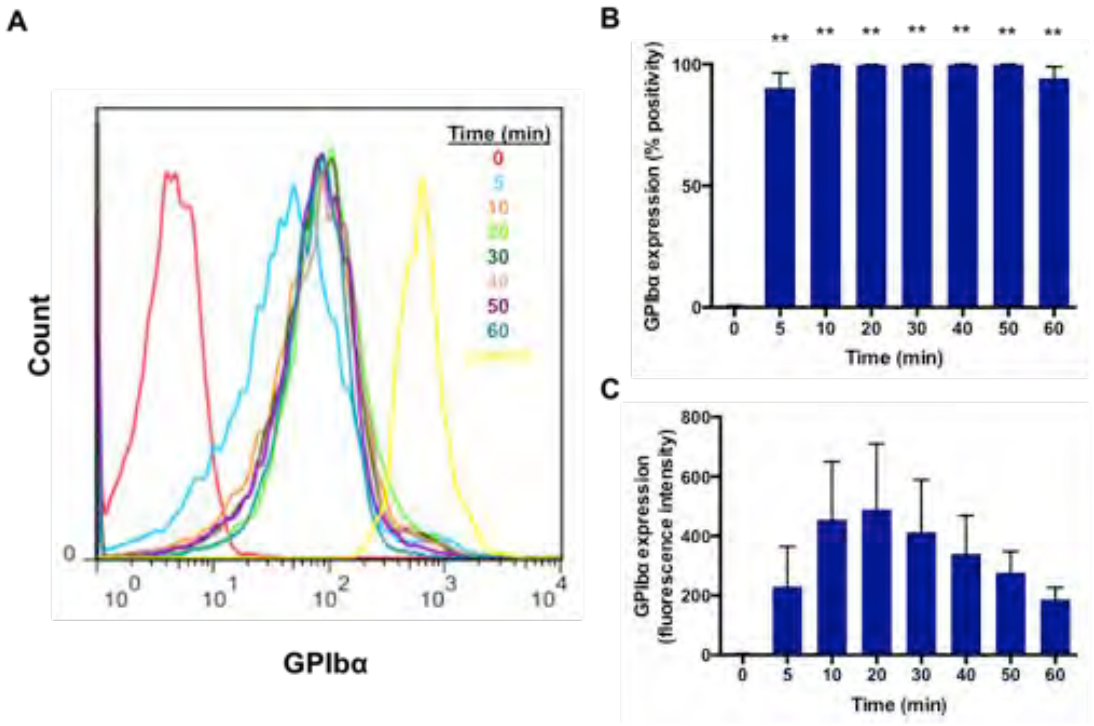

Figure 5.11. Formation of aggregates between washed CD16-ve monocytes and washed PEV over time

(A) Representative FACS overlay histograms demonstrating GPIbα expression on CD16-ve monocytes over time. The trace of platelets is overlaid. **(B)** Percentage of GPIbα+ve CD16-ve monocytes over time. **(C)** Median GPIbα expression on CD16-ve monocytes. Data are represented as mean +/- SEM of 3-4 experiments. Data were analysed by One-way ANOVA to determine effect of time and by Dunnett's multiple comparison test. ** indicates P<0.01.

5.3.4.2 Formation of Aggregates between PEV and CD16+ve Monocytes

Representative flow cytometry dot-plots can be found in the Supplementary Material (**Fig. 12.12**). The GPIbα expression histograms for CD16+ve at all time points are shown in **Figure 5.12A**. The expression profile for platelets is also overlaid. CD16-ve monocytes exhibit one peak of positive GPIbα expression; Lower than that of platelets. Hence, CD16+ve monocytes aggregated with PEV. The expression profile of monocytes from 10 minutes of incubation onwards is about the same. The expression profile of monocytes at 5 minutes of incubation is lower. Hence, heterotypic aggregation

is time-dependent, but after10 minutes of incubation, monocytes reach a point of saturation.

Upon statistical analysis, the percentage of CD16-ve monocytes was found to increase significantly with time (**Fig. 5.12B**). However, the median GPIbα expression does not change significantly by time (**Fig. 5.12C**). However, there seems to be a clear trend with CD16-ve monocytes acquiring GPIbα at an increasing trend up to 20 minutes of incubation, reaching a maximum, and subsequently start decreasing the amount of GPIbα on them.

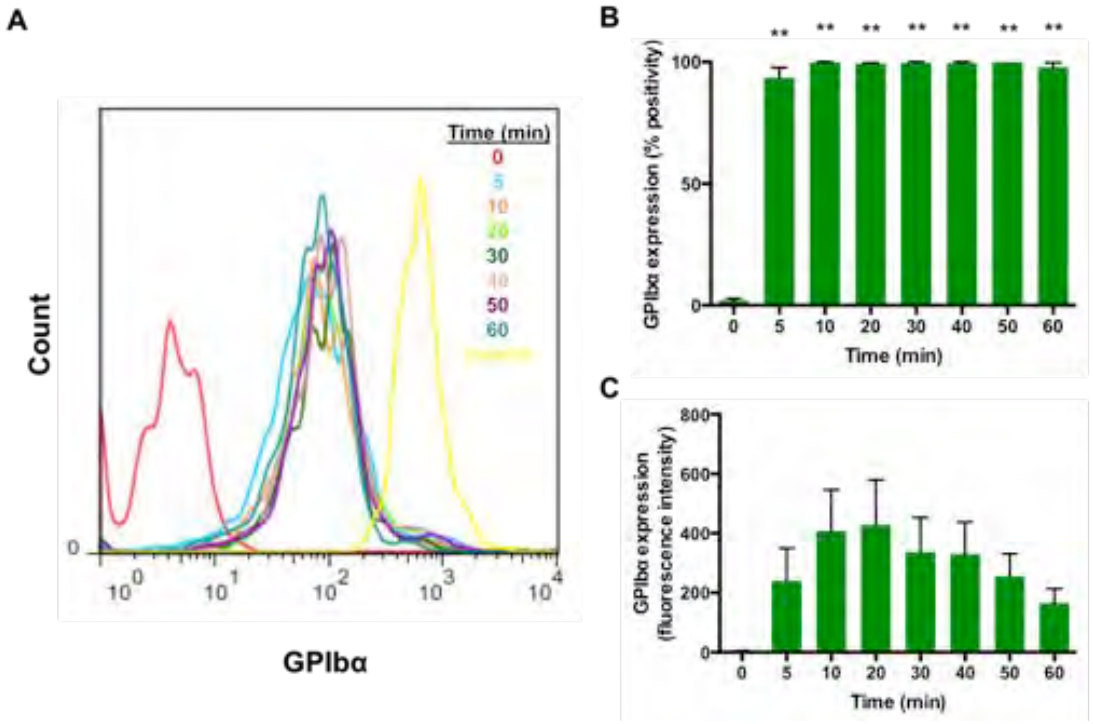

Figure 5.12. Formation of aggregates between washed CD16+ve monocytes and washed PEV over time

(A) Representative FACS overlay histograms demonstrating GPIbα expression on CD16+ve monocytes over time. The trace of platelets is overlaid. **(B)** Percentage of GPIbα+ve CD16+ve monocytes over time. **(C)** Median GPIbα expression on CD16+ve monocytes. Data are represented as mean +/- SEM of 3-4 experiments. Data were analysed by One-way ANOVA to determine effect of time, and by Dunnett's multiple comparison test. ** indicates P<0.01.

5.4 Discussion

The potential of PEV released from activated platelets to form aggregates with leukocytes was investigated. To our knowledge this was the first study to assess formation of aggregates between leukocytes and exogenously added PEV. PEV were produced from stimulation of washed platelets with CRP-XL and they were subsequently incubated with whole blood or washed monocytes under conditions of roller mixing. Heterotypic aggregation was detected by FACS, based on presence of platelet/PEV markers on the leukocytes. The dynamics of this experiment are different from the previous experiment in Chapter 4 where platelets were being stimulated continuously in the blood, and blood was stained for platelet/PEV markers at the end of incubation. In this case, PEV were exogenously provided so that a stable number of PEV to leukocytes. In addition, these PEV are purified and stained before incubation with blood so that platelet contamination is limited and so we can observe only stained PEV-leukocyte interactions without platelet interference.

Overall, PEV exhibited a preferential affinity for binding monocytes. The neutrophils and the lymphocytes exhibited some indications of binding with PEV, however this behaviour was significantly lower than the behaviour of monocytes. The two monocyte subsets exhibited similar mode of PEV acquisition. The binding of PEV to both monocyte subsets is time-dependent and proportional to the PEV concentration. These results agree with our results in Chapter 4.

Presence of PEV on the monocytes was confirmed by antigen expression GPIb and presence of PEV membrane (PKH67 dye). GPIb is a receptor for von Willebrand factor (VWF). Binding of GPIb to VWF initiates platelet deposition on the compromised vessel wall and upon platelet activation this complex is cleaved (Morrison et al., 2014).

Platelet activation has been shown to cause a decrease in GPIb on platelets (Bergmeier et al., 2004; Wang et al., 2010; Gardiner et al., 2007), due to both shedding and its incorporation and release into PMV.

A higher percentage of aggregates between monocytes and PEV was noted when exogenous PEV were marked with PKH67 dye rather than with an anti-GPIbα antibody, hence staining EV with antibodies might cover a significant area of the surface of the EV, this way obstructing EV-cell interactions. Also this could be due to the fact that not all PEV express these glycoproteins; we found that the majority of the larger PMV express them but we do not know if this is also true for the smaller PMV that could not get detected by flow cytometry and the exosomes. A higher percentage of aggregates between monocytes and PEV was also noted when PEV were incubated with washed monocytes than with blood. This was expected, as other cells or other vesicles and compounds in the blood may in theory physically obstruct access of PEV to monocytes. In addition, some PEV form aggregates with other leukocytes as we observed, and they may also form aggregates with the platelets in the blood. Hence, a portion of PEV might get consumed elsewhere, leaving lower numbers available to interact with monocytes.

The number of PEV bound per monocyte/leukocyte could not be determined precisely in these experiments as we used two different flow cytometers. A BD Accuri was used to run unpurified/purified PEV and determine staining levels, whereas lysed blood and purified monocytes were ran on a Dako Cyan ADP to determine platelet/PEV markers staining level on leukocytes. A Cyan ADP cannot detect vesicles hence we could not compare fluorescence intensity of GPIb/PKH67 on a single PEV with fluorescence intensity of one of these markers on leukocytes in the blood to get an idea on how many PEV bound leukocytes.

Presence of PEV-borne GPIbα in monocytes raised the critical prospect of this adopted GPIbα being functional. GPIbα is part of the GPIb-IX complex receptor for von Willebrand factor (VWF) that mediates initial platelet binding to the subendothelium (Savage et al.; 1996; Savage et al., 1998; Morrison et al., 2014). Indeed, further studies from our group revealed that perfusion of monocytes 'decorated' with PEV across immobilised human VWF resulted in significantly higher monocyte recruitment compared to monocytes perfused alone. This behaviour was GPIbα-dependent as monocyte recruitment was inhibited by the use of a function-neutralizing antibody against GPIbα (Chimen et al.; under review). This represents a novel thrombo-inflammatory pathway of leukocyte recruitment to the vessel wall, that may be relevant in atherosclerosis.

Conclusions

Exogenous PEV exhibit a high affinity for forming heterotypic aggregates preferentially with monocytes. This binding is time-dependent and not specific to a particular monocyte subset. PEV showed lower affinity for binding other leukocyte types such as lymphocytes and neutrophils. This interaction might be relevant in monocyte recruitment in atherosclerosis.

6 INTERNALISATION OF PEV BY MONOCYTES

6.1 Introduction

In chapters 4 and 5, it was found that PEV are able to form aggregates with leukocytes, preferentially monocytes. Experiments using acid (Feng et al., 2010) or trypsin (Franzen et al., 2014) that strip surface-bound EV off and staining EV with fluorescent lipid membrane dyes such as PKH67 (Na¨slund et al., 2014; Christianson et al., 2013) have proven microscopically that EV in general are largely endocytosed. Hence, we speculated that PEV could also get endocytosed in monocytes.

Endocytosis is the internalisation of extracellular material without passing through the cell membrane. There are four main distinct endocytic pathways; phagocytosis, macropinocytosis, clathrin-mediated and caveolae-mediated endocytosis (**Fig. 6.1**).

Phagocytosis is the receptor-mediated internalization of opsonised particles into plasma membrane-derived vacuoles called phagosomes. Upon detachment from the plasma membrane, the phagosomes fuse with endosomes and lysosomes, forming phagolysosomes, which degrade the internalized particles (Botelho and Grinstein, 2011). This process is largely and efficiently used by monocytes, macrophages and neutrophils mainly to kill pathogens, hence for material >1 μm in size (Akinc and Battaglia, 2013). However there is evidence that even small particles such as exosomes can also get phagocytosed (Feng et al., 2010). Phagocytosis blocking is often achieved by Phosphoinositide 3-kinases (PI3Ks) inhibition (Feng et al., 2010).

Macropinocytosis is a non-selective mechanism of extracellular fluid internalisation associated with cell surface ruffling. It is actin-driven, induced by activation of growth factor signalling pathways and requires Na+/H+ exchanger activity (Kerr and Teasdale, 2009). Extracellular material is endocytosed as part of the

extracellular fluid without direct contact with the membrane ruffles, hence it can accommodate a range of cargo sizes, reaching up to 1 μm (Swanson, 2008). Inhibition of this mechanism is often achieved by blocking the sodium/proton exchanger (Fitzner et al., 2011; Escrevente et al., 2011).

Clathrin-mediated endocytosis refers to progressive and sequential formation of vesicles covered with the coat-protein clathrin. These vesicles cause the membrane to collapse into a vesicular bud that matures and pinches off. This process continues with clathrin uncoating and fusion of the uncoated vesicle with the endosome with associated release of its contents. Clathrin-mediated entry is associated with particles with sizes ranging from 10 nm to 300 nm (Wasylewski et al., 1986; Heuser and Reese, 1973; Ehrlich et al., 2004).

Caveolin-dependent endocytosis involves caveolae, which are small cave-like invaginations of the plasma membrane, which, like clathrin-coated pits, get internalised in the cytoplasm. Caveolae are mainly composed of cholesterol, sphingolipids and proteins of the caveolin gene family (caveolin-1. -2, -3) (Kiss and Botos, 2009). This route has been shown to facilitate the entry of nanoparticles up to 100 nm in diameter (Wang et al., 2009). Clathrin- and caveolin-dependent endocytosis both require dynamin2 for the formation and expansion of the endocytic vesicles and its inhibition ablates endocytosis (Barre's et al., 2010).

EV have also been shown to gain entry for their cargo in recipient cells by non-endocytic pathways i.e. by EV membrane fusion with the plasma membrane of the recipient cells, followed by EV cytosol merging with the recipient cell cytoplasm (Montecalvo et al., 2012).

It is important to discover the internalisation mechanism as it determines the trafficking and intracellular fate of particles. EV uptake is affected by EV size, shape, material and surface coating and acceptor cell type, age and cellular environment (Iversen et al., 2011; Rejman et al., 2004; Yacobi et al., 2008; Doherty et al., 2009; Kumari et al., 2010; Sakhtianchi et al., 2013).

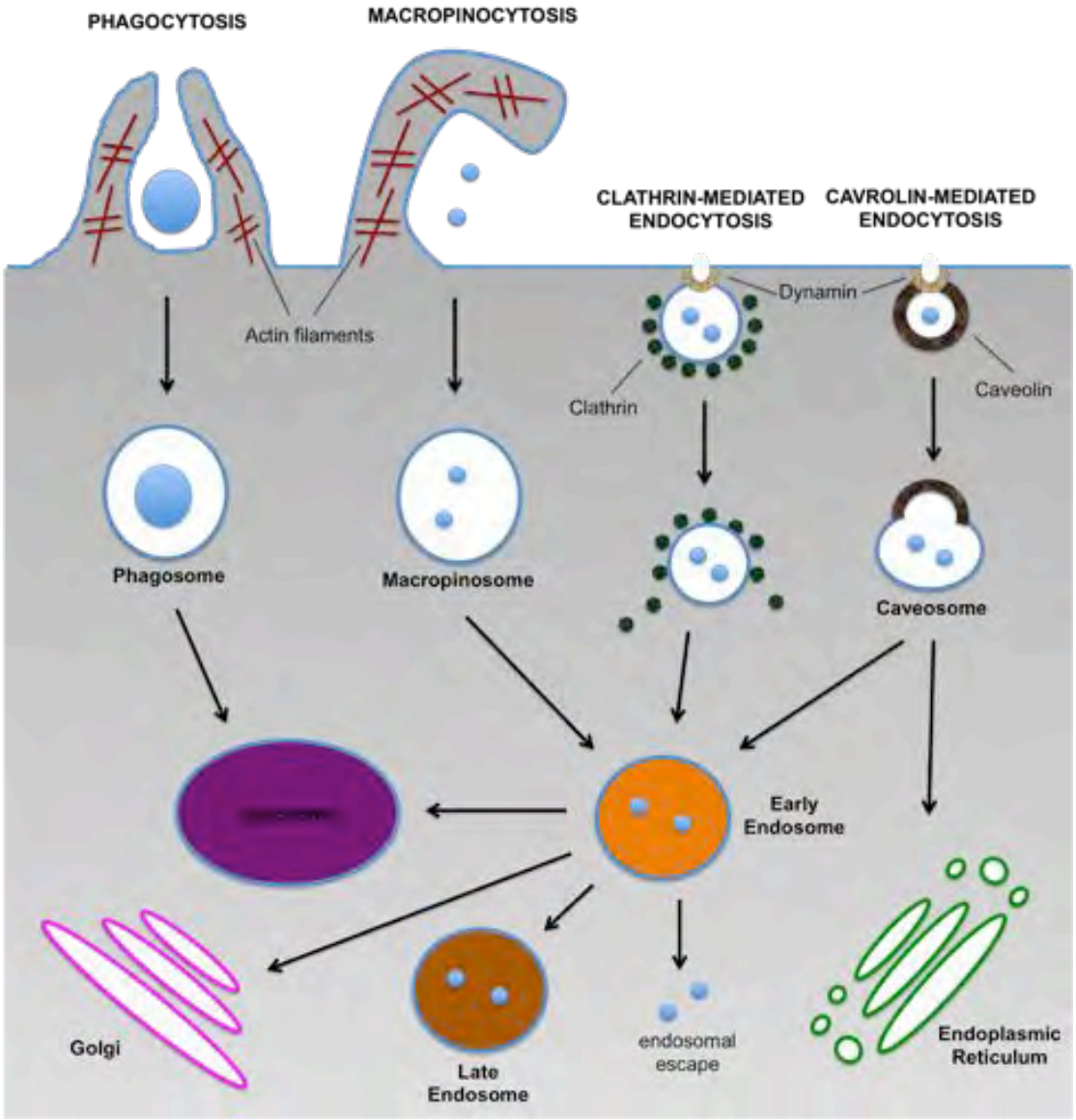

Figure 6.1. Main Pathways of Endocytosis

Extracellular matter is mainly internalised by phagocytosis or macropinocytosis that depend largely on the actin-mediated remodelling of the cell membrane, or by clathrin-

mediated endocytosis and caveolin-mediated endocytosis that depend on dynamin-mediated formation of endocytic vesicles.

PEV internalisation investigation by monocytes could provide us with insights on atherosclerosis pathology as it could be linked to the dysregulation of the LDL uptake cycle. In normal cells, the low-density lipoprotein receptor mediates the endocytosis of LDL, which provides the cells with the essential lipids to be used for growth of their membranes and as an energy source. The LDL is transferred to late endosomes and lysosomes, where lysosomal enzymes digest the cholesteryl esters of the LDL, releasing cholesterol and fatty acids (Goldstein and Brown, 2009). The cholesterol is either stored in the macrophages as cholesteryl esters in lipid droplets or effluxed to HDL particles that transfer it to the liver (Maxfield and Tabas, 2005).

In atherosclerosis, this process is dysregulated. Macrophages internalise excessive amounts of LDL, their cytoplasm becomes filled with cholesteryl ester lipid droplets and they enlarge and eventually the cells die of intracellular stress (Maxfield and Tabas, 2005; Moore and Tabas, 2011).

Platelets contain lysosomes that digest phagocytic and cytosolic components, similarly to nucleated cells. The function of platelet lysosomes has not been studied well, but platelet lysosomal glycohydrolases were found to be released "*in vivo*" in humans upon platelet activation (Ciferri et al., 2000). In addition, platelet-specific ablation of PIKfyve kinase, whose activity is essential for vesicle trafficking and cargo transport along the endosomal-lysosomal pathway (McCartney et al., 2014), resulted in impaired lysosomal secretion associated with accelerated arterial thrombosis and macrophage accumulation (Sang et al., 2014). Hence, there seems to be a link between platelet lysosomes and macrophage action in atherosclerosis and we further speculate that such an action could be mediated by PEV. PEV might get internalised into

monocytes and their contents might act on the monocyte lysosomes causing lysosomal dysfunction.

The aims for this chapter were to:

1. Discover whether PEV get internalised into monocytes.
2. Image PEV inside monocytes and determine distribution and fate (transfer into monocyte lysosomes?).
3. Investigate the mechanism(s) of internalisation.

6.2 Methodology

6.2.1 Investigation of PEV Internalisation

Purified PEV were incubated with washed monocytes for 30 minutes at 37˚C on a roller mixer. Monocytes were then centrifuged to remove unbound PEV and were either a) first stained with anti-GPIbα antibody for 30 minutes before fixation and permeabilisation (this procedure lasted 30 minutes), or b) were first fixed and permeabilised and secondly stained with anti-GPIbα antibody. All monocytes were analysed by FACS (Cyan ADP) to measure surface PEV signal and total PEV signal (surface + intracellular). Statistical analysis was performed using Graph Pad Prism 6. (For further detail see methods chapter 3).

6.2.2 Imaging of internalised PEV

Purified PEV (unstained or stained with the lipophilic PKH67 dye) were incubated with washed monocytes for 30 minutes at 37˚C on a roller mixer. Monocytes were then centrifuged to remove unbound PEV and were cultured in plates at 37°C for 30 minutes or as indicated. The cells were then fixed and stained with anti-GPIbα or isotype control, anti-CD14 antibody, anti-LAMP1 (lysosomal marker), and DAPI in the

presence of FcR blocking reagent. Monocytes were imaged using confocal microscopy. Images were analysed using FIJI software. Statistical analysis was performed using Graph Pad Prism 6. (For further detail see methods chapter 2).

6.2.3 Inhibition of Endocytosis

Washed monocytes were incubated with various endocytosis inhibitors (Cytochalasin D, Ly294002, EIPA or Dynasore) for 30 minutes. Purified PEV were then incubated with the monocytes for 30 minutes at 37˚C on a roller mixer in the presence of the inhibitors. Monocytes were then centrifuged to remove unbound PEV and were either a) first stained with anti-GPIbα antibody for 30 minutes before fixation and permeabilisation (this procedure lasted 30 minutes) in the presence of the inhibitors, or b) were first fixed and permeabilised in the presence of the inhibitors and secondly stained with anti-GPIbα antibody. All monocytes were analysed by FACS (Cyan ADP) to measure surface PEV signal and total PEV signal (surface + intracellular). Statistical analysis was performed using Graph Pad Prism 6. (For further detail see methods chapter 3).

6.3 Results

6.3.1 Investigation of PEV Internalisation

In order to determine whether PEV get internalized into monocytes the PEV signal (GPIbα) from the surface of monocytes and the total signal (surface and intracellular) was measured for the CD16-ve and the CD16+ve monocytes.

6.3.1.1 Internalisation by CD16-ve Monocytes

Representative flow cytometry dotplots show acquisition of PEV-borne GPIbα by the CD16-ve monocyte subset on the surface only and total acquisition (i.e. surface and

intracellular) (**Fig. 6.2A**). We can observe that the percentage of GPIbα+ve events slightly increases in the total expression sample.

The GPIbα histograms were also analyzed. The traces of the surface and total expression were overlaid. The distribution curve is shifted towards higher expression for the total expression sample compared to the surface expression (**Fig. 6.2B**).

The percentage of GPIbα+ve events and the median GPIbα expression were analyzed graphically and statistically. The percentage of CD16-ve monocytes that express GPIbα on their surface only, is not significantly different than the percentage of total expression (**Fig. 6.2C**), however the total median GPIbα expression is significantly higher than the surface median GPIbα expression (**Fig. 6.2D**), suggesting that there is an amount of GPIb located intracellularly.

6.3.1.2 Internalisation by CD16+ve Monocytes

Representative flow cytometry dotplots show acquisition of PEV-borne GPIbα by the CD16+ve monocyte subset on the surface only and total acquisition (surface and intracellular) (**Fig. 6.3A**). We can observe that the percentage of GPIbα+ve events slightly increases in the total expression sample.

The GPIbα histograms were also analyzed. The traces of the surface and total expression were overlaid. The distribution curve is shifted towards higher expression for the total expression sample compared to the surface expression (**Fig. 6.3B**).

The percentage of GPIbα+ve events and the median GPIbα expression were analyzed graphically and statistically. The percentage of total expression is not significantly higher than the percentage of surface expression (**Fig. 6.3C**), however the

total median GPIbα expression is significantly higher than the surface median GPIbα expression (**Fig. 6.3D**).

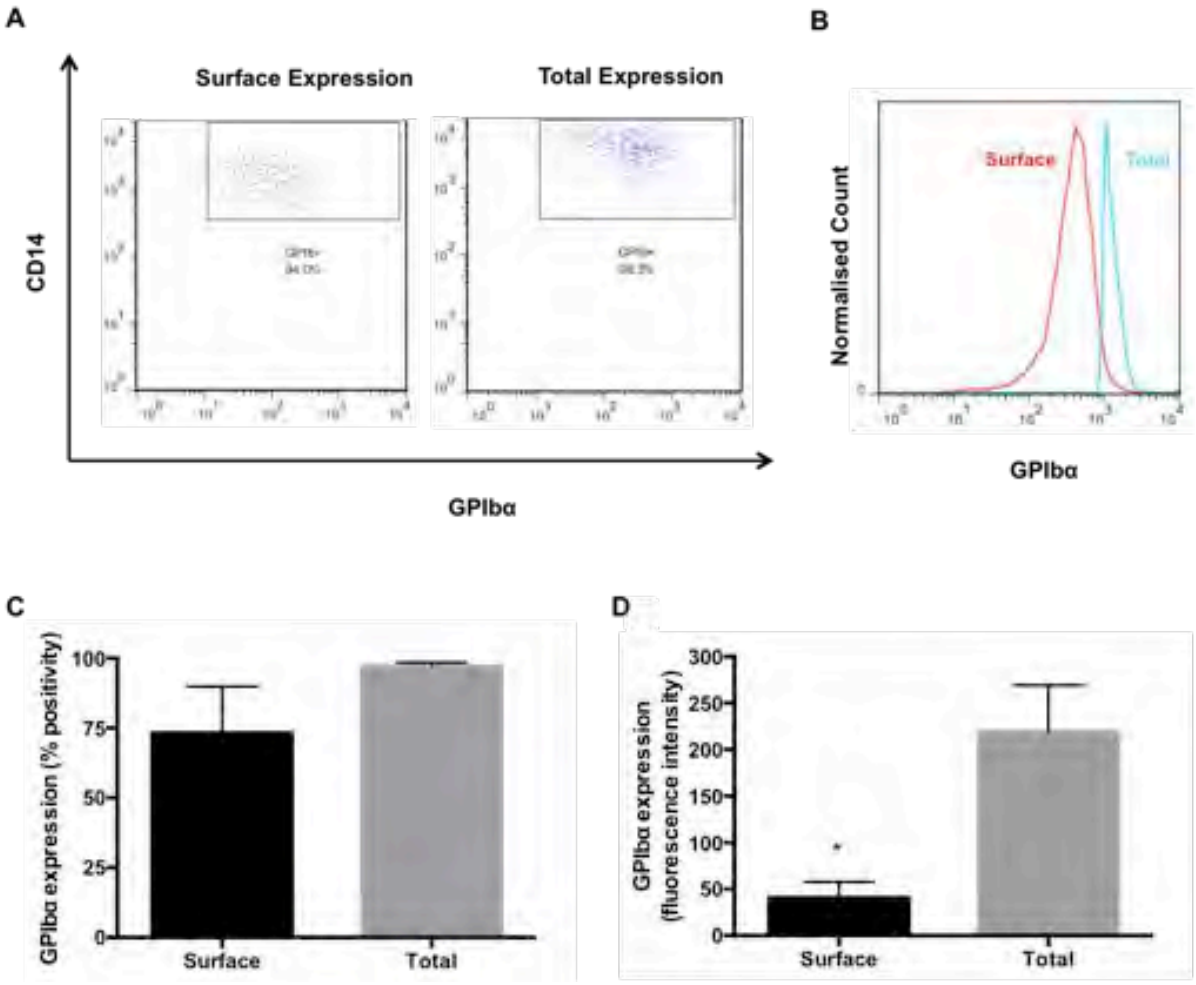

Figure 6.2. Surface and Total expression of GPIbα in CD16-ve Monocytes

(A) Representative FACS dotplots indicating percentage of cells expressing GPIbα on their surface and total (surface and intracellular) GPIbα expression upon 30 minutes incubation with PEV. **(B)** Representative FACS overlay histograms demonstrating the surface and the total GPIbα expression. **(C)** Percentage of cells expressing GPIbα on their surface and total GPIbα expression and **(D)** median GPIbα expression. Data are represented as mean +/- SEM of 3 experiments. T-tests were performed between surface and total expression. * indicates $P<0.05$.

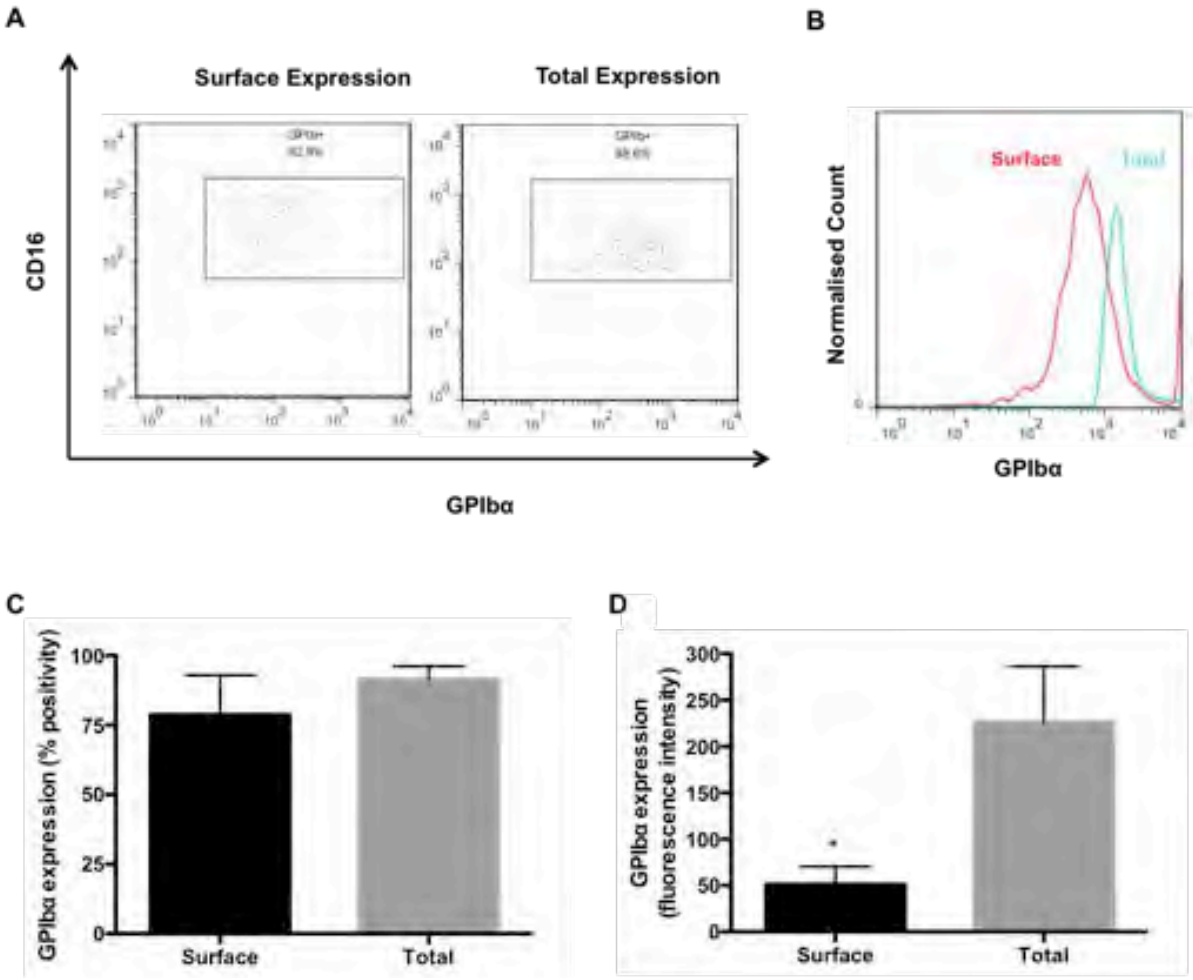

Figure 6.3. Surface and Total expression of GPIbα in CD16+ve Monocytes

(A) Representative FACS dotplots indicating percentage of cells expressing GPIbα on their surface and total (surface and intracellular) GPIbα expression upon 30 minutes incubation with PEV. **(B)** Representative FACS overlay histograms demonstrating the surface and the total GPIbα expression. **(C)** Percentage of cells expressing GPIbα on their surface and total GPIbα expression and **(D)** median GPIbα expression. Data are represented as mean +/- SEM of 3 experiments. T-tests were performed between surface and total expression. * indicates $P<0.05$.

6.3.2 Imaging of internalised PEV

FACS analysis suggested that PEV get internalised into monocytes since the fluorescence intensity of GPIbα on monocytes (both subsets) was higher upon staining after cell permeabilisation compared to staining before cell permeabilisation. This observation raised questions regarding the fate of internalised PEV, which we attempted to answer by imaging the heterotypic aggregates.

6.3.2.1 Detection of PEV-derived GPIbα

Figure 6.4 shows successive frames from z-stacks of plated monocytes that have aggregated with PEV. Aggregated monocytes were stained for GPIbα (**Fig. 6.4A**) to visualise PEV or with an isotype control (**Fig. 6.4B**) to check for any non-specific signal in the green channel. Each successive frame shows signal 0.6μm deeper into the cell. Individual cells were identified by a DAPI-stained nucleus and CD14-stained surface (not shown on the z-stack frames). Clearly, numerous, distinct, green dots appear at different frames of the z-stack, away from the top (frame 1) and bottom (frame 10) cell surfaces suggesting that the majority of PEV are located inside the monocyte. Monocytes stained with an isotype control show very low non-specific staining.

The z-stack frames were combined together to form a single image of total signal (maximum projection of each pixel) using FIJI software in order to view all PEV on and in the monocyte (**Fig. 6.5**). Clearly, the GPIbα+ve particles are in the sub-micron range and evenly distributed in all directions of the cell (**Fig. 6.5A**). The composite image for the isotype control revealed numerous particles scattered everywhere as well, however the fluorescence intensity of these is much lower (**Fig. 6.5B**).

The signal intensity in the green channel per cell and the individual particles were analyzed using the FIJI software and are shown graphically in **Fig. 6.6**. The signal intensity in the green channel is significantly higher in the GPIbα-stained aggregates compared to the isotype control (**Fig. 6.6A**). The number of particles per cell is not higher in the GPIbα-stained sample compared to the isotype control (**Fig. 6.6B**), however the particles in the GPIbα-stained sample are significantly larger in size than the particles of the control sample (**Fig. 6.6C**).

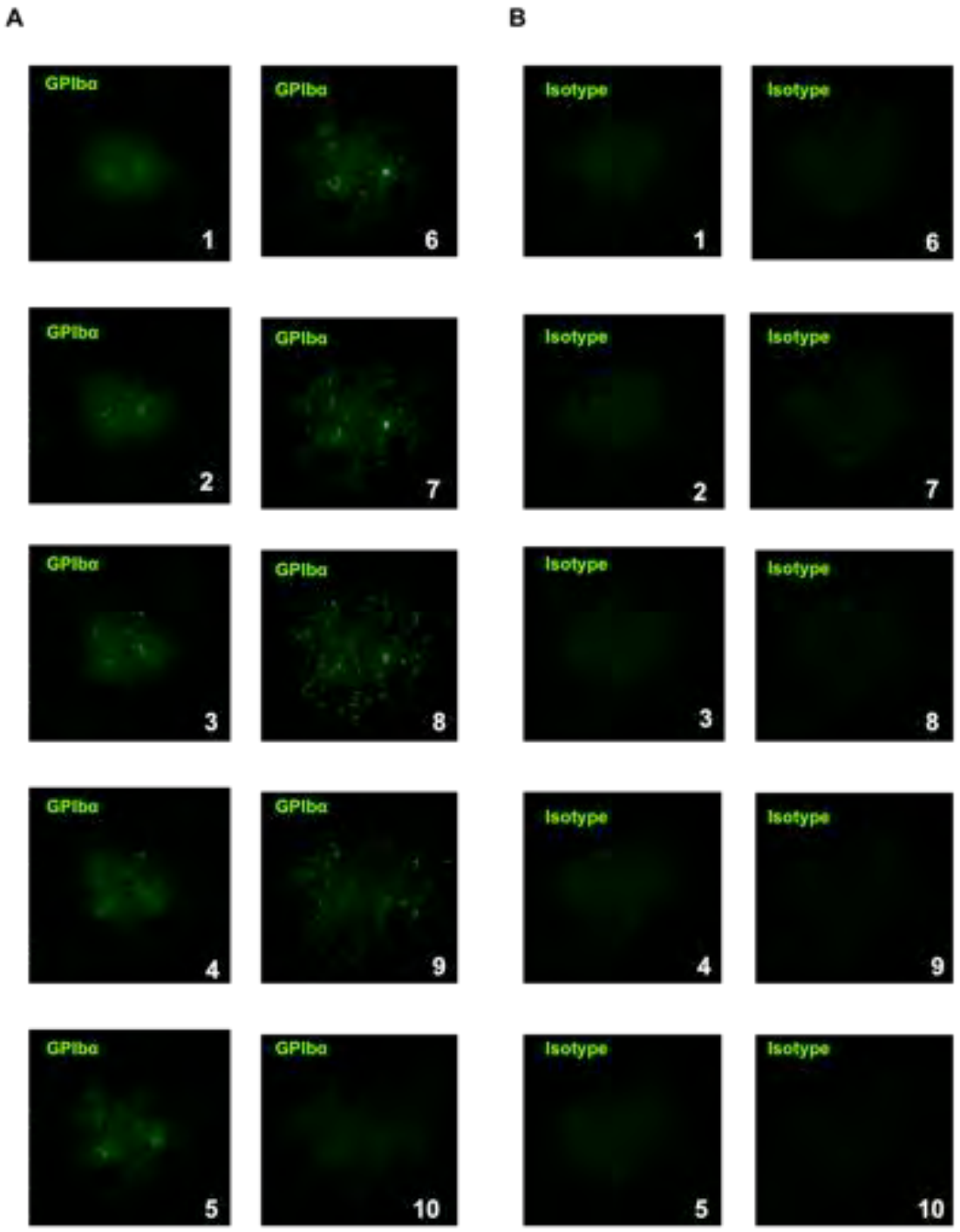

Figure 6.4. GPIbα distribution in monocytes after 1 hour of initial PEV introduction

Representative successive frame images from z-stacks of monocyte-PEV aggregates. PEV were labelled with anti-GPIbα antibody tagged with alexa-488 fluorochrome **(A)** or with isotype control **(B)**. The cell depth between successive images is 0.6μm.

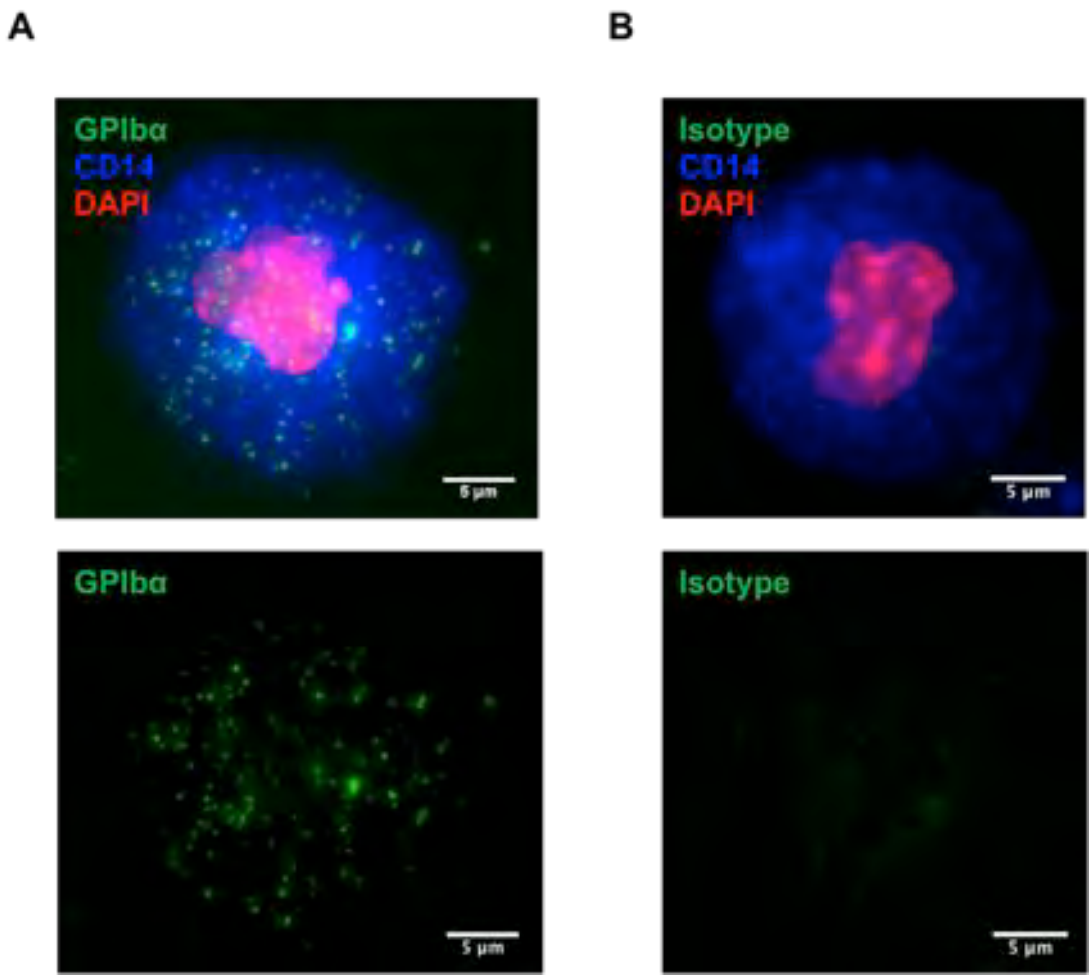

Figure 6.5. GPIbα distribution in monocytes after 1 hour of initial PEV introduction

Representative composite images from z-stacks of monocyte-PEV aggregates. PEV were labelled with anti-GPIbα antibody tagged with alexa-488 fluorochrome **(A)** or with isotype control **(B)**. The composite signal from all channels and from the green channel alone are shown in individual images.

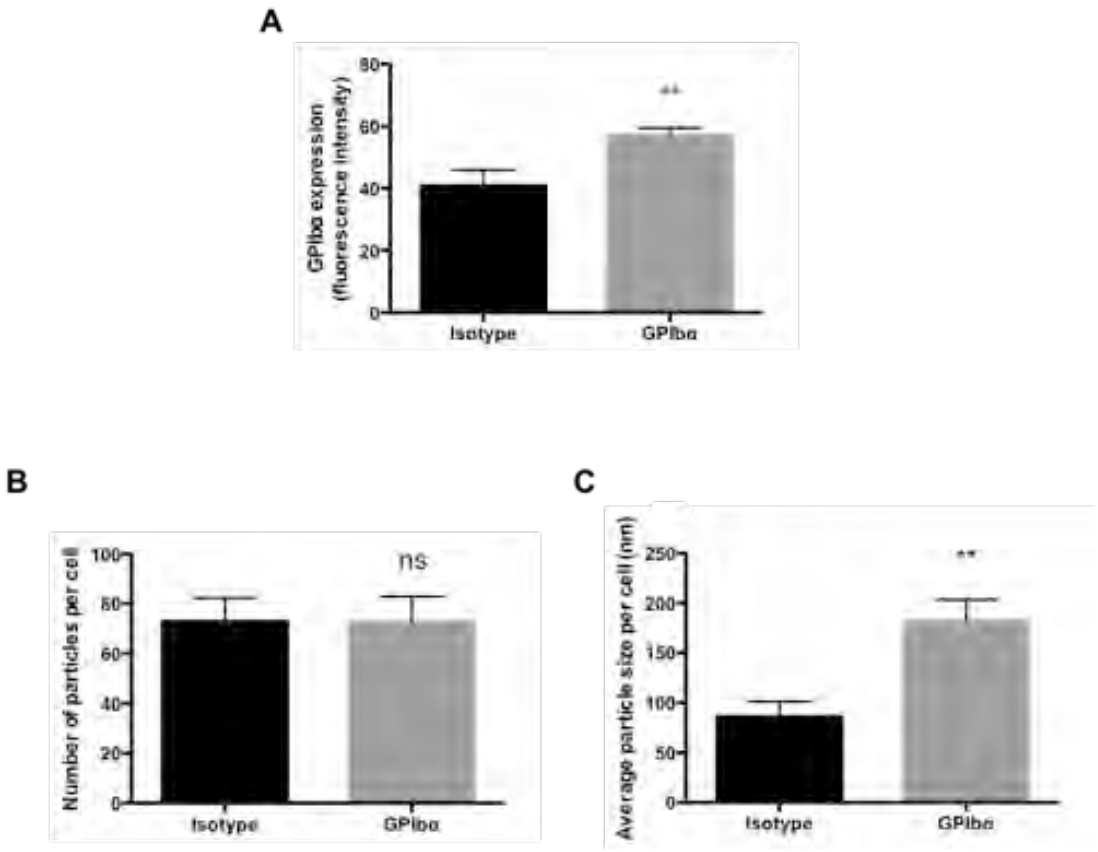

Figure 6.6. PEV-derived GPIbα in monocytes after 1 hour of initial introduction

Mean expression of GPIbα or isotype control per monocyte **(A),** number **(B**) and average particle size **(C)** upon staining with GPIbα or isotype control as determined using the FIJI software. Data are represented as mean +/- SEM of 3 independent experiments. T-tests were performed between surface and total expression. ** indicates $P<0.01$, ns indicates no statistical significance.

6.3.2.2 Detection of PEV Membrane

Figure 6.7 shows successive frames from z-stacks of plated monocytes that have aggregated with PEV. PEV were stained with the PKH67 dye before incubation with monocytes. Each successive frame shows signal 0.6μm deeper into the cell. Individual cells were identified by a DAPI-stained nucleus and CD14-stained surface (not shown on the z-stack frames). Some particles are seen to be located inside the monocytes as they are most clearly seen on the middle frames.

The z-stack frames were combined together to form a single image of total signal (maximum projection of each pixel) using FIJI software in order to view all PEV on and in the monocyte (**Fig. 6.8**). The PKH67+ve particles are in the sub-micron range and evenly distributed in all directions of the cell. Some of them are seem to be located on the extracellular surface of the cell (**Fig. 6.8A**). The composite image for the unstained control revealed only some minimal fluorescence in the green channel coming from the DAPI-stained nucleus (**Fig. 6.8B**). An unstained sample was considered to be an adequate control because the PKH67 dye showed no signs of "leaking" out of the vesicles in Chapter 5, as judged from the fact that lymphocytes for example did not acquire significant PKH67 signal upon incubation with exogenous PKH67-stained PEV.

The signal intensity in the green channel per cell and the individual particles were analyzed using the FIJI software and are shown graphically in **Fig. 6.9**. The signal intensity in the green channel is significantly higher in the PKH67-stained sample compared to the unstained control (**Fig. 6.9A**). The number of particles per cell (**Fig. 6.9B**) and their size in the PKH67-stained sample are significantly higher than the particles of the control sample (**Fig. 6.9C**).

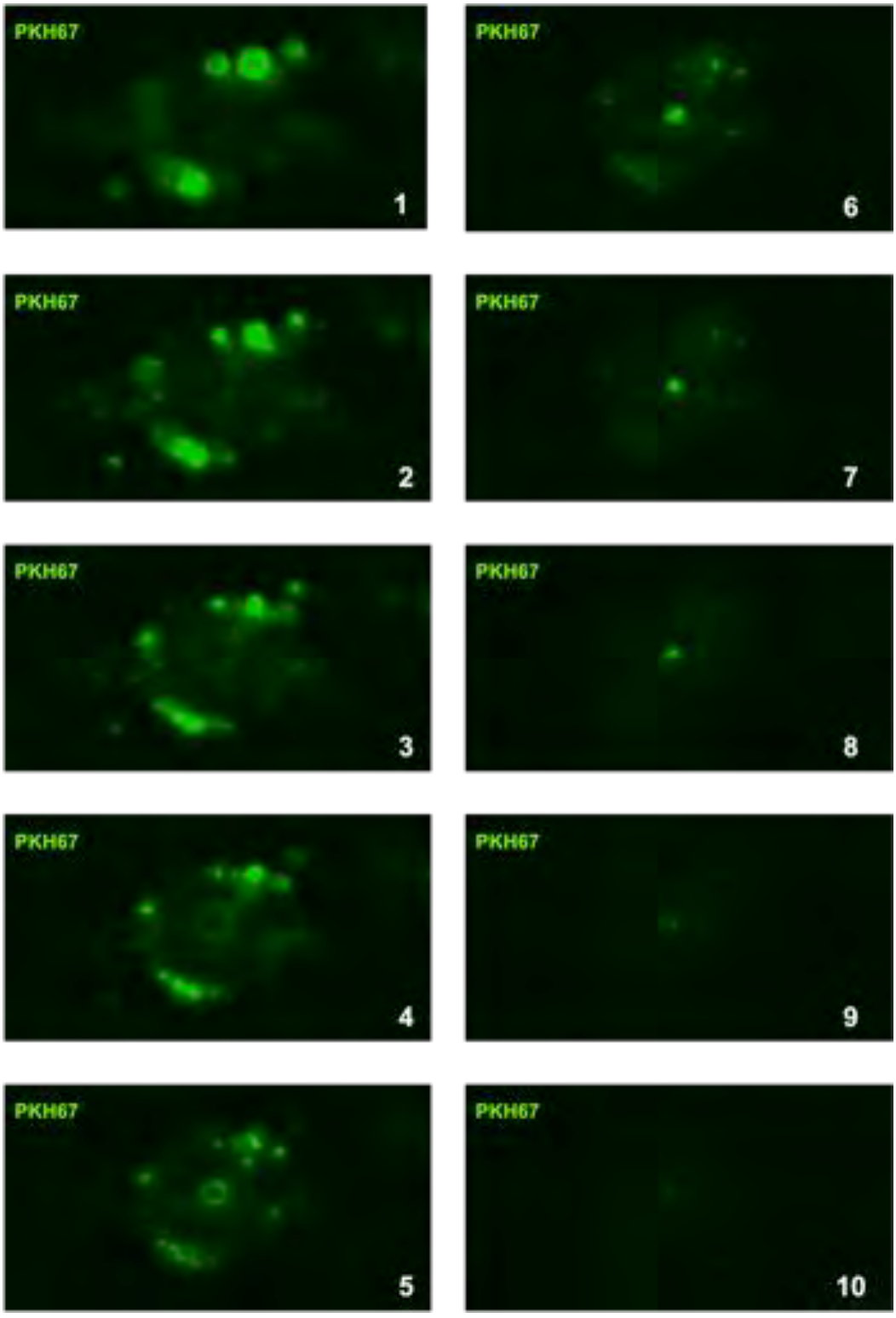

Figure 6.7. PEV membrane distribution in monocytes after 1 hour of initial PEV introduction

Representative successive frame images from z-stacks of monocyte-PEV aggregates. PEV were labelled with PKH67 dye. The cell depth between successive images is 0.6μm.

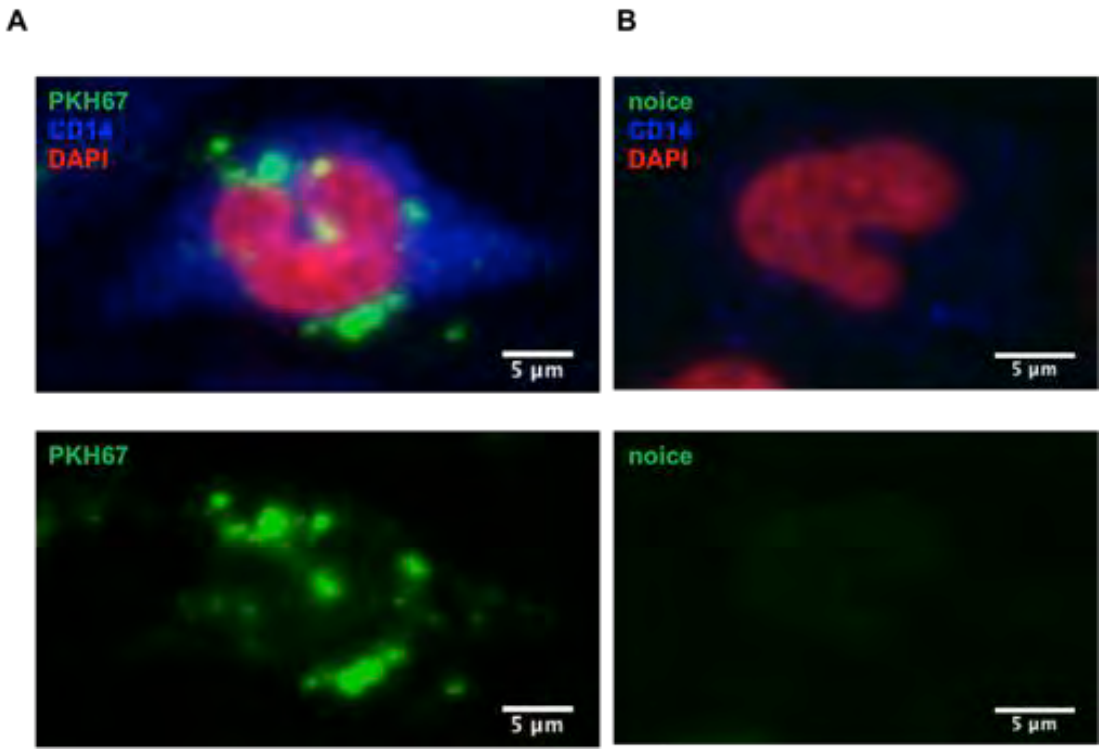

Figure 6.8. PEV membrane distribution in monocytes after 1 hour of initial PEV introduction

Representative composite images from z-stacks of monocyte-PEV aggregates. PEV were labelled with PKH67 dye. The composite signal from all channels and from the green channel alone are shown in individual images.

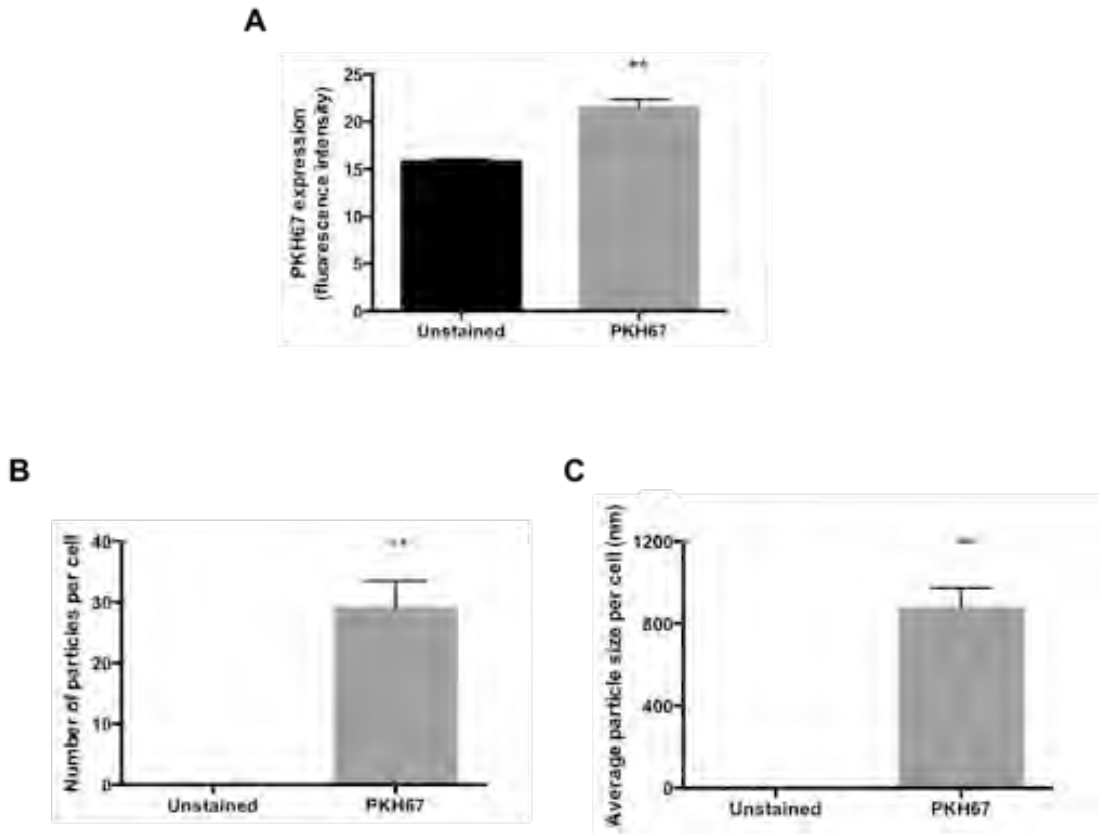

Figure 6.9. PEV membrane in monocytes after 1 hour of initial PEV introduction

Mean fluorescence intensity in the green channel for the PKH67-stained and the unstained PEV **(A),** number **(B**) and average particle size **(C)** as determined using the FIJI software. Data are represented as mean +/- SEM of 3 independent experiments. T-tests were performed between surface and total expression. ** indicates $P<0.01$.

6.3.2.3 Investigation of PEV transfer into Monocytes Lysosomes

After observing that PEV get internalized into monocytes, we wondered where they end up inside the monocytes; whether they get transferred into lysosomes for degradation or whether they get recycled and used somewhere by monocytes? In order to determine whether PEV get trafficked into lysosomes, plated monocyte-PEV aggregates were stained for GPIbα and LAMP1, a lysosomal and late endosomal marker, to check colocalization. Cells were imaged by confocal microscopy by z-stacking 1 hour, 3 hours and 20 hours post-plating.

The z-stack frames were combined together to form a single image of total signal (maximum projection of each pixel) using FIJI software in order to view all PEV and all lysosomes in the monocytes (**Fig. 6.10**). We clearly see numerous lysosomes and PEV. These do not seem to colocalise by eye observation. Only in the 20-hour sample we can see two individual lysosomes exhibiting GPIbα signal (appearing as yellow in the composite image).

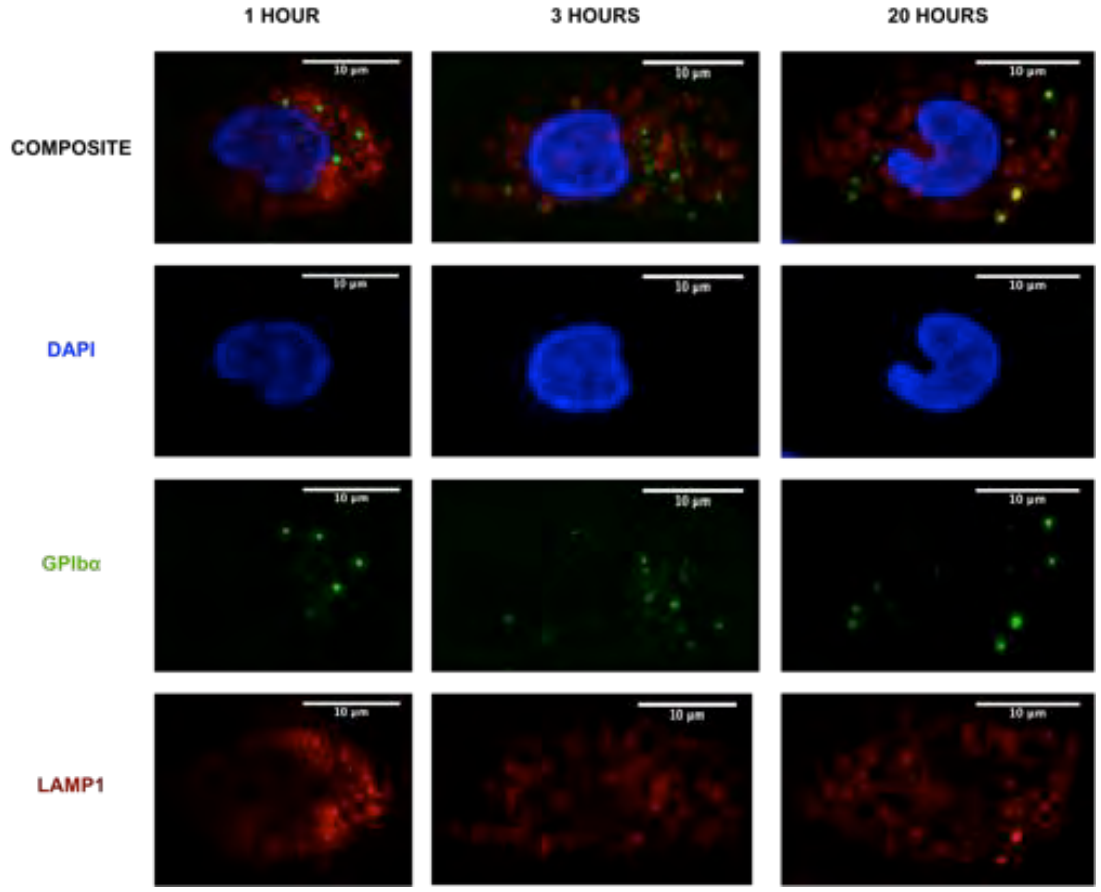

Figure 6.10. PEV-derived GPIbα localization in monocyte lysosomes

Representative composite images from z-stacks of monocyte-PEV aggregates. Monocyte-PEV aggregates were labelled with anti-GPIbα antibody tagged with alexa-488 fluorochrome, anti-LAMP1 tagged with alexa-647 and DAPI. The composite signal from all channels and from individual colour channels.

The colocalization coefficient (Pearson's) was determined at each time point using FIJI software and was analyzed statistically. It was found to increase significantly with time

however even after 20 hours, the colocalization value is low meaning that a small number of PEV (≈25%) colocalize with lysosomes; most of them do not (**Fig. 6.11A**). The number of individual GPIbα+ve particles was also counted at each time point using FIJI software and was found not to change significantly with time. In addition, the number of GPIbα+ve particles at 20h was not significantly different than at 3h (**Fig. 6.11B**).

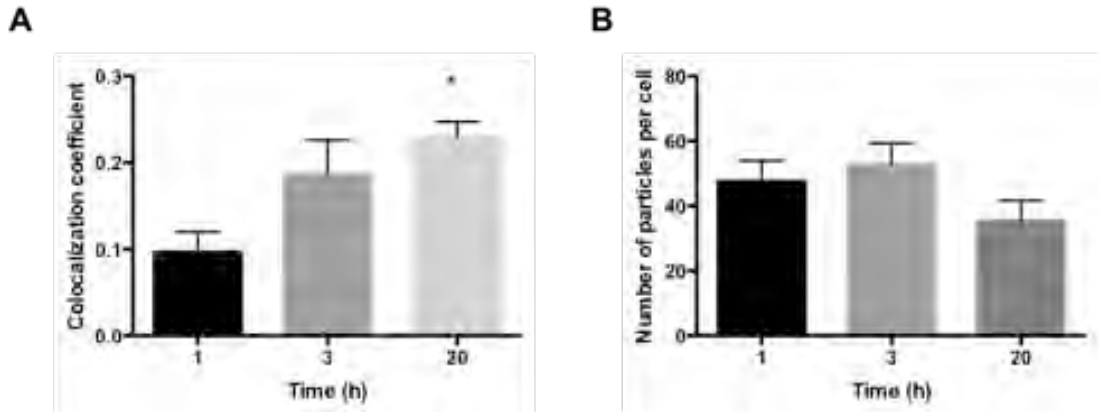

Figure 6.11. PEV-derived GPIbα localization in monocyte lysosomes

(A) Pearson's colocalization coefficient of GPIbα and LAMP1 as calculated using FIJI software in monocytes over time. **(B)** Number of GPIbα+ve particles. Data are represented as mean +/- SEM of 3 experiments. One-way ANOVA was performed to determine effect of time. T-test was performed between number of particles at 3h and 20h. * indicates $p<0.05$.

6.3.3 Investigation of the PEV Internalisation Mechanism

Upon observing that PEV get internalised by monocytes, the mechanism of internalisation was investigated. Purified PEV were incubated with various endocytosis inhibitors and the level of endocytosed PEV was measured.

6.3.3.1 Role of Actin Polymerisation

The role of actin polymerization, which is important in phagocytosis macropinocytosis and clathrin-dependent endocytosis, on the uptake of PEV was

investigated using the chemical inhibitor Cytochalasin D (C.D) which depolymerizes F-actin.

Representative flow cytometry dotplots show surface acquisition of PEV-borne GPIbα and total acquisition (surface and intracellular) by monocytes in the presence of DMSO vehicle or actin polymerization inhibitor Cytochalasin D (**Fig. 6.12**). We can observe that the percentage of GPIbα+ve events decreases in the Cytochalasin D-treated sample.

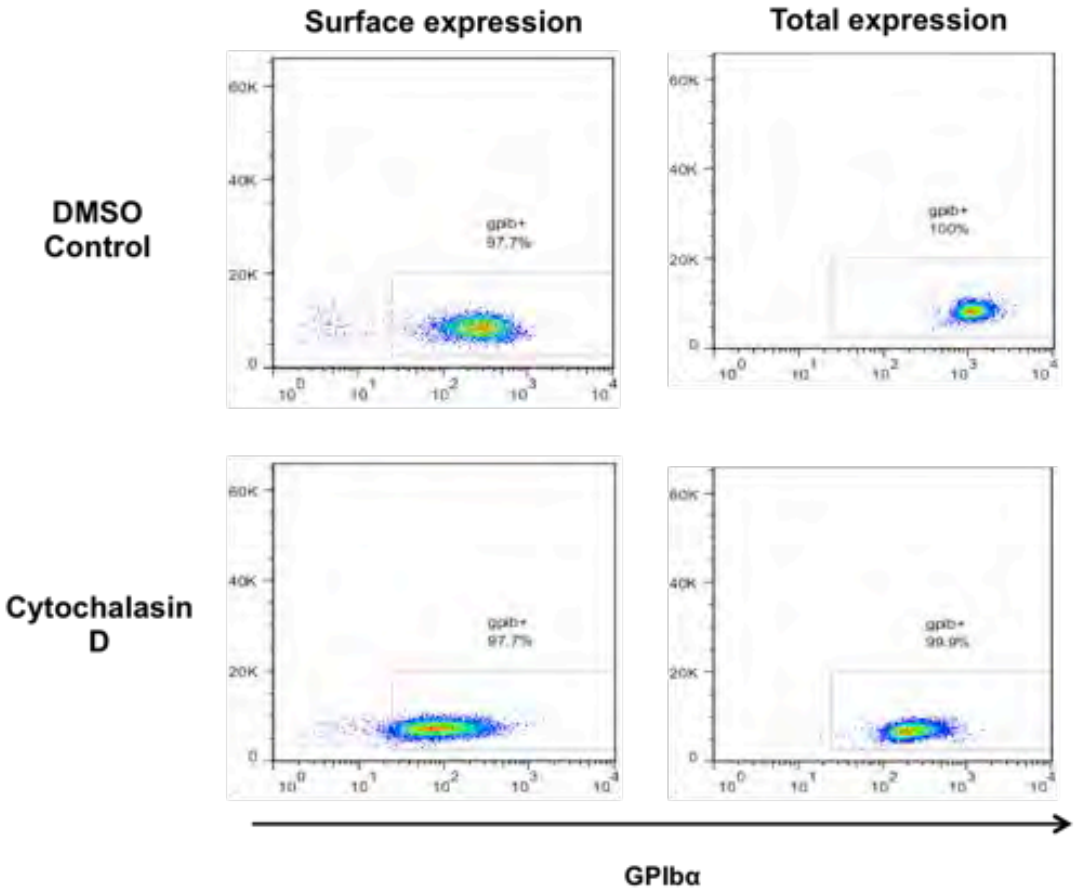

Figure 6.12. Role of Actin polymerization on the uptake of PEV by Monocytes

Representative FACS dotplots indicating percentage of monocytes that express GPIbα on their surface and total (surface and intracellular) GPIbα expressionn upon 30 minutes incubation with PEV in the presence of Cytochalasin D or DMSO control which blocks actin polymerization.

The GPIbα histograms were also analyzed. The traces of the surface and total expression of DMSO and Cytochalasin D were overlaid. The distribution curve is shifted towards lower surface and total expression for the Cytochalasin D-treated sample compared to the DMSO control (**Fig. 6.13**).

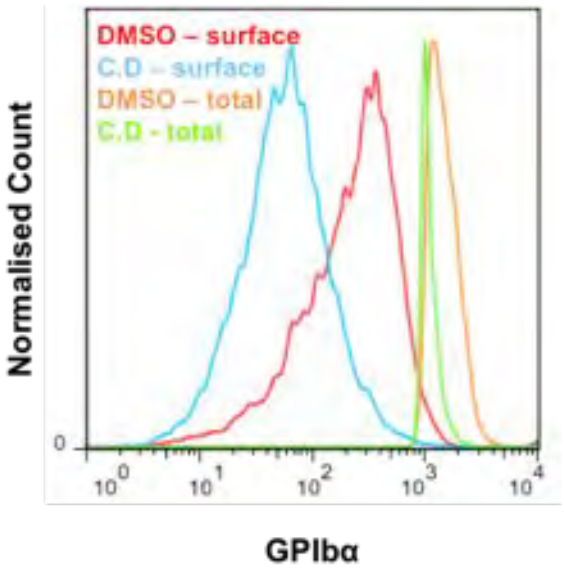

Figure 6.13. Role of Actin polymerization on the uptake of PEV by Monocytes

Representative FACS overlay histograms demonstrating the surface and the total GPIbα expression on monocytes upon 30 minutes incubation with PEV in the presence of Cytochalasin D (C.D) or DMSO control which blocks actin polymerization.

The percentage of GPIbα+ve events and the median GPIbα expression were analyzed graphically and statistically (**Fig. 6.14**). The percentage of surface and total expression of Cytochalasin D is not significantly lower than the percentage of the DMSO expression (**Fig. 6.14A**). The median total GPIbα expression in the presence of Cytochalasin D. is significantly lower than the median total GPIbα expression of the control, however the median surface GPIbα expression in the presence of Cytochalasin D is not significantly lower than the median total GPIbα expression of the control. The median total GPIbα expression in the presence of Cytochalasin D is significantly higher

than the median surface GPIbα expression of (**Fig. 6.14B**), hence Cytochalasin D decreases the intercellular GPIbα expression i.e. (partly) inhibits GPIbα internalization.

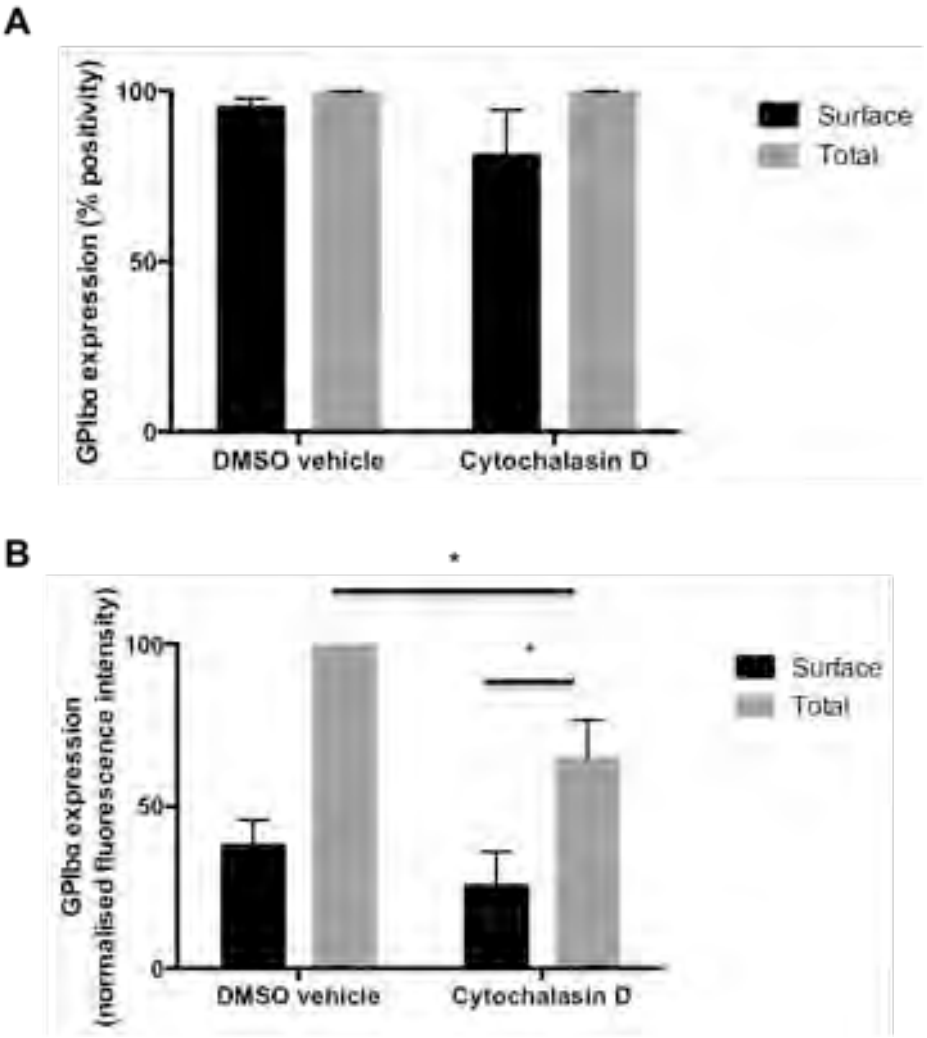

Figure 6.14. Role of Actin polymerization on the uptake of PEV by Monocytes

Percentage of monocytes that express GPIbα on their surface and total GPIbα expression **(A)** and median GPIbα expression **(B)** upon 30 minutes incubation with PEV in the presence of Cytochalasin D or DMSO control. Data are represented as mean +/- SEM of 3 experiments. T-tests were performed between surface and total expression with Cytochalasin D, between surface expression of DMSO vehicle and surface expression of Cytochalasin D and between total expression of DMSO vehicle and total expression of Cytochalasin D. * indicates $P<0.05$, absence of * indicates no significance.

6.3.3.2 Role of PI3K

The role of phosphoinositide 3-kinases (PI3K), which are important in phagocytosis (Feng et al., 2010), on the uptake of PEV was investigated using the chemical inhibitor Ly294002.

Representative flow cytometry dotplots show surface acquisition of PEV-borne GPIbα and total acquisition (surface and intracellular) by monocytes in the presence of DMSO control or Ly294002 (**Fig. 6.15**). We can observe that the percentage of GPIbα+ve events is about the same in the Ly294002-treated samples compared to the controls.

The GPIbα histograms were also analyzed. The traces of the surface and total expression of DMSO and Ly294002 were overlaid. The distribution curves of the Ly294002 samples lie exactly on those of the controls i.e. there is no shift towards lower GPIbα expression (**Fig. 6.16**).

The percentage of GPIbα+ve events and the median GPIbα expression were analyzed graphically and statistically (**Fig. 6.17**). The percentage of surface and total expression of Ly294002 is the same as the percentage of the DMSO sample (**Fig. 6.17A**). The median total and surface GPIbα expression in the presence of Ly294002 is also the same as the median GPIbα expression of the control (**Fig. 6.17B**), hence Ly294002 does not have any effect on PEV internalisation.

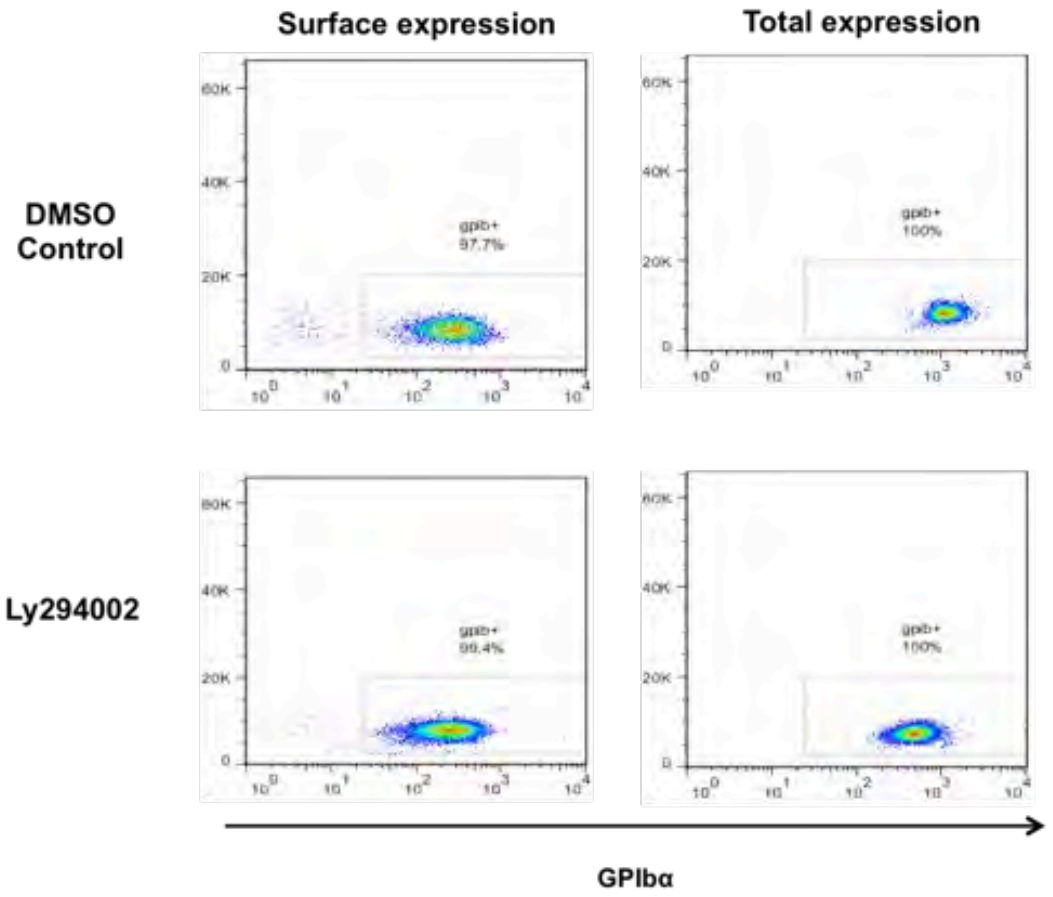

Figure 6.15. Role of PI3K on the uptake of PEV by Monocytes

Representative FACS dotplots indicating percentage of monocytes that express GPIbα on their surface and total (surface and intracellular) GPIbα expressionn upon 30 minutes incubation with PEV in the presence of Ly294002, which inhibits PI3K action or DMSO control.

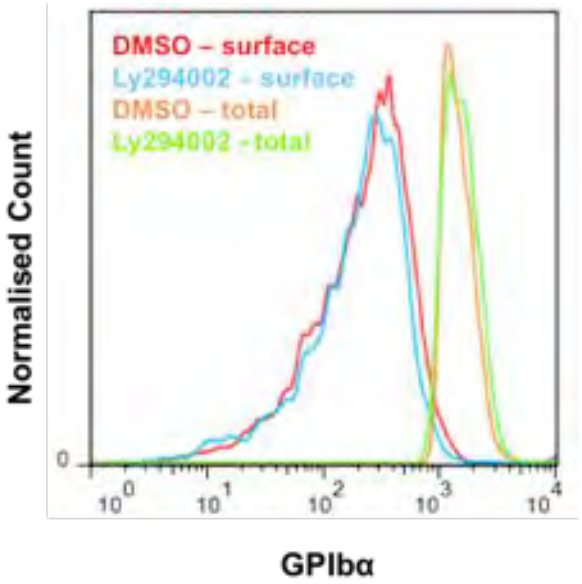

Figure 6.16. Role of PI3K on the uptake of PEV by Monocytes

Representative FACS overlay histograms demonstrating the surface and the total GPIbα expression on monocytes upon 30 minutes incubation with PEV in the presence of Ly294002 which inhibits PI3K action or DMSO control.

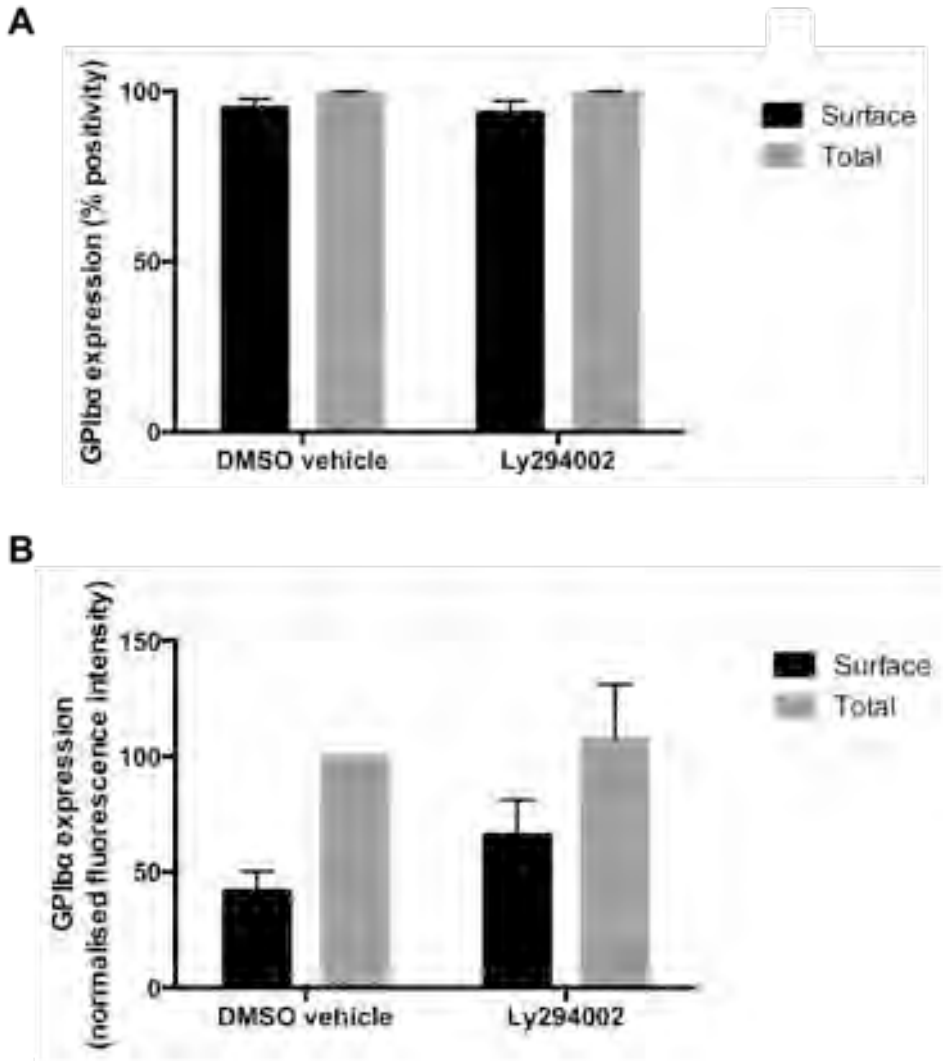

Figure 6.17. Role of PI3K on the uptake of PEV by Monocytes

Percentage of monocytes that express GPIbα on their surface and total GPIbα expression **(A)** and median GPIbα expression **(B)** upon 30 minutes incubation with PEV in the presence of Ly294002, which inhibits PI3K action or DMSO control. Data are represented as mean +/- SEM of 3 experiments. T-tests were performed between surface and total expression with Ly294002, between surface expression of DMSO vehicle and surface expression of Ly294002 and between total expression of DMSO vehicle and total expression of Ly294002. Absence of * indicates no significance.

6.3.3.3 Role of Sodium/ Proton Exchanger

The role of sodium/proton exchanger, which is important in macropinocytosis, on the uptake of PEV was investigated using the chemical inhibitor 5-(N-Ethyl-N-isopropyl)amiloride (EIPA) (Fitzner et al., 2011; Escrevente et al., 2011).

Representative flow cytometry dotplots show surface acquisition of PEV-borne GPIbα and total acquisition (surface and intracellular) by monocytes in the presence of DMSO vehicle or macropinocytosis inhibitor EIPA (**Fig. 6.18**). We can observe that the percentage of GPIbα+ve events decreases in the EIPA-treated samples.

The GPIbα histograms were also analyzed. The traces of the surface and total expression of DMSO and EIPA were overlaid. The distribution curve is shifted towards lower surface and total expression for the EIPA-treated sample compared to the DMSO control (**Fig. 6.19**).

The percentage of GPIbα+ve events and the median GPIbα expression were analyzed graphically and statistically (**Fig. 6.20**). The percentage of surface and total expression of EIPA is not significantly lower than the percentage of the DMSO expression (**Fig. 6.20A**). The median total GPIbα expression in the presence of EIPA is significantly lower than the median total GPIbα expression of the control, however the median surface GPIbα expression in the presence of EIPA is not significantly lower than the median total GPIbα expression of the control. The median total GPIbα expression in the presence of EIPA is not significantly higher than the median surface GPIbα expression of (**Fig. 6.20B**), hence EIPA decreases the intercellular GPIbα expression i.e. inhibits most GPIbα internalization.

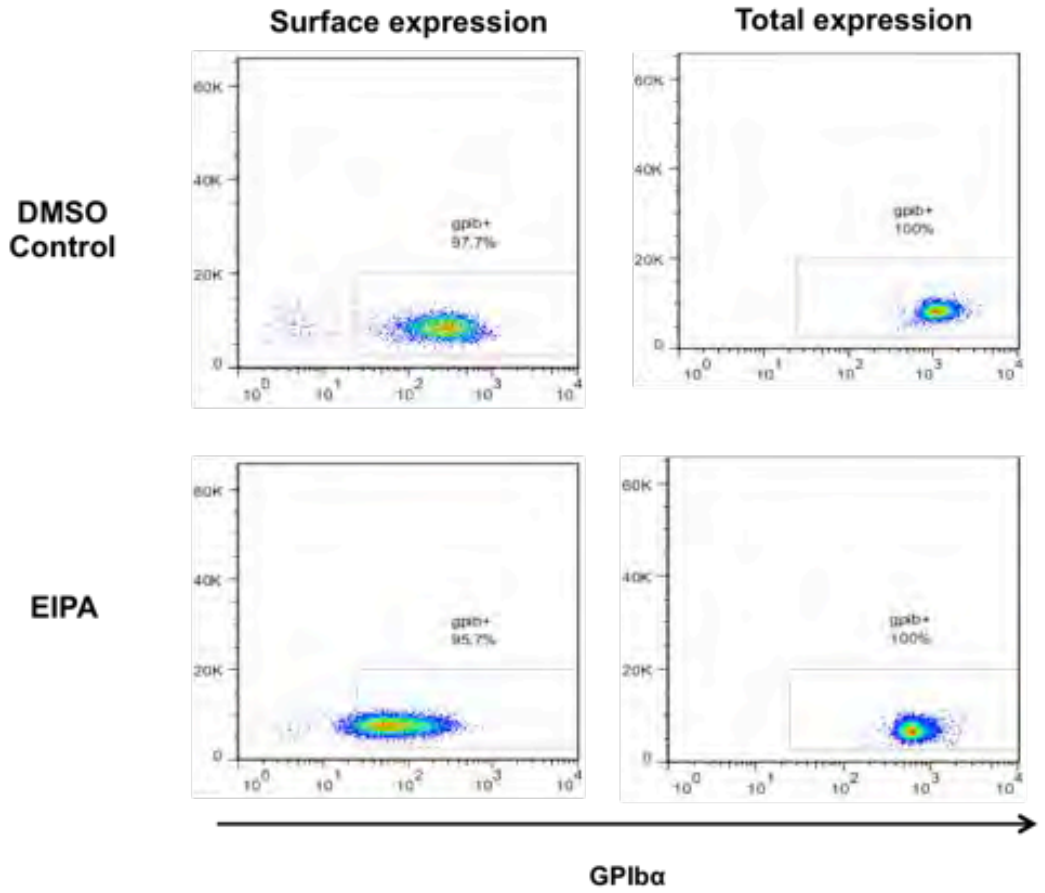

Figure 6.18. Role of the sodium/proton exchanger on the uptake of PEV by Monocytes

Representative FACS dotplots indicating percentage of monocytes that express GPIbα on their surface and total (surface and intracellular) GPIbα expressionn upon 30 minutes incubation with PEV in the presence of EIPA, which inhibits the action of the sodium/proton exchanger or DMSO control.

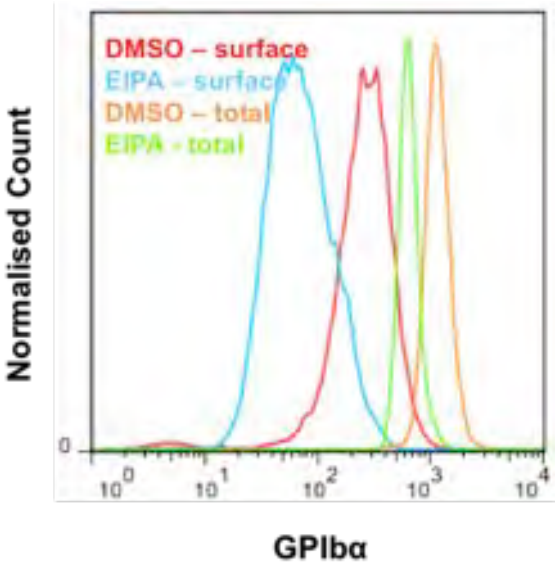

Figure 6.19. Role of the sodium/proton exchanger on the uptake of PEV by Monocytes

Representative FACS overlay histograms demonstrating the surface and the total GPIbα expression on monocytes upon 30 minutes incubation with PEV in the presence of EIPA, which inhibits the action of the sodium/proton exchanger or DMSO control.

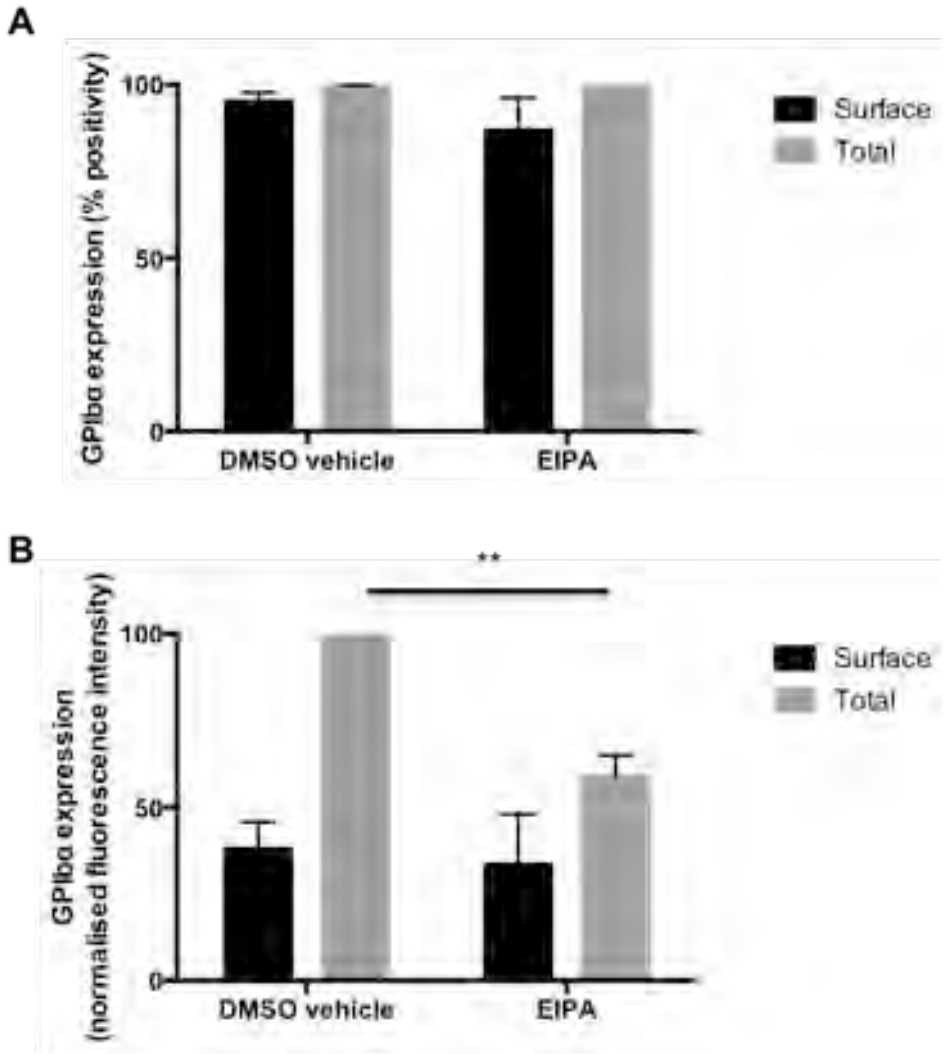

Figure 6.20. Role of the sodium/proton exchanger on the uptake of PEV by Monocytes

Percentage of monocytes that express GPIbα on their surface and total GPIbα expression **(A)** and median GPIbα expression **(B)** upon 30 minutes incubation with PEV in the presence of EIPA, which inhibits the action of the sodium/proton exchanger or DMSO control. Data are represented as mean +/- SEM of 3 experiments. T-tests were performed between surface and total expression with EIPA, between surface expression of DMSO vehicle and surface expression of EIPA and between total expression of DMSO vehicle and total expression of EIPA. ** indicates $p<0.01$, absence of * indicates no significance.

6.3.3.4 Role of Dynamin

The role of dynamin, which is important in clathrin-and caveolin-mediated endocytosis, on the uptake of PEV was investigated using the pharmacological inhibitor Dynasore which blocks the GTPase activity of dynamin.

Representative flow cytometry dotplots show surface acquisition of PEV-borne GPIbα and total acquisition (surface and intracellular) by monocytes in the presence of DMSO vehicle or clathrin-mediated endocytosis inhibitor Dynasore (**Fig. 6.21**). We can observe that the percentage of GPIbα+ve events decreases in the Dynasore-treated samples.

The GPIbα histograms were also analyzed. The traces of the surface and total expression of DMSO and Dynasore were overlaid. The distribution curve is shifted towards lower total expression for the Dynasore-treated sample compared to the DMSO control (**Fig. 6.22**). The surface curve is the same for both samples.

The percentage of GPIbα+ve events and the median GPIbα expression were analyzed graphically and statistically (**Fig. 6.23**). The percentage of surface and total expression of Dynasore is not significantly different than the percentage of the DMSO sample (**Fig. 6.23A**). The median total GPIbα expression in the presence of Dynasore is significantly lower than the median total GPIbα expression of the control. The median surface GPIbα expression in the presence of Dynasore is a little higher than the median surface GPIbα expression of the control, however it does not reach significance. The median total GPIbα expression in the presence of Dynasore is not significantly higher than the median surface GPIbα expression of Dynasore (**Fig. 6.23B**), hence Dynasore completely blocks internalization of GPIbα.

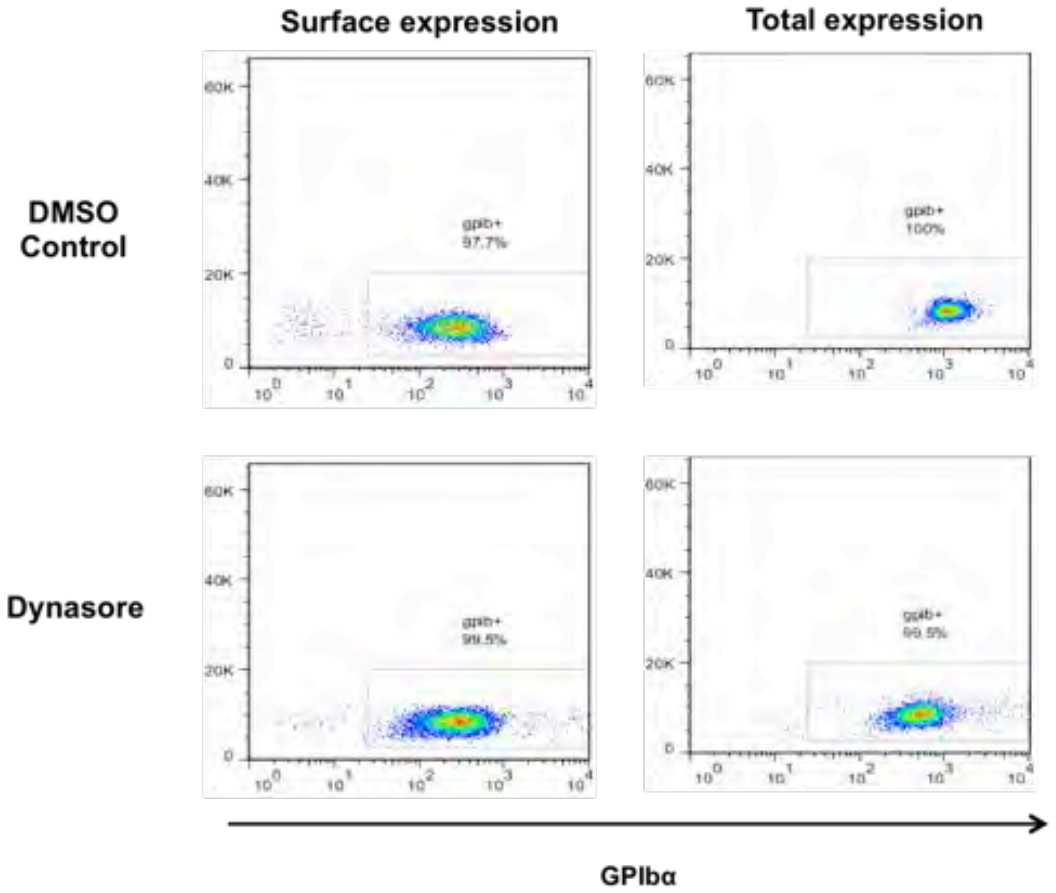

Figure 6.21. Role of Dynamin-2 on the uptake of PEV by Monocytes

Representative FACS dotplots indicating percentage of monocytes that express GPIbα on their surface and total (surface and intracellular) GPIbα expressionn upon 30 minutes incubation with PEV in the presence of Dynasore, which blocks the action of Dynami-2 or DMSO control.

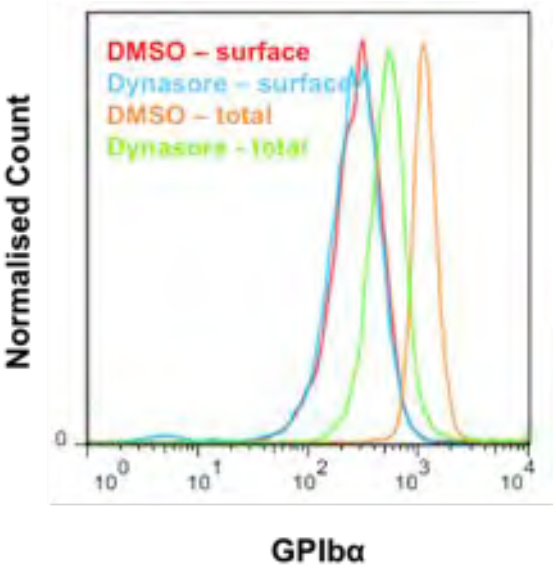

Figure 6.22. Role of Dynamin-2 on the uptake of PEV by Monocytes Representative FACS overlay histograms demonstrating the surface and the total GPIbα expression on monocytes upon 30 minutes incubation with PEV in the presence of Dynasore, which blocks the action of Dynamin-2 or DMSO control.

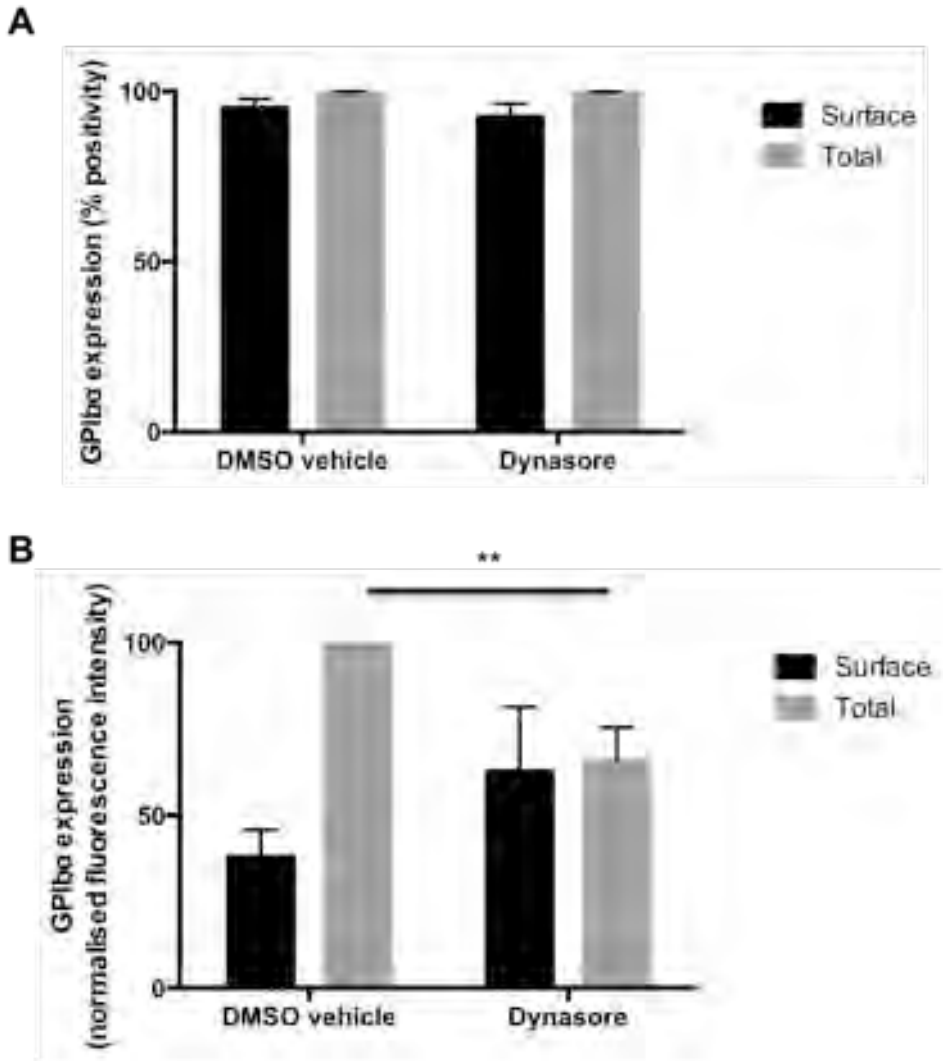

Figure 6.23. Role of Dynamin-2 on the uptake of PEV by Monocytes Percentage of monocytes that express GPIbα on their surface and total GPIbα expression **(A)** and median GPIbα expression **(B)** upon 30 minutes incubation with PEV in the presence of Dynasore, which blocks the action of Dynamin-2 or DMSO control. Data are represented as mean +/- SEM of 3 experiments. T-tests were performed between surface and total expression with Dynasore, between surface expression of DMSO vehicle and surface expression of Dynasore and between total expression of DMSO vehicle and total expression of Dynasore. ** indicates $p<0.01$, absence of * indicates no significance.

6.4 Discussion

The potential of monocytes to internalize PEV was investigated by FACS analysis. Monocyte-PEV aggregates were stained for GPIbα before and after cell permeabilization in order to compare surface with total signal. A significant difference between surface and total GPIbα signal revealed that the majority of GPIbα molecules were located

intracellularly. This observation was not surprising as EV in general are largely endocytosed by various cells (Feng et al., 2010; Franzen et al., 2014; Na¨slund et al., 2014; Christianson et al., 2013).

The two main monocyte subsets; CD16-ve and CD16+ve, exhibited the same capacity to internalise PEV. This is in contrast to the literature where one subset (not always the same one) is shown to be more phagocytic than the other (Mosig et al., 2008; Mukherjee et al., 2015; Boyette et al., 2017). However, this observation led us to speculate that PEV get internalized in a non-phagocytotic mechanism.

In order to shed some light on the post-internalisation fate of PEV, PEV were imaged. Confocal imaging of monocyte-PEV aggregates revealed the presence of numerous GPIbα+ve particles in the microvesicle size range (100-200nm diameter), scattered throughout the cells. Labeling PEV with the lipophilic dye PKH67 resulted in larger particles (sized 600-1000nm) but fewer in number. In addition, the PKH67+ve particles were not clearly located inside the cells and they appeared to be located closer to the surface of the cells, away from the cells' core. Lipophilic dyes, such as the PKH67 dye used in our experiments, associate with lipids, whereas antibodies, such as our anti-GPIbα antibody, associate with proteins. Different EV molecules might separate and have different post-internalization fate inside the monocytes. A study deduced that EV proteins start separating from the EV membrane within 3 hours of endocytosis. The separation occurred possibly by fusion of EV to endosome or acidified environment in late endosome. EV lipids in these experiments were transported to the plasma membrane, whereas EV membrane proteins were transported to lysosomes (Tian et al., 2010). In other studies, internalized EV components were transferred from endosomal vesicles to the ER (Heusermann et al., 2016). Double staining of PEV using a lipophilic

dye and an antibody targeting a PEV protein i.e. GPIbα could help us understand better whether PEV are internalized as whole, or whether their membrane fuses with the monocytes's plasma membrane and only the non-membrane contents get internalized, or whether the different components of PEV (i.e. lipids and proteins) separate and have a different post-internalization fates.

There is concern that the presence of fluorescent molecules in membrane-binding dyes or the presence of antibodies might affect the behavior of EV. The fluorescent molecules from the lipophilic dyes might in theory leach from EV onto the recipient cell's plasma membrane. A significant improvement to our experiment in order to visualize our PEV would be the use fluorescent proteins, such as GFP, fused with vesicular proteins (Keller et al., 2011; Koumangoye et al., 2011).

In order to gain a deeper understanding and further investigate this possibility, the internalization mechanism was sought. PEV were incubated with monocytes in the presence of various endocytosis inhibitors. The chemical compound Cytochalasin D which depolymerizes F-actin and inhibits most endocytic pathways (phagocytosis, macropinocytosis and clathrin-dependent endocytosis) decreased significantly internalization of PEV by monocytes, however the chemical compound Ly294002 that inhibits phagocytosis only, by blocking the action of PI3Ks, did not have any effect on the uptake of PEV by monocytes. Hence, it is most likely that PEV do not get endocytosed by phagocytosis and that the inhibitory effect observed with Cytochalasin D is attributed to macropinocytosis or/and clathrin-dependent endocytosis.

Contribution of macropinocytosis was further confirmed by the use of another chemical macropinocytosis inhibitor, EIPA, that acts by blocking the sodium/proton exchanger, which also (partly) inhibited internalization of GPIbα. Nonetheless, EIPA did

not block internalization of PEV completely, suggesting that PEV get internalized into monocytes via non-macropinocytotic mechanisms as well. This observation agrees with literature where EV are usually taken up by cells via more than one mechanism (Barre`s et al., 2010; Feng et al., 2010; Morelli et al., 2004; Tian et al., 2010; Escrevente et al., 2011; Hao et al., 2007).

Since macropinocytosis blocking did not block PEV internalization completely, the contribution of other endocytic pathways was evaluated. The pharmacological inhibitor Dynasore, which blocks the GTPase activity of dynamin and clathrin/caveolin-mediated endocytosis, completely hindered internalization of PEV, suggesting that this is the main pathway(s) used by the monocytes to internalise PEV. Future experiments should include tracking of PEV into monocytes in real time, along with staining of endocytic components such as clathrin/caveolin/early endosome and markers of endocytosis-related organelles such as endoplasmic reticulum and Golgi.

Endocytosed molecules inside endosomes are either recycled usually back to the plasma membrane via transport vesicles or, if considered “useless” or harmful, they are transferred to the lysosomes for degradation. The distribution of GPIbα inside the monocytes (numerous particles scattered throughout inside of cells) and the fact that PEV were found to be internalized into monocytes via endocytosis (macropinocytosis and clathrin/caveolin-mediated endocytosis) led us to speculate that PEV might end up in monocyte lysosomes. Such an observation would strengthen our hypothesis that PEV might contribute to the lysosomal dysfunction that might cause atherosclerosis. However, after 1, 3 or 20 hours of initial introduction, GPIbα+ve molecules did not localize inside lysosomes. There seems to be a variation in the time it takes for EV to reach lysosomes. EV have been shown to localize into lysosomes 2 hours upon initial

introduction (Fitzner et al., 2011). However, another study found colocalized EV membrane proteins with lysosomes 12 hours upon initial EV introduction (Tian et al., 2010) and another study found high colocalization (50-60%) of EV with lysosomes in fibroblasts after 48 hours upon addition of EV (Heusermann et al., 2016). Hence it is possible that the time points in our experiment were not appropriate. However, this might be a true result. The GPIbα protein might be recycled by monocytes. Indeed, it was found in our lab that monocytes pre-incubated with PEV bound to human immobilized vWF or stimulated cultured endothelial cells in flow in a GPIbα-dependent way (Chimen et al., unpublished).

Uptake of EV by cells is usually mediated by protein-protein interactions. Platelets and monocytes contain various tetraspanins, integrins, immunoglobulins, proteoglycans and lectins that could possibly be involved in the PEV uptake by monocytes and could be the focus of future studies.

Conclusions

Monocytes internalize PEV by macropinocytosis and clathrin/caveolin-dependent endocytosis. Both CD16-ve and CD16+ve exhibit the same efficiency in internalizing PEV. The majority of PEV-derived GPIbα does not end up in monocyte lysosomes upon endocytosis. Further experimentation and live tracking is required to dissect the trafficking and fate of PEV and PEV components inside monocytes and to unravel the functional consequence, if any, in atherosclerosis.

7 INVESTIGATION OF PEV-DERIVED MITOCHONDRIA INTERNALISATION BY MONOCYTES

7.1 Introduction

We have shown by FACS and confocal microscopy in Chapter 6 that PEV are internalized by monocytes. This raises the interesting prospect of transfer of PEV components that can affect monocyte behavior in atherosclerosis. An interesting observation made by Boudreau et al. (2014) is the presence of mitochondria in PEV. Upon internalization by neutrophils and subsequent hydrolysis of the PEV-derived mitochondrial membrane by the bactericidal phospholipase A2 (PLA2 IIA), different inflammatory stimuli were produced; in particular lysophospholipid, fatty acids and mtDNA. These mediators activated neutrophils *in vivo* (Boudreau et al., 2014) and are known to activate leukocytes and promote the progression of atherosclerosis. Hence, we hypothesized that PEV can transfer platelet mitochondria to monocytes and confer monocyte mitochondrial dysfunction, associated with atherosclerosis.

Mitochondria can regulate cell death, inflammation, ROS generation and metabolism. Hence, mitochondrial DNA (mtDNA) damage that leads to mitochondrial dysfunction can directly promote atherosclerosis (Yu and Bennet, 2014). ROS are responsible for oxidation of the lipids that accumulate at sites of endothelial damage in atherosclerosis and are mainly generated as a byproduct of mitochondrial respiration (Turrens, 2003). Thus, prolonged mitochondrial dysfunction may cause high levels of oxidative stress (Logan et al., 2014).

The human mitochondrial genome encodes 13 respiratory chain subunits as well as rRNAs and tRNAs (Larsson, 2010). mtDNA is not protected by histones like nuclear DNA and is located close to the site of ROS production, conditions that render it susceptible to damage. Damaged mtDNA was discovered in blood cells and in atherosclerotic plaques in patients with coronary artery disease and was associated

with high-risk plaques in humans, implying that it has a role in atherosclerosis progression independently of ROS (Botto et al., 2005; Corral-Debrinski et al., 1992; Yu et al., 2013). Monocytes exhibited increased apoptosis and a proinflammatory status. Damaged mtDNA promoted atherosclerosis also in animal models (Trifunovic et al., 2004).

mtDNA contains high levels of unmethylated DNA as CpG islands (regions of DNA where a cytosine nucleotide is followed by a guanine nucleotide in the linear sequence of bases along its 5' -> 3' direction). These can act as DAMPs (damage-associated molecular patterns) and activate TLR9 (Toll-like receptor 9) (Zhang et al., 2010). Activated TLR9 increases nuclear factor kappa B (NFκB) signaling that results in proinflammatory cytokine expression (Oka et al., 2012). Mitochondrial dysfunction can promote inflammation also through activation of the NRLP3 inflammasome through ROS, mtDNA release, cardiolipin release and by altering NAD/NADH ratios (Yu and Bennet, 2014).

Mitochondrial dysfunction promotes cell apoptosis. Apoptotic signals in the cells might reach the mitochondrial proteins Bax and Bak, which form pores on the mitochondrial outer membrane. This allows proapoptotic factors such as cytochrome c to escape the mitochondria and activate the cascade that executes apoptosis (Marino et al., 2014). However, the exact mechanism of this remains unclear.

Mitochondria also affect metabolism. They do so by generating ATP using compounds from the Krebs cycle, which are obtained from lipids, sugars and proteins. Dysfunctional mitochondria that result in insufficient levels of ATP, lead to the activation of AMP-activated protein kinase (AMPK) that inhibits gluconeogenesis and adipogenesis (Hardie et al., 2012).

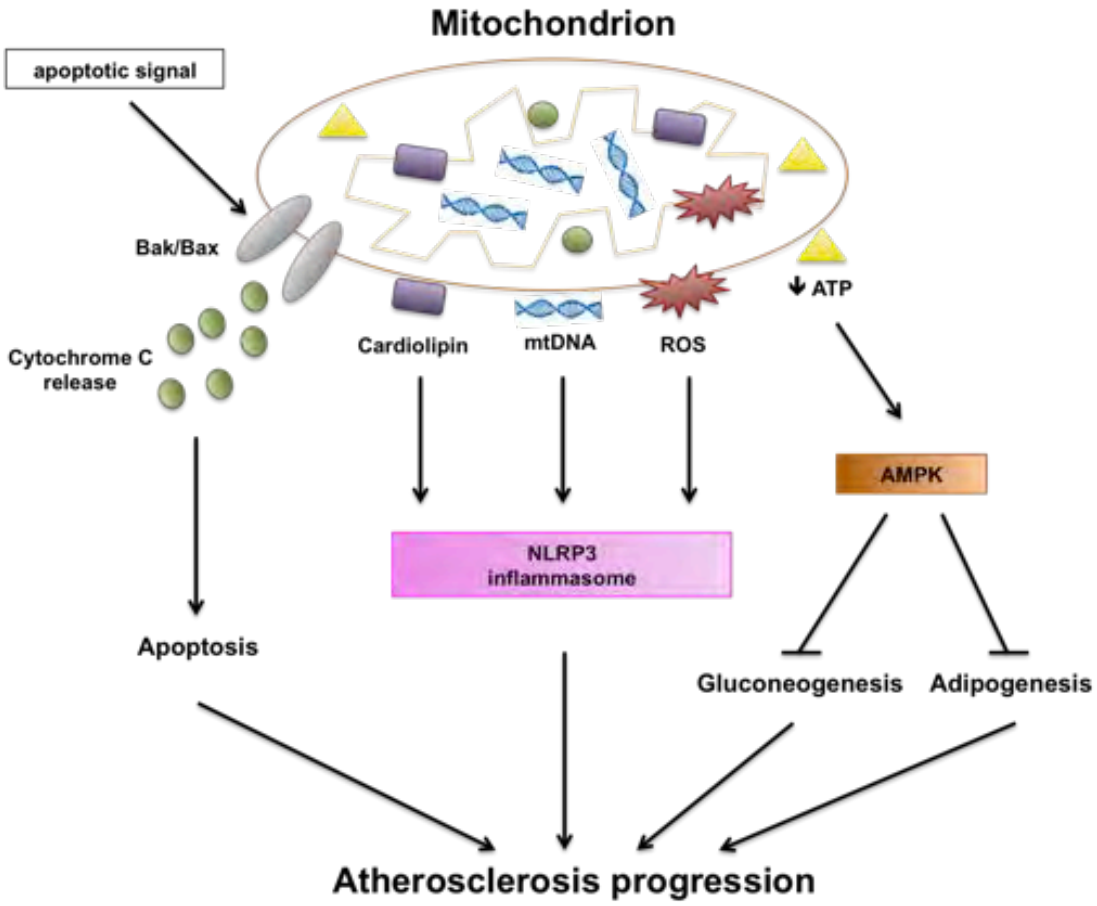

Figure 7.1. Mitochondrial dysfunction and Atherosclerosis

Mitochondrial dysfunction can directly promote atherosclerosis. Dysfunctional mitochondria produce reactive oxygen species (ROS), release cardiolipin and damaged mitochondrial DNA (mtDNA) that can activate the NLRP3 inflammasome. They can also release cytochrome C upon sensing apoptotic signals that further promotes cellular apoptosis. Insufficient production of ATP, leads to the activation of AMP-activated protein kinase (AMPK) that inhibits gluconeogenesis and adipogenesis.

Mitochondria are highly dynamic organelles that constantly undergo fusion and fission (division) forming mitochondrial networks. Integrity of these networks is vital for cell survival and health. Hence, we speculate that internalized PEV into monocytes transfer mitochondria, which can get integrated in the existing mitochondrial networks. However, in atherosclerosis PEV-borne mitochondria might disrupt the function of monocyte mitochondrial networks, this way contributing to atherosclerosis.

The aims for this chapter were to:

1. Check whether PEV contain mitochondria.
2. Discover whether PEV-borne mitochondria get internalised into monocytes.
3. Discover whether PEV-borne mitochondria get integrated into monocyte mitochondrial networks.

7.2 Methodology

7.2.1 Staining of PEV Mitochondria

Resting platelets were stained with MitoTracker dyes (Green/ Deep Red) at different concentrations and with PKH67 dye where necessary and washed extensively. Stained platelets were stimulated using CRP-XL/ thrombin to shed PEV-containing mitochondria. Stained PEV were purified by differential centrifugation and were analyzed by FACS (Accuri C6). Statistical analysis was performed using Graph Pad Prism 6. (For further detail see methods section 2).

7.2.2 Staining and Imaging of Live Monocyte Mitochondria

Washed monocytes were stained with MitoTracker dyes (Green/ Deep Red) at different concentrations and washed extensively. Stained monocytes were plated onto glass surfaces in culture medium and imaged in real time by STORM (Stochastic Optical Reconstruction Microscopy).

7.2.3 Investigation of transfer of PEV-derived Mitochondria to Monocytes

Monocytes unstained or MitoTracker-stained were incubated with MitoTracker-stained PEV or the filtrate from the PEV suspensions (filtered through 0.25 μm pores) in order to remove the bigger PMV that contain mitochondria; or platelets or the filtrate from platelet suspensions. Monocyte uptake of exogenous mitochondria was assessed

by by FACS (Cyan ADP) and confocal microscopy. Images were analysed using FIJI software. Statistical analysis was performed using Graph Pad Prism 6. (For further detail see methods section 2).

7.3 Results

7.3.1 Investigation of Mitochondria presence in PEV

In order to determine whether PEV contain mitochondria and whether these are enclosed in vesicular membranes or are "naked" mitochondria, platelets were stained with the mitochondrial dye MitoTracker Deep Red and/or with the membrane dye PKH67 before stimulation and subsequent shedding of PEV. The level of staining was assessed by FACS. **Fig. 7.2** shows representative histograms of MitoTracker Deep Red/PKH67 expression by PEV. When PEV were only stained with MitoTracker, >90% of PEV appeared positive, indicating that many of the PEV detectable by FACS contained high presence of mitochondria (**Fig. 7.2A, left histogram**). However, when PEV were also stained with PKH67 in order to see what percentage of the mitochondria were membrane-enclosed or not, the level of MitoTracker staining decreased by approximately one third (**Fig. 7.2A, right histogram**). All MitoTracker+ve particles were also positive for PKH67, indicating that mitochondria were always shed within an envelopeof platelet membrane (**Fig. 7.2B, left histogram**). When PEV were stained only with PKH67 dye, almost 100% of them were found positive (**Fig. 7.2B, right histogram**).

The percentage of MitoTracker+ve/PKH67+ve events was analysed graphically and statistically from a number of experiments (**Fig. 7.3**). The percentage of MitoTracker+ve vesicles decreases significantly when PEV were also stained with

PKH67 dye (**Fig. 7.3A**). All PEV and all MitoTracker+ve PEV were also positive for PKH67 (**Fig. 7.3B**).

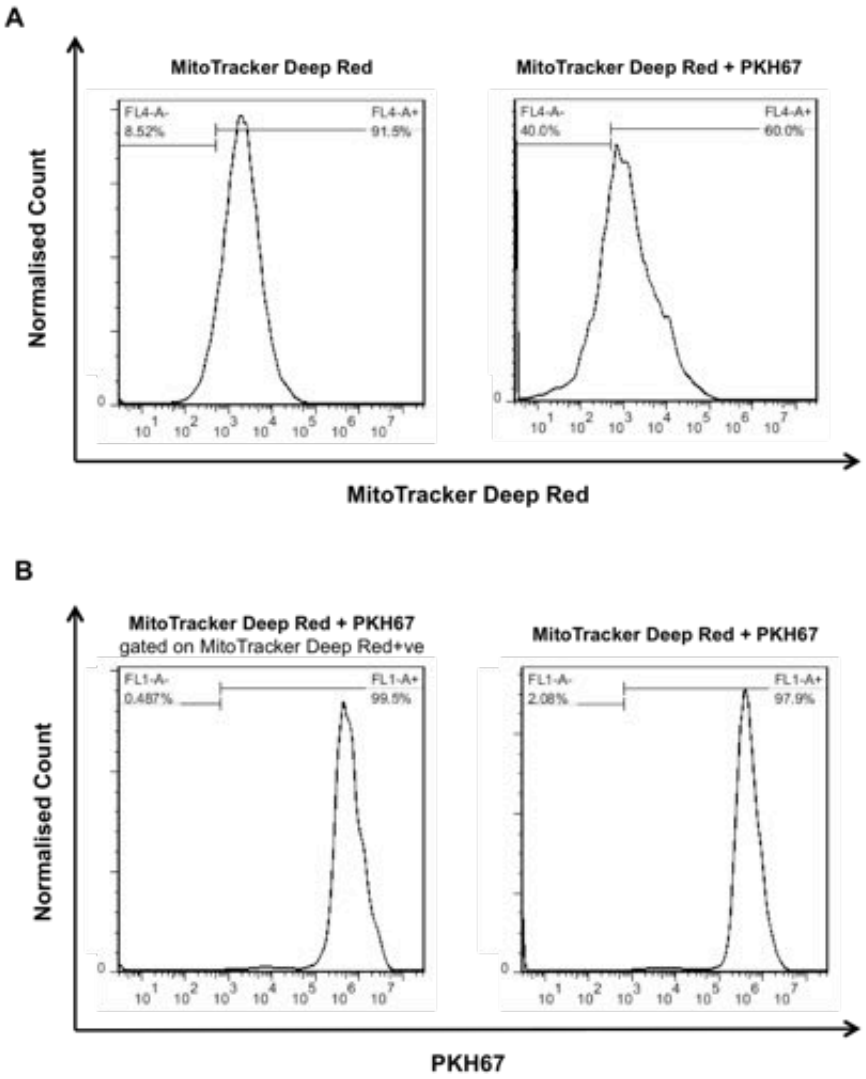

Figure 7.2. Presence of Mitochondria in PEV

(A) Representative histograms of MitoTracker Deep Red expression by PEV stained for MitoTracker Deep Red dye only or MitoTracker Deep Red and PKH67 dye, as detected by flow cytometry. **(B)** Representative histogram of PKH67 expression by PEV, stained with MitoTracker Deep Red and PKH67 dye, gated on MitoTracker Deep Red+ve events or ungated. The gates were set using unstained controls (not shown).

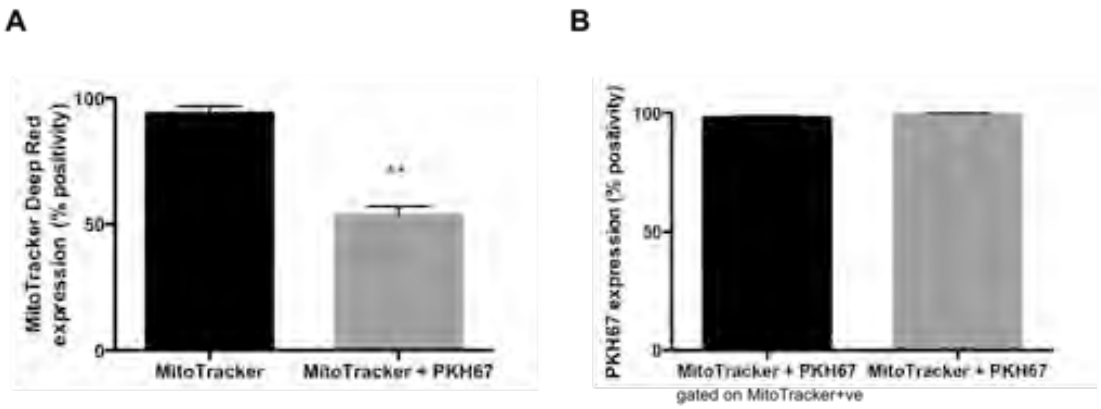

Figure 7.3. Presence of Mitochondria in PEV

(A) Percentage of PEV stained with MitoTracker Deep Red only or MitoTracker Deep Red and PKH67 dye expressing MitoTracker Deep Red. **(B)** Percentage of PEV stained with MitoTracker Deep Red and PKH67 dye gated on MitoTracker Deep Red+ve events or ungated expressing PKH67. Data are represented as mean +/- SEM of 3 experiments. All data were analysed by t-test. ** indicates $P<0.01$.

7.3.2 Characterisation of Mitochondria in Monocytes

Before introduction of PEV mitochondria to monocytes, we wanted to first observe and characterize the behaviour of endogenous mitochondria in monocytes, as well as optimise imaging conditions. Live mitochondria were stained with MitoTracker Deep Red and imaged in real time by STORM (Stochastic Optical Reconstruction Microscopy). **Figure 7.4** shows representative images of mitochondria in two live monocytes stained with MitoTracker Deep Red. Upon careful observation, individual mitochondria can be seen to be located at different positions within the cells, indicating that they are constantly moving.

The path of individual mitochondria was tracked over the course of 50 seconds using the Trackmate plugin on FIJI software and is shown in different colours in **Fig. 7.5**. Individual mitochondria were constantly moving, fusing with each other and dividing, forming tubular networks i.e. elongated structures from the fusion of mitochondria.

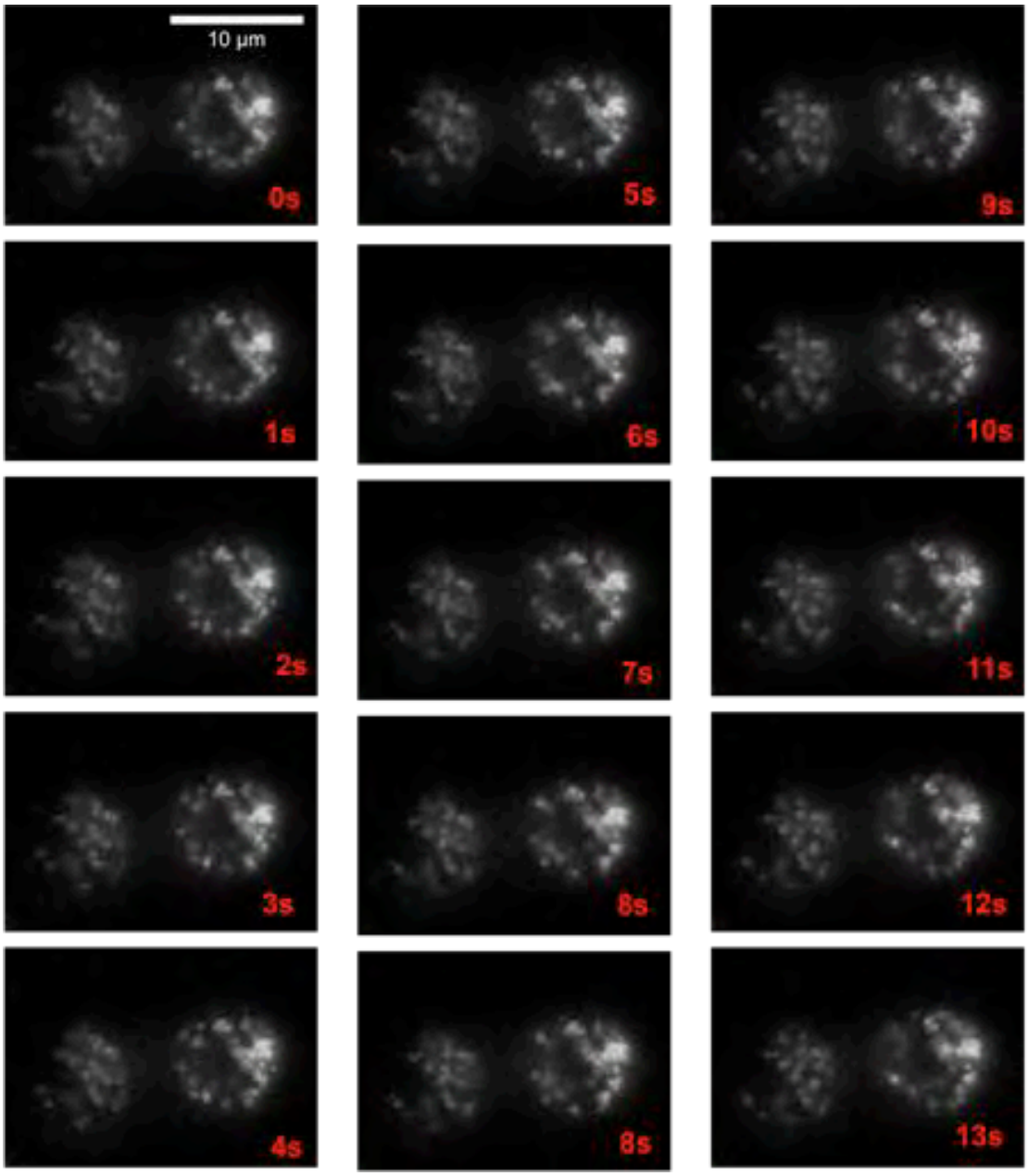

Figure 7.4. The behaviour of Mitochondria in Monocytes

Live monocytes stained with MitoTracker Deep Red were imaged by STORM live. Images were captured every second. White dots represent individual mitochondria.

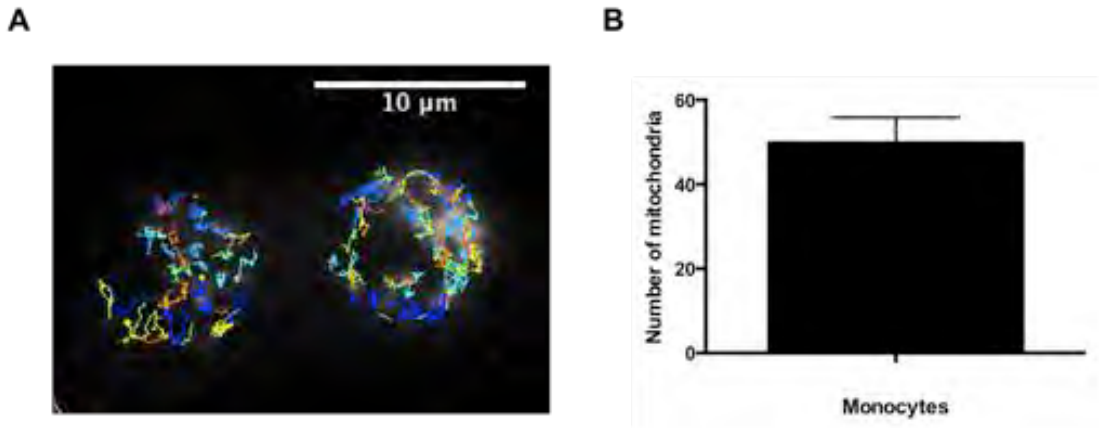

Figure 7.5. The trajectory of Mitochondria in Monocytes

(A) Individual mitochondria trajectories in representative monocytes over the course of 50 seconds as tracked by FIJI software. **(B)** Quantification of mitochondria in monocytes based on differential trajectories. Data is mean + / - SEM of 10 monocytes.

7.3.3 Investigation of transfer of PEV-derived Mitochondria to Monocytes

Since PEV were found to carry mitochondria and since PEV were found in Chapter 6 to be internalized by monocytes, we hypothesized that PEV-borne mitochondria can also gain entry into monocytes. In order to investigate this possibility, induced-PEV were stained with MitoTracker dyes and incubated with washed monocytes over a 50-minute time-course. As a control, the filtrate (filtration through 0.25um pores) from the PEV suspension was also incubated with washed monocytes.

7.3.3.1 Investigation by FACS

Acquisition of PEV-derived mitochondria by monocytes is shown in flow cytometry dotplots in **Figure 7.6.** PEV were stained with MitoTracker Green. Almost all monocytes become positive for MitoTracker Green upon incubation with PEV or with the filtrate at all time points. Monocytes seem to acquire MitoTracker Green with increased intensity by time.

The histograms of MitoTracker Green expression by monocytes were also analysed. They show clearly that most monocytes become positive for MitoTracker Green upon incubation with both PEV or the filtrate from PEV at all time points. The fluorescence intensity however increases with time with both PEV and filtrate. The signal starts to saturate between 30-50 minutes (**Fig. 7.7**).

The percentage of MitoTracker Green+ve monocytes and the median fluorescence intensity of monocytes were plotted graphically and analysed statistically (**Fig. 7.8**). Most monocytes become positive with MitoTracker Green when incubated with PEV suspension or the filtrate from PEV from as early as 5 minutes of incubation (**Fig. 7.8A**). The fluorescence intensity increases significantly with time up to 50 minutes with both PEV and the filtrate from them. The signal of monocytes with the filtrate is significantly lower than the signal with the PEV (**Fig. 7.8B**).

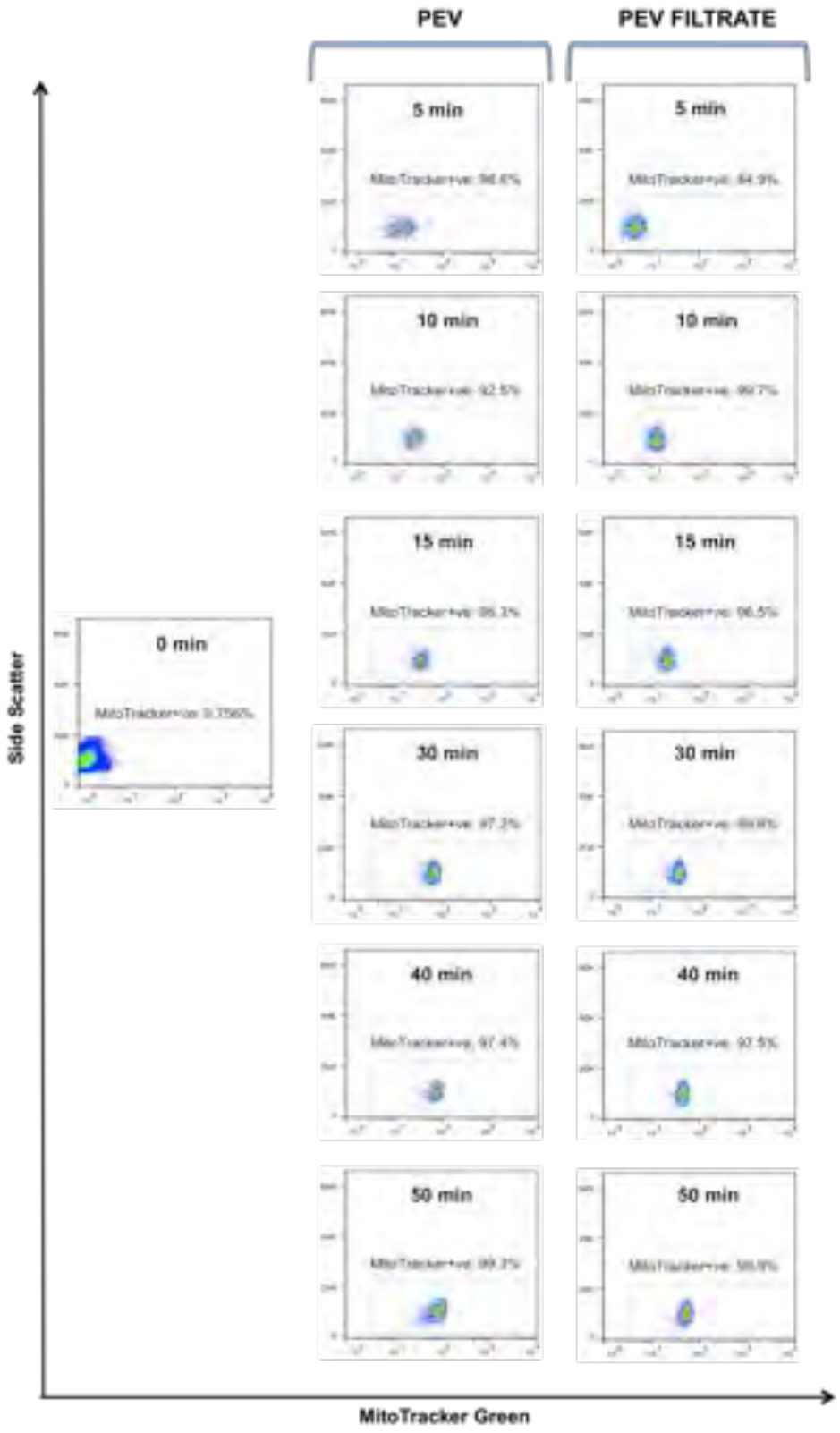

Figure 7.6. Uptake of PEV-derived Mitochondria by Monocytes

Monocytes were incubated with PEV stained with MitoTracker Green or with the filtrate from the PEV suspension over the course of 50 minutes under shear stress conditions.

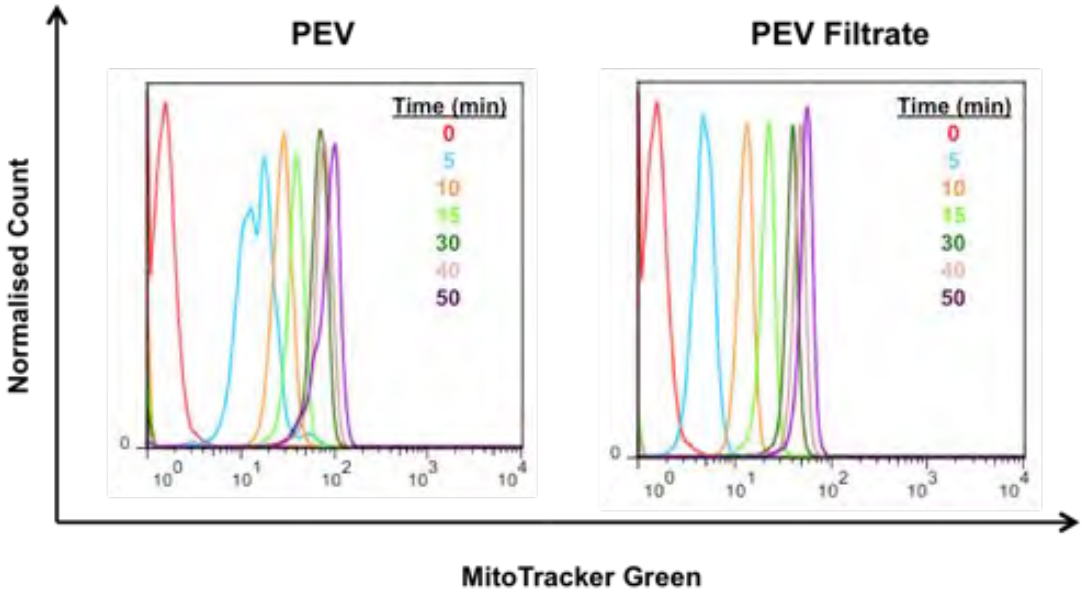

Figure 7.7. Uptake of PEV-derived Mitochondria by Monocytes

Monocytes were incubated with PEV stained with MitoTracker Green or with the filtrate from the PEV suspension over the course of 50 minutes under shear.

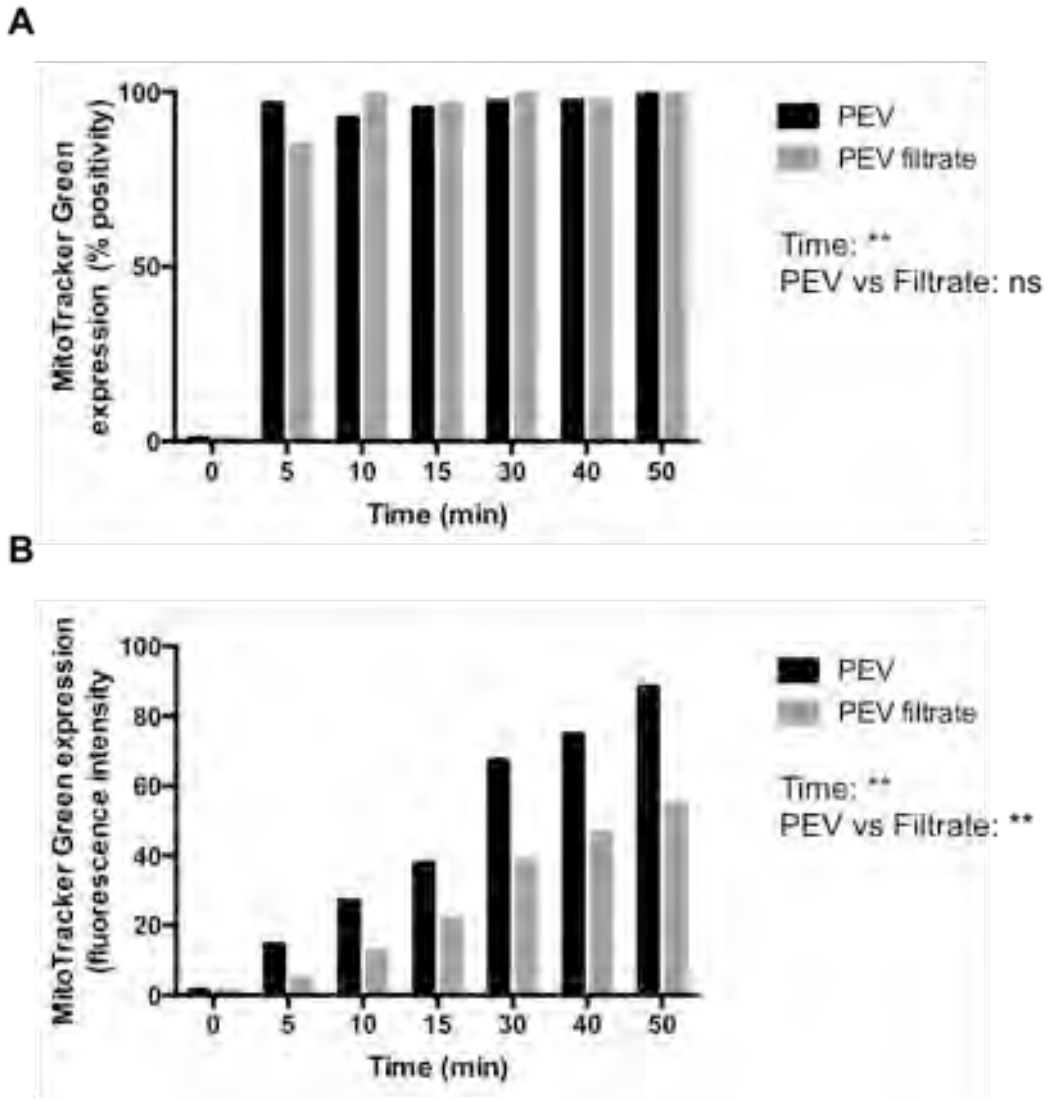

Figure 7.8. Uptake of MitoTracker Green by Monocytes

Monocytes exposed to PEV or a filtered supernatant from PEV suspensions were analysed by flow cytometry for fluorescent stain. Two-way ANOVA tests were performed for both graphs to determine effect of time and any difference between PEV and filtrate. ** indicates $P<0.01$, ns indicates no statistical significance.

7.3.3.2 Investigation by Microscopy

Incubation of monocytes with the filtrate of PEV (control sample) resulted in detectable signal on the monocytes that significantly increased by time. However, this signal was significantly lower than the signal with the PEV. We wanted to image monocytes incubated with the filtrate by PEV, in order to check whether the signal is

detectable by confocal microscopy or whether it is minimal and should be disregarded as background signal. Monocytes in these experiments were fixed before imaging.

Representative images are shown in **Fig. 7.9**. The positive control (monocytes stained with MitoTracker Green) shows clearly defined dots of high fluorescent intensity. The unstained monocyte that was incubated with PEV stained with MitoTracker shows less-defined dots that are of lower fluorescent intensity. The unstained monocytes that were incubated with the filtrate from MitoTracker-stained PEV shows low green fluorescence. Individual dots cannot get identified.

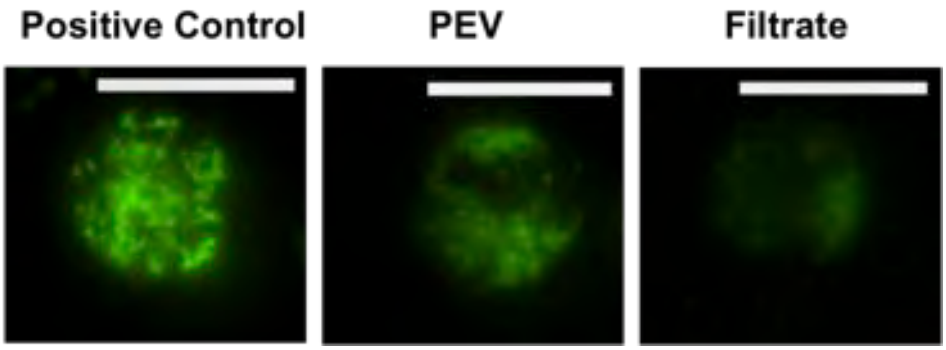

Figure 7.9. Mitochondria signal in Monocytes

Monocytes were either stained with MitoTracker Green or were incubated with PEV stained with MitoTracker Green or with the filtrate from stained PEV. Scale bar is 10um.

The fluorescence intensity from a number of cells was quantified using FIJI software (**Fig. 7.10**). The mean fluorescence intensity on the monocytes that were incubated with the PEV suspension was significantly lower than the control sample and significantly higher than the filtrate sample.

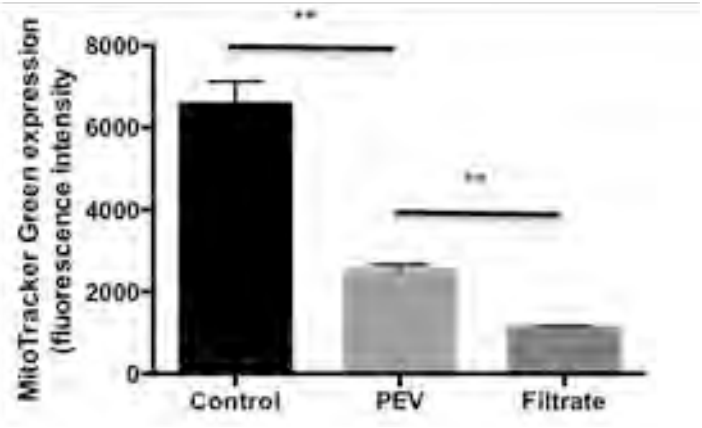

Figure 7.10. Mitochondria signal from Monocytes

Monocytes were either stained with MitoTracker Green or were incubated with PEV stained with MitoTracker Green or with the filtrate from stained PEV. T-tests were performed between groups. > 20 randomly selected cells were analysed per group. ** indicates P<0.01.

7.3.4 Investigation of Dye Leakage

7.3.4.1 Investigation by Microscopy

Upon observing that incubation of monocytes with the filtrate from PEV suspension results in significant mitochondrial signal expressed by monocytes, we decided to perform a control experiment. Monocytes stained with MitoTracker Green and resting platelets stained with MitoTracker Deep Red were incubated together for 30 minutes, washed and imaged live by confocal microscopy. In theory, monocytes should appear green and platelets red without any overlap.

However, most mitochondria, either in the monocytes or in the platelets appeared stained with both colours (this was not due to spectral overlap) (**Fig. 7.11A**). Monocytes and platelets are distinguished by their difference in size. The monocyte in the white dashed circle appears only green in the merged image. However in the single colour images, a low level of red fluorescence is revealed. The platelet in the blue dashed circle clearly contains both red and green mitochondria aligned next to each other. These are however the same mitochondria, stained with both green and red

MitoTracker, but because stained live, they appear as misaligned because of the lag time it takes for the microscope to change lasers and image in the next colour channel. The next monocyte in the purple dashed circle contains dots in different shades/intensities of green, yellow and orange. This shows that monocyte mitochondria acquired MitoTracker Deep Red dye. Hence, there is a large level of dye leakage.

Colocalization analysis using FIJI software revealed two different correlations between the green and red fluorescence intensities (dashed blue and green lines). The overall correlation coefficient was 0.82, which is indicative of high correlation (**Fig. 7.11B**). The existence of two correlations reveals the presence of two separate entities. The blue-lined correlation represents mitochondria originally stained with MitoTracker Green and later stained with MitoTracker Deep Red (these show higher green fluorescence and lower red fluorescence) and the green-lined correlation represents mitochondria originally stained with MitoTracker Deep Red and later stained with MitoTracker Green (these show higher red fluorescence and lower green fluorescence).

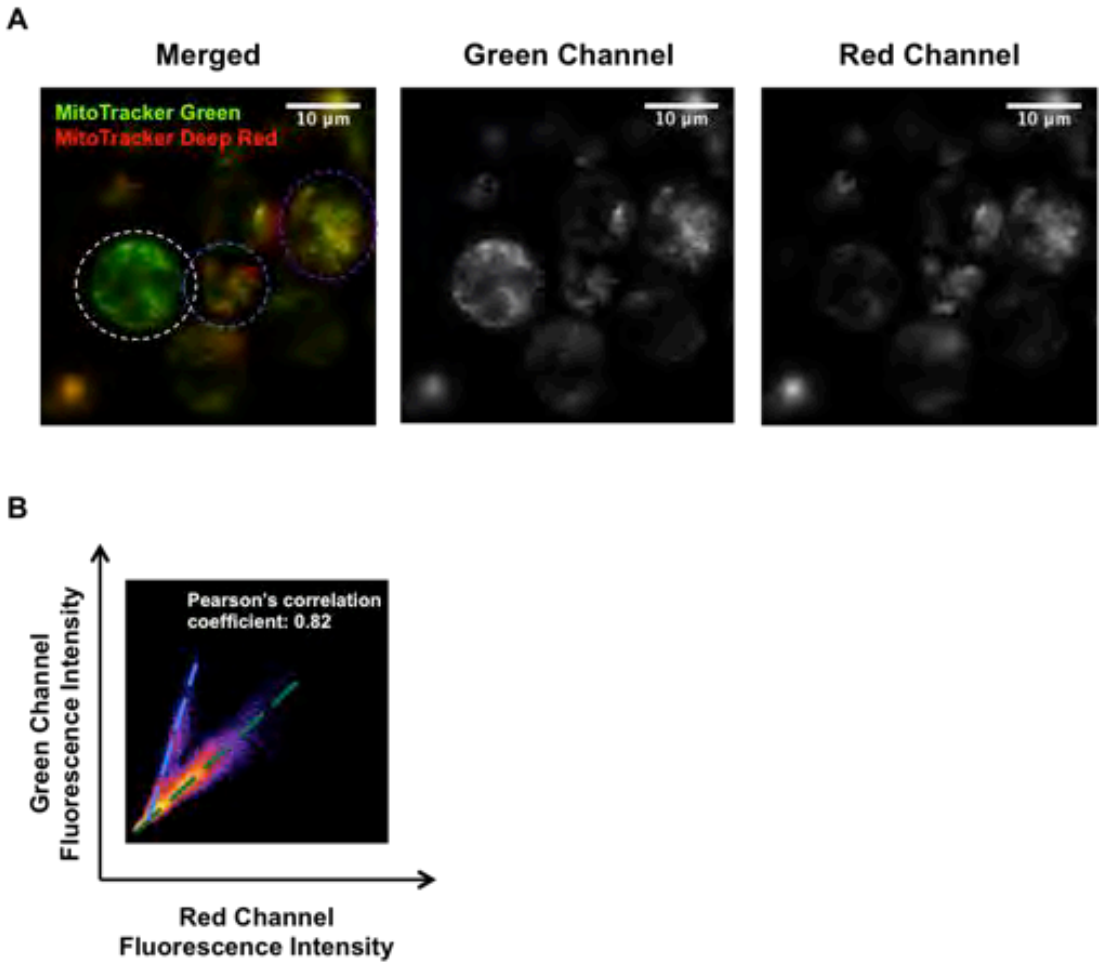

Figure 7.11. MitoTracker dye leakage

Monocytes stained with MitoTracker Green were incubated with resting platelets stained with MitoTracker Deep Red and imaged live by confocal microscopy. **(A)** Representative images of monocytes and platelets, **(B)** Correlation of the fluorescence intensity in the Red versus the Green channel by FIJI analysis. The calculated correlation coefficient is indicated.

7.3.4.2 Investigation by FACS

Unstained monocytes were incubated with resting platelets or platelet filtrate or PEV or PEV filtrate, all stained with MitoTracker Deep Red for 30 minutes and the level of MitoTracker Deep Red expression on the monocytes was assessed by FACS. A representative overlay histogram indicates that all monocytes become positive for MitoTracker Deep Red upon incubation with any suspension or solution. The lowest fluorescence is acquired with the platelet filtrate, followed by PEV filtrate, PEV and

platelets in ascending order of fluorescence. Incubation with the filtrates resulted in lower fluorescence than that expressed by platelets, whereas incubation with platelets or PEV resulted in higher MitoTracker expression than that expressed by platelets on the monocytes.

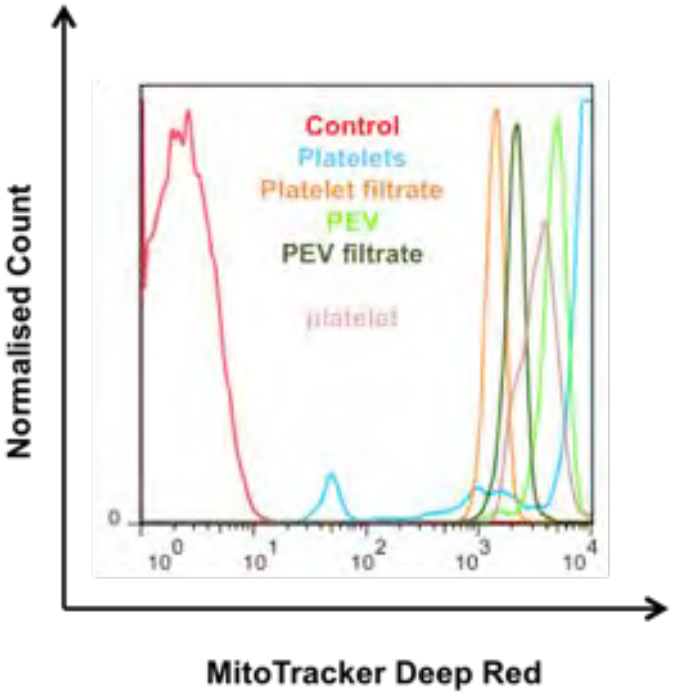

Figure 7.12. MitoTracker dye leakage

Overlay histogram of MitoTracker Deep Red expression on monocytes upon incubation with resting platelets/platelet filtrate/PEV/PEV filtrate, all stained with MitoTracker Deep Red, as analysed by FACS. The trace of MitoTracker expression on the platelets is also shown as reference.

The percentage and fluorescence intensity were assessed graphically and statistically from a number of experiments. All monocytes became positive for MitoTracker Deep Red upon incubation with platelets/PEV/filtrates. However the fluorescence acquired by monocytes varies in each case. Incubation with the filtrate from platelets results in very low MitoTracker expression by monocytes; significantly lower than the expression when incubated with platelets. This means that the high expression encountered when incubated with platelets is not the result of inadequate

washing of the platelets that results in high levels of free dye outside of the cells and into the solution. The expression of MitoTracker Deep Red on the monocytes upon incubation with the PEV filtrate is not significantly lower than the signal seen with the PEV and is higher than the signal with the platelet filtrate.

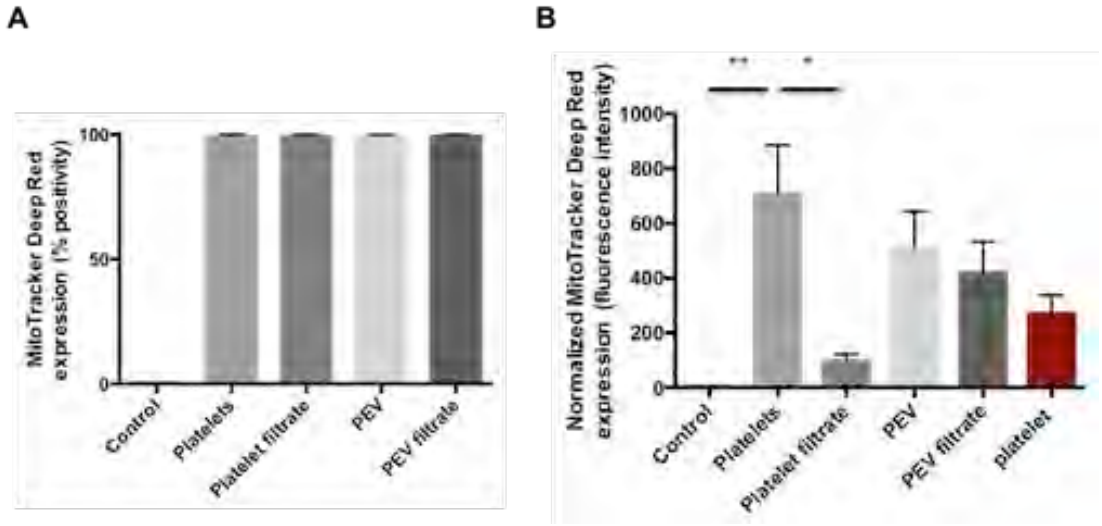

Figure 7.13. MitoTracker dye leakage

(A) Graphical percentage of monocytes expressing MitoTracker Deep Red. **(B)** Graphical median fluorescence intensity of MitoTracker Deep Red on monocytes. The fluorescence intensity of platelets is also shown as a reference. Data are represented as mean +/- SEM of three independent experiments. One way ANOVA test with multiple comparisons was performed. * indicates $P < 0.05$, ** indicates $P < 0.01$.

7.4 Discussion

There is now evidence to suggest that monocyte mitochondrial dysfunction can directly promote atherosclerosis. A recent publication showed that activated platelets can release free mitochondria and mitochondria enclosed in extracellular vesicles (Boudreau et al., 2014). Hence, since PEV can get internalized into monocytes (Chapter 6), we hypothesized that PEV can also transfer mitochondria or mitochondrial components into monocytes and that in atherosclerosis, PEV-derived mitochondria/mitochondrial components can somehow cause monocyte mitochondrial dysfunction, thus contributing to the progression of atherosclerosis.

We attempted to replicate this result in our experiments. Platelets were co-stained with the MitoTracker Deep Red dye that marks mitochondria and with the PKH67 dye that marks cell membrane. >90% of PEV were found positive for mitochondria. However, all mitochondria detected were membrane-enclosed. No free mitochondria were detected. This contradicts the observations of Boudreau and colleagues (2014). This outcome could be due to size detection limitation of the flow cytometer (Accuri C6 has a 0.5 μm cut-off). Boudreau et al. used a high sensitivity flow cytometry configuration that according to them allowed detection of particles from 100 nm in size to be detected simultaneously. Further investigation with a more sensitive flow cytometer is hence required in order to say with confidence whether naked mitochondria exist in our preparations or not.

Live imaging of monocyte mitochondria revealed that monocyte mitochondria are highly motile and that they constantly move in a relatively organized way forming mitochondrial networks. Due to the high and fast motility of monocyte mitochondria it is difficult to image them live if two-coloured laser is required, i.e. when PEV mitochondria are also stained with a different colour MitoTracker.

The MitoTracker dyes contain a mildly thiol-reactive chloromethyl moiety that passively diffuse across the plasma membrane and stain active mitochondria. They have been used extensively in the literature (Bosnjak et al., 2012; Arnaudeau et al., 2002; Jambrina et al., 2003; Hobbs et al., 2001). However, in our studies these proved to be unsuitable as incubation of monocytes with the filtrate from PEV suspension resulted in mitochondrial signal to monocytes. In addition, monocyte incubation with resting platelets stained with MitoTracker resulted in intercellular staining of monocyte mitochondria with platelet mitochondria dye and vice versa. As resting platelets do not

form aggregates with monocytes (Chapter 4) and since resting platelets do not release mitochondria (observation in our lab, not shown here), it is unlikely that this result represents true mitochondria transfer. It seems to be the result of dye transfer.

MitoTracker staining of mitochondria depends on mitochondrial membrane potential. A loss in membrane potential causes the dye to get washed off; so it can travel as free dye until it finds other mitochondria with the right membrane potential to stain. Hence even if no excess dye is used, there is still high chance that free dye is mobilised once mitochondrial integrity is compromised. Incubation with platelet filtrate resulted in minimal monocyte MitoTracker signal; hence not much free dye is present extracellularly, but when the filtrate from PEV is incubated with monocytes, this results in higher signal on the monocytes. We cannot exclude the possibility of inadequate filtration. A syringe system was used to push PEV through a 250nm pore filter. The resulting filtrate that in theory contains vesicles smaller than 250nm, could not be assessed by FACS in order to check whether it contained mitochondria, as our flow cytometer has a 500nm cut-off. Hence, the high signal with the PEV filtrate could be the result of insufficient exclusion of mitochondria. However, there is another possible explanation for the presence of MitoTracker dye in the PEV filtrate. When the platelets are activated to shed PEV, mitochondria tend to depolarize, which could result in uncoupling of the dye that later diffuses through the monocyte membrane and stains monocyte mitochondria. Our results are in accordance with studies from Cselenyak and colleagues (2010). This group also found that MitoTracker dyes are unsuitable for determining mitochondrial transfer in co-cultures, because there is passive diffusion of the dye.

One way to overcome this would be to double-stain PEV with a MitoTracker and an antibody that binds PEV, i.e. anti-GPIb as in Chapter 6. In this case, mitochondria inside monocytes that also express GPIb would be identified as PEV-derived. In this experiment MitoTracker dye needs to be added first when PEV are active (i.e. alive, at the platelet stage before stimulation to shed the PEV), whereas anti-GPIb antibody needs to be added second, after PEV are incubated with monocytes, because we found that antibody presentation on PEV inhibits PEV aggregation with monocytes (not shown). However, when this was attempted we could not detect any signal for GPIb. According to Thermo Fisher Scientific the chloromethyl group of the MitoTracker dyes may covalently bind to proteins in the cell so it is possible to interfere with antibody binding.

The use of the MitoTracker dyes has another weakness in our experimental setting. Most MitoTracker dyes are non-fluorescent in aqueous solutions and become fluorescent only on sequestration and association with lipids within the mitochondria. This is a major advantage in general because it means that the signal detected by FACS or by fluorescence microscopy comes only from mitochondria and not from free dye in the cells. However, in our experiments it constitutes a disadvantage because we cannot assess whether there is free dye in our PEV suspension outside of PEV or dye trapped in PEV without presence of mitochondria. (Staining of PEV with MitoTrackers was assessed by flow cytometry and >90% were found positive. However the Accuri flow cytometer only detects <1% of PEV, only the larger PMV. Smaller PMV and exosomes cannot be detected by Accuri as proved in Chapter 3 and these could contain free dye) When the PEV suspension is incubated with our monocyte suspension any free dye can diffuse into the monocyte and stain monocyte mitochondria, which again could be mistakenly interpreted as PEV-derived mitochondria.

In order to overcome these issues, two future approaches are proposed. Firstly, the use of fluorescent proteins such as GFP could be employed. Transgenic mice that express a fluorescent protein coupled to their mitochondria such as the *Gt(ROSA)26Sor*$^{tm1(CAG\text{-}mCherry/GFP)Ganl}$ mouse strain (McWilliams et al., 2016) could be used in theory to generate PEV with fluorescent mitochondria. PEV could be then incubated with wild type mouse monocytes and their uptake could be investigated by microscopy.

Another approach involves the use of mitochondrial antibodies. However, the use of a mitochondrial antibody pre-requires that the cells/vesicles are permeabilized. Mitochondria cannot be stained with an antibody while in the platelet, because permeabilised platelets cannot be stimulated to shed PEV. Hence, PEV mitochondria have to be stained after incubation with monocytes and subsequent permeabilization. However, this would stain also monocyte mitochondria. This problem could be overcome if we take an inter-species approach. For example, human PEV could be incubated with mouse monocytes. Upon internalization (assuming this will happen), cells will get permeabilized and stained using human mitochondria-specific antibodies such as the anti-mitochondria antibody 113-1 from Abcam.

Conclusions

The majority of PMV contain a mitochondrion. No further conclusions can be made with certainty as to whether PEV transfer their mitochondria into monocytes. This remains to be investigated in future studies. However, this does not seem impossible since PEV in general are readily internalized by monocytes (Chapter 6) and PEV commonly contain mitochondria.

8 INTRAVITAL IMAGING OF INTERACTIONS BETWEEN MONOCYTE-PEV AGGREGATES AND BLOOD ENDOTHELIUM IN ATHEROSCLEROSIS

8.1 Introduction

Any damage to the vascular endothelium that exposes the subendothelial extracellular matrix (ECM) triggers platelet recruitment at the injured site. Circulating platelets initially decelerate over the compromised site due to transient interactions with the extracellular matrix. These initial interactions trigger platelet activation, which results in the activation of specialized integrins that then enable firm adhesion of platelets to the ECM.

Initial interaction between platelets and the subendothelium is influenced by the rheological conditions of the blood. In veins and microvessels, where there is low shear stress, platelets bind directly to exposed collagen, fibronectin and laminin. However under conditions of high shear stress, such as those in the large arteries, platelet binding to the subendothelium is achieved indirectly, through binding plasma VWF that itself rapidly binds exposed collagen (Savage et al., 1998; Jackson et al., 2003).

Platelets initially bind VWF through the platelet receptor GPIba (Sakariassen et al., 1986), a subunit of GPIb-IX-V. This binding has a fast dissociation rate; hence it is incapable of mediating stable adhesion. However, this interaction keeps platelets in close proximity with the vessel surface, with rolling along the VWF in the direction of blood flow. The resulting deceleration or “rolling” enables another platelet receptor, called glycoprotein-VI (GPVI), to interact with exposed collagen. GP VI binds collagen with low affinity; therefore it is incapable of mediating stable adhesion either. However, it induces intracellular signaling that activates platelets and transforms platelet integrins to a high-affinity state. Platelet activation, results in the activation of integrin receptor αIIbβ3 (glycoprotein IIbIIIα, GPIIbIIIa), forming a stable bond with VWF (Savage et al., 1998; Jackson et al., 2003).

Many studies investigated whether the ability of platelets to bind compromised endothelium can be exploited by monocytes in inflammation. In a model of allergic inflammation circulating platelets were found to form aggregates with leukocytes and to be essential for their recruitment (Pitchford et al., 2003). In addition, our group has shown in the past that in cocultures of ECs and secretory SMCs (the phenotype seen in atherosclerotic vessel wall), a matrix of vWF is presented to flowing blood, allowing platelets to attach to the endothelium (Tull et al., 2006). These adhered platelets can serve as adhesive bridges between flowing monocytes in blood and the EC surface (Kuckleburg et al., 2011).

However, not much research has gone into PEV or PEV-mediated recruitment. Studies by Merten and colleagues (1999) showed that infusion of PEV into the abdominal aorta of rabbits after induction of endothelial injury resulted in increased recruitment at the iliac artery. In addition, recent *in vitro* studies from our group revealed that perfusion of monocytes that are "decorated" with PEV on their surface over immobilized vWF or TGFβ-stimulated endothelial cells up-regulates monocyte adhesion (Chimen et al.; under review). Our group also replicated this result *in vivo* in the microcirculation of a mouse model of induced inflammation (Chimen et al.; under review). These observations led us to speculate that PEV might act as adhesive intermediates that bridge monocytes with inflamed endothelium in atherosclerosis.

The aim for this chapter was to:

- Investigate whether PEV up-regulate monocyte recruitment in atherosclerosis.

8.2 Methodology

8.2.1. Aggregation of human monocytes with murine PEV

Murine PEV, generated from purified mouse platelets, were incubated with human monocytes (due to difficulty in obtaining adequate numbers of murine monocytes from the circulation) for 30 minutes at 37°C. The cells were stained with anti-GPIbα antibody for FACS analysis or with Cell-Tracker Orange for intra-vital microscopy. Stained monocytes were purified from free PEV by centrifugation (For further detail see methods section 2).

8.2.2. Intra-vital Microscopy

ApoE-/- mice with established atherosclerosis (fed a high fat diet for six weeks from 10 weeks of age) were injected with Cell-Tracker Orange-stained monocytes (derived from human blood) alone or monocytes aggregated with PEV (derived from murine platelets) in the circulation through the left common carotid artery through a cannula.

Interaction of injected cells with the vessel wall was monitored *in vivo* by fluorescent video-microscopy in the right common carotid artery at the athero-prone "fork" site. The number, velocity and duration of adhesion interactions were manually analysed using the SlideBook 6 Reader Software. Statistical analysis was performed using Graph Pad Prism 6. (For further detail see methods section 2).

8.3. Results

8.3.1. Aggregation between human monocytes and mouse PEV

Before testing *in vivo* whether PEV bound to monocytes can mediate recruitment of monocytes to athero-compromised endothelium, it was essential to confirm that

murine PEV and human monocytes are also capable of forming heterotypic aggregates, like the human PEV and monocytes in chapters 4 and 5. However, our yield of purified monocytes from the mouse circulation was very low so we decided to try an inter-species approach i.e. to perfuse heterotypic aggregates of human monocytes with murine PEV into the mouse circulation and check whether these would get recruited to the endothelium. Before infusing these aggregates, we checked by FACS whether this inter-species heterotypic aggregation could take place.

Figure 8.1. shows the expression of mouse GPIbα on human monocytes that were incubated with mouse PEV, as opposed to the expression of mouse GPIbα on human monocytes before the introduction of the PEV. It is clear that almost all monocytes become highly positive for GPIbα once incubated with the PEV, suggesting that human monocytes are capable of forming aggregates with mouse PEV.

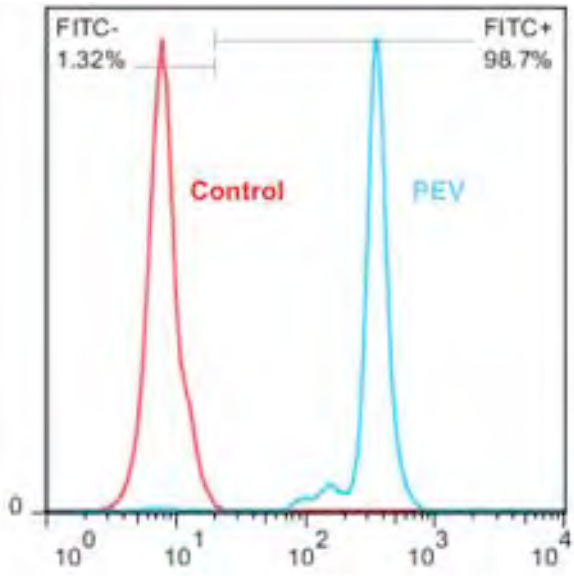

Figure 8.1. Expression of mouse GPIbα on human monocytes

Representative histogram showing expression of mouse GPIbα on human monocytes before and after incubation with mouse PEV.

8.3.2. Monocyte Adhesion to the carotid artery in the *ApoE* KO mouse

Upon injection of human monocyte-mouse PEV aggregates (Cell-Tracker Orange-stained) in the *ApoE* KO mouse circulation, a number of stable and unstable (rolling) interactions were noted at the fork site of the right common carotid artery. A representative monocyte exhibiting both types of adhesive behavior is shown in **Fig. 8.2**.

The stable and rolling interactions were quantified from a number of experiments (**Fig. 8.3**). The total number of adhered monocytes (sum of stable and rolling) when monocytes were “decorated” with PEV was higher than when monocytes were perfused alone.

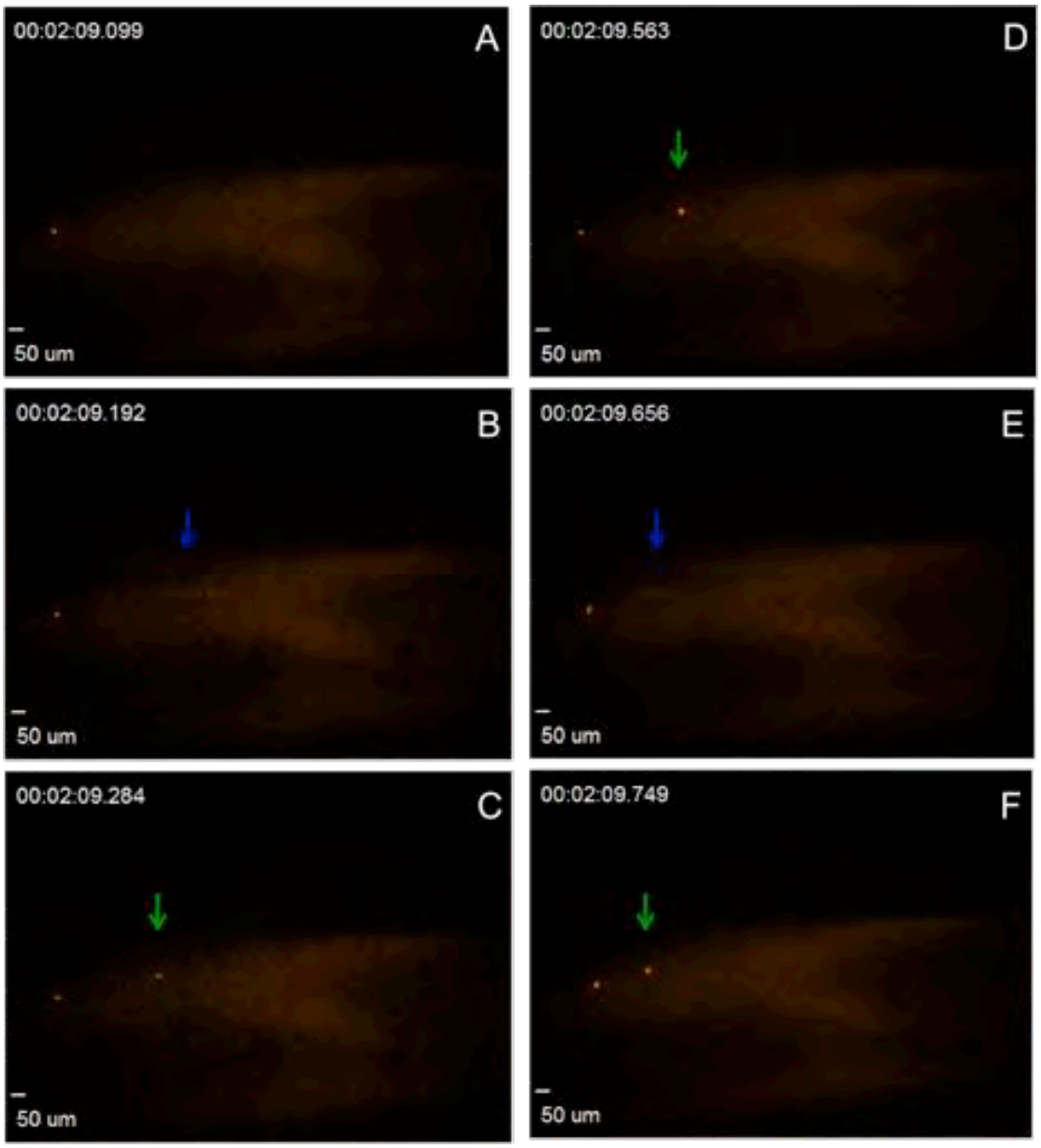

Figure 8.2. Stable and Unstable Monocyte adhesion in the carotid artery of the ApoE KO mouse

Monocytes stained with Cell Tracker Orange were injected in the mouse circulation and adhesive interactions onto the mouse endothelium in the carotid artery were video-recorded. A representative monocyte is shown here exhibiting mixed adhesion modes. The time passed post cell injection is shown on the top left corner. The blue arrow shows rolling adhesion and the green arrow shows stable adhesion. **(A)** Before an interaction was observed, **(B)** a monocyte is seen rolling, **(C)** the monocyte firmly adheres, **(D)** the monocyte is still firmly adhered after 279ms, **(E)** the monocyte rolls for a second time, **(F)** the monocyte firmly adheres for a second time.

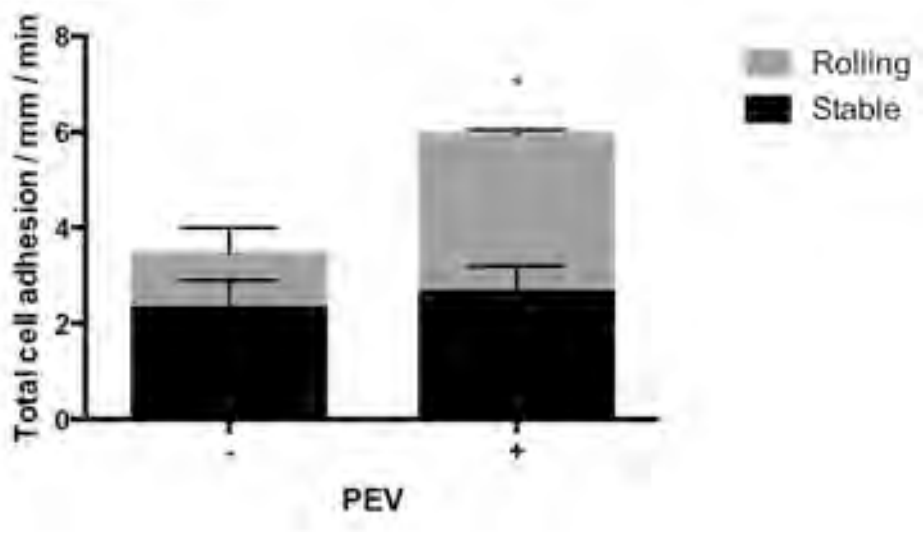

Figure 8.3. Quantification of Monocyte Stable and Rolling interactions in the carotid artery of the ApoE KO mouse

Total number of monocytes exhibiting stable or rolling adhesion onto mouse endothelium when monocytes were injected alone or when monocytes were decorated with PEV during the first six minutes post-cell injection. Data are shown as Mean +/- SEM of 2 independent experiments. Data were analysed by t-test. * indicates $P< 0.05$.

8.3.3. Stable Interactions

The duration of stable interactions was quantified **(Fig. 8.4)**. When monocytes carried PEV on their surface their stable interactions lasted significantly longer.

The majority of stable interactions took place in the first three minutes passed post-cell introduction. A higher percentage of stable interactions occurred in the first three minutes with the monocyte-PEV aggregates (> 75%) than when monocytes were perfused alone (< 75%), whereas a higher percentage of stable interactions occurred in the last three minutes of imaging with the no PEV sample (> 25%) than with the PEV sample (< 25%) (**Fig. 8.5**).

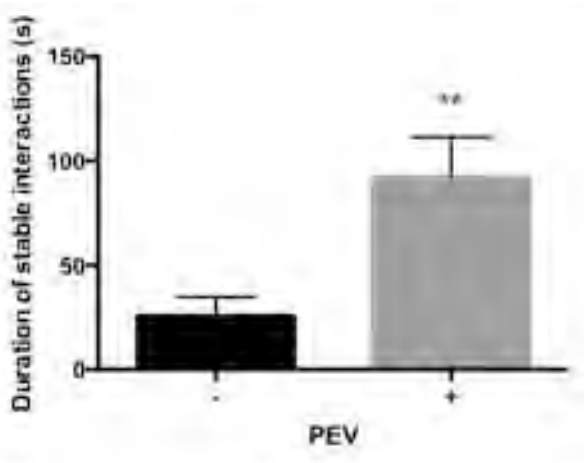

Figure 8.4. Duration of Stable interactions

Duration of stable cell interactions when monocytes were injected alone or when monocytes were decorated with PEV. Data are shown as Mean +/- SEM from 2 independent experiments of at least 17 interactions per group. Data were analysed by t-test. ** indicates $p < 0.01$.

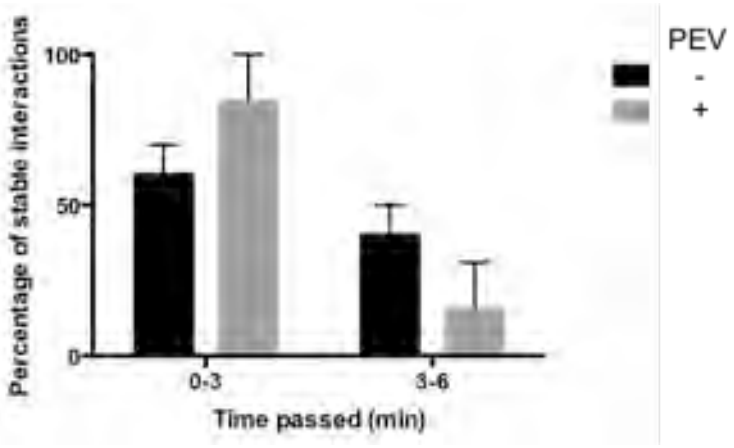

Figure 8.5. Time passed post-cell injection when stable interactions take place

Percentage of stable cell interactions taking place in the first 3 minutes passed post-cell injection versus in the last 3 minutes of video-recording, when monocytes were injected alone or when monocytes were decorated with PEV. Data are shown as SEM from 2 independent experiments. Data were analysed by two-way ANOVA.

8.3.4. Rolling Interactions

The velocity of rolling interactions was quantified. No difference was noted between monocytes perfused alone compared to monocytes that carried PEV on their surface (**Fig. 8.6**).

The majority of rolling interactions took place in the first three minutes passed post-cell introduction for the PEV sample, whereas an equal number of rolling interactions occurred in the first versus the last three minutes of imaging post-cell injection (**Fig. 8.7**).

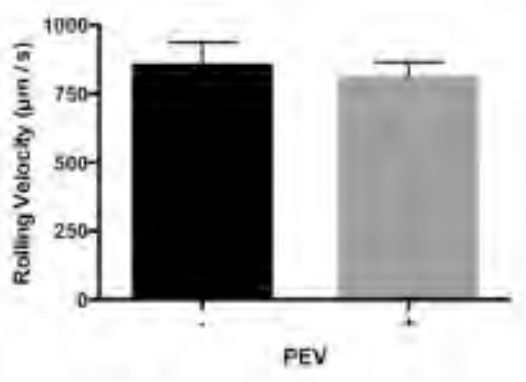

Figure 8.6. Velocity of Monocytes rolling in the carotid artery of the ApoE KO mouse

Velocity of rolling cell interactions when monocytes were injected alone or when monocytes were decorated with PEV. Data are shown as SEM from 2 independent experiments. Data were analysed by t-test.

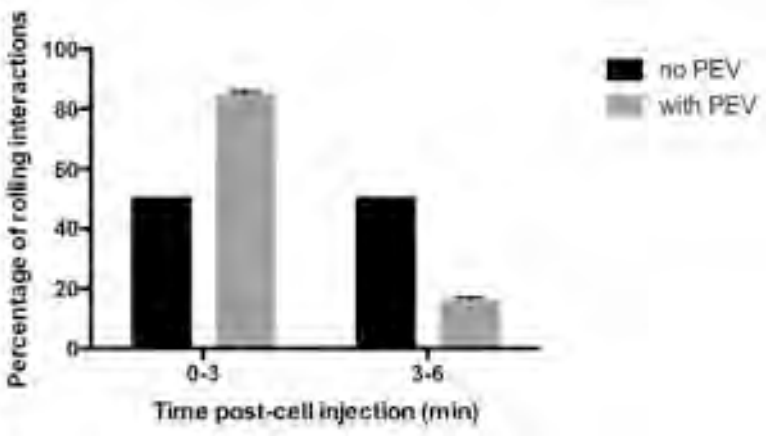

Figure 8.7. Changes with time in the number of cells rolling in the carotid artery of the *ApoE* KO mouse

Percentage of rolling cell interactions taking place in the first 3 minutes passed post-cell injection versus in the last 3 minutes of video-recording, when monocytes were injected alone or when monocytes were decorated with PEV. Data are shown as SEM from 2 independent experiments. Data were analysed by two-way ANOVA.

8.4. Discussion

In this chapter, monocyte-PEV aggregates were infused in the circulation of mice with established atherosclerosis and subsequent interactions with the inflamed endothelium were observed at the athero-prone "fork" site of the right common carotid artery. Another group investigated previously indirect PEV-mediated recruitment of monocytes in an *ex vivo* setting with extracted carotid arteries and found that PEV can deliver the chemokine RANTES to the athero-compromised endothelium, which enhanced subsequent monocyte arrest on the inflamed endothelium (Mause et al., 2005). However, our study is the first to date to investigate direct PEV-monocyte interactions resulting in monocyte recruitment in atherosclerosis *in viv*o.

Due to higher availability, human monocytes were used instead of mouse monocytes (upon confirming that mouse PEV could also aggregate with human monocytes). Human and mouse monocytes exhibit extensive gene and protein homology (Ingersoll et al., 2010), which could translate into compatible human monocyte – mouse PEV adhesion receptors. Also human and mouse platelet receptors share high homology. Jesse et al. (2011) found that 58% of the mRNAs expressed by human platelets are also found in the mouse platelets.

The observed "compatibility" between human monocytes and murine PEV might be specifically owed to platelet P-selectin. P-selectin has been found to mediate PEV-monocyte aggregation (Chimen et al., under review; McEver and Cummings, 1997). Liu et al. (2010) made transgenic mice that constitutively expressed human P-selectin in platelets and observed that leukocytes rolled similarly on human or murine P-selectin on activated murine platelets and in venules of the cremaster muscle upon trauma,

suggesting that P-selectin is functionally and phenotypically conserved in human and mouse.

Apart from P-selectin, platelet phosphatidylserine has also been found to have a role in mediating monocyte-PEV binding (Chimen et al., under review). Murine PEV also express phosphatidylserine on their outer surface, hence this fact could also explain the observed high affinity of human monocytes for murine PEV. In these experiments we confirmed that human monocytes can form heterotypic aggregates with murine PEV. However, we did not investigate whether human monocytes could also internalize these vesicles. This aspect was beyond the scope of these experiments, as in these experiments we just wanted to test any direct adhesion benefit to the monocytes i.e. from utilizing the PEV adhesion receptors on the surface of the monocytes.

Upon infusing the monocytes in the mouse circulation we observed two modes of adhesion on the endothelium; a) stable adhesion which was defined as cells staying "still" at the same position for over 100ms and b) unstable adhesion which was defined as cells in decelerating motion that take the form of a "stream" that indicates cell rolling, typically lasting < 100ms.

Monocytes exhibited higher adhesion when pre-incubated with PEV. This observation is in accordance with observations made by Mause and colleagues (2005), who found increased monocyte adhesion to atherosclerotic endothelium with pre-perfusion of PEV. Monocytes exhibited higher rolling adhesion when pre-incubated with PEV, whereas firm adhesion was not affected by PEV, in our experiments. Accordingly, Mause et al. (2005) found that perfused PEV do not undergo firm adhesion largely, but instead they engage in rolling interactions with carotid endothelium.

Increased PEV-mediated rolling adhesion in our experiments might result from monocyte adoption of PEV-derived GPIb, as Mause and colleagues (2005) observed inhibition of monocyte adhesion with GPIb blocking. GPIb is the known platelet adhesion partner of vWF in compromised endothelium and this interaction is known to be unstable (Sakariassen et al., 1986). In addition, similar studies from our group found that monocyte-bound PEV up-regulated adhesive interactions of monocytes with the endothelium in the mouse cremaster muscle microcirculation in a GPIb-dependent way as well in a model of induced inflammation (Chimen et al.; under review). The velocity of blood in the mouse carotid, which is typically 500-600 μm in diameter, ranges between 2.5-18 cm/s (Parzy et al., 2009). Based on these measurements, the rolling monocytes in our experiments exhibited 30-200-fold deceleration.

Stable adhesion lasted longer for the monocytes that carried PEV on their surface. This fact could be the result of monocyte utilisation of another PEV receptor; GPIIb. GPIIb is the platelet receptor that mediates stable adhesion between platelets and exposed ECM upon platelet activation (Savage et al., 1998; Jackson et al., 2003). Mause and colleagues showed that GPIIb blocking also decreases monocyte rolling on atherosclerotic endothelium.

Apart from monocyte adoption of PEV adhesion molecules that remains to be explored in future experiments, another PEV-mediated mechanism of monocyte recruitment to the vessel wall involves PEV-mediated activation of monocytes, resulting in up-regulation of endogenous monocyte adhesion molecules on the surface of monocytes. Montoro-Garcia and colleagues (2014) have found that PEV can induce up-regulation of ICAM-1 on the monocyte surface. In addition, PEV have been shown to

promote monocyte adhesion indirectly via the deposition of RANTES to the endothelium (Mause et al., 2005).

Atheromatous plaques are rich in various endothelial cell adhesion molecules (CAMs) such as P-selectin, ICAM-1 and VCAM-1 (Patel et al., 1998; Poston et al., 1992; Johnson-Tidey et al., 1994; O'Brien 1993) that facilitate monocyte recruitment. In an oscillatory flow study, Hsiai and colleagues (2003) simulated the moving and unsteady separation point at the arterial bifurcation with high spatial and temporal resolution and found that monocytes also underwent rolling, binding, dissociation and firm adhesion on EC. Monocytes also exhibited increased rolling in the carotid artery from ApoE KO mice *ex vivo* compared to wild type mice (Ramos et al., 1999). In these experiments, cell rolling was mediated by P-selectin and VCAM-1. Hence, an advancement to our experiment would be to extract the carotid artery post-video recording and stain with a lipid dye (such as Oil Red O) in order to investigate whether firmly adhered monocytes are directly adhered onto plaques. Plaque staining with dyes or PEV protein staining with antibodies during perfusion *in vivo* is prohibited due to the toxic effects on the mouse.

Conclusions

The presence of PEV on the monocyte surface enhances monocyte recruitment in atherosclerosis in acute experiments. The effect of circulating monocyte-PEV aggregates in the long-term with regards to atherosclerosis remains to be investigated.

9. CHARACTERISATION OF APOE KO-HIL4RA/GPIBA-TG MOUSE

9.1. Introduction

In chapter 8 it was shown that *in vivo* infusion of monocytes that are decorated with PEV in the circulation of a mouse with established atherosclerosis up-regulates monocyte adhesion to the carotid artery wall. Hence, we speculate that PEV might contribute to atherosclerosis progression by recruiting circulating monocytes to the inflamed vessel wall.

In order to investigate the potential of PEV to directly affect atherogenesis there is need for an atherosclerosis animal model that is free of platelets. This is required because PEV are capable of activating platelets and recruiting them to compromised endothelium (Owens et al., 1992; Merten et al., 1999). Hence, it could be argued that any effect on atherogenesis upon PEV injection might have been caused by endogenous platelets rather than PEV.

An atherosclerosis animal model that is free of platelets did not exist to our knowledge, so we aimed to generate one by breeding the *ApoE KO* mouse, which is a widely used mouse for atherosclerosis studies, with the transgenic mouse *hiL-4Rα/GPIbα-Tg* (Kanaji et al., 2002).

The *ApoE KO* mouse lacks the apolipoprotein-E (ApoE) gene. ApoE mediates receptor recognition of intermediate-density lipoprotein and chylomicron remnant in the liver. It is essential for maintaining plasma cholesterol and triglyceride levels by clearance of remnant lipoproteins (Eichner et al., 2002). As a consequence, the ApoE KO mouse develops severe hypercholesterolemia and atherosclerosis when fed a high-fat diet (McNeil et al., 2010).

The hiL-4Rα/GPIbα-Tg mouse expresses a chimeric protein that is composed of the extracellular domain of the human IL4-R and the transmembrane and cytoplasmic

sequences of human GPIbα on the platelets instead of the murine GPIbα (Kanaji et al., 2002). Upon injection with anti-human IL-4 receptor α antibodies, the endogenous circulating platelets are effectively cleared from the circulation (Boulaftali et al., 2013). The antibodies only target endogenous platelets; hence it allows the adoptive transfer of exogenous wildtype platelets or PEV.

In theory, this new mouse ApoE KO-hiL4Rα/GPIbα-Tg would be athero-prone and free of platelets and would allow the investigation of injected PEV in the progression of atherosclerosis.

The aims for this chapter were to:

1. Generate and characterise *ApoE* KO *hiL-4Rα/GPIbα-Tg* mouse.
2. Investigate atherogenesis in *ApoE hiL-4Rα/GPIbα-Tg* mouse.
3. Investigate platelet clearance by antiplatelet antibody.

9.2. Methodology

9.2.1. Generation of ApoE KO-hiL4Rα/GPIbα-Tg Mouse

ApoE$^{-/-}$ hiL4R/GPIbα-Tg mice were generated by crossing ApoE$^{-/-}$ with hiL4R/GPIbα-Tg mice to first generate double heterozygous ApoE$^{+/-}$ hiL4R/GPIbα-Tg$^{+/-}$ mice. Heterozygous mice were crossed among themselves to generate different genotype combinations of which only the ApoE$^{-/-}$ hiL4R/GPIbα-Tg$^{+/+}$ and ApoE$^{-/-}$ hiL4R/GPIbα-Tg$^{+/-}$ mice were used in experiments. Presence of the ApoE gene was assessed by PCR. Presence of the hiL4Rα gene was assessed by FACS. Further details can be found in Chapter 2.

9.2.2. Characterisation of the ApoE KO-hiL4Rα/GPIbα-Tg Mouse Platelets and PEV

EDTA-anti-coagulated peripheral blood from 10-week old *ApoE* KO *hiL-4Rα/GPIbα-Tg* mice was analysed on a mouse blood haemocytometer to count numbers and measure size. The blood was also stained with anti-hiL4R and anti-GPIIb antibodies and platelet/PEV expression was analysed by FACS. Blood from ApoE and hiL4Rα/GPIbα-Tg mice was also analysed.

9.2.3. Investigation of Atherogenesis

ApoE KO *hiL-4Rα/GPIbα-Tg* female mice were placed on a high fat diet for 14 weeks from 10 weeks of age. Mice were weighed weekly. Their aorta was extracted and stained with Oil Red O to visualize atheromatous plaque. Their liver was extracted and stained with H & E to measure steatosis. Blood samples were collected before and after feeding on the diet for 14 weeks to measure serum lipids. Statistical analysis was performed using Graphpad Prism 6. More details can be found in Chapter 2.

9.2.4. Platelet Depletion

Endogenous platelets in the ApoE KO-hiL4R/GPIbα-Tg mouse were depleted by intra-venous injection of 2.5 μg or 5μg / g body weight of anti-hiL4Rα (R & D Systems). Blood cells were analysed using a Pentra hematocytometer over the course of the next 9 days following the antibody injection. Statistical analysis was performed using Graphpad Prism 6. More details can be found in Chapter 2.

9.3. Results

9.3.1. Characterisation of Platelets and PEV

Platelet counts and size of ApoE, hiL4Rα/GPIbα-Tg and ApoE KO-hiL4Rα/GPIbα-Tg are shown in **Fig. 9.1.,** as measured by haemacytometry. The number of platelets in the blood of hiL4Rα mice was significantly lower than the number of circulating platelets in ApoE mice (**Fig. 9.1A**). ApoE hiL4Rα platelets were significantly larger than ApoE platelets and significantly smaller than hiL4Rα mice (**Fig. 9.1B**).

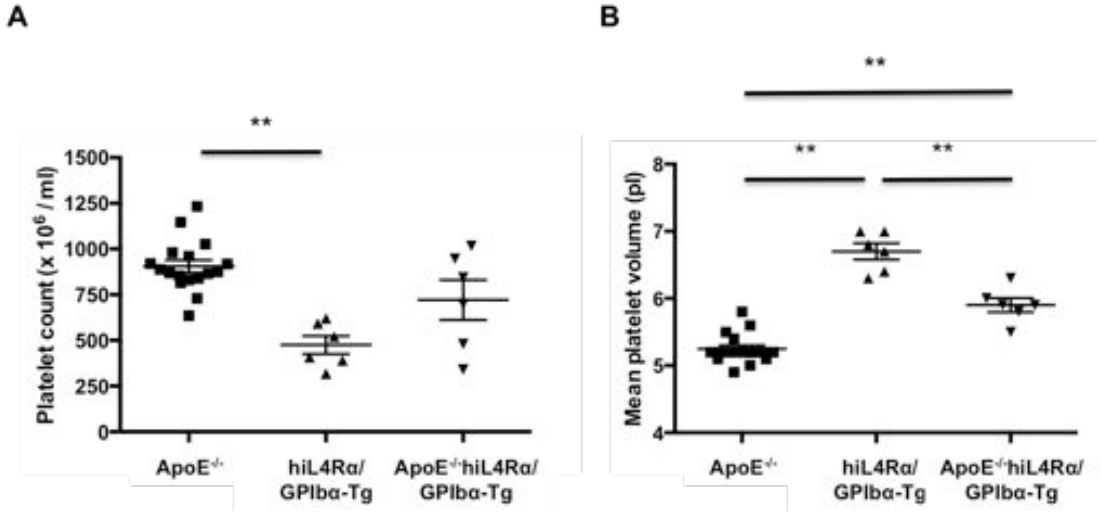

Figure 9.1. Platelet Counts and Size

Platelets in anti-coagulated peripheral blood were analysed on a Pentra haemocytometer for **(A)** numbers and **(B)** size. Data are shown as Mean +/- SEM. Data were analysed by one-way ANOVA test. ** indicates $p < 0.01$.

Upon observing differences between hiL4Rα/GPIbα-Tg and ApoE KO-hiL4Rα/GPIbα-Tg platelets, the two strains were compared for their platelet hiL4Rα protein expression levels (**Fig. 9.2**). Upon selecting for GPIIb+ve events, we observed two distinct entities of characteristic forward and side scatter location of platelets and EV (**Fig. 9.2A**). Platelets and PEV were independently analyzed for hiL4Rα protein expression (**Fig. 9.2B**). Most platelets and PEV from hiL4Rα/GPIbα-Tg and ApoE KO-

hiL4Rα/GPIbα-Tg mice express hiL4Rα protein (**Fig. 9.3A**). Platelets and PEV from hiL4Rα/GPIbα-Tg mice exhibit statistically the same levels of hiL4Rα protein with those from ApoE KO-hiL4Rα/GPIbα-Tg mice (**Fig. 9.3B**).

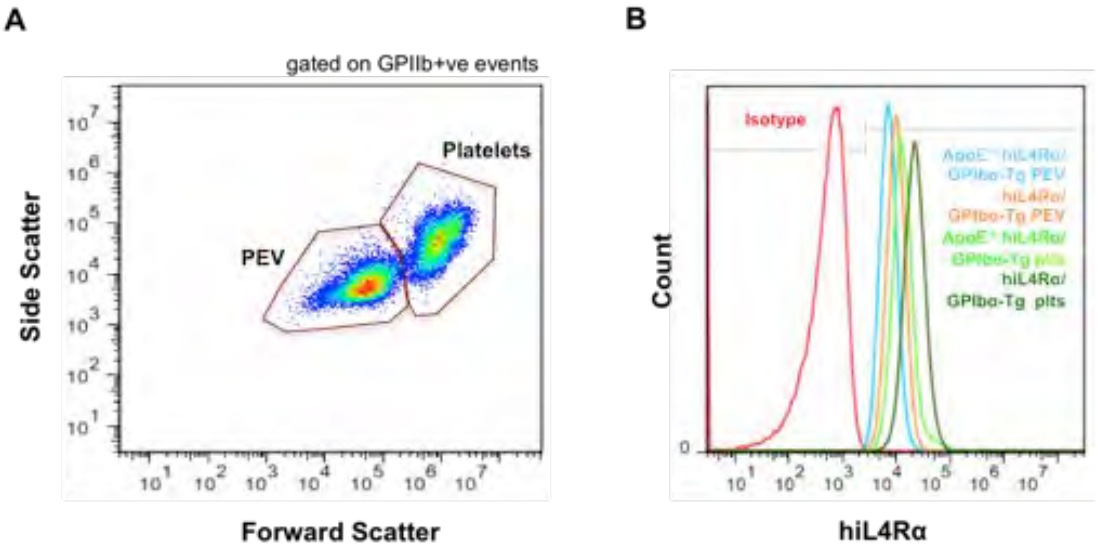

Figure 9.2. Expression of hiL4Rα on platelets and PEV

Anticoagulated peripheral blood was co-stained with anti-GPIIb and anti-hiL4Rα antibodies and analyzed by FACS. **(A)** Representative forward vs side scatter plot, as gated on GPIIb+ve events, showing platelets and PEV. **(B)** Overlay histogram of hiL4Rα expression expressed by platelets or PEV of hiL4Rα/GPIbα-Tg or ApoE KO-hiL4Rα/GPIbα-Tg mice.

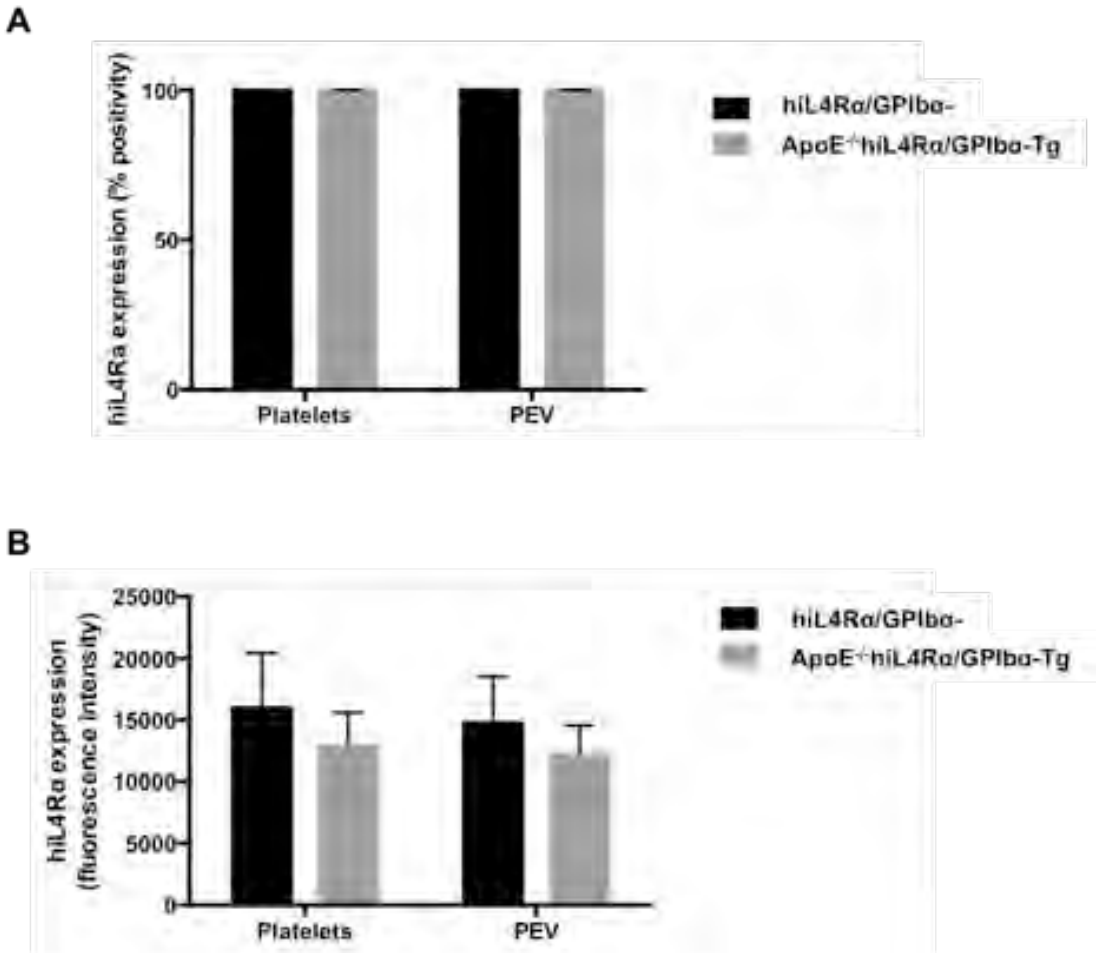

Figure 9.3. Expression of hiL4Rα on Platelets and PEV

(A) Percentage of platelets or PEV from hiL4Rα/GPIbα-Tg or ApoE KO-hiL4Rα/GPIbα-Tg mice expressing hiL4Rα and **(B)** respective mean fluorescence intensity. Data are shown as Mean +/- SEM of 5-6 mice. Data were analyzed by two-way ANOVA test.

9.3.2. Atherogenesis in the ApoE KO-hiL4Rα/GPIbα-Tg Mouse

In order to test athero-propensity, ApoE KO-hiL4Rα/GPIbα-Tg mice were placed on a high fat diet for 14 weeks from 10 weeks old. ApoE mice were used as the control group. All mice were weighed regularly over the course of the treatment. Their weight gain is shown in **Fig. 9.4** as a percentage of the starting weight. Both strains gained weight significantly with time, however the ApoE hiL4Rα mice gained weight at a significantly higher rate than the ApoE mice.

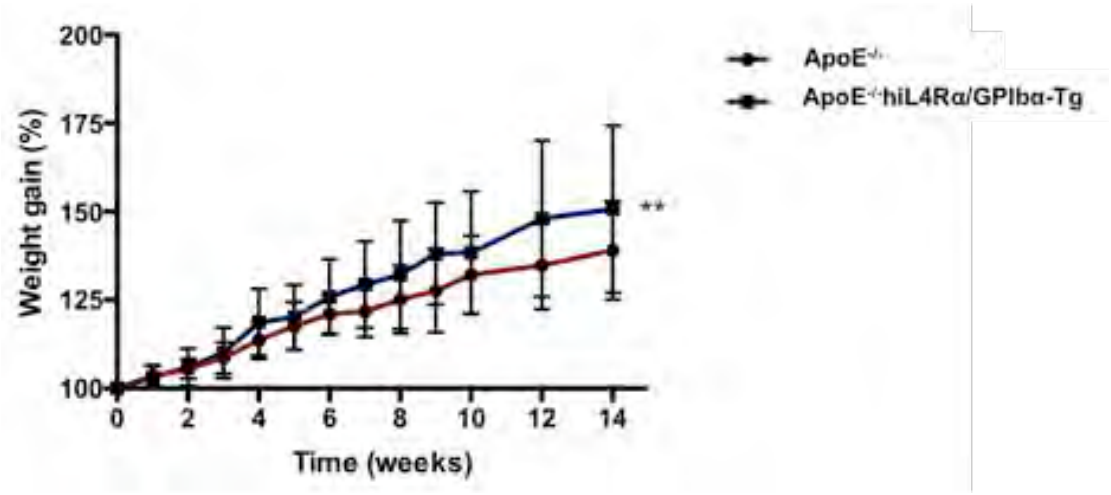

Figure 9.4. Weight gain while on a high fat diet

The weight of ApoE KO and ApoE KO-hiL4Rα/GPIbα-Tg mice as a percentage of starting weight over the course of 14 weeks on the high fat diet. Data are shown as Mean +/- SEM OF 8-10 mice. Data were analyzed by two-way ANOVA test. ** indicates $p < 0.01$.

9.3.2.1. Atheromatous Plaque Formation

To test whether differences in weight reflected differences in level of disease, mouse aortas were extracted to measure level of plaque formation. Representative aortas are shown in **Fig. 9.5**. Upon quantification, no differences in plaque formation were noted between the two strains in the different aortic sites (**Fig. 9.6**). The size and number of individual lesions was also analyzed and was found to be statistically the same (**Fig. 9.7**). These mice also exhibited similar numbers of circulating monocytes (**Fig. 9.8**). The difference in platelet counts and size between the two mouse strains remained evident throughout the HFD regimen (**Supplementary Material Fig. 12.13**).

Figure 9.5. Aortic Plaque formation in response to a high fat diet for 14 weeks

ApoE KO and ApoE KO-hiL4Rα/GPIbα-Tg mice were placed on a high fat diet from 10 weeks old. Their aortas were extracted and stained with Oil Red O before imaging. Red colour depicts plaque presence.

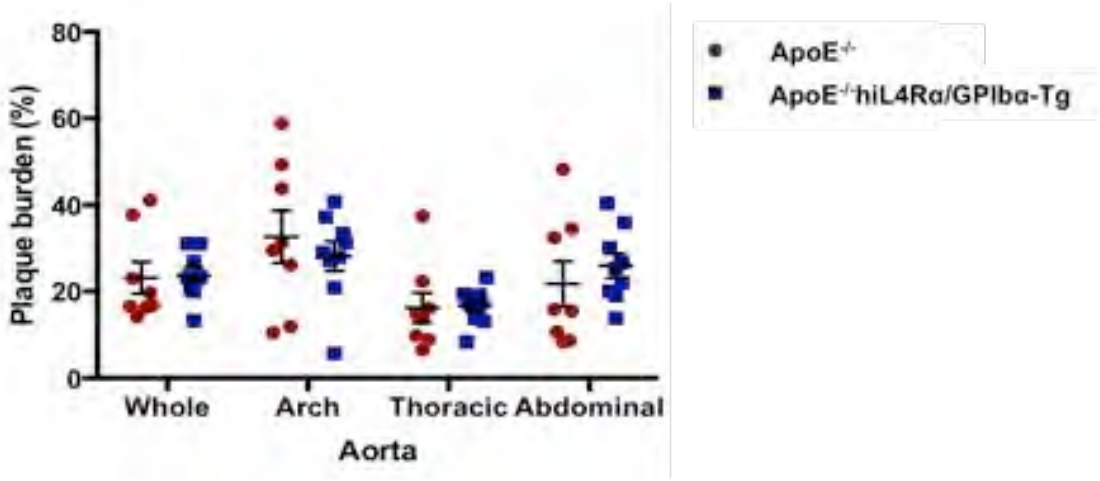

Figure 9.6. Aortic Plaque burden in response to a high fat diet for 14 weeks

Plaque burden at different aorta sites of ApoE KO and ApoE KO-hiL4Rα/GPIbα-Tg mice was quantified using FIJI software. Data are shown as Mean +/- SEM from 7-8 mice. Data were analyzed by t-tests.

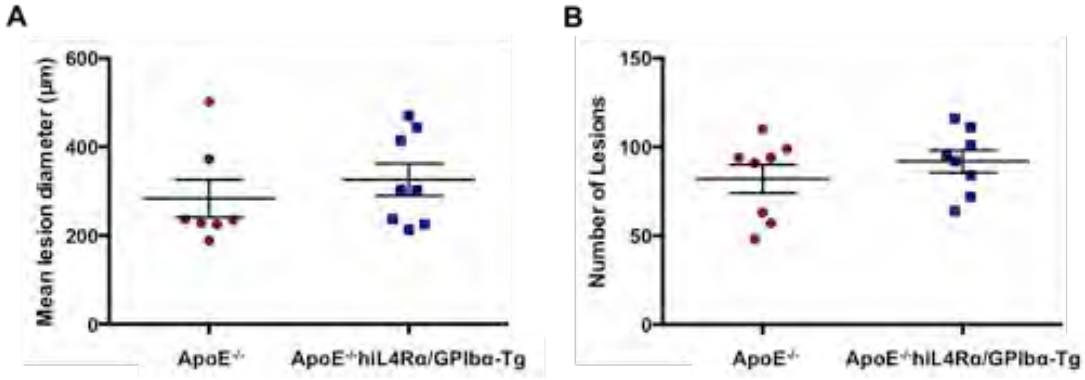

Figure 9.7. Aortic Lesion characteristics in response, to a high fat diet for 14 weeks

(A) Mean diameter and **(B)** number of lesions formed in aortas of ApoE KO or ApoE KO-hiL4Rα/GPIbα-Tg mice upon 14-week fed a high fat diet from 10 weeks old. Data are shown as Mean +/- SEM from 7-8 mice. Data were analyzed by t-test.

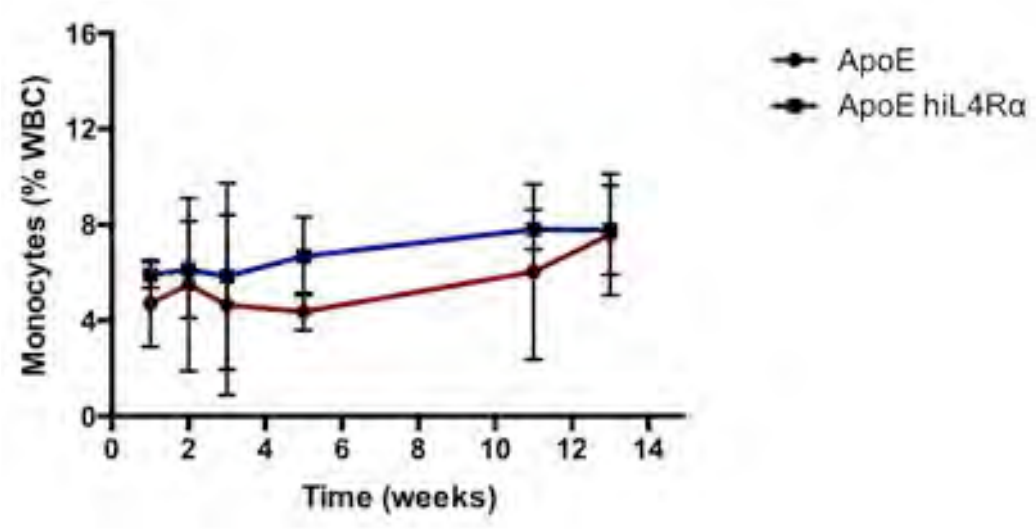

Figure 9.8. Circulating monocyte levels on a high fat diet

Circulating monocytes in as a percentage of white blood cells in the ApoE and ApoE KO-hiL4Rα/GPIbα-Tg over the course of 14 weeks on the high fat diet. Data are shown as Mean +/- SEM of 8-10 mice. Data were analyzed by two-way ANOVA test.

9.3.2.2. Liver Steatosis

Another feature of atherosclerosis, which is the steatotic liver, was also analyzed for the two strains. **Fig. 9.9** shows representative sections of livers, as stained with H & E. Liver steatosis was quantified but no significant differences were noted between the two strains (**Fig. 9.10**). The weight of the livers of the two strains can be found in the Supplementary Material (**Fig. 12.14**).

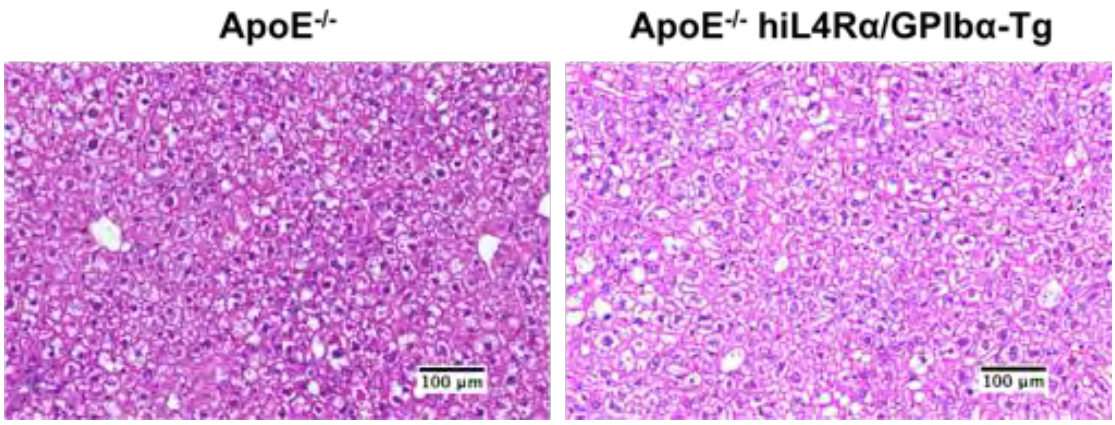

Figure 9.9. Liver steatosis in response to a high fat diet for 14 weeks

Representative images of liver sections of ApoE KO and ApoE KO-hiL4Rα/GPIbα-Tg mice stained with H & E as imaged using an AxioScan microscope. White colour depicts fat accumulation.

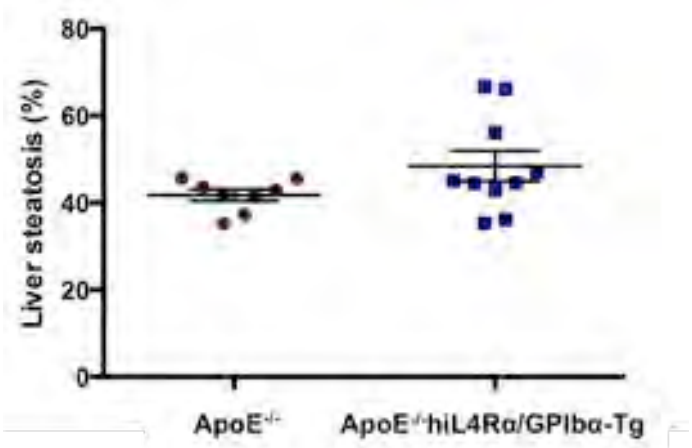

Figure 9.10. Liver steatosis in response to a high fat diet for 14 weeks

The percentage of liver steatosis in ApoE KO and ApoE KO-hiL4Rα/GPIbα-Tg mice was quantified using FIJI. Data are shown as Mean +/- SEM. Data were analyzed by t-test.

9.3.2.3. Blood Lipids

The levels of the different lipids in the blood were measured before and after feeding the mice a high fat diet for 14 weeks. Total cholesterol levels increased significantly for both strains upon feeding a high fat diet for 14 weeks compared to starting levels, as expected. However, total cholesterol levels of ApoE KO-hiL4Rα/GPIbα-Tg mice were significantly lower than ApoE total cholesterol levels at the

end of 14 weeks (**Fig. 9.11A**). Triglyceride levels increased significantly for both strains upon feeding a high fat diet for 14 weeks compared to starting levels. However, triglyceride levels of ApoE KO-hiL4Rα/GPIbα-Tg mice were significantly higher than ApoE triglyceride levels at the end of 14 weeks (**Fig. 9.11B**). HDL increased significantly in the ApoE mouse upon feeding the high fat diet, however the HDL of the ApoE KO-hiL4Rα/GPIbα-Tg mouse was significantly lower than that of the ApoE mouse after feeding on the high fat diet (**Fig. 9.11C**). LDL increased significantly in the ApoE mouse upon feeding the high fat diet, however the LDL of the ApoE KO-hiL4Rα/GPIbα-Tg mouse was significantly higher than that of the ApoE mouse before starting the high fat diet (**Fig. 9.11D**).

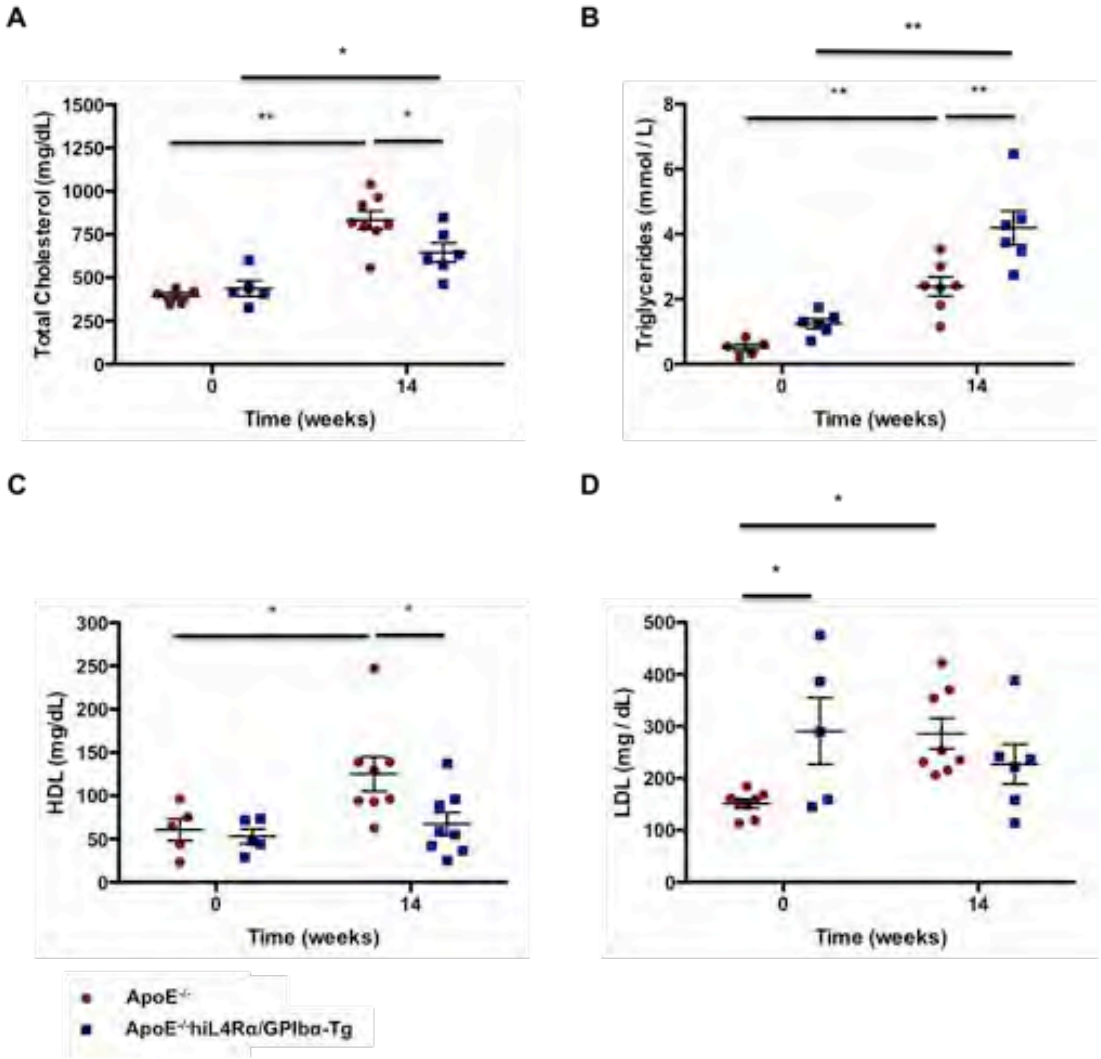

Figure 9.11. Changes in Blood Lipids in response to a high fat diet for 14 weeks

(A) Total cholesterol, **(B)** Triglyceride, **(C)** HDL and **(D)** LDL levels before and after 14 weeks of high fat diet in the ApoE KO versus ApoE KO-hiL4Rα/GPIbα-Tg mouse. Data are shown as Mean +/- SEM. Data were analysed by two-way ANOVA test with multiple comparisons. * indicates $p < 0.05$, ** indicates $p < 0.01$.

9.3.3. Induction of Platelet Clearance

In order to determine whether ApoE KO-hiL4Rα/GPIbα-Tg mice are also capable of clearing their platelets upon injection with anti-hiL4Rα antibodies like it was shown in the literature for the hiL4Rα/GPIbα-Tg mice, ApoE KO-hiL4Rα/GPIbα-Tg mice were injected intravenously with 2.5 μg/g of anti-hiL4Rα antibody. This caused circulating platelets and PEV to drop dramatically (**Fig. 9.12**). Platelet counts remained minimal

(about 85% decreased) for at least 4 days post-injection. Platelet counts recovered by the 7th day post-injection (**Fig. 9.13A**). The size of platelets was also measured during the 9-day follow up period post-injection. Circulating platelets were significantly larger after the antibody injection and remained abnormally large for at least 4 days passed post-injection. Platelets returned to their normal size by the 7th day post-injection (**Fig. 9.13B**). The WBC counts of the mice injected did not change significantly over the 9-day period post-injection (**Fig. 9.14**).

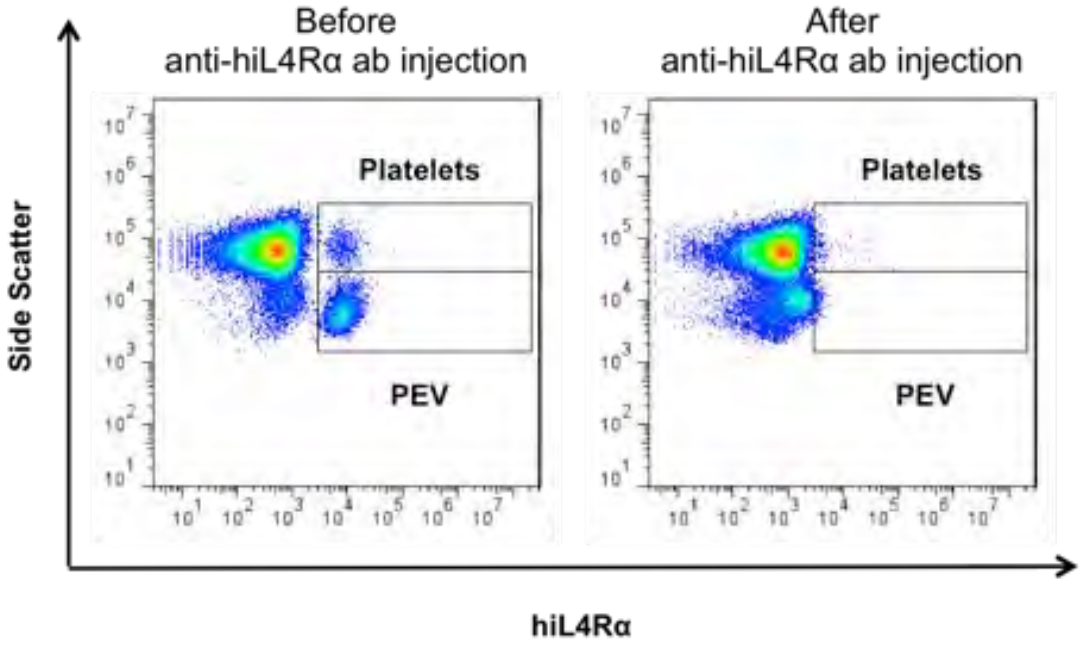

Figure 9.12. Platelet and PEV clearance in response to injection with 2.5 µg/g anti-hiL4Rα antibody

Representative FACS plots indicating the presence of hiL4Rα-positive events (platelets and PEV) in the ApoE KO-hiL4Rα/GPIbα-Tg mouse (left plot) and the absence of hiL4Rα-positive events (platelets and PEV) 45-minutes after i/v injection with 2.5 µg/g anti-hiL4Rα antibody (right plot).

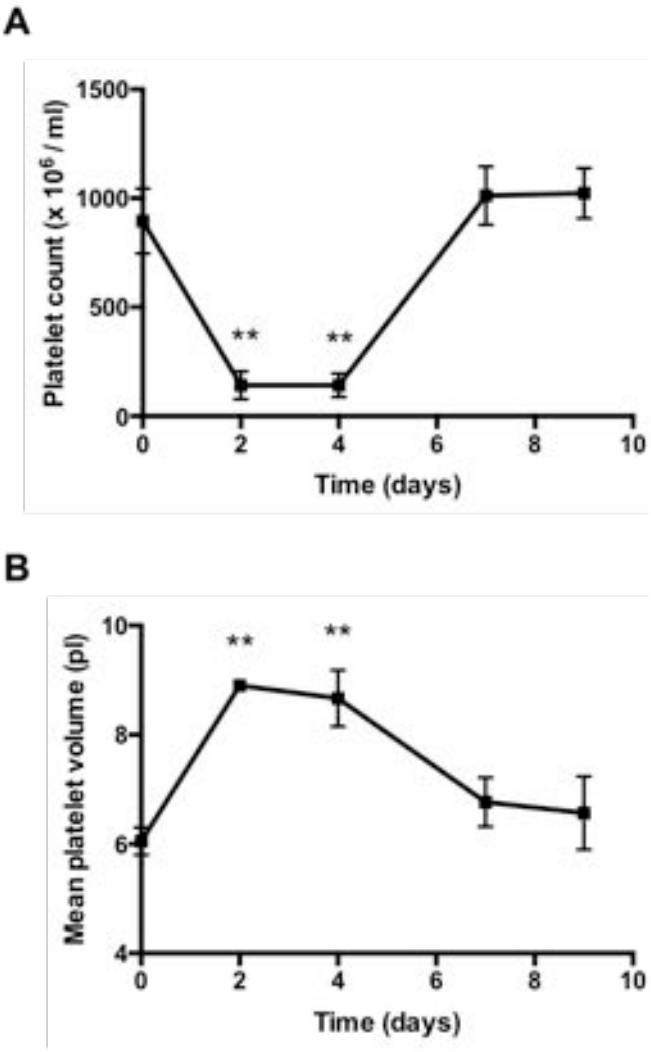

Figure 9.13. Time-course of platelet clearance in response to injection with 2.5 µg/g anti-hiL4Rα antibody

(A) Blood platelet counts and **(B)** platelet size upon injection of 2.5 µg/g anti-hiL4Rα antibody over the course of 9 days in the ApoE KO-hiL4Rα/GPIbα-Tg mouse. Data are shown as Mean +/- SEM of 3 independent samples. Data were analysed by one-way ANOVA test with multiple comparisons. ** indicates $p < 0.01$.

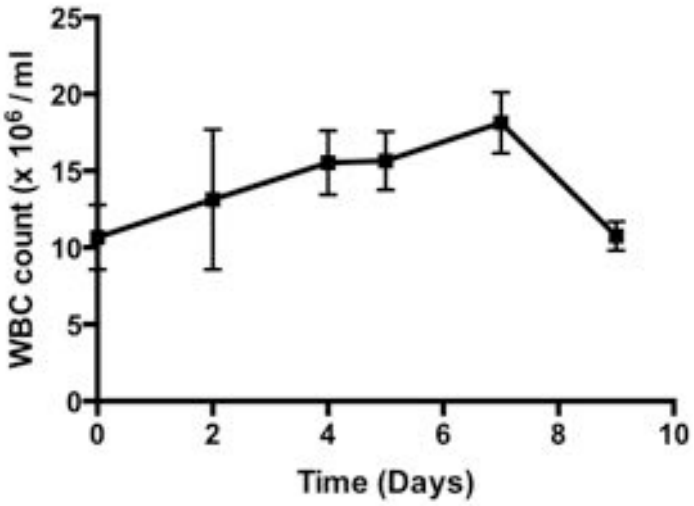

Figure 9.14. Circulating WBC counts in response to hiL4Rα antibody injection

Circulating WBC counts in the ApoE KO-hiL4Rα/GPIbα-Tg mouse in response to i/v injection with 2.5 µg/g hiL4Rα antibody over time. Data are shown as Mean +/- SEM of 3 mice. Data were analyzed by one-way ANOVA test.

9.4. Discussion

In this chapter the *ApoE* KO mouse was crossed with the *hiL-4Rα/GPIbα-Tg* mouse to generate a new mouse strain that is athero-prone and inducible of platelet clearance. We named the resulting mouse ApoE KO-hiL4Rα/GPIbα-Tg mouse. This new mouse would allow the investigation of injected PEV in the progression of atherosclerosis, independently of platelets. The aim of this chapter was to characterize this new mouse model.

9.4.1. Characterisation of Platelets and PEV

We counted the number and size of circulating platelets in the new mouse. Previous studies had indicated that the platelets from the hiL4Rα KI mouse are larger and fewer in numbers than WT platelets (Kanaji et al., 2002). However, these deviations were not as dramatic as those seen in pathological thrombocytopenia disorders. Increased mean platelet volume is typical of newly formed platelets and suggests

increased thrombopoiesis by the bone marrow (Corash et al., 1987; Levin et al., 1982), which is usually the response to thrombocytopenia. Similarly, platelets derived from the hiL4Rα KI mouse in our experiments, exhibited larger and fewer platelets than those derived from ApoE KO mice of 10 weeks of age on a normal diet. It has been shown that GPIb deficiency results in mild thrombocytopenia and circulation of 'giant platelets' (Ware et al., 2000). However, the new mouse generated exhibited platelets of an intermediate phenotype. These platelets were smaller than those derived from the hiL4Rα KI mouse, but bigger than the ApoE KO platelets. These platelets were also higher in numbers than hiL4Rα KI platelets but not as high as ApoE KO platelets. Apolipoprotein E has been found to inhibit agonist-induced platelet aggregation and activation *in vitro* (Nofer et al., 2002; Desai et al., 1989; Higashihara et al., 1991; Riddell et al., 1997). Hence, the observed differences in platelet counts and size in the ApoE KO-hiL4Rα/GPIbα-Tg mouse compared to the hiL4Rα/GPIbα-Tg mouse might be directly attributed to the absence of ApoE protein.

In addition, ApoE KO mice are characterized by hyperlipidemia. Hypercholesterolemia is suggested to promote platelet biogenesis, hence increases circulating platelet counts (Wang and Tall, 2016; Fessler et al., 2013).

Another explanation for the platelet count and size differences could be that the mice tested were heterozygous for the hiL4Rα gene. Unfortunately, because the mice were genotyped by FACS, we could only determine whether the platelets contained the hiL4Rα protein or not but we could not distinguish with absolute certainty whether the mice were heterozygote or homozygote KI for the hiL4Rα gene. Genotyping by PCR needs to be employed for future experiments with these mice in our group. We cannot know with certainty whether heterozygocity/homozygocity for the hiL4Rα gene would

result in variations in platelet characteristics. The literature does not mention anything about the phenotype of hiL4Rα KI heterozygous mice (Kanaji et al., 2002). However, GPIbα heterozygous expression results in intermediate platelet counts compared to platelets from WT or GPIbα null mice (Ware et al., 2000), hence this could hold also true for ApoE$^{-/-}$-hiL4Rα$^{+/-}$ mice. This is consistent with our observation that platelets and PEV from ApoE hiL4Rα mice exhibit a little lower amount of hiL4Rα protein on their surface than hiL4Rα.

As expected, the *hiL-4Rα/GPIbα-Tg* mouse has adhesion problems due to inability to bind vWF. In this mouse model, platelets were incapable of binding to injured endothelium and forming thrombi (Boulaftali et al., 2013). In addition, these mice exhibited prolonged tail bleeding times compared to WT controls (Kanaji et al., 2002). However, our experiments suggest that activation is normal in these platelets, as circulating blood contains numerous PEV. Further characterization of our new mouse should include platelet aggregation assays and flow adhesion assays over immobilised vWF.

9.4.2. Atherogenesis

The main hypothesis of this PhD project is that PEV drive the progress of atherogenesis through interacting with monocytes. One way PEV could promote the inflammatory activities of monocytes in atherosclerosis is through facilitating monocyte recruitment to the endothelium. Indeed, our group has shown that PEV increase adhesion of monocytes to immobilized stimulated vWF or to stimulated endothelial cells in *in vitro* flow assays. Our group also replicated this result *in vivo* in the microcirculation of a mouse model of induced inflammation (Chimen et al.; under review). In addition, in chapter 8 it was shown that injection of monocytes-PEV

aggregates in the circulation of mice with established atherosclerosis results in increased adhesive interactions with the carotid endothelium. Injection of activated WT platelets into ApoE KO mice has been shown to increase atherosclerosis (Huo et al., 2003). However, we have not yet investigated the long term effect of injected PEV in atherosclerosis.

The new mouse was generated to allow studying the role of PEV in atherogenesis independently of platelets. This requires clearance of endogenous platelets, followed by infusion of exogenous PEV. Prior to investigating the effect of infused PEV into thrombocytopenic mice in atherosclerosis, appropriate controls need to be established to allow future comparisons. A first control is the study of basal atherogenesis in ApoE KO-hiL4Rα/GPIbα-Tg mice without induction of platelet depletion and injection of PEV, just by feeding a high fat diet; this was our treatment group for this study. ApoE mice were used as a control. Since *hiL-4Rα/GPIbα*-Tg mice reportedly had adhesion complications (Kanaji et al., 2002; Boulaftali et al., 2013) we speculated that the ApoE KO-hiL4Rα/GPIbα-Tg mice might exhibit decreased levels of atherosclerosis, arising from decreased levels of PEV-mediated monocyte recruitment. Our speculation was strengthened by the studies of Massberg and colleagues (2002), who found that inhibition of platelet (and PEV) adhesion by GPIbα-blocking antibodies significantly reduced atheromatous plaque formation.

Our ApoE KO-hiL4Rα/GPIbα-Tg mouse did not however exhibit decreased plaque formation in the aorta compared to the ApoE mouse. In addition, the individual plaques exhibited the same characteristics in the two mouse models. This result agrees with the results by Koltsova and colleagues (2014), who performed similar atherosclerosis studies with the *hiL-4Rα/GPIbα*-Tg mouse using a different

atherosclerosis mouse model. Ldlr$^{-/-}$ mice lethally irradiated and fed on a high fat diet reconstituted with GPIbα$^{-/-}$ bone marrow reported lower atherosclerosis than wt controls. However, ldlr$^{-/-}$ mice reconstituted with *hiL-4Rα/GPIbα*-Tg bone marrow that lacks only the extracellular domain of GPIbα, exhibited atherosclerotic lesions similar to wt mice. Hence, the authors concluded that the decreased atherosclerosis seen in mice deficient of GPIbα is most likely not the result of defective GPIbα binding, but rather results from associated low blood platelet counts and platelet dysfunction. This might hold true in our case as well.

Despite the presence of similar atheromata in our two strains of mice tested, the two mice exhibited some differences in lipid metabolism. Both blood triglyceride and total cholesterol levels rose as expected upon feeding on a high fat diet in both strains. However, the ApoE KO-hiL4Rα/GPIbα-Tg mice had lower total cholesterol and HDL but higher triglyceride and LDL levels than the ApoE mouse. A combination of higher triglyceride levels (and sometimes lower cholesterol levels) with thrombocytopenia or enlarged platelets is also seen in acute hantavirus infections, nephropathia epidemica and subclinical hypothyroidism, even though the exact mechanism is unknown (Clement et al., 2016; Martynova et al., 2016; Yilmaz et al., 2011). Hence, we believe that the differences observed in lipid metabolism parameters in the ApoE KO-hiL4Rα/GPIbα-Tg mouse compared to the ApoE mouse in our studies, are due to differences in platelet counts, size and functionality.

9.4.3. Induction of Platelet Clearance

The use of antiplatelet antibodies is an efficient way to cause platelet clearance *in vivo*. These antibodies mimic the mechanism of platelet auto-destruction seen in the bleeding disease autoimmune thrombocytopenic purpura (ITP), where autoantibodies

target the individual's own platelets, resulting in Fc-mediated platelet destruction by macrophages in the reticuloendothelial system (RES) (Semple et al., 1998). Monoclonal antibodies (mAbs) targeting mouse GPIIbIIIa, GPIIIa, GPIbα, GPIb-IX, GPV and CD31 have been evaluated (Nieswandt et al., 2000).

Intravenous injection of anti-hiL4Rα antibody into our ApoE KO-hiL4Rα/GPIbα-Tg mice caused circulating platelet counts to drop dramatically as also shown by Boulaftali and colleagues (2013). The platelets stayed as low as 15% of their original counts for at least four days post-injection. Platelet counts were restored seven days after the injection. Platelet size was inversely correlated to counts. Upon platelet depletion, the newly formed platelets are abnormally larger in size as expected and go back to their normal size between four and seven days after the injection.

These mice appeared to have no complications (normal WBC/neutrophil levels, no lethal internal bleedings) during the course of the 9-days in general (mice were kept in separated cages each during this time to prevent injuring each other during play or fight time which could lead to lethal hemorrhage due to absence of platelets). However, when successive injections of the antibody (same concentration) were attempted at a weekly frequency in order to prolong the platelet-free period, the mice exhibited anaphylaxis-like symptoms (mice extremely hypo-energetic on second injection, spasms on third injection).

Nieswandt and colleagues (2000) also reported an anaphylaxis-like reaction with associated hypothermia and a decrease in hematocrit due to internal bleeding with administration of anti-GPIIbIIIa antibodies (10μg). These side effects were PAF-mediated and Fc-dependent. However, when Nieswandt et al., (2000) gave repeated injections of low doses of anti-GPIIbIIIa antibodies (7 x 7.5μg i/p within 8 hours) no

acute systemic responses were noted, suggesting that there is a dose threshold and this threshold was not reached by repeated concentrations possibly because PAF has a very short half-life.

In our case, we gave an injection of 2.5 μg/g antibody (IgG_{2A}) (to replicate data from Boulaftali et al., 2013); for an average mouse of 20g this is 50 μg, followed by the same dose 7 days after. However, administrating only one injection of a double dose (5 μg/g) (result not shown) caused no adverse effects. Only when a second injection was administered 7 days after the first one, the mice exhibited severe side effects. Hence, we conclude that our mice developed immune hypersensitivity that caused anaphylactic shock. The sensitizing agent in the antibody most likely is the IgG_{2A} . IgG_{2A}, as well as other IgG subclasses (IgG_1 and IgG_{2B}), have been reported to induce systemic anaphylaxis in the mouse (Khodoun et al., 2013; Miyajima et al., 1997; Jonsson et al., 2011). Hence, future approaches to prolong platelet-free period in ApoE KO-hiL4Rα/GPIbα-Tg mice by repeated anti- hiL4Rα antibodies should try alternative anti-hiL4Rα antibodies, where the anti- hiL4Rα region is fused to non-immunogenic immunoglobulins.

In addition, the efficiency of anti-hiL4Rα $F(ab)_2$ fragments could be evaluated in causing thrombocytopenia in future investigations. Administration of anti-GPIbα antibodies caused virtually complete thrombocytopenia (without any associated side effects) in Fc-independent mechanisms in mice (Nieswandt et al., 2000), suggesting that the RES was not involved here. Hence, antibody-mediated platelet destruction depends on the antigenic specificity of the injected antibody. If anti-hiL4Rα-mediated platelet destruction does not involve the Fc portion of the antibody, then injecting anti-hiL4Rα

$F(ab)_2$ fragments should achieve the same levels of thrombocytopenia without the observed immunotoxic effects.

As it stands, we are currently unable to investigate the role of PEV in atherosclerosis independently of platelets in chronic experiments as we are currently unable to maintain ApoE KO-hiL4Rα/GPIbα-Tg mice free of endogenous platelets for prolonged periods of time (i.e. for 6 weeks which is the usual minimum time for observing differences in plaque formation in ApoE KO mice on a high fat diet) and constantly injecting PEV. However, our model allows the study of PEV in acute experiments. We have already performed a preliminary investigation of the fate of injected stained PEV (from WT platelets) into endogenous platelet-depleted ApoE KO-hiL4Rα/GPIbα-Tg mouse. We could not find any PEV localized at the aortic root, spleen or lung of the mouse two hours post-PEV-injection (results not shown). However, this was a premature study and this result needs to be validated in further experiments. Intravenously injected HEK293T-derived EV in rodents have been found to localise predominantly in the liver, spleen, lungs and kidneys within a few hours (Lai et al., 2014).

Conclusions

The ApoE KO-hiL4Rα/GPIbα-Tg mouse is a relatively healthy mouse (no severe phenotype) that has fewer but larger circulating platelets than the ApoE mouse (these differences are not dramatic). This mouse when fed a high fat diet develops atheromatous plaques, similar to those exhibited by ApoE KO mice. However, this new mouse exhibits some differences in lipid metabolism, with higher circulating triglycerides (associated with a little higher steatosis and higher weight gain rate) and lower circulating total cholesterol, most likely resulting from the quantitative and

qualitative differences in their platelets. This new mouse is also inducible of endogenous platelet clearance using anti- hiL4Rα antibodies. Hence it can serve as a model for studying the effect of injected PEV in acute and also possibly in chronic atherosclerosis experiments.

10. GENERAL DISCUSSION

Background and Project hypothesis

Increased levels of PEV have been reported to circulate in atherosclerosis patients (Michelsen et al., 2009) and they correlate with atheromatous plaque formation (Lukasik et al., 2013). Furthermore, elevated levels of monocyte-platelet aggregates have been reported to circulate in atherosclerosis (Shantsila and Lip, 2009). In addition, studies on certain atherosclerosis medications, such as statins, have attributed, at least part of their cardioprotective effect, on the associated reduction in (P)EV concentration (Suades et al., 2013). Hence, we hypothesized that PEV may contribute to disease development via formation of heterotypic aggregates with monocytes and associated impact on monocyte function.

The role of PEV in monocyte recruitment in Atherosclerosis

One of the hallmarks of atherosclerosis is monocyte recruitment to the artery wall that involves direct interaction between monocytes and endothelial cells, trans-endothelial migration into the intima layer of the vessel wall, maturation into macrophages and uptake of fats, becoming foam cells (Libby et al., 2011).

In atherosclerosis, the endothelial cells express L-, P- and E-selectins and intercellular adhesion molecules (ICAMs), such as ICAM-1 (Borregaard, 2010; Galkina and Ley, 2007; Johnson-Tidey et al., 1994). These adhesion molecules are recognised by the P-selectin glycoprotein ligand-1 (PSGL-1) and L-selectin on the surface of leukocytes that mediate capture from flow. Sequential formation and dissolution of these bonds under the shear forces generated by blood flow results in rolling adhesion along the luminal endothelial cells (Kansas 1996; McEver and Cummings, 1997). This initial interaction results in the activation of the β2 integrins lymphocyte function-associated antigen 1 (LFA-1) and Macrophage-1 antigen (Mac-1) on the leukocytes which then

bind to the ICAM-1 immunoglobulin receptors of the endothelium; leading to arrest of rolling and “firm adhesion” (Woollard and Geissmann, 2010; Yago et al., 2010; Mueller et al., 2010; Ley et al., 2007; Campbell et al., 1998).

PEV interactions with monocytes can result in monocyte activation, an essential step for monocyte recruitment to take place. Indeed, PEV have been found to promote adhesion of monocytes to activated endothelial cells *in vitro* in a PEV-derived arachidonic acid- dependent manner. When PMV get exposed to phospholipase A2, they release arachidonic acid (Barry et al., 1997). PMV-released arachidonic acid transactivates monocytes and endothelial cells leading to increased monocyte adhesion to endothelial cells through intracellular cell adhesion molecule-1 (ICAM-1) expression and binding and elevated chemotaxis of monocytoid cells (Barry et al., 1998; Forlow et al., 2000; Lukasik et al., 2013). The arachidonic acid also induces synthesis of cyclooxygenase-2 (COX-2)-derived prostacyclin (PGI2) (Barry et al., 1999; Barry et al., 1997). PEV were found to deliver proinflammatory mediators, such as the chemokine CXCR4 (Rozmyslowicz et al., 2003), IL-1 (Boilard et al., 2010) and other receptors such as PAR-1 to cancer cells and hematopoietic stem-progenitor cells. As a result, adhesion to endothelium or fibrinogen was enhanced (Janowska-Wieczorek et al., 2004; Janowska-Wieczorek et al., 2001). PEV can also activate cells through exposure of platelet activating factor (Iwamoto et al., 1996).

In this thesis, it was found that released EV from activated platelets exhibit preferential affinity for binding monocytes in the blood. Leukocytes acquired the PEV receptors GPIb / GPIIb mostly in quanta that are significantly smaller than whole platelets at resting conditions. This suggested that leukocytes bound PEV, instead of whole platelets. Only minimal binding of whole platelets was noted to the leukocytes, a

result that contradicts the observations of other groups (Nagasawa et al., 2013; Xiao and Theroux, 2004; Jensen et al., 2001) that found high levels of whole platelets instead of PEV bound to leukocytes. I argue that their contradictory observation is most likely an artefact arising from the fact that their experiments were performed under static conditions.

Upon this heterotypic aggregate formation, I observed that PEV got endocytosed by the monocytes, even though the endocytosis mechanism(s) was/were not fully elucidated. The internalization of PEV by monocytes opens up the possibility of various molecules and components from the PEV such as inflammatory mediators or miRNAs to be transferred to the monocytes and affect monocyte action towards an inflammatory phenotype in atherosclerosis.

One such constituent that could in theory be transferred to monocytes from PEV is mitochondria. From this project I found that released PEV from activated platelets may contain mitochondria inside them. Contradictory to Laffont et al. (2016), I did not observe any “naked” mitochondria, i.e. without surrounding membrane being shed, which could be the result of different detection technique. Internalized PEV mitochondria by neutrophils can serve as a substrate for phospholipase A2 (PLA2 IIA) that leads to the formation of inflammatory mediators e.g. lysophospholipids and fatty acids from the mitochondrial membrane (Boudreau et al., 2014). Such mediators are known to activate leukocytes and promote the progression of atherosclerosis.

PEV were also found to transfer various miRNAs affecting recipient cell function (Janowska-Wieczorek et al., 2004; Laffont et al., 2013). PEV have been reported to increase monocyte phagocytic activity (Forlow et al., 2000; Jy et al., 1995) via miR-126-3p transfer (Laffont et al., 2016). Increased phagocytosis of lipoproteins and apoptotic

cells contributes to foam cell formation (Schrijvers et al., 2007). In addition, PEV-derived miR-24 was found to target the mitochondrial gene mt-Nd2, causing mitochondrial dysfunction and cell apoptosis (Michael et al., 2016). Mitochondrial dysfunction can directly promote atherosclerosis (Yu and Bennet, 2014).

This interaction between monocytes and PEV increased monocyte recruitment to mouse atherosclerotic carotid endothelium *in vivo* in my experiments. Mause and colleagues (2005), studied indirect effect of PEV on monocyte recruitment to carotid endothelium by *ex vivo* infusion of free PEV in the mouse circulation, followed by infusion of free monocytes. By using sttroboscopic epifluorescence illumination microscopy, they observed increased monocyte interactions with the atheromatous endothelium with pre-perfusion of PEV. The underlying mechanism in this case was PEV-mediated deposition of the chemokine RANTES (CCL5) to the inflamed endothelium during transient PEV-endothelium interactions.

My study however was the first to date in our knowledge to investigate direct and *in vivo* PEV-mediated monocyte recruitment in atherosclerosis using intra-vital microscopy. In my study monocytes-PEV aggregates were perfused instead. Though the underlying mechanism was not investigated, we speculate that the increased monocyte recruitment observed was due to monocyte adoption of PEV adhesion receptors. PEV contain various adhesion receptors on their surface as stated previously, such as glycoproteins Ia/Ib/IIa/IIb/IIIa/VI (Aatonen et al., 2014; Garcia et al., 2005), which are known to bind to the subendothelium (directly or indirectly through vWF) (Sakariassen et al., 1986; Savage et al. 1998; Jackson et al., 2003). Indeed, PEV have been found to promote adhesion of monocytes to activated endothelial cells *in vitro* and *in vivo,* in a PEV-mediated GPIb-dependent manner (Chimen et al., unpublished).

Despite the different strategies employed (perfusion of free PEV, followed by perfusion of free monocytes versus perfusion of monocyte-PEV aggregates), both Mause et al. (2005) and us observed higher rolling adhesion with PEV, whereas firm adhesion was not affected significantly. This result further suggests involvement of GPIb, which is part of the GPIb-IX complex receptor for von Willebrand factor (VWF) that mediates initial and transient platelet binding to the sub-endothelium (Savage et al.; 1996; Savage et al., 1998; Morrison et al., 2014).

Upon monocyte incubation with PEV in our experiments, we detected numerous GPIbα particles inside monocytes scattered around the cells' nucleus, independent of monocyte lysosomes. The fact that PEV-derived GPIbα did not seem to get targeted for destruction in lysosomes, further suggests that it may be recycled by monocytes and exploited to enable monocyte adherence to the endothelium. Interestingly, PEV-derived lipids appeared closer to the cell's edges, away form the cell's core. This differential localisation pattern suggests deconstruction of PEV and separation of the different components. Other EV studies have also reported separation of EV proteins from the EV membrane following endocytosis by recipient cells, with EV lipids fusing with the recipient cell's membrane and EV proteins getting transported to lysosomes or the ER (Tian et al., 2010; Heusermann et al., 2016).

Compared to platelets, PEV appear as more powerful agents in affecting atherosclerosis. According to the concept of size-dependent radial distribution of particles in flow (Nobis et al., 1985; Tangelder et al., 1982), PEV are expected to flow farther in the periphery of the blood stream than platelets because of their smaller size, however their function appears to be comparable to that of activated platelets (Gilbert et al., 1991). Hence, they are expected to bind to athero-compromised endothelium first,

and potentially acting as a substrate for monocyte recruitment. However, we argue that platelets and PEV do not function competitively, but instead synergistically. PEV are released from activated platelets and then PEV can bind to subendothelial matrix and act as a substrate for platelet recruitment (Merten et al., 1999). In addition, PEV can lead to further platelet activation (Montoro-Garcia et al., 2014).

In conclusion, the results from our experiments strengthen the general idea that PEV provide an additional vehicle for monocyte recruitment in atherosclerosis, though the underlying mechanism(s) remain to be fully identified. **Figure 10.1.** shows our proposed mechanism of PEV-mediated monocyte recruitment to atherosclerotic endothelium that remains to be fully investigated. If increased PEV-mediated recruitment translates into acceleration or exacerbation of atherosclerosis, then by blocking the interaction between monocytes and PEV, we could potentially decrease monocyte recruitment in atherosclerosis, ultimately leading to deceleration of disease progression. The effect of chronically preventing monocytes and PEV from forming aggregates, with subsequent prohibition of PEV internalization by monocytes and associated blocking of PEV transfer of various molecules (e.g. adhesion receptors and pro-inflammatory mediators) should be evaluated. PEV were found to bind leukocytes through p-selectin – PSGL-1 interaction (Forlow et al., 2000; Jy et al., 1995), however the effect of chronically blocking this interaction for example, has not been evaluated in atherosclerosis.

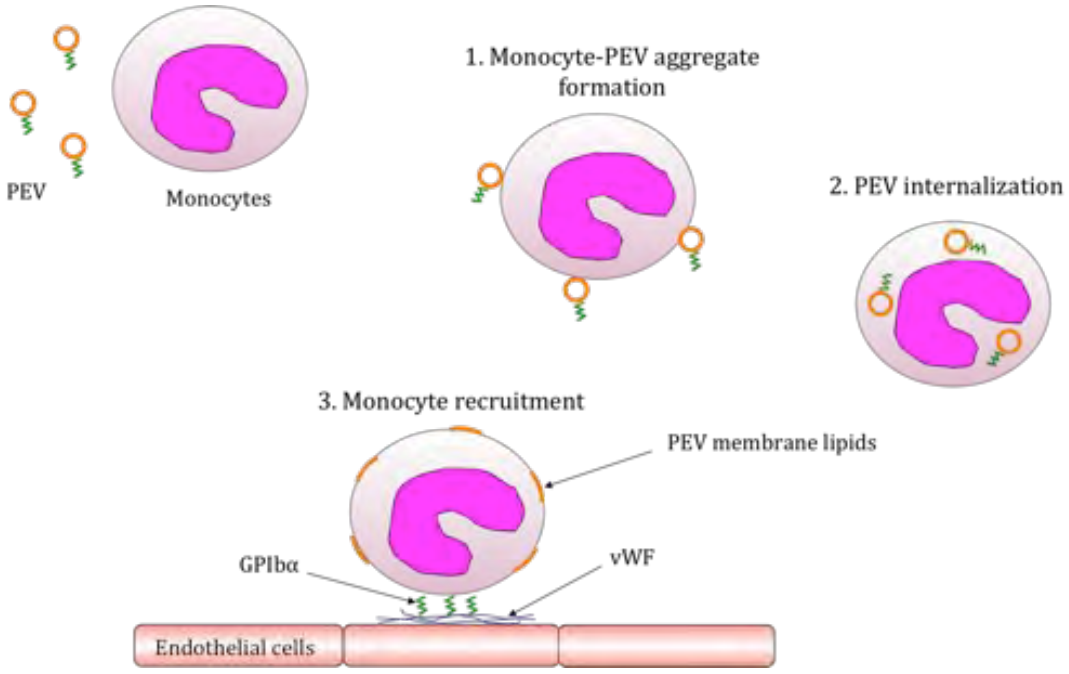

Figure 10.1. Model for PEV-mediated monocyte recruitment in atherosclerosis.

PEV preferentially bind monocytes in the blood (1). Upon this heterotypic aggregate formation, PEV get endocytosed by the monocytes (2). PEV membrane lipids separate from PEV proteins e.g. GPIbα. PEV-derived GPIbα is utilized by the monocytes to facilitate monocyte attachment to blood endothelium in atherosclerosis (3).

Strategy to study the long-term effects of PEV in Atherosclerosis

In order to study the long-term effects of PEV in atherosclerosis progression, one strategy is to systematically inject exogenous PEV in the circulation of a mouse model of atherosclerosis and then check the effect on atherosclerosis progression. However, injecting PEV in a mouse that already contains endogenous PEV might not result in a detectable additional effect if this system is "saturated" in terms of PEV numbers, hence there is need for a PEV-free system. Platelets and PEV can be targeted for endogenous destruction by injecting antibodies against platelet/PEV surface proteins i.e. monoclonal antibodies (mAbs) targeting mouse GPIIbIIIa, GPIIIa, GPIbα, GPIb-IX, GPV and CD31 (Nieswandt et al., 2000). However, these antibodies also target exogenous PEV for destruction. Hence there is need for differentiation between endogenous and

exogenous PEV. During this project, this was achieved by using the *hiL-4Rα/GPIbα-Tg* mouse, that expresses a chimeric protein that is composed of the extracellular domain of the human IL4-R and the transmembrane and cytoplasmic sequences of human GPIbα on the platelets instead of the murine GPIbα (Kanaji et al., 2002). Upon injection with anti-human IL-4 receptor α antibodies, the endogenous circulating platelets are temporarily effectively cleared from the circulation (Boulaftali et al., 2013). The antibodies only target endogenous platelets and PEV; hence it allows the adoptive transfer of exogenous wildtype platelets and/ or PEV. In this project, the *hiL-4Rα/GPIbα-Tg* mouse was crossed with the *ApoE* KO, so a new mouse was created that lacked Apolipoprotein E and also contained the human version of IL-4 on the surface of its platelets and PEV. After first injection with an anti-hIL4R*α* antibody the platelets in the mice were effectively cleared from the circulation and recovered fully within a week. However when repetitive injections with the antibody were given to the mice in order to prolong the PEV-free period, the mice developed anaphylaxis, hence the experiments had to be terminated. To our knowledge, this was the first study to assess effect of repetitive dose of anti-hIL4R*α* antibody. Hence, we conclude that caution must be taken when injecting anti-PEV/platelet antibodies in the mouse circulation. Other strategies, such as using antibodies where the anti- hiL4Rα region is fused to non-immunogenic immunoglobulins or injection of anti-hiL4Rα $F(ab)_2$ fragments (Nieswandt et al., 2000) should be evaluated in the future in terms of both efficiency and safety.

The successful chronic clearance of only endogenous platelets and PEV from the mouse circulation is expected to revolutionise the platelet field in general as this would enable infusion of platelets and/or PEV with various modifications and defects to be studied *in vivo* in different chronic diseases and conditions.

In conclusion, PEV are a rich source of biomolecules that may potentially contribute to atherosclerosis through their preferential interactions with monocytes. PEV up-regulate monocyte recruitment in atherosclerosis, though the underlying mechanism remains to be identified. The new mouse that we hope to generate in future studies may become a useful tool for assessing further PEV-mediated effects in atherosclerosis, such as increase in phagocytosis activity. By dissecting the interactions between PEV and monocytes in atherosclerosis, we hope to find promising targets for future pharmacological intervention.

Open Questions Further Areas of Study

A hallmark of advanced atherosclerosis is the excess accumulation of lipids in the lysosomes of foam cells (Jerome, 2006), due to defects in the process of lysosomal hydrolysis. What causes this lysosomal dysfunction is unknown. Cell-internalized EV usually end up in lysosomes for degradation (Tian et al., 2013; Tian et al., 2010). Hence, PEV or certain PEV components are expected to ultimately traffic into monocyte lysosomes upon internalization. Our experiments have found minimal localization of PEV-derived GPIbα in monocyte lysosomes; however transfer of the rest PEV components into lysosomes has not been assessed. Since PEV have been found to contain various lysosomal molecules such as lysosomal-associated membrane protein-3 (LAMP3) (Perez-Pujol et al., 2007), we speculate that internalized PEV might cause or contribute to lysosomal dysfunction, ultimately contributing to atherosclerosis progression by transformation into foam cells.

The differential distribution of PEV-derived GPIb and PEV membrane inside the monocytes led us speculate that PEV get deconstructed and that the various PEV components lead a different post-internalization fate. It remains to determine which

components if any are transferred to monocyte lysosomes, endosomal vesicles, ER, monocyte membrane or elsewhere and whether they are recycled by the monocytes intact or whether broken down in lysosomes. Live molecule tracking needs to be employed to achieve this.

Attempts to test whether PEV can transfer their mitochondria into monocytes were unsuccessful because the MitoTracker dyes used, proved to be unsuitable for determining mitochondrial transfer in co-cultures due to passive diffusion of the dye. In order to overcome these issues, two future approaches are proposed. Firstly, the use of fluorescent proteins such as GFP could be employed. Transgenic mice that express a fluorescent protein coupled to their mitochondria such as the *Gt(ROSA)26Sor*$^{tm1(CAG-mCherry/GFP)Ganl}$ mouse (McWilliams et al., 2016) could be used in theory to generate PEV with fluorescent mitochondria. PEV could be then incubated with wild type mouse monocytes and their uptake could be investigated by microscopy.

Another approach involves the use of mitochondrial antibodies. However, the use of a mitochondrial antibody pre-requires that the cells/vesicles are permeabilized. Mitochondria cannot be stained with an antibody while in the platelet, because permeabilized platelets may not be able to get stimulated and shed PEV. Hence, PEV mitochondria have to be stained after incubation with monocytes and subsequent permeabilization. However, this would stain also monocyte mitochondria. This problem could be overcome if we take an inter-species approach. For example, human PEV could be incubated with mouse monocytes. Upon internalization (assuming this will happen), cells will get permeabilized and stained using human mitochondria-specific antibodies such as the anti-mitochondria antibody 113-1 from Abcam.

In this project we attempted to develop a new mouse strain to enable the study of long-term effects of injected PEV in atherosclerosis. The biodistribution of PEV upon administration into the mouse circulation will have to be investigated. Intravenously injected HEK293T-derived EV in rodents localised predominantly in the liver, spleen, lungs and kidneys within a few hours (Lai et al., 2014). *In vivo* biodistribution of EV depends on the cell source, the route of administration and targeting (Wiklander et al., 2015).

11. REFERENCES

Aatonen MT, Öhman T, Nyman TA, Laitinen S, Grönholm M, Siljander PR-M. Isolation and characterization of platelet-derived extracellular vesicles. *Journal of Extracellular Vesicles*. 2014; 3: 10.3402/jev.v3.24692.

Admyre C, Johansson SM, Qazi KR, Filén JJ, Lahesmaa R, Norman M, Neve EP, Scheynius A, Gabrielsson S. Exosomes with immune modulatory features are present in human breast milk. *Journal of Immunology 2007;* 179 (3): 1969-78.

Akinc Akin, Battaglia Giuseppe. Exploiting Endocytosis for Nanomedicines. Cold Spring Harb Perspect Biol., 2013; 5(11): a016980.

Akool el, S, Kleinert, H, Hamada, FM *et al.* Nitric oxide increases the decay of matrix metalloproteinase 9 mRNA by inhibiting the expression of mRNA-stabilizing factor HuR. *Mol Cell Biol,* 2003; **23**: 4901– 16.

Ambrose AR, Alsahli MA, Kumani SA, Goodall AH. Comparison of the release of microRNAs and extracellular vesicles from platelets in response to different agonists. Platelets, 2018; 29 (5): 446-454.

Ando M, Iwata A, Ozeki Y, Tsuchiya K, Akiba T, Nihei H. Circulating platelet-derived microparticles with procoagulant activity may be a potential cause of thrombosis in uremic patients. Kidney Int, 2002; 62 (5): 1757-63.

Andreou I, Antoniadis AP, Shishido K, et al. How do we prevent the vulnerable atherosclerotic plaque from rupturing? Insights from in vivo assessments of plaque vascular remodelling and local endothelial shear stress. J Cardiovasc Pharmacol Ther, 2015; 20: 261-275.

Armento EP, Ehsani N, Palmer H, Libby P. Cytokines and growth factors positively and negatively regulate interstitial collagen gene expression in human vascular smooth muscle cells. Arterioscler Thromb, 1991; 11 (5): 1223-30.

Arnaudeau S, Frieden M, Nakamura K, Castelbou C, Michalak M, Demaurex N. Calreticulin differentially modulates calcium uptake and release in the endoplasmic reticulum and mitochondria. J Biol Chem, 2002; 277: 46696-46705.

Arraud N, Linares R, Tan S, Gounou C, Pasquet JJ, Mornet S, Brisson AR. Journal of Thrombosis and Haemostasis, 2014; 12 (5): 614-627.

Asea A, Jean-Pierre C, Kaur P, Rao P, Linhares IM, Skupski D, Witkin SS. Heat shock protein-containing exosomes in mid-trimester amniotic fluids. Journal of Reproductive Immunology, 2008; 79 (1): 12-17.

Bahra P, Nash GB. Sparsely adherent platelets support capture and immobilization of flowing neutrophils. The Journal of Laboratory and Clinical Medicine, 1998; 132 (3): 223-228.

Barre`s C, Blanc L, Bette-Bobillo P, Andre´ S, Mamoun R, Gabius HJ, et al. Galectin-5 is bound onto the surface of rat reticulocyte exosomes and modulates vesicle uptake by macrophages. Blood. 2010; 115: 696-705.

Barry OP, Kazanietz MG, Pratico D, Fitzgerald GA. Arachidonic acid in platelet microparticles up-regulates cyclooxygenase-2-dependent prostaglandin formation via a protein kinase C/mitogen-activated protein kinase-dependent pathway. The Journal of biological chemistry, 1999; 274 (11): 7545-56.

Barry OP, Pratico D, Lawson JA, Fitzgerald GA. Transcellular activation of platelets and endothelial cells by bioactive lipids in platelet microparticles. The journal of clinical investigation, 1997; 99 (9): 218-27.

Barry OP, Pratico D, Savani RC, Fitzgerald GA. Modulation of monocyte-endothelial cell interactions by platelet microparticles. The Journal of clinical investigation, 1998; 102 (1): 136-44.

Basavaraj MG, Osterud B, Hansen JB. Influence of different anticoagulants on monocyte procoagulant functions and monocyte-platelet aggregates formation. Journal of Thrombosis and Haemostasis, 2012; 10 (8): 1698-1702.

Baumgartner HR, Haudenschild C. Adhesion of platelets to subendothelium. Ann. N. Y. Acad. Sci., 1972; 201: 22-36.

Berckmans RJ, Nieuwland R, Kraan MC, Schaap MC, Pots D, Smeets TJ, Sturk A, Tak PP. Synovial microparticles from arthritic patients modulate chemokine and cytokine release by synoviocytes. Arthritis Res Ther 2005; **7**: 536–544.

Berk BC. Atheroprotective signaling mechanisms activated by steady laminar flow in endothelial cells. Circulation. 2008; 117:1082–1089.

Bernal-Mizrachi L, Jy W, Jimenez J, Pastor J, Mauro L, Horstman L, de Marchena E, Ahn Y. High levels of circulating endothelial microparticles in patients with acute coronary syndromes. The American Heart Journal, 2003; 145 (6): 962-970.

Bergmeier W, Boulaftali Y. Adoptive transfer method to study platelet function in mouse models of disease. Thrombosis Research, 2014; 133: S3-S5.

Bergmeier W, Piffath CL, Cheng G, Dole VS, Zhang Y, von Andrian UH, Wagner DD. Tumor necrosis factor-alpha-converting enzyme (ADAM17) mediates GPIbalpha shedding from platelets in vitro and in vivo. Circ Res 2004; 95: 677–683.

Bevers EM, Comfurius P, Dekkers DW, Zwaal RF. Lipid translocation across the plasma membrane of mammalian cells. Biochim Biophys Acta 1999; 18; 1439 (3): 317-30.

Bevers EM, Williamson PL. Phospholipid scramblase: An update**.** FEBS Letters, 2010; 584 (13); 2724-2730.

Beyer C Pisetsky DS. The role of microparticles in the pathogenesis of rheumatic diseases. Nat Rev Rheumatol 2010; **6**: 21–29.

Bode AP, Knupp CL. Effect of cold storage on platelet glycoprotein Ib and vesiculation. Transfusion, 1994; 34 (8): 690-6.

Bode AP, Orton SM, Frye MJ, Udis BJ. Vesiculation of platelets during in vitro aging. Blood, 1991; 77 (4): 887-95.

Boilard E, Nigrovic PA, Larabee K, Watts GFM, Coblyn JS, Weinblatt ME, Massarotti EM, Remold-O'Donnell E, Farndale RW, Ware J, Lee DM. Platelets amplify inflammation in arthritis via collagen-dependent microparticle production. Science, 2010; 327 (5965): 580-3.

Bombrie A, Colombo M, Raposo G, Thery C. Exosome secretion: molecular mechanisms and roles in immune responses. Traffic, 2011; 12 (12): 1659-68.

Booth AM, Fang Y, Fallon JK, Yang JM, Hildreth JE, Gould SJ. Exosomes and HIV Gag bud from endosome-like domains of the T cell plasma membrane. J Cell Biol 2006; **172**: 923–935.

Bosnjak ZJ, Yan Y, Canfield S, Muravyeva MY, Kikuchi C, Wells CW, Corbett JA, Bai X. Ketamine induces toxicity in human neurons differentiated from embryonic stem cells via mitochondrial apoptosis pathway. Curr Drug Saf, 2012; 7: 106-119.

Botelho RJ, Grinstein S. Phagocytosis. Current Biology, 2011; 21 (14): 533-538.

Botto N, Berti S, Manfredi S, Al-Jabri A, Federici C, Clerico A, Ciofini E, Biagini A, Andreassi MG. Detection of mtDNA with 4977 bp deletion in blood cells and atherosclerotic lesions of patients with coronary artery disease. Mutation Research/Fundamental and Molecular Mechanisms of Mutagenesis, 2005; 570 (1): 81-88.

Boudreau LH, Duchez AC, Cloutier N, Soulet D, Martin N, Bollinger J, Pare A, Rousseau M, Naika GS, Levesque T, Laflamme C, Marcoux G, Lambeau G, Farndale RW, Pouliot M, Hamzeh-Cognasse H, Cognasse F, Garraud O, Nigrovic PA, Guderley H, Lacroix S, Thibault L, Semple JW, Geib MH, Boilard E. Platelets release mitochondria serving as substrate for bactericidal group IIA-secreted phospholipase A2 to promote inflammation. Blood, 2014; 124 (14): 2173-83.

Boulaftali Y, Hess PR, Getz TM, Cholka A, Stolla M, Mackman N, et al. Platelet ITAM signaling is critical for vascular integrity in inflammation. J Clin Invest 2013; 123: 908–16.

Boulanger MC, Scoazec MA, Ebrahimian MT, Henry MP, Mathieu ME, Tedgui MA, Mallat MZ. Circulating Microparticles From Patients With Myocardial Infarction Cause Endothelial Dysfunction. Circulation: Journal of the American Heart Association, 2001; 104 (22): 2649-2652.

Bournazos S, Rennie J, Hart SP, Dransfield I. Choice of anticoagulant critically affects measurement of circulating platelet-leukocyte complexes. Arterioscler Thromb Vasc Biol 2008; 28: e2-3.

Box CL, Harrison P, Nash H, Watson S, Harper L, Rainger E. Interactions between platelets and platelet derived microvesicles in inflammation (PhD Thesis). University of Birmingham, 2014.

Boyette LB, Macedo C, Hadi K, Elinoff BD, Walters JT, Ramaswami B, Chalasani G, Taboas JM, Lakkis FG, Metes DM. PLoS One, 2017; 12 (4): e0176460.

Brass LF. Thrombin and Platelet Activation. CHEST, 2003; 124 (3): 18S-25S.

Brill A, Dashevsky O, Rivo J, Gozal Y, Varon D. Platelet-derived microparticles induce angiogenesis and stimulate post-ischemic revascularization. Cardiovasc. Research, 2005; 67 (1): 30-8.

Brisson AR, Tan S, Linares R, Gounou C, Arraud N. Extracellular vesicles from activated platelets: a semiquantitative cryo-electron microscopy and immune-gold labelling study. Platelets, 2017; 28 (3): 263-271.

Burger JA, Kipps TJ. CXCR4: a key receptor in the crosstalk between tumor cells and their microenvironment. Blood, 2006; 107: 1761-1767.

Buttrum SM, Hatton R, Nash GB. Selectin-mediated rolling of neutrophilson immobilized platelets. Blood, 1993; 82 (4): 1165-74.

Cai, H, Harrison, DG. Endothelial dysfunction in cardiovascular diseases: the role of oxidant stress. *Circ Res* 2000; **87**: 840– 4.

Campbell JJ, Hedrick J, Zlotnik A, Siani MA, Thompson DA, Butcher EC. Chemokines and the Arrest of Lymphocytes Rolling Under Flow. Science, 1998; 279 (5349): 381-384.

Castaman G, Yu-Feng L, Rodeghiero F. A bleeding disorder characterised by isolated deficiency of platelet microvesicle generation. The Lancet, 1996;347 (9002): 700-701.

Cauwenberghs S, Feijge MAH, Harper AGS, Sage SO, Curvers J, Heemskerk JWM. Shedding of procoagulant microparticles from unstimulated platelets by integrin-mediated destabilization of actin cytoskeleton. FEBS Letters, 2006; 580 (22): 5313-5320.

Chaput N, Théry C. Exosomes: immune properties and potential clinical implementations. Semin Immunopathol 2011; **33**:419–440.

ChatzizisisYS, Coskun AU, Jonas M, et al. Role of endothelial shear stress in the natural history of coronary atherosclerosis and vascular remodelling: molecular, cellular, and vascular behaviour. J Am Coll Cardiol, 2007; 49: 2379-2393.

Chen, HH, Wang, DL. Nitric oxide inhibits matrix metalloproteinase-2 expression via the induction of activating transcription factor 3 in endothelial cells. *Mol Pharmacol* 2004; **65**: 1130– 40.

Chen Z, Mondal NK, Ding J, Koenig SC, Slaughter MS, Griffith BP, Wu ZJ. Activation and shedding of platelet glycoprotein IIb/IIIa under non-physiological shear stress. Mol Cell Biochem, 2015; 409 (0): 93-101.

Cheng C, van Haperen R, de Waard M, et al. Shear stress affects the intracellular distribution of eNOS: direct demonstration by a novel in vivo technique. Blood, 2005; 106: 3691– 8.

Chien S. Mechanotransduction and endothelial cell homeostasis: the wisdom of the cell. Am J Physiol Heart Circ Physiol. 2007; 292:H1209–H1224.

Chien S. Molecular and mechanical bases of focal lipid accumulation in arterial wall. Prog Biophys Mol Biol. 2003; 83:131–151.

Chimen M, Evryviadou A, Box CL, Harrrison MJ, Hazeldine J, Dib LH, Kuravi SJ, Payne H, Kavanagh D, Lax S, Kalia N, Brill A, Thomas SG, Belli A, Crombie N, Adams RA, Evans SA, Deckmyn H, Lord JM, Harrison P, Watson SP, Nash GB, Rainger GE. A novel thrombo-inflammatory pathway of leukocyte recruitment: Appropriation of GPIbα from platelet extracellular vesicles supports monocyte recruitment in systemic inflammation. European Heart Journal (under review).

Chiu JJ, Chien S. Effects of disturbed flow on vascular endothelium: pathophysiological basis and clinical perpectives. Physiol Rev, 2011; 91: 327-387.

Christianson HC, Svensson KJ, van Kuppevelt TH, Li JP, Belting M. Cancer cell exosomes depend on cell-surface heparan sulfate proteoglycans for their internalization and functional activity. Proc Natl Acad Sci U S A. 2013; 110: 17380-5.

Ciferri S, Emiliani C, Guglielmi G, Orlacchio A, Nenci G, Gresele P. Platelets release their Lysosomal Content In Vivo in Humans upon Activation. Thrombosis and Haemostasis, 2000; 83 (1): 157-164.

Clement J, Colson P, Saegeman V, Lagrou K, Ranst M. 'Bedside assessment' of acute hantavirus infections and their possible classification into the spectrum of haemophagocytic syndromes. European Journal of Clinical Microbiology & Infectious Diseases, 2016; 35 (7): 1101-1106.

Cochain C, Zernecke A. Macrophages in vascular inflammation and atherosclerosis, Pflugers Arch., 2017; 469: 485–499.

Comfurius P, Senden JMG, Tilly RHJ, Schroit AJ, Bevers EM, Zwaal RFA. Loss of membrane phospholipid asymmetry in platelets and red cells may be associated with calcium-induced shedding of plasma membrane and inhibition of aminophospholipid translocase. BBA-Biomembranes, 1990; 1026 (2): 153-160.

Corash L, Chen HY, Levin J, et al. Regulation of thrombopoiesis: effects of the degree of thrombocytopenia on megakaryocyte ploidy and platelet volume. Blood, 1987; 70: 177-185.

Corral-Debrinski, Shoffner JM, Lott MT, Wallace DC. Association of mitochondrial DNA damage with aging and coronary atherosclerotic heart disease. Mutation/Research/DNAging, 1992; 275 (3-6): 169-180.

Cowan DH, Robertson AL, Shook P, Giroski P. Platelet adherence to collagen: role of plasma, ADP, and divalent cations. 1981; 47 (2): 257-67.

Cramer EM, Norol F, Guichard J, Breton-Gorius J, Vainchenker W, Masse JM, Debili N. Ultrastructure of platelet formation by human megakaryocytes cultured with the Mpl ligand. Blood, 1997; 89 (7): 2336-2346.

Cselenyak A, Pankotai E, Csordas A, Kiss L, Lacza Z. Live-Cell Fluorescent Imaging of Membrane or Mitochondrion Transfer between Connected Cells in Culture. Microscopy, Science, Technology, Applications and Education, 2010; 1: 764-771.

Daleke DL. Regulation of transbilayer plasma membrane phospholipid asymmetry. Journal of Lipid Research, 2003; 44 (2): 233-42.

Danesh A, Inglis HC, Jackman RP, Wu S, Deng X, Muench MO, Heitman JW, Norris PJ. Exosomes from red blood cell units bind to monocytes and induce inflammatory cytokines, boosting T-cell responses in vitro. Blood, 2013; 123: 687-696.

Dashevsky O, Varon D, Brill A. Platelet-derived microparticles promote invasiveness of prostate cancer cells via upregulation of MMP-2 production. International Journal of Cancer, 2009; 124 (8): 1773-1777.

Del Cacho E, Gallego M, Lee SH, Lillehoj HS, Quilez J, Lillehoj EP, Sánchez-Acedo C. Induction of protective immunity against Eimeria tenella infection using antigen-loaded dendritic cells (DC) and DC-derived exosomes. Vaccine, 2011; **29**: 3818–3825.

Desai K, Bruckdorfer KR, Hutton RA, Owen JS. Binding of apoE-rich high density lipoprotein particles by saturable sites on human blood platelets inhibits agonist-induced platelet aggregation. J Lipid Res, 1989; 30 (6): 831-40.

Diehl P, Aleker M, Helbing T, Sossong V, Beyersdorf F, Olschewski M, Bode C, Moser M. Enhanced microparticles in ventricular assist device patients predict platelet, leukocyte and endothelial cell activation. Interactive CardioVascular and Thoracic Surgery, 2010; 11 (2): 133-137.

Distler JH, Distler O. Inflammation: Microparticles and their roles in inflammatory arthritides. Nat Rev Rheumatol, 2010; **6**: 385–386.

Distler JH, Jüngel A, Huber LC, Seemayer CA, Reich CF 3rd., Gay RE, Michel BA, Fontana A, Gay S, Pisetsky DS, Distler O. The induction of matrix metalloproteinase and cytokine expression in synovial fibroblasts stimulated with immune cell microparticles. Proc Natl Acad Sci USA 2005; **102**: 2892–2897.

Doherty GJ, McMahon HT. Mechanisms of Endocytosis. Annu Rev Biochem, 2009; 78: 857–902.

Dollery CM, Libby P. Atherosclerosis and proteinase activation. Cardiovascular research, 2006; 69 (3): 625-635.

Ehrlich M, Boll W, Van Oijen A, Hariharan R, Chandran K, Nibert ML, Kirchhausen T. Endocytosis by random initiation and stabilization of clathrin-coated pits. Cell, 2004; 118: 591–605.

Eichner JE, Dunn ST, Perveen G, Thompson DM, Stewart KE, Stroehla BC. Apolipoprotein E polymorphism and cardiovascular disease: a HuGE review. Am J Epidemiol, 2002; 155 (6): 487-95.

Eitan E, Green J, Bodogai M, Mode NA, Baek R, Jorgensen MM, Freeman DW, Witwer KW, Zonderman AB, Biragyn A, Matson MP, Hooten NN, Evans MK. Age-related Changes in Plasma Extracellular Vesicle Characteristics and Internalization by Leukocytes. Scientific Reports, 2017; 7 (1342).

Escola JM, Kleijmeer MJ, Stoorvogel W, Griffith JM, Yoshie O, Geuze HJ. Selective enrichment of tetraspan proteins on the internal vesicles of multivesicular endosomes and on exosomes secreted by human B-lymphocytes. J Biol Chem 1998; **273**:20121–20127.

Escrevente C, Keller S, Altevogt P, Costa J. Interaction and uptake of exosomes by ovarian cancer cells. BMC Cancer. 2011; 11: 108.

Esser J, Gehrmann U, D'Alexandri FL, Hidalgo-Estévez AM, Wheelock CE, Scheynius A, Gabrielsson S, Rådmark O. Exosomes from human macrophages and dendritic cells contain enzymes for leukotriene biosynthesis and promote granulocyte migration. J Allergy Clin Immunol 2010; **126**:1032–1040, 1040.e1–1040.e4.

Fang Y, Wu N, Gan X, Yan W, Morrell JC, Gould SJ. Higher-order oligomerization targets plasma membrane proteins and HIV gag to exosomes. PLoS Biol 2007; **5**:e158.

Fang Y, Wu N, Gan X, Yan W, Morrell JC, Gould SJ. Higher-order oligomerization targets plasma membrane proteins and HIV gag to exosomes. PLoS Biol 2007; **5**:e158.

Febbraio M, Podrez EA, Smith JD, Hajjar DP, Hazen SL, Hoff HF, Sharma K, Silverstein RL. Targeted disruption of the class B scavenger receptor CD36 protects against atherosclerotic lesion development in mice. The Journal of clinical investigation, 2000; 105 (8): 1049-56.

Feng D, Zhao WL, Ye YY, Bai XC, Liu RQ, Chang LF, et al. Cellular internalization of exosomes occurs through phago- cytosis. Traffic. 2010; 11: 675-87.

Feinstein MB, Fraser C: Human platelet secretion and aggregation induced by calcium ionophores. J Gen Physiol, 1975; 66: 561.

Fessler MB, Rose K, Zhang Y, Jaramillo R, Zeldin DC. Relationship between serum cholesterol and indices of erythrocytes and platelets in the US population. J Lipid Res, 2013; 54 (11): 3177-3188.

Fitzner D, Schnaars M, van Rossum D, Krishnamoorthy G, Dibaj P, Bakhti M, et al. Selective transfer of exosomes from oligodendrocytes to microglia by macropinocytosis. J Cell Sci. 2011; 124: 447-58.

Flaumenhaft R, Dilks JR, Richardson J, et al. Megakaryocyte-derived microparticles: direct visualization and distinction from platelet-derived microparticles. Blood, 2009; 113 (5): 1112-21.

Flaumenhaft R. Formation and fate of platelet microparticles. Blood Cells, 2006; 36 (2): 182-187.

Forlow S, McEver RP, Nollert MU. Leukocyte-leukocyte interactions mediated by platelet microparticles under flow. Blood, 2000; 95: 1317-23.

Franzen CA, Simms PE, Van Huis AF, Foreman KE, Kuo PC, Gupta GN. Characterization of uptake and internaliza- tion of exosomes by bladder cancer cells. Biomed Res Int. 2014; 2014: 619829.

Freeman DW, Noren Hooten N, Eitan E, Green J, Mode NA, Bodogai M, Zhang Y, Lehrmann E, Zonderman AB, Biragyn A, Egan J, Becker KG, Mattson MP, Ejiogu N, Evans MK. Altered Extracellular Vesicle Concentration, Cargo and Function in Diabetes Mellitus. Diabetes, 2018; db171308.

Freyssinet JM, Toti F. Membrane microparticle determination: at least seeing what's being sized! Journal of Thrombosis and Haemostasis, 2010; 8 (2), 311-314.

Furie B, Furie BC. Thrombus formation in vivo. The Journal of Clinical Investigation, 2005; 115 (12): 3355-3362.

Furman MI, Benoit SE, Barnard MR, Valeri CR, Borbone ML, Becker RC, Hechtman HB, Michelson AD. Increased Platelet Reactivity and Circulating Monocyte-Platelet Aggregates in Patients With Stable Coronary Artery Disease. Journal of the American College of Cardiology, 1998; 31 (2): 352-358.

Gabriel DA, Giordano K. Microparticle sizing and counting using light scattering methods. Semin Thromb Hemost, 2010; 36 (8): 824-32.

Galis Z, Sukhova G, Lark M, Libby P. Increased expression of matrix metalloproteinases and matrix degrading activity in vulnerable regions of human atherosclerotic plaques. *J Clin Invest* 1994; **94**: 2493 503.

Galkina E, Ley K. Vascular adhesion molecules in atherosclerosis. Arteriosclerosis, Thrombosis, and Vascular Biology, 2007; 27: 2292-2301.

Galli M, Grassi A, Barbui T. Platelet-derived microvesicles in thrombotic thrombocytopenic purpura and haemolytic uremic syndrome. Thromb Haemost, 1996; 75 (3): 427-31.

Gambillara V, Chambaz C, Montorzi G, Roy S, Stergiopulos N, Silacci P. Plaque-prone hemodynamics impair endothelial function in pig carotid arteries. Am J Physiol Heart Circ Physiol., 2006; 290: 434.

Garcia BA, Smalley DM, Jun H, Shabanowitz J, Ley K, Hunt DF. The platelet Microparticle Proteome. J Proteome Res., 2005; 4 (5): 1516-1521.

Gardiner EE, Karunakaran D, Shen Y, Arthur JF, Andrews RK, Berndt MC. Controlled shedding of platelet glycoprotein (GP) VI and GPIb-IX-V by ADAM family metalloproteinases. J Thromb Haemost., 2007; 5: 1530–1537.

Gasser O, Schifferli JA. Activated polymorphonuclear neutrophils disseminate anti-inflammatory microparticles by ectocytosis. Blood, 2004; 104: 2543-2548.

Gemmell CH, Ramirez SM, Yeo EL, Sefton MV. Platelet activation in whole blood by artificial surfaces: identification of platelet-derived microparticles and activated platelet binding to leukocytes as material-induced activation events. J Lab Clin Med, 1995; 125 (2): 276-87.

George JN. Platelets. Lancet, 2000; 355 (9214): 1531-9.

Gilbert GE, Sims PJ, Wiedmer T, Furie B, Furie BC, Shattil SJ. Platelet-derived microparticles express high affinity receptors for factor VIII. The Journal of biological chemistry, 1991; 266 (26): 17261-8.

Go YM, Boo YC, Park H, et al. Protein kinase B/Akt activates c-Jun NH(2)-terminal kinase by increasing NO production in response to shear stress. J Appl Physiol 2001; 91: 1574 – 81.

Goldstein JL, Brown MS. The LDL receptor. Arterioscler Thromb Vasc Biol, 2009; **29**: 431–438.

Goncalves GS, Duarte RCF, Campos FMF, de Fatima Oliveira Silva I, se Sousa LP, Faria MC, Filho OAM, Bicalho MAC, de Moraes EN, Teixeira AL, Silveira JN, Das Gracas Carvalho M. Elevated platelet microparticles levels are associated with lipidic oxidation and inflammatory profiles in Alzheimer's disease. European Geriatric Medicine, 2016; 7 (4): 352-359.

Hafiane A, Genest J. ARP binding cassette A1 (ABCA1) mediates microparticle formation during high-density lipoprotein (HDL) biogenesis. Atherosclerosis, 2017; 257: 90-99.

Hansson GK. Mechanisms of Disease: Inflammation, Atherosclerosis, and Coronary Artery Disease. The New ngland Journal of Medicine, 2005; 352 (16): 1685-95.

Hao S, Bai O, Li F, Yuan J, Laferte S, Xiang J. Mature dendritic cells pulsed with exosomes stimulate efficient cytotoxic T-lymphocyte responses and antitumour immunity. Immunology. 2007; 120: 90-102.

Hardie D, Ross F, Hawley S. AMPK: a nutrient and energy sensor that maintains energy homeostasis. Nature Reviews. Molecular Cell Biology, 2012; 13 (4): 251-62.

Harding C, Heuser J, Stahl P. Receptor-mediated endocytosis of transferrin and recycling of the transferrin receptor in rat reticulocytes. J Cell Biol, 1983; **97**: 329–339.

Harding SA, Sommerfield AJ, Sarma J, Twomey PJ, Newby DE, Frier BM, Fox KAA. Increased CD40 ligand and platelet-monocyte aggregates in patients with type 1 diabetes mellitus. Atherosclerosis, 2004; 176 (2): 321-325.

Harrison DG, Widder J, Grumbach I, Chen W, Weber M, Searles C. Journal of Internal Medicine, 2006; 259 (4): 351-363.

Heemskerk JW, Kuijpers MJ, Munnix IC, Siljander PR. Platelet collagen receptors and coagulation. A characteristic platelet response as possible target for antithrombotic treatment. Trends Cardiovasc Med, 2005; 15 (3): 86-92.

Heemskerk JW, Siljander P, Vuist WM, Breikers G, Reutelingsperger CP, Barnes MJ et al. Function of glycoprotein VI and integrin alpha2beta1 in the procoagulant response of single, collagen-adherent platelets. Thromb Haemost. 1999; 81: 782–92.

Heijnen HF, Schiel AE, Fijnheer R, Geuze HJ, Sixma JJ. Activated platelets release two types of membrane vesicles: microvesicles by surface shedding and exosomes derived from exocytosis of multivesicular bodies and alpha-granules. Blood, 1999; **94**:3791–3799.

Henney AM, Wakeley PR, Davies MJ *et al*. Localization of stromelysin gene expression in atherosclerotic plaques by in situ hybridization. *Proc Natl Acad Sci USA* 1991; **88**: 8154 58.

Hernandez M, Wright SD, Cai TQ. Critical role of cholesterol ester transfer protein nicotinic acid-mediated HDL elevation in mice. Biochem Biophys Res Commun, 2007; 355 (1075-1080).

Hezel MEV, Nieuwland R, Bruggen RV, Juffermans NP. The ability of extracellular vesicles to induce a pro-inflammatory host response. Int. J. Mol. Sci., 2017; 18 (6).

Heuser JE, Reese TS. Evidence for recycling of synaptic vesicle membrane during transmitter release at the frog neuromuscular junction. J Cell Biol., 1973; 57: 315–344.

Heusermann W, Hean J,Trojer D, Steib E, von Bueren S, Graff-Meyer A, Genoud C, Martin K, Pizzato N, Voshol J, Morrissey DV, Andaloussi SEL, Wood MJ, Meisner-Kober N. Exosomes surf on filopodia to enter cells at endocytic hot spots, traffic within endosomes, and are targeted to the ER. Journal of Cell Biology, 2016; 213 (2): 173-184.

Higashihara M, Kinoshita M, Kume S, Teramoto T, Kurokawa K. Inhibition of platelet function by highdensity lipoprotein from a patient with apolipoprotein E deficiency. Biochem Biophys Res Commun, 1991; 181: 1331–1336.

Higashihara M, Kinoshita M, Teramoto T, Kume S, Kurokawa K. The role of apoE in inhibitory effects of apoE-rich HDL on platelet function. FEBS Lett,, 1991; 282: 82-86.gg

Himburg HA, Grzybowski DM, Hazel AL, Lamack JA, Li XM, Friedman MH. Spatial coparison between wall shear stress measures and porcine arterial endothelial permeability. American Journal of Physiology, 2004; 286 (5): HH1916-22.

Hobbs AE, Srinivasan M, McCaffery JM, Jensen RE. Mmm1p, a mitochondrial outer membrane protein, is connected to mitochondrial DNA (mtDNA) nucleoids and required for mtDNA stability. J Cell Biol, 2001; 152: 401-410.

Holme PA, Solum NO, Brosstad F, Pedersen T, Kveine M. Microvesicles bind soluble fibrinogen, adhere to immobilized fibrinogen and coaggregate with platelets. Thromb Haemost. 1998; 79: 389–94.

Hoffman M, Monroe DM, Roberts HR. Coagulation factor IXa binding to activated platelets and platelet-derived microparticles: a flow cytometric study. Thromb Haemost, 1992; 68 (1): 74-8.

Horstman LL, Ahn., YS. Platelet microparticles: a wide-angle perspective. Critical Reviews in Oncology and Hematology, 1999; 30: 111-142.

Hourdillé, P., Gralnick, H.R., Heilmann, E., et al. von Willebrand factor bound to glycoprotein Ib is cleared from the platelet surface after platelet activation by thrombin. Blood, 1992; 79 (8): 2011–21.

Hourdillé, P., Heilmann, E., Combrié, R., et al. Thrombin induces a rapid redistribution of glycoprotein Ib-IX complexes within the membrane systems of activated human platelets. Blood, 1990; 76 (8): 1503–13.

Hovig T. Release of a platelet-aggregating substance (adenosine diphosphate) from rabbit blood platelets induced by saline "extract" of tendons. Thromb Diath Haemorrh. 1963;9:264–278.

Hsiai TK, Cho SK, Wong PK, Ing M, Salazar A, Sevanian A, Navab M, Demer LL, Ho CM. Monocyte recruitment to endothelial cells in response to oscillatory shear stress. FASEB Journal, 2003; 17 (12): 1648-1657.

Hsiai TK, Cho SK, Reddy S, Hama S, Navab M, Demer LL, Honda HM, Ho CM. Pulsatile flow regulates monocyte adhesion to oxidized lipid-induced endothelial cells. Arterioscler Thromb Vasc Biol. 2001; 21:1770–1776.

Hugues J, Lapière CM. Nouvelles recherches sur l'accolement des plaquettes aux fibres de collagén. Thromb Diath Haemorrh. 1964; 11: 327–354.

Hughes M, Hayward CP, Warkentin TE, Horsewood P, Chorneyko KA, Kelton JG. Morphological analysis of microparticle generation in heparin-induced thrombocytopenia. Blood, 2000; 96 (1): 188-94.

Huo Y, Schober A, Forlow SB, Smith DF, Hyman MC, Jung S, Littman DR, Weber C, Ley K. Circulating activated platelets exacerbate atherosclerosis in mice deficient in apolipoprotein E. Nat Med., 2003; 9(1): 61-7.

Hwang J, Ing MH, Salazar A, Lassègue B, Griendling K, Navab M, Sevanian A, Hsiai TK. Pulsatile versus oscillatory shear stress regulates NADPH oxidase subunit expression: implication for native LDL oxidation. Circ Res. 2003; 93:1225–1232.

Hwang J, Saha A, Boo YC, Srescu GP, McNally JS, Holland SM, Dikalov S, Giddens DP, Griendling KK, Oscillatory shear Harrison DG, Jo H. stress stimulates endothelial production of O2- from p47-dependent NAD(P)H oxidases, leading to monocyte adhesion. J Biol Chem, 2003: 47291-47298.

Ikonen E. Cellular cholesterol trafficking and compartmentalization. Nat. Rev. Mol. Cell Biol., 2008; 9 (2): 125–138.

Inami N, Nomura S, Kikuchi H, Kajiura T, Yamada K, Nakamori H, Takahashi N, Tsuda N, Hikosaka M, Masaki M, Iwasaka T. P-selectin and Platelet-Derived Microparticles Associated with Monocyte Activation Markers in Patients with Pulmonary Embolism. Clinical and Applied Thrombosis/Hemostasis, 2003; 9 (4): 309-316.

Ingersoll MA, Spanbroek R, Lottaz C, Gautier EL, Frankenberger M, Hooffmann R, Lang R, Haniffa M, Collin M, Tacke F, Habenicht AJR, Ziegler-Heitbrock L, Randolph GJ. Comparison of gene expression profiles between human and mouse monocyte subsets. Blood, 2010; 115: e10-e19.

Ivandic B, Castellani LW, Wang XP, Qiao JH, Mehrabian M, Navab M, Fogelman AM, Grass DS, Swanson ME, De Beer MC, De Beer F, Lusis AJ. Role of Group II Secretory Phospholipase A2 in Atherosclerosis and Altered Lipoproteins in Transgenic Mice Expressing Group IIa Phospholipase A2. Arteriosclerosis, Thrombosis, and Vascular Biology, 1999; 19 (5): 1284-1290.

Iversen TG, Skotland T, Sandvig K. Endocytosis and intracellular transport of nanoparticles: Present knowledge and need for future studies. Nano Today, 2011; 6 (2): 176-185.

Iwamoto S, Kawasaki T, Kambayashi J, Ariyoshi H, Monden M. Microparticles: a carrier of platelet-activating factor? Biochem BiophysRes Commun, 1996; 218 (3): 940-4.

Jackson SP, Nesbitt WS, Kulkarni S. Signaling events underlying thrombus formation. Journal of Thrombosis and Haemostasis, 2003; 1 (7): 1602-1612.

Jambrina E, Alonso R, Alcalde M, del Carmen Rodríguez M, Serrano A, Martínez-A C, García-Sancho J, Izquierdo M. Calcium influx through receptor-operated channel induces mitochondria-triggered paraptotic cell death. J Biol Chem, 2003; 278: 14134-14145.

Janowska-Wieczorek A, Majka M, Kijowski J, Baj-Krzyworzeka M, Reca R, Turner AR, Ratajczak J, Emerson SG, Kowalska MA, Ratajczak MZ. Platelet-derived microparticles bind to hematopoietic stem/progenitor cells and enhance their engraftment. Blood, 2001; 98 (10): 3143-9.

Janowska-Wieczorek A, Wysoczynnski M, Kijowski J, Marquez-Curtis L, Machalinski B, Ratajczak J, Ratajczak MZ. Microvesicles derived from activated platelets induce metastasis and angiogenesis in lung cancer. International Journal of Cancer, 2004; 113 (5): 752-60.

Jensen, M.K., de Nully Brown, P., Lund, B. V, et al. Increased circulating platelet-leukocyte aggregates in myeloproliferative disorders is correlated to previous thrombosis, platelet activation and platelet count. European journal of haematology, 2001; 66 (3): 143–51.

Jerome WG. Advanced atherosclerotic foam cell formation has features of an acquired lysosomal storage disorder. Rej Res, 2006; 9: 245-255.

Jia LX, Zhang WM, Li TT, Liu Y, Piao CM, Ma YC, Lu Y, Wang Y, Liu TT, Qi YF, Du J. ER stress dependent microparticles derived from smooth muscle cells promote endothelial dysfunction during thoracic aortic aneurysm and dissection. Clinical Science Volume, 2017; 131 (12): 1287-1299.

Johnson-Tidey RR, McGregor JL, Taylor PR, Poston RN. Increase in the adhesion molecule P-selectin in endothelium overlying atherosclerotic plaques: coexpression with intercellular adhesion molecule-1. *Am J Pathol.* 1994;**144**: 952–961.

Jones RC, Jacobson M, Capen D. Quantitative analysis of PDGF-AA/PDGF-R alpha and interstitial fibroblasts recruited as perivascular progenitor smooth muscle cells (mural cells)) in adult pulmonary hypertension (PH): imaging microvessel wall structure and regulation of PDGF signalin. Faseb Journal, 2005; 19 (5): 1507.

Jonsson F, Mancardi DA, Kita Y, Karasuyama H, Iannascoli B, Van Rooijen N, Shimizu T, Daeron M, Bruhns P. Mouse and human neutrophils induce anaphylaxis. J Clin Invest, 2011; 121 (4): 1484-96.

Jonsson F, Mancardi DA, Zhao W, Kita Y, Iannascoli B, Khun H, van Rooijen N, Shimizu T, Schwartz LB, Daeron M, Bruhns P. Humna FcγRIIA induces anaphylactic and allergic reactions. Blood, 2012; 119 (11): 2533-44.

Joop K, Berckmans RJ, Nieuwland R, Berkhout J, Romijn FPHTM, Hack E, Sturk A. Microparticles from Patients with Multiple Organ Dysfunction Syndrome and Sepsis Support Coagulation through Multiple Mechanisms. Thromb Haemost, 2001; 85 (5): 810-820.

Joseph JE, Harrison P, Mackie IJ, Isenberg DA, Machin SJ. Increased circulating platelet-leucocyte complexes and platelet activation in patients with antiphospholipid syndrome, systemic lupus erythematosous and rheumatoid arthritis. Br J Haematol, 2001; 115 (2): 451-9.

Jy W, Mao WW, Horstman LL, Tao J, Ahn YS. Platelet microparticles bind, activate and aggregate neutrophils in vitro. Blood Cells Mol Dis, 1995; 21.

Kanaji T, Russell S, Ware J. Amelioration of the macrothrombocytopenia associated with the murine Bernard-Soulier syndrome. Blood, 2002; 100: 2102-2107.

Kansas G. Selectins and their ligands: Current concepts and controversies. Blood, 1996; 88 (9): 3259-3287.

Kapustin AN, Chatrou MLL, Drozdov I, Zheng, Y, Davidson SM, Soong D, Furmanik M, Sanchis P, De Rosales RTM, Alvarez-Hernandez D, Shroff R, Yin X, Muller K, Skepper JN, Mayr M, Reutelingsperger CP, Chester A, Bertazzo S, Schurgers LJ, Shanahan CM. Vascular smooth muscle cell calcification is mediated by regulated exosome secretion. Circulation Research, 2015; 116 (8): 1312-1323.

Kelton JG, Warkentin TE, Hayward CPM, Murphy WG, Moore JC. Calpain activity in patients with thrombotic thrombocytopenic purpura is associated with platelet microparticles. Blood, 1992; 80 (90): 2246-2251.

Kerr MC, Teasdale RD. Defining Macropinocytosis. Traffic, 2009; 10 (4): 364-371.

Khodoun MV, Kucuk ZY, Strait RT, Krishnamurthy D, Janek K, Clay CD, Morris SC, Finkelman FD. Rapid desensitization of mice with anti-FcγRIIb/FcγRIII mAb safely prevents IgC-mediated anaphylaxis. Food, drug, insect sting allergy, and anaphylaxis, 2013; 132 (6): 1375-1387.

Kilicli Camur N, Demirtune R, Konuralp C, Eskiser A, Basaran Y. Could mean platelet volume be a predictive marker for acute myocardial infarction? Med Sci Monit, 2005; 11: 387–392.

Kim HK, Song KS, Chung JH, Lee KR, Lee SN. Platelet microparticles induce angiogenesis in vitro. British Journal of Haematology, 2004; 124 (3): 376-384.

Kiss AL, Botos E. Endocytosis via caveolae: alternative pathway with distinct cellular compartments to avoid lysosomal degradation? Journal of Cellular and Molecular Medicine, 2009; 13 (7): 1228-1237.

Koga H, Sugiyama S, Kugiyama K, Fukushima H, Watanabe K, Sakamoto T, Yoshimura M, Jinnouchi H, Ogawa H. Elevated levels of remnant lipoproteins are associated with plasma platelet microparticles in patients with type-2 diabetes mellitus without obstructive coronary artery disease. European Heart Journal, 2006; 27 (7): 817-823.

Koltsova EK, Sundd P, Zarpellon A, Ouyang H, Mikulski Z, Zampolli A, Ruggeri ZM, Ley K. Genetic deletion of platelet glycoprotein Ib alpha but not its extracellular domain protects from atherosclerosis. Thromb Haemost, 2014; 112(6): 1252-1263.

Koiou E, Tziomalos K, Katsikis I, Kalaitzakis E, Kandaraki EA, Tsourdi EA, Delkos D, Papadakis E, Panidis D. Circulating platelet-derived microparticles are elevated in women with polycystic ovary syndrome diagnosed with the 1990 criteria and correlate with serum testosterone levels. European journal of endocrinology, 2011; 165 (1): 63-8.

Kraiss LW, Geary RL, Mattsson EJR, Vergel S, Au YPT, Clowes AW. Acute reductions in blood flow and shear stress induce platelet-derived growth factor-A expression in baboon prosthetic grafts. Circ Res. 1996; 79:45–53.

Kuckleburg CJ, Yates CM, Kalia N, Zhao Y, Nash GB, Watson SP, Rainger GE. Endothelial cell-borne platelet bridges selectively recruit monocytes in human and mouse models of vascular inflammation. Cardiovascular Research, 2011; 91 (1): 134-141.

Kumari S, Swetha S, Mayor S. Endocytosis unplugged: multiple ways to enter the cell. Cell Res, 2010; 20: 256–275.

Lacroix R, Plawinski L, Robert S, Doeuvre L, Sabatier F, de Lizarrondo SM, Mezzapesa A, Anfosso F, Leroyer AS, Poullin P, Jourde N, Njock MS, Boulanger CM, Anglés-Cano E, Dignat-George F. Leukocyte-and endothelial-derived microparticles: A circulating source for fibrinolysis. Haematologica, 2012; 97 (12): 1864-1872.

Laffont B, Corduan A, Ple H, Duchez AC, Cloutier N, Boilard E, Provost P. Activated platelets can deliver mRNA regulatory Ago2-microRNA complexes to endothelial cells via microparticles. Blood, 2013; 122 (2): 253-61.

Laffont B, Corduan A, Rousseau M, Duchez A, Lee C, Boilard E, Provost P. Platelet microparticles reprogram macrophage gene expression and function. Thromb and Haemost, 2016; 115 (2): 311-323.

Lai C. P., Mardini O., Ericsson M., et al. Dynamic biodistribution of extracellular vesicles in vivo using a multimodal imaging reporter. *ACS Nano*, 2014; 8(1): 483–494.

Lalor P, Nash GB. Adhesion of flowing leucocytes to immobilized platelets. British Journal of Haematology, 1995; 89 (4): 725-32.

Lam CF, Peterson TE, Richardson DM, et al. Increased blood flow causes coordinated upregulation of arterial eNOS and biosynthesis of tetrahydrobiopterin. Am J Physiol Heart Circ Physiol 2006; 290: H786 –93.

Lanza F, Beretz A, Stierle A, Hanau D, Kubina M, Cazenave JP. Epinephrine potentiates human platelet activation but is not an aggregating agent. Am J Physiol., 1988; 255 (6Pt2): H1276-88.

Larsson NG. Somatic mitochondrial DNA mutations in mammalian aging. Annu Rev Biochem, 2010; 79: 683-706.

Lee HH, Elia N, Ghirlando R, Lippincott-Schwartz J, Hurley JH. Midbody targeting of the ESCRT machinery by a noncanonical coiled coil in CEP55. Science 2008; 322 (5901): 576-80.

Lee YJ, Jy W, Horstman LL, Janania J, Reyes Y, Kelley RE, Ahn YS. Elevated platelet microparticles in transient ischemic attacks, lacunar infarcts, and multiinfarct dementias. Thromb Res, 1993; 72 (4): 295-304.

Leeksma CH, Cohen JA. Determination of the life of human blood platelets using labelled diisopropylfluorophosphanate. Nature, 1955; 175 (4456): 552-3.

Lenassi M, Cagney G, Liao M, Vaupotic T, Bartholomeeusen K, Cheng Y, Krogan NJ, Plemenitas A, Peterlin BM. HIV Nef is secreted in exosomes and triggers apoptosis in bystander CD4+ T cells. Traffic, 2010; **11**: 110–122.

Leroyer AS, Rautou PE, Silvestre JS, Castier Y, Leseche G, Devue C, Duriez M, Brandes RP, Lutgens E, Tedgui A, Boulanger CM. CD40 ligand+ microparticles from human atherosclerotic plaques stimulate endothelial proliferation and angiogenesis a potential mechanism for intraplaque neovascularization. J. Am. Coll. Cardiol., 2008; 52: 1302-1311.

Levin J, Levin FC, Hull DF III, et al. The effects of thrombopoietin on megakaryocyte-CFC, megakaryocytes, and thrombopoiesis: with studies of ploidy and platelet size. Blood, 1982 (60): 989-998.

Ley K, Laudanna C, Cybulsky MI, Nourshargh S. Getting to the site of inflammation: the leukocyte adhesion cascade. Nature Reviews Immunology, 2007; 7 (9): 678

Li L, Masica D, Ishida M, Tomuleasa C, Umegaki S, Kalloo AN, Georgiades C, Singh VK, Khashab M, Amateau S, et al. Human bile contains MicroRNA-laden extracellular vesicles that can be used for cholangiocarcinoma diagnosis. Hepatology 2014; 60: 896–907.

Li YS, Haga JH, Chien S. Molecular basis of the effects of shear stress on vascular endothelial cells. J Biomech. 2005; 38:1949–1971.

Libby P, Ridker PM, Hansson GK. Progress and challenges in translating the biology of atherosclerosis. Nature, 2011; 473 (7347): 317.

Liu ML, Reilly MP, Casasanto P, McKenzie SE, Williams KJ. Cholesterol enrichment of human monocyte/macrophages induces surface exposure of phosphatidylserine and the release of biologically active tissue factor-positive microvesicles. Arterioscler. Thormb. Vasc. Biol., 2007; 27 (2): 430-435.

Logan A, Shabalina IG, Prime TA, Rogatti S, Kalinovich AV, Hartley RC, Budd RC, Cannon B, Murphy MP. *In vivo* levels of mitochondrial hydrogen peroxide increase with age in mtDNA mutator mice. Agin Cell, 2014; 12212.

Lood C, Tyden H, Gullstrand B, Nielsen CT, Heegaard NHH, Linge P, Jonsen A, Hesselstrand R, Kahn R, Bengtsson AA. Decreased platelet size is associated with platelet activation and anti-phospholipid syndrome in systemic lupus erythematosus. Rheumatology, 2017; 56 (3): 408-416.

Lukasik M, Rozalski M, Luzak B, Michalak, Ambrosius W, Watala C, Kozubski W. Enhanced platelet-derived micro- particle formation is associated with carotid atherosclerosis in convalescent stroke patients. Platelets, 2013; 24: 63e70.

Lusis AJ. Atherosclerosis. Nature, 2000; 407 (6801): 233.

Machlus KR, Thon JN, Italiano JE. Interpreting the developmental dance of the megakaryocyte: a review of the cellular and molecular processes mediating platelet formation. BJH, 2014; 165 (2): 12758.

Malek AM, Gibbons GH, Dzau VJ, Izumo S. Fluid shear stress differentially modulates expression of genes encoding basic fibroblast growth factor and platelet-derived growth factor B chain in vascular endothelium. J Clin Invest. 1993; 92: 2013–2021.

Mallat Z, Hugel B, Ohan J, Leseche G, Freyssinet JM, Tedgui A. Shed membrane microparticles with procoagulant potential in human atherosclerotic plaques: a role for apoptosis in plaque thrombogenicity. Circulation, 1999; 99 (3): 348-353.

Manno S, Takakuwa Y, Mohandas N. Identification of a functional role for lipid asymmetry in biological membranes: Phosphatidylserine-skeletal protein interactions modulate membrane stability. Proceedings of the National Academy of Sciences of the United States of America 2002; 99 (4): 1943-8.

Marathe JS, Kuriakose JG, Williams JK, Tabas JI. Sphingomyelinase, an Enzyme Implicated in Atherogenesis, Is Present in Atherosclerotic Lesions and Binds to Specific Components of the Subendothelial Extracellular Matrix. Arteriosclerosis, thrombosis, and vascular biology, 1999; 19 (11): 2648-2658.

Marcos-Ramiro B, Oliva Nacarino P, Serrano-Pertierra E, Blanco-Gelaz M, Weksler B, Romero I, Couraud P, Tunon A, Lopez-Larrea C, Millan J, Cernuda-Morollon E. Microparticles in multiple sclerosis and clinically isolated syndrome: effect on endothelial barrier function. BMCNeuroscience, 2014; 15: 110.

Marino G, Niso-Santano M, Baehrecke EH, Kroemer G. Self-consumption: the interplay of autophagy and apoptosis. Nature Reviews Molecular Cell Biology, 2014; 15: 81-94.

Martynova EV, Valiullina AH, Gusev OA, Davidyuk YN, Garanina EE, Shakirova VG, Khaertynova I, Anokhin VA, Rizvanov AA, Khaiboullina SF. High Triglycerides are associated with low thrombocyte counts and high VEGF in Nephropathia Epidemica. JIR, 2016; 2016: 8528270.

Maruyama K, Morishita E, Sekiya A, Omote M, Kadono T, Asakura H, Hashimoto M, Kobayashi M, Nakatsumi Y, Takada S, Ohtake Shigeki. Plasma levels of platelet-derived microparticles in patients with obstructive sleep apnea syndrome. Journal of atherosclerosisand thrombosis, 2012; 19 (1): 98-104.

Massberg S, Brand K, Gruner S, Page S, Muller I, Bergmeier W, Richter T, Lorenz M, Konrad I, Nieswandt B, Gawaz M. A Critical Role of Platelet Adhesion in the Initiation of Atherosclerotic Lesion Formation. JEM, 2002; 196 (7): 887-896.

Mathivanan S, Ji H, Simpson RJ. Exosomes: extracellular organelles important in intercellular communication. J Proteomics, 2010; **73**: 1907–1920.

Mause FS, von Hundelshausen RP, Zernecke RA, Koenen RR, Weber RC. Platelet Microparticles: A Transcellular Delivery System for RANTES Promoting Monocyte Recruitment on Endothelium. Arteriosclerosis, Thrombosis, and Vascular Biology, 2005; 25 (7): 1512-1518.

Maxfield FR, Tabas I. Role of cholesterol and lipid organization in disease. Nature, 2005; **438**: 612–621.

Maxfield FR, van Meer G, Cholesterol, the central lipid of mammalian cells, Curr. Opin. Cell Biol., 2010; 22 (4): 422–429.

McCartney AJ, Zolov SN, Kauffman EJ, Zhang Y, Strunk BS, Weisman LS, Sutton MA. Activity-dependent PI(3,5) synthesis controls AMPA receptor trafficking during synaptic depression. PNAS USA, 2014; 111 (45): E4896.

McEver RP, Cummings RD. Perspectives series: cell adhesion in vascular biology. Role of PSGL-1 binding to selectins in leukocyte recruitment. The journal of clinical investigation, 1997; 100 (3): 485-91.

McNally J, Davis M, Giddens D, Saha A. Role of xanthine oxidorecustase and NAD(P)H oxidase in endothelial superoxide production in response to oscillatory shear stress. American Journal of Physiology, 2003; 54 (6): 2290-2297.

McWilliams TG, Prescott AR, Allen GFG, Tamjar J, Munson MJ, Thomson C, Muqit MMK, Ganley IG. Mito-QC illuminates mitophagy and mitochondrial architecture in vivo. J Cell Bio, 2016; 214 (3): 333-345.

Merten M, Pakala R, Thiagarajan P, Benedict CR. Platelet Microparticles Promote Platelet Interaction With Subendothelial Matrix in a Glycoprotein IIb/IIIa-Dependent Mechanism. Circulation, 1999; 99: 2577-2582.

Michael JV, Wurtzel JGT, Fen Mao G, Koneti Rao A, Hoffman NE, Rajan S, Madesh M, Jana F, Nieman M, Rowley JW, Weyrich AS, Goldfinger LE. Platelet microparticles infiltrating solid tumors transfer miRNAs and modulate tumor angiogenesis and growth. In: AACR; Cancer Res 2016; 76 (14 Suppl): Abstract nr 2667.

Michelsen, AE, Noto AT, Brodin E, Mathiesen EB, Brosstad F, Hansen JB. Elevated levels of platelet microparticles in carotid atherosclerosis and during the postprandial state. Thromb Res, 2009; 123 (6): 881-6.

Michelson AD, Benoit SE, Kroll MH, et al. The activation-induced decrease in the platelet surface expression of the glycoprotein Ib-IX complex is reversible. Blood, 1994; 83 (12): 3562-73.

Milioli M, Ibanez-Vea M, Sidoli S, Palmisano G, Careri M, Larsen MR. Quantitative proteomics analysis of platelet-derived microparticles reveals distinct protein signatures when stimulated by different physiological agonists. *J. Proteomics, 2015;* 121: 56–66.

Mills DC, Smith JB. The influence on platelet aggregation of drugs that affect the accumulation of adenosine 3':5'-cyclic monophosphate in platelets. Biochem J. 1971; 121(2): 185–96.

Mills DCB, Robb IA, Roberts GCK. The release of nucleotides, 5-hydroxytryptamine and enzymes from human blood platelets during aggregation. J Physiol. 1968; 195: 715–729.

Miranda KC, Bond DT, Mckee M, Skog J, Păunescu TG, Da Silva N, Brown, D, Russo LM. Nucleic acids within urinary exosomes/microvesicles are potential biomarkers for renal disease. Kidney International 2010; 78 (2): 191-99.

Miyajima DD, Martin TR, Ravetch JV, Kinet JP, Galli SJ. Systemic anaphylaxis in the mouse can be mediated largely through IgG1 and Fc gammaRIII. Assessment of the cardiopulmonary changes, mast cell degranulation, and death associated with active or IgE- or IgG1-dependent passive anaphylaxis. J Clin Invest, 1997; 99 (5): 901-14.

Miyazaki Y, Nomura S, Miyake T, Kagawa H, Kitada C, Taniguchi H, Komiyama Y, Fujimura Y, Ikeda Y, Fukuhara S. High shear stress can initiate both platelet aggregation and shedding of procoagulant containing microparticles. Blood, 1996; 88 (9): 3456-64.

Moake JL, Cimo PL, Widmer K, Peterson DM, Gum JR: Effects of prostaglandins, derivatives of cyclic 3':5'-AMP, theophylline, cholinergic agents and colchicine on clot retraction in dilute platelet-rich plasma and gel-separated platelet test systems. Thromb Haemostas, 1977; 38: 420, 1977.

Montecalvo A, Larregina AT, Shufesky WJ, Stolz DB, Sullivan ML, Karlsson JM, et al. Mechanism of transfer of functional microRNAs between mouse dendritic cells via exosomes. Blood, 2012; 119: 756-66.

Montoro-Garcia S, Shantsila E, Hernandez-Romero D, Jover E, Valdes M, Marin F, Lip GY. Small-size platelet microparticles trigger platelet and monocyte functionality and modulate thrombogenesis via P-selectin.*Br. J. Haematol, 2014;* 166 (4): 571–580.

Moore KJ, Tabas I. Macrophages in the pathogenesis of atherosclerosis.Cell, 2011; **145**: 341–355.

Morrison A, McMillan L, Radwanski K, Blatchford O, Min K, Petrik J. Storage of apheresis platelet concentrates after manual replacement of >95% of plasma with PAS 5. Vox Sang. 2014; 107(3): 247–53.

Morton LF, Peachey AR, Barnes MJ. Platelet-reactive sites in collagens type I and type III. Evidence for separate adhesion and aggregatory sites, Biochem J, 1989; 258 (1): 157-63.

Mosig AS, Rennert K, Krause S, Kzhyshkowska J, Neunubel K, Heller R, Funke H. Different functions of monocyte subsets in familial hypercholesterolemia: Potential function of CD14+CD16+ monocytes in detoxification of oxidized LDL. The FASEB Journal, 2008; 23 (3): 866-74.

Mostefai HA, Agouni A, Carusio N, Mastronardi ML, Heymes C, Henrion D, et al. Phosphatidylinositol 3-kinase and xanthine oxidase regulate nitric oxide and reactive oxygen species productions by apoptotic lymphocyte microparticles in endothelial cells. J Immunol 2008; **180**: 5028–35.

Mueller H, Stadtmann A, van Aken H, Hirsch E, Wang D, Ley K, Zarbock A. Tyrosine kinase Btk regulates E-selectin-mediated integrin activation and neutrophil recruitment by controlling phospholipase C (PLC) gamma2 and PI3Kgamma pathways. Blood, 2010; 115 (15): 3118-27.

Mukherjee Ratnadeep, Barman PK, Thatoi PK, Tripathy R, Das BK, Ravindran B. Non-classical monocytes display inflammatory features: Validation in Sepsis and Systemic Lupus Erythematous. Scientific Reports, 2015; 13886.

Murugappan S, Shankar H, Kunapuli SP. Platelet receptors for adenine nucleotides and thromboxane A2. Semin Thromb Hemost, 2004; 30 (4): 411-8.

Nagasawa A, Matsuno K, Tamura S, Hayasaka K, Shimizu C, Moriyama T. The basis examination of leukocyte-platelet aggregates with CD45 gating as a platelet activation marker. International Journal of Laboratory Hematology, 2013; 35 (5): 534-541.

Nandi S, Ma L, Denis M, Karwatsky J, Li Z, Jiang XC, Zha X. ABCA1-mediated cholesterol efflux generates microparticles in addition to HDL through processes governed by membrane rigidity. J. Lipid Res., 2009; 50 (3): 456-466.

Na¨slund TI, Paquin-Proulx D, Paredes PT, Vallhov H, Sandberg JK, Gabrielsson S. Exosomes from breast milk inhibit HIV-1 infection of dendritic cells and subsequent viral transfer to CD4 T cells. AIDS. 2014; 28: 171-80.

Nieswandt B, Bergmeier W, Rackebrandt K, Gessner JE, Zimgibl H. Identification of critical antigen-specific mechanisms in the development of immune thrombocytopenic purpura in mice. Blood, 2000; 96 (7): 2520-7.

Nieuwland R, Berckmans RJ, McGregor S, Böing AN, Romijn FP, Westendorp RG, Hack CE, Sturk A. Cellular origin and procoagulant properties of microparticles in meningococcal sepsis. Blood 2000; **95**: 930–935.

Nieuwland R, Berckmans RJ, Rotteveel-Eijkman RC, Maquelin KN, Roozendaal KJ, Jansen PG, ten Have K, Eijsman L, Hack CE, Sturk A. Cell-derived microparticles generated in patients during cardiopulmonary bypass are highly procoagulant.Circulation 1997; **96**:3534–3541.

Nieuwland R, Sturk A. 2007. Platelet-Derived Microparticles. In: Michelson AD. ed. *Platelet.* Burlington: Elsevier, pp. 403-413.

Nieuwland R, van der Pol E, Gardiner C, Sturk A. Platelet-Derived Microparticles-Chapter 22. In: Platelets, 2013: 453-467.

Nikkari ST, O'Brien KD, Ferguson M, Hatsukami T, Welgus HG, Alpers CE, Clowes AW. Interstitial collagenase (MMP-1) expression in human carotid atherosclerosis. *Circulation,* 1995; **92**: 1393-98.

Niu C, Wang X, Zhao M, Cai T, Liu P, Li J, Willard B, Zu I, Zhou E, Li Y, Pan B, Yang F, Zheng L. Macrophage foam cell-derived extracellular vesicles promote vascular smooth muscle cell migration and adhesion. J. Am. Heart Assoc., 2016; 5 (10).

Nobis U, Pries AR, Cokelet GR, Gaehtgens P. Radial distribution of white cells during blood flow in small tubes. Microvasc Res, 1985; 29: 295-304.

Nofer JR, Kehrel B, Fobker M, Levkau B, Assmann G, von Eckardstein A. HDL and arteriosclerosis: Beyond reverse cholesterol transport. Atherosclerosis, 2002; 161: 1–16.

Nomura S, Kanazawa S, Fukuhara S. Effects of efonidipine on platelet and monocyte activation markers in hypertensive patients with and without type 2 diabetes mellitus. J Hum Hypertens, 2002; 16 (8): 539-47.

Nomura S, Shimizu M. Clinical significance of procoagulant microparticles. Journal of Intensive Care, 2015; 3 (1): 2.

Nording HM, Seizer P, Langer HF. Platelets in Inflammation and Atherogenesis. Frontiers in Immunology, 2015; 6: 98.

Nurden AT. Platelets, inflammation and tissue regeneration. Thrombosis and haemostasis, 2011; 105 (1): 13-33.

Nurden AT, Nurden P, Sanchez M, Andia I, Anitua E. Platelets and wound healing. Front Biosci, 2008; 13: 3532-48.

O'Brien KD, Allen MD, McDonald TO, Chait A, Harlan JM, Fishbein D, McCarty J, Ferguson M, Hudkins K, Benjamin CD, et al. Vascular cell adhesion molecule-1 is expressed in human coronary atherosclerotic plaques. Implications for the mode of progression of advanced coronary atherosclerosis. *J Clin Invest,* 1993; **92**: 945–951.

Oka T, Hikoso S, Yamaguchi O, Taneike M, Takeda T, Tamai T, Oyabu J, Murakawa T, Nakayama H, Nishida K, Akira S, Yamamoto A, Komuro I, Otsu K. Mitochondrial DNA that escapes from autophagy causes inflammation and heart failure. Nature, 2012; 485 (7397): 251-255.

Owens MR, Holme S, Cardinali S. Platelet microvesicles adhere to subendothelium and promote adhesion of platelets. Thromb Res, 1992; 66 (2-3): 247-58.

Palmer, RM, Ferrige, AG, Moncada, S. Nitric oxide release accounts for the biological activity of endothelium-derived relaxing factor. *Nature,* 1987; **327**: 524– 6.

Palumbo R, Gaetano C, Antonini A, Pompilio G. Different effects of high and low shear stress on platelet-derived growth factor isoform release by endothelial cells: Consequences for smooth muscle cell migration. Arteriosclerosis, Thrombosis and Vascular Biology, 2002; 22 (3): 405-11.

Pan BT, Teng K, Wu C, Adam M, Johnstone RM. Electron microscopic evidence for externalization of the transferrin receptor in vesicular form in sheep reticulocytes. J Cell Biol, 1985; **101**: 942–948.

Patel SS, Thiagarajan R, Willerson JT, Yeh ET. Inhibition of α_4 integrin and ICAM-1 markedly attenuate macrophage homing to atherosclerotic plaques in ApoE-deficient mice. *Circulation.*1998; **97**: 75–81.

Paul BZS, Jin J, Kunapuli SP. Molecular Mechanism of Thromboxane A2-induced Platelet Aggregation. The Journal of Biological Chemistry, 1999; 274 (41): 29108-29114.

Paulus JM. Platelet size in man. Blood, 1975; 46 (3): 321-36.

Parzy E, Miraux S, Jean-Michel Franconi, Thiaudiere E. In vivo quantification of blood velocity in mouse carotid and pulmonary arteries by ECG-triggered 3D time-resolved magnetic resonance angiography.. NMR in Biomedicine, 2009; 22 (5): 532-537.

Pedersen EM, Oyre S, Agerbaek M, et al. Distribution of early atherosclerotic lesions in the human abdominal aorta correlates with wall shear stresses measured in vivo. Eur J Vasc Endovasc Surg, 1999; 18: 328-333.

Pegtel DM, Cosmopoulos K, Thorley-Lawson DA, van Eijndhoven MA, Hopmans ES, Lindenberg JL, de Gruijl TD, Würdinger T, Middeldorp JM. Functional delivery of viral miRNAs via exosomes. Proc Natl Acad Sci USA, 2010; **107**:6328–6333.

Peng P, Yan Y, Keng S. Exosomes in the ascites of ovarian cancer patients: Origin and effects on anti-tumor immunity. Oncology Reports 2011; 25: 749-762.

Perez-Casal M, Thompson V, Downey C, Welters I, WyncollD, Thachill J, Toh c. The clinical and functional relevance of microparticles induced by activated prorein C treatment in sepsis. Critical Care, 2011; 15 (4): R195.

Perez-Pujol S, Marker PH, Key NS. Platelet microparticles are heterogeneous and highly dependent on the activation mechanism: Studies using a new digital flow cytometer. Cytometry Part A, 2007; 71A (1): 38-45.

Pfister LS. Role of Platelet Microparticles in the Production of Thromboxane by Rabbit Pulmonary Artery. Hypertension: Journal of the American Heart Association, 2004; 43 (2): 428-433.

Phillipson M, Heit B, Colarusso P, Liu L, Ballantyne CM, Kubes P. Intraluminal crawling of neutrophils to emigration sites: a molecularly distinct process from adhesion in the recruitment cascade. The Journal of Experimental Medicine, 2006; 203 (12): 2569-2575.

Piccin A, Murphy WG, Smith OP. Circulating microparticles: pathophysiology and clinical implications. Blood Rev, 2007; 21 (3): 157-71.

Pienimaeki-Roemer A, Konovalova T, Musri MM, Sigruener A, Boettche A, Meister G, Schmitz G. Transcriptomic profiling of platelet senescence and platelet extracellular vesicles. Transfusion, 2017; 57(1): 144-156.

Pitchford SC, Yano H, Lever R, Riffo-Vasquez Y, Ciferri S, Rose MJ, Giannini S, Moni S, Spina D, O'Connor B, Gresele P, Page CP. The Journal of Allergy and Clinical Immunology, 2003; 112 (1): 109-118.

Pittoni V, Valesini G. The clearance of apoptotic cells: implications for autoimmunity. Autoimmun. Rev., 2002; 1: 154-161.

Pizzirani C, Ferrari D, Chiozzi P, Adinolfi E, Sandonà D, Savaglio E, Di Virgilio F. Stimulation of P2 receptors causes release of IL-1beta-loaded microvesicles from human dendritic cells. Blood, 2007; **109**:3856–3864.

Podrez, EA, Febbraio M, Sheibani N, Schmitt D, Silverstein RL, Hajjar DP, Cohen PA, Frazier WA, Hoff HF, Hazen SL. Macrophage scavenger receptor CD36 is the major receptor for LDL modified by monocyte-generated reactive nitrogen species. JCI, 2000; 105 (8): 1095-108.

Poole AW, Watson SP. Regulation of cytosolic calcium by collagen in single human platelets. Br J Pharmacol, 1995; 115 (1): 101-6.

Poston RN, Haskard DO, Coucher JR, Gall NP, Johnson-Tidey RR. Expression of intercellular adhesion molecule-1 in atherosclerotic plaques. *Am J Pathol.* 1992; **140**: 665–673.

Preston RA, Jy w, Jimenez JJ, Mauro LM, Horstman LL, Valle M, Aime G, Ahn YS. Effects of severe hypertension on endothelial and platelet microparticles. Hypertension, 2003; 41 (2): 211-7.

Qiu Y, Tarbell JM. Interaction between wall shear stress and circumferential strain affects endothelial cell biochemical production. Journal of Vascular Research, 2000; 37 (3): 147-157.

Qu Y, Franchi L, Nunez G, Dubyak GR. Nonclassical IL-1 beta secretion stimulated by P2X7 receptors is dependent on inflammasome activation and correlated with exosome release in murine macrophages. J Immunol, 2007; **179**: 1913–1925.

Ramos CL, Huo Y, Jung U, Ghosh S, Manka DR, Sarembock IJ, Ley K. Direct demonstration of P-selectin– and VCAM-1–dependent mononuclear cell rolling in early atherosclerotic lesions of apolipoprotein E–deficient mice. *Circ Res.* 1999; **84**: 1237–1244.

Rand ML, Wang H, Bang KW, Packham MA, Freedman J. Rapid clearance of procoagulant platelet-derived microparticles from the circulation of rabbits. J Thromb. Haemost, 2006; 4: 1621-1623.

Raposo G, Nijman HW, Stoorvogel W, Liejendekker R, Harding CV, Melief CJ, Geuze HJ. B lymphocytes secrete antigen-presenting vesicles. J Exp Med 1996; **183**:1161–1172.

Rautou PE, Leroyer AS, Ramkhelawon B, Devue C, Duflaut D, Vion AC, Nalbone G, Castier Y, Leseche G, L ehoux S, Tedgui A, Boulanger CM. Microparticles from human atherosclerotic plaques promote endothelial ICAM-1-dependent monocyte adhesion and transendothelial migration. Circ Res 2011; **108**: 335–343.

Record M, Subra C, Silvente-Poirot S, Poirot M. Exosomes as intercellular signalosomes and pharmacological effectors. Biochem Pharmacol, 2011; **81**:1171–1182.

Reiss AB, Cronstein BN. Regulation of foam cells by adenosine, Arterioscler. Thromb. Vasc. Biol., 2012; 32 (4): 879–886.

Rejman J, Oberle V, Zuhorn I S, Hoekstra D. Size-dependent internalization of particles via the pathways of clathrin- and caveolae-mediated endocytosis. Biochem J, 2004; 377 (1): 159-169.

Riddell DR, Graham A, Owen JS. Apolipoprotein E inhibits platelet aggregation through the L-arginine: nitric oxide pathway. Implications for vascular disease. J Biol Chem, 1997; 272 (1): 89-95.

Ross R. Atherosclerosis- an inflammatory disease. The New England journal of medicine, 1999; 340 (2): 115-126.

Royo F, Diwan I, Tackett MR, Zuniga P, Sanchez-Mosquera P, Loizaga-Iriarte A, Ugalde-Olano A, Lacasa I, Perez A, Unda M, Carracedo A, Falcon-Perez JM. Comparative miRNA Analysis of Urine Extracellular Vesicles isolated through Five Different Methods. Cancers 2016; 8 (12); doi:10.3390/cancers8120112.

Rozmyslowicz LT, Majka OM, Kijowski NJ, Murphy ZS, Conover ZD, Poncz ZM, Ratajczak ZN, Gaulton ZG, Ratajczak ZM. Platelet- and megakaryocyte-derived microparticles transfer CXCR4 receptor to CXCR4-null cells and make them susceptible to infection by X4-HIV. AIDS, 2003; 17 (1): 33-42.

Sabatier F, Darmon P, Hugel B, Combes V, Sanmarco M, Velut J, Arnoux D, Charpiot P, Freyssinet J, Oliver C, Sampol J, Dignat-George F. Type 1 and type 2 diabetic patients display different patterns of cellular microparticles. Diabetes, 2002; 51 (9): 2840-2845.

Sakariassen KS, Fressinaud E, Girma JP, Baumgartner HR. Meyer D. Mediation of platelet adhesion to fibrillar collagen in flowing blood by a proteolytic fragment of human von Willebrand factor. Blood, 1986; 67 (5): 1515-8.

Sakhtianchi R, Minchin R F, Lee KB, Alkilany AM, Serpooshan V, Mahmoudi M. Exocytosis of nanoparticlesfrom cells: role in cellular retention and toxicity. Adv Colloid Interface Sci, 2013; 201 (201): 18-29.

Salzman EW, Kensler PC, Levine L. Cyclic 3',5'-adenosine monophosphate in human blood platelets. IV. Regulatory role of cyclic amp in platelet function. Ann N Y Acad Sci. 1972; 201: 61–71.

Sang M, Suzuki A, Stalker T, Zhao L, Wang Y, Mckennan C, Riese M, Guzman J, Zhang S, Lian L, Joshi R, Meng R, Seeholzer S, Choi J, Koretzky G, Marks M, Abrams C. Loss of PIKfyve in platelets causes a lysosomal disease leading to inflammation and thrombosis in mice. Nature Communications, 2014; 5: 4691.

Santoro SA, Walsh JJ, Staatz WD, Baranski KJ. Distinct determinants on collagen support alpha 2 beta 1 integrin-mediated platelet adhesion and platelet activation, 1991; 2 (11): 905-13.

Savage B, Saldivar E, Ruggeri ZM. Initiation of Platelet Adhesion by Arrest onto Fibrinogen or Translocation on von Willebrand Factor. Cell, 1996; 84: 289-297.

Savage B, Almus-Jacobs F, Ruggeri ZM. Specific Synergy of Multiple Substrate-Receptor Interactions in Platelet Thrombus Formation under Flow. Cell, 1998; 94 (5): 657-666.

Schmitz, G., Rothe, G., Ruf, A., et al. European working group on clinical cell analysis: consensus protocol for the flow cytometric characterisation of platelet function. Thrombosis and haemostasis, 1998; 79 (5): 885–96.

Schonbeck U, Mach F, Sukhova GK, Herman M, Graber P, Kehry MR, Libby P. CD40 Ligation induces Tissue Factor Expression in Human Vascular Smooth Muscle Cells. The American Journal of Pathology, 2000; 156 (1): 7-14.

Schonbeck U, Sukhova GK, Shimizu K, Mach F, Libby, P. Inhibition of CD40 signaling limitsevolution of established atherosclerosis in mice. *Proc. Natl Acad.Sci., 2000;* **97**: 7458–7463.

Schrijvers DM, De Meyer GRY, Herman AG, Martinet W. Phagocytosis in atherosclerosis: Molecular mechanisms and implications for plaque progression and stability. Cardiovascular Research, 2007; 73 (3): 470-480.

Schwartz GC, Olsson AG, Abt M, Ballantyne CM, Barter PJ, Brumm J, Chaitman BR, Holme IM, Kallend D, Leiter LA, Leitersdorf, E, Mcmurray JJV, Mundl H, Nicholls SJ, Shah PK, Tardif JC, Wright RS. The New England Journal of Medicine, 2012; 367 (22): 2089-2099

Seigneuret M, Zachowski, A, Hermann A, Devaux PF. Asymmetric lipid fluidity in human erythrocyte membrane: new spin-label evidence. Biochemistry 1984; 23 (19): 4271-5.

Semple JW, Lazarus AH, Freedman J. The cellular immunology associated with autoimmune thrombocytopenic purpura: an update. Transfus Sci., 1998; 19: 245-251.

Sewify EM, Sayed D, Abdel Aal RF, Heba M, Abdou MA. Increased circulating red cell microparticles (RMP) and platelet microparticles (PMP) in immune thrombocytopenic purpura. Thrombosis Research, 2013; 131 (2): 59-63.

Shai E, Rosa I, Parguina AF, Motahedeh S, Varon D, Garcia A. Comparative analysis of platelet-derived microparticles reveals differences in their amount and proteome depending on the platelet stimulus. Journal of Proteomics, 2012; 76: 287-296.

Shan Z, Qin S, Li W, Wu W, Yang J, Chu M, Li X, Huo X, Schaer GL, Wang S, Zhang C. An endocrine Genetic Signal Between blood cells and vascular smooth muscle cells: Role of MicroRNA-233 in Smooth Muscle Function and Atherogenesis. Am. Coll. Cardiol.,, 2015; 65 (23): 2526-2537.

Shantsila, E, Lip, GYH. The role of monocytes in thrombotic disorders. Insights from tissue factor, monocyte-platelet aggregates and novel mechanisms. Thrombosis and haemostasis, 2009; 102 (5): 916–24.

Shantsila E, Wrigley B, Tapp L, Apostolakis S, Montoro-Garcia S, Drayson MT, Lip GYH. Immunophenotypic characterization of human monocyte subsets: possible implications for cardiovascular disease pathophysiology. Journal of Thrombosis and Haemostasis, 2011; 9: 1056-1066.

Shyy YJ, Hsieh HJ, Usami S, Chien S. Fluid shear stress induces a biphasic response of human monocyte chemotactic protein 1 gene expression in vascular endothelium. Proc Natl Acad Sci USA. 1994; 91:4678–4682.

Shyy JY, Li YS, Lin MC, Chen W, Yuan S, Usami S, Chien S. Multiple cis-elements mediate shear stress-induced gene expression. J Biomech. 1995; 28:1451–1457.

Shyy JY, Lin MC, Han J, Lu Y, Petrime M, Chien S. The cis-acting phorbol ester "12-O-tetradecanoylphorbol 13-acetate"-responsive element is involved in shear stress-induced monocyte chemotactic protein 1 gene expression. Proc Natl Acad Sci USA. 1995; 92:8069–8073.

Simons M, Raposo G. Exosomes–vesicular carriers for intercellular communication. Curr Opin Cell Biol 2009; 21: 575–581.

Sims PJ, Faioni EM, Wiedmer T, Shattil SJ. Complement proteins C5b-9 cause release of membrane vesicles from the platelet surface that are enriched in the membrane receptor for coagulation factor Va and express prothrombinase activity. The Journal of biological chemistry, 1988; 263 (34): 18205-12.

Sims PJ, Wiedmer T, Esmon CT, Weiss HJ, Shattil SJ. Assembly of the platelet prothrombinase complex is linked to vesiculation of the platelet plasma membrane. Studies in Scott syndrome: an isolated defect in platelet procoagulant activity. J Biol Chem. 1989; 264: 17049–57.

Sinauridze EI, Kireev DA, Popenko NY, Pichugin AV, Panteleev MA, Krymskaya OV, Ataullakhanov FI. Platelet microparticle membranes have 50- to 100-fold higher specific procoagulant activity than activated platelets. Thrombosis and haemostasis, 2007; 97 (3): 425-34.

Stary HC, Chandler AB, Dinsmore RE, Fuster V, Glagov S, Insull J, Rosenfeld ME, Schwartz CJ, Wagner WD, Wissler RW. A Definition of Advanced Types of Atherosclerotic lesions and a histological classification of Atherosclerosis: A report from the committee on vascular lesions of the council on Arteriosclerosis, American Heart Association. Circulation, 1995; 92 (5): 1355-1374.

Street JM, Barran PE, Mackay CL, Weidt S, Balmforth C, Walsh TS, Chalmers RTA, Webb DJ, Dear JW. Journal of Translational Medicine 2012; 10:5. doi:10.1186/1479-5876-10-5.

Suades R, Padro T, Alonso R, Mata P, Badimon L. Lipid-lowering therapy with statins reduces microparticle shedding from endothelium, platelets and inflammatory cells. Thromb. Haemost., 2013; 110: 366-377.

Subra C, Laulagnier K, Perret B, Record M. Exosome lipidomics unravels lipid sorting at the level of multivesicular bodies. Biochimie 2007; 89 (2): 205-212.

Sun Cheng, Zhao WB, Chen Y, Hu HY. Higher Plasma Concentrations of Platelet Microparticles in Patients With Acute Coronary Syndrome: A Systematic Review and Meta-analysis. The Canadian journal of cardiology, 2016; 32 (11): 1325.

Suzuki H, Kurihara Y, Takeya M, Kamada N, Kataoka M, Jishage K, Ueda et al. A role for macrophage scavenger receptors in atherosclerosis and susceptibility to infection. Nature, 1997; 386: 292-296.

Suzuki-Inoue K, Fuller GLJ, García A, Eble JA, Pöhlmann S, Inoue O, Gartner TK, Hughan SC, Pearce AC, Laing GD, Theakston RDG, Schweighoffer E, Zitzmann N, Morita T, Tybulewicz VLJ, Ozaki Y, Watson SP. A novel Syk-dependent mechanism of platelet activation by the C-type lectin receptor CLEC-2. Blood, 2006; 107 (2): 542-549.

Swanson JA. Shaping cups into phagosomes and macropinosomes. Nat Rev Mol Cell Biol., 2008; 9: 639–649.

Tak T, Tesselaar K, Pillay J, Borghans JA, Koenderman L. "What's your age again? Determination of human meutrophil half-lives revisited". Journal of Leukocyte Biology, 2013; 94 (4): 595-601.

Takahashi Y., Nishikawa M., Shinotsuka H., et al. Visualization and in vivo tracking of the exosomes of murine melanoma B16-BL6 cells in mice after intravenous injection. *Journal of Biotechnology*. 2013; 165 (2): 77–84.

Tamagawa-Mineoka R, Katoh N, Kishimoto S. Platelet activation in patients with psoriasis: Increased plasma levels of platelet-derived microparticles and soluble P-selectin. Journalof the American Academy of Dermatology, 2010; 62 (4): 621-626.

Tan KT, Tayebjee MH, Lim HS, Lip GYH. Clinically apparent atherosclerotic disease in diabetes is associated with an increase in platelet microparticle levels. Diabetic Medicine, 2005; 22 (12): 1657-1662.

Tangelder GJ, Slaaf DW, Teirlinck HC, Alewijnse R, Reneman RS. Localization within a thin optical section of fluorescent blood platelets flowing in a microvessel. Microvasc Res. 1982; 23: 214-230.

Taraboletti G, D'Ascenzo S, Borsotti P, Giavazzi R, Pavan A, Dolo V. Shedding of the matrix metalloproteinases MMP-2, MMP-9, and MT1-MMP as membrane vesicle-associated components by endothelial cells. Am. J. Pathol., 2002; 160: 673-680.

Tekelioglu Y, Uzun H, Hasan Gucer. Circulating platelet-leukocyte aggregates in patients with inflammatory bowel disease. Journal of the Chinese Medical Association, 2013; 76 (4): 182-185.

Tesselaar ME, Romijn FP, Van Der Linden IK, Prins FA, Bertina RM, Osanto S. Microparticle-associated tissue factor activity: a link between cancer and thrombosis? J Thromb Haemost, 2007; **5**: 520–527.

Théry C, Boussac M, Véron P, Ricciardi-Castagnoli P, Raposo G, Garin J, Amigorena S. Proteomic analysis of dendritic cell-derived exosomes: a secreted subcellular compartment distinct from apoptotic vesicles. J Immunol, 2001; **166**:7309–7318.

Théry C, Duban L, Segura E, Véron P, Lantz O, Amigorena S. Indirect activation of naive CD4+ T cells by dendritic cell-derived exosomes. Nat Immunol, 2002; **3**:1156–1162.

Théry C, Ostrowski M, Segura E. Membrane vesicles as conveyors of immune responses. Nat Rev Immunol 2009; **9**: 581–593.

Thiagarajan P, Tait JF. Collagen-induced exposure of anionic phospholipid in platelets and platelet-derived microparticles. The Journal of biological chemistry, 1991; 266 (36): 24302-7.

Thomas LM, Salter RD. Activation of macrophages by P2X7-induced microvesicles from myeloid cells is mediated by phospholipids and is partially dependent on TLR4. J Immunol, 2010; **185**: 3740–3749.

Thushara RM, Hemshekhar M, Kemparaju K, Rangappa KS, Devraja S, Girish KS. Therapeutic drug-induced platelet apoptosis: an overlooked issue in pharmacotoxicology. Archives of Toxicology, 2014; 88 (2): 185-198.

Tian T, Wang Y, Wang H, Zhu Z, Xiao Z. Visualizing of the cellular uptake and intracellular trafficking of exosomes by live-cell microscopy. J Cell Biochem. 2010; 111: 488-96.

Tian T, Zhu YL, Hu FH, Wang YY, Huang NP, Xiao ZD. Dynamics of exosome internalization and trafficking. Journal of Cellular Physiology, 2013; 228 (7): 1487-95.

Tontonoz P, Nagy L, Alvarez JGA, Thomazy VA, Evans RM. PPARγ Promotes Monocyte/Macrophage Differentiation and Uptake of Oxidized LDL. Cell, 1998; 93 (2): 241-252.

Trajkovic K, Hsu C, Chiantia S, Rajendran L, Wenzel D, Wieland F, Schwille P, Brügger B, Simons M. Ceramide triggers budding of exosome vesicles into multivesicular endosomes. Science 2008; **319**: 1244–1247.

Trams EG, Lauter CJ, Norman SJ, Heine U. Exfoliation of membrane ecto-enzymes in the form of micro-vesicles. BBA-Biomembranes, 1981; 645 (1): 63-70.

Traub O, Berk BC. Laminar shear stress: mechanisms by which endothelial cells transduce an atheroprotective force. Arterioscler Thromb Vasc Biol. 1998; 18:677–685.

Trifunovic A, Wredenberg A, Falkenberg M, Spelbrink JN, Rovio AT, Bruder CE, Bohlooly-Y M, Gldlöf S, Oldfors A, Wibom, R., Törnell J, Jacobs HT, Larsson NG. Premature ageing in mice expressing defective mitochondrial DNA polymerase. Nature, 2004; 429 (6990): 417-423.

Tsiantoulas D, Perkmann T, Afonyushkin T, Mangold A, Prohaska TA, Papac-Milicevic N, Millischer V, Bartel C, Hörkkö S, Boulanger CM, Tsimikas S, Fischer MB, Witztum JL, Lang IM, Binder CJ. Circulating microparticles carry oxidation-specific epitopes and are recognized by natural IgM antibodies. J Lipid Res., 2015; 56 (2): 440-8.

Tull SP, Anderson SI, Hughan SC, Watson SP, Nash GB, Rainger GE. Cellular pathology of atherosclerosis: smooth muscle cells promote adhesion of platelets to cocultured endothelial cells. *Circ Res*, 2006; 98: 98-104.

Turiák L, Misják P, Szabó TG, Aradi B, Pálóczi K, Ozohanics O, Drahos L, Kittel A, Falus A, Buzás EI, Vekey K.Proteomic characterization of thymocyte-derived microvesicles and apoptotic bodies in BALB/c mice. J Proteomics, 2011; **74**: 2025–2033.

Turrens JF. Mitochondrial formation of reactive oxygen species. Journal of physiology, 2003; 552: 335-344.

Upchurch, GR, Ford, JW, Weiss, SJ *et al.* Nitric oxide inhibition increases matrix metalloproteinase-9 expression by rat aortic smooth muscle cells in vitro. *J Vasc Surg* 2001; **34**: 76– 83.

Valadi H, Ekstrom K, Bossios A, Sjostrand M, Lee JJ, Lotvall JO. Exosome-mediated transfer of mRNAs and microRNAs is a novel mechanism of genetic exchange between cells. Nat. Cell Biol 2007; 9:654–59.

van der Pol E, Boing AN, Harrison P, Sturk A, Nieuwland R, Mattson MP. Classification, Functions, and Clinical Relevance of Extracellular Vesicles. Pharmacological Reviews 2012; 64 (3): 676-705.

van der Pol E, Coumans FAW, Grootemaat AE, Gardiner C, Sargent IL, Harrison P, Sturk A, van Leeuwen TG, Nieuwland R. Particle size distribution of exosomes and microvesicles determined by transmission electron microscopy, flow cytometry, nanoparticle tracking analysis, and resistive pulsing. Journal of Thrombosis and Haemostasis, 2014; 12 (7): 1182-1192.

van der Zee PM, BiroE, Ko Y, de Winter RJ, Hack CE, Sturk A, Nieuwland R. P-selectin- and CD63-exposing platelet microparticles reflect platelet activation in peripheral arterial disease and myocardial infarction. Clin Chem, 2006; 52 (4): 657-64.

Vanhaverbeke M, Gal D, Holvoet P. Advances in Experimental Medicine and Biology, 2017; 998: 45-58.

van Helvoort A, Smith AJ, Sprong H, Fritzsche I, Schinkel AH, Borst P, van Meer G. MDR1 P-glycoprotein is a lipid translocase of broad specificity, while MDR3 P-glycoprotein specifically translocates phosphatidylcholine Cell 1996; 87: pp. 507-517.

Vanwijk MJ, Svedas E, Boer K, Nieuwland R, Vanbavel E, Kublickiene KR. Isolated microparticles, but not whole plasma, from women with preeclampsia impair endothelium-dependent relaxation in isolated myometrial arteries from healthy pregnant women. Am J Obstet Gynecol 2002; **187**:1686–1693.

Vanwijk MJ, VanBavel E, Sturk A, Nieuwland R. Microparticles in cardiovascular diseases. Cardiovasc Res, 2003; 59 (2): 277-87.

Virmani R, Kolodgie F, Burke A, Farb A, Schwartz S. Lessons from sudden coronary death: A comprehensive morphological classification scheme for atherosclerotic lesions. Arteriosclerosis, Thrombosis and Vascular Biology, 2000; 20 (5): 1262-75.

Vojtech L, Woo S, Hughes S, Levy C, Ballweber L, Sauteraud RP, Strobl J, Westerberg K, Gottardo R, Tewari M, Hladik F. Exosomes in human semen carry a distinctive repertoire of small non-coding RNAs with potential regulatory functions. Nucleic Acids Research 2014; 42 (11): 7290–7304.

Wang, W, Viappiani, S, Sawicka, J *et al.* Inhibition of endogenous nitric oxide in the heart enhances matrix metalloproteinase-2 release. *Br J Pharmacol* 2005; **145**: 43– 9.

Wagner DD, Burger PC. Platelets in inflammation and thrombosis. Arterioscler Thromb Vasc Biol, 2003; 23 (12): 2131-7.

Wang H, Wang ZH, Kong J, Yang MY, Jiang GH, Wang XP, Zhong M, Zhang Y, Deng JT, Zhang W. Oxidized Low-Density Lipoprotein-Dependent Platelet-Derived Microvesicles Trigger Procoagulant Effects and Amplify Oxidative Stress. Mol Med, 2012; 18 (1): 159-166.

Wang N, Tall AR. Cholesterol in platelet biogenesis and activation. Blood, 2016; 127 (16): 1949-1953.

Wang JG, Williams JC, Davis BK, Jacobson K, Doerschuk CM, Ting JP, Mackman N. Monocytic microparticles activate endothelial cells in an IL-1beta-dependent manner. Blood 2011; **118**: 2366–2374.

Wang W, Hein TW, Zhang C, Zawieja DC, Liao JC, Kuo L. Oxidised low-density lipoprotein inhibits nitric oxide-mediated coronary arteriolar dilation by up-regulating endothelial arginase I. Microcirculation, 2011; 18 (1): 36-45.

Wang Z, Shi Q, Yan R, Liu G, Zhang W, Dai K. The role of calpain in the regulation of ADAM17-dependent GPIbalpha ectodomain shedding. Arch Biochem Biophys., 2010; 495: 136–143.

Wang Z, Tiruppathi C, Minshall RD, Malik AB. Size and dynamics of caveolae studied using nanoparticles in living endothelial cells. ACS Nano, 2009; 3: 4110–4116.

Ware J, Russell S, Ruggeri ZM. Generation and Rescue of a Murine Model of Platelet Dysfunction: The Bernard-Soulier Syndrome. PNAS, 2000; 97 (6): 2803-2808.

Wasylewski Z, Stryjewski W, Wasniowska A, Potempa J, Baran K. Effect of calcium binding on conformational changes of staphylococcal metalloproteinase measured by means of intrinsic protein fluorescence. Biochim Biophys Acta, 1986; 871: 177–181.

Watson AD, Leitinger N, Navab M, Faull KF, Hörkkö S, Witztum JL, Palinski W, Schwenke D, Salomon RG, Sha W, Subbanagounder G, Fogelman AM, Berliner JA. Structural identification by mass spectrometry of oxidizedphospholipids in minimally oxidized low density lipoprotein that induce monocyte/endothelialinteractions and evidence for their presence in vivo. *J.Biol. Chem., 1997;* 272: 13597–13607.

Watson KE, Bostrom K, Ravindranath R, Lam T, Norton B,Demer LL. TGF-β1 and 25-hydroxycholesterol stimulate osteoblast-likevascular cells to calcify. *J. Clin. Invest., 1994* **93**: 2106–2113.

Weber J, Clayton A. How pure are your vesicles? Journal of Extracellular Vesicles, 2013; 2: 19861.

Weiss R, Groger M, Raucher S, Fendl B, Eichhorn T, Fischer MB, Spittler A, Weber V. Differential Interaction of Platelet-Derived Extracellular Vesicles with Leukocyte Subsets in Human Whole Blood. Scientific Reports, 2018; 8 (1): 6598.

Wiedmer T, Hall SE, Ortel TL, Kane WH, Rosse WF, Sims PJ. Complement-induced vesiculation and exposure of membrane prothrombinase sites in platelets of paroxysmal nocturnal hemoglobinuria. Blood, 1993; 82 (4): 1192-6.

Wiklander OP, Nordin JZ, O'Loughlin A, et al. Extracellular vesicle in vivo biodistribution is determined by cell source, route of administration and targeting. J Extracell Vesicles, 2015; 4: 26316.

Wilcox JN, Smith KM, Williams LT, Schwartz SM, Gordon D. Platelet-derived growth factor mRNA detection in human atherosclerotic plaques by in situ hybridization. J Clin Invest. 1988; 82:1134–1143.

Willis GR, Connolly K, Ladell K, Davies TS, Guschina IA,Ramji D, Miners K, Price DA, Clayton A, James PE, Rees DA. Young women with polycystic ovary syndrome have raised levels of circulating annexin V-positive platelet microparticles. Human Reproduction, 2014; 29 (12): 2756-2763.

Wolf P. The nature and significance of platelet products in human plasma. Br J Haematol, 1967; **13**:269–288.

Woollard KJ, Geissmann F. Monocytes in atherosclerosis: subsets and functions. Nature Reviews Cardiology, 2010; 7: 77-86.

Wrigley BJ, Shantsila E, Tapp LD, Lip GY. Increased formation of monocyte-platelet aggregates in ischemic heart failure. Circ Heart Fail, 2013; 6 (1): 127-35.

Wubbolts R, Leckie RS, Veenhuizen PT, Schwarzmann G, Möbius W, Hoernschemeyer J, Slot JW, Geuze H J, Stoorvogel W. Proteomic and biochemical analyses of human B cell-derived exosomes. Potential implications for their function and multivesicular body formation. J Biol Chem 2003; **278**: 10963–10972.

Xiao, Z, Théroux, P. Clopidogrel inhibits platelet-leukocyte interactions and thrombin receptor agonist peptide-induced platelet activation in patients with an acute coronary syndrome. Journal of the American College of Cardiology, 2004; 43 (11): 1982–8.

Xiao H, Wong DT. Proteomic analysis of microvesicles in human saliva by gel electrophoresis with liquid chromatography-mass spectrometry. Analytica Chimica Acta 2012; 723:61-7.

Xu Y, Wang L, Buttice G, Sengupta PK, Smith BD. Interferon gamma repression of collagen (COL1A2) transcription is mediated by the RFX5 complex. J Biol Chem, 2003; 278 (49): 49134-44..

Yacobi N R, DeMaio L, Xie J, Hamm-Alvarez S F, Borok Z, Kim KJ, Crandall ED. Polystyrene nanoparticle trafficking across alveolar epithelium. Nanomedicine; 2008; 4: 139–145.

Yago Tadayuki, Fu Jianxin, Mcdaniel JM, Miner JJ, Mcever RP, Xia L. PNAS USA, 2010; 107 (20): 9204-9.

Yilmaz H, Ertugrul O, Ertugrul B, Ertugrul D. Mean platelet volume in patients with subclinical hypothyroidism. Platelets, 2011; 22 (2): 143-147.

Yin M, Loyer X, Boulanger CM. Extracellular vesicles as new pharmacological targets to treat atherosclerosis. Eur. J. Pharmacol., 2015; 763 (Pt A): 90-103.

Yip C, Ignjatovic V, Attard C, Monagle P, Linden MD. First report of elevated monocyte-platelet aggregates in healthy children. PLOS One, 2013; 8 (6): e67416.

Yuana Y, Oosterkamp TH, Bahatyrova S, Ashcroft B, Garcia Rodriguez P, Bertina RM, Osanto S. Atomic force microscopy: a novel approach to the detection of nanosized blood microparticles. Journal of thrombosis and haemostasis. 2010; 8 (2): 315-23.

Yu E, Calvert PA, Mercer JR, Harrison J, Baker L, Figg NL, Kumar S, Wang JC, Hurst LA, Obaid DR, Logan A, West NEJ, Clarke MCH, Vidal-Puig A, Murphy MP, Bennett MR. Mitochondrial DNA damage can promote atherosclerosis independently of reactive oxygen species through effects on smooth muscle cells and monocytes and correlates with higher-risk plaques in humans. Circulation, 2013; 128 (7): 702-712.

Yu EPK, Bennett MR. Mitochondrial DNA damage and atherosclerosis. Trends in Endocrinology & Metabolism, 2014;25 (9): 481-487.

Zakharova L, Svetlova M, Fomina AF. T cell exosomes induce cholesterol accumulation in human monocytes via phosphatidylserine receptor. J. Cell. Physiol., 2007; 212 (1): 174-181.

Zhang Q, Raoof M, Chen Y, Sumi Y, Sursal T, Junger W, Brohi K, Itagaki K, Hauser CJ. Circulating mitochondrial DAMPs cause inflammatory responses to injury. Nature, 2010; 464 (7285): 104-107.

Zhao C, Zhang H, Wong WC, Sem X, Han H, Ong SM, Tan YC, Yeap WH, Gan CS, Ng KQ, Koh MBC, Kourilsky P, Sze SK, Wong SC. Journal of proteome research, 2009; 8 (8): 4028-38.

Zhao Y, Li Y, Luo P, Gao Y, Yang J, Lao KH, Wang G, Cockerill G, Hu Y, Xu Q, Li T, Zeng L. XBP1 splicing triggers miR-150 transfer from smooth muscle cells to endothelial cells via extracellular vesicles. Sci Rep, 2016; 6: 28627.

Ziegler T, Bouzourene K, Harrison VJ, Brunner HR, Hayoz D. Influence of oscillatory and unidirectional flow environments on the expression of endothelin and nitric oxide synthase in cultured endothelial cells. Arterioscler Thromb Vasc Biol, 1998; 18 (5): 686-92.

Zucker MB, Borrelli J. Platelet clumping produced by connective tissue suspensions and by collagen. Proc Soc Exp Biol Med. 1962;109:779–787.

Zwaal RFA, Schroit AJ. Pathophysiologic Implications of Membrane Phospholipid Asymmetry in Blood Cells. Blood, 1997; 89: 1121-1132.

12. SUPPLEMENTARY MATERIAL

	% GPIbα Expression											
	CD16-ve Monocytes			CD16+ve Monocytes			Neutrophils			Lymphocytes		
Time (min)	Whole population	PEV gate	Plt gate	Whole population	PEV gate	Plt gate	Whole population	PEV gate	Plt gate	Whole population	PEV gate	Plt gate
0	0.8 ± 0.3	0.7 ± 0.4	0.1 ± 0.1	7.8 ± 4.7	2.9 ± 1.2	1.4 ± 1.0	1.0 ± 0.2	1.0 ± 0.3	0.1 ± 0.0	1.3 ± 0.4	1.0 ± 0.4	0.3 ± 0.2
10	29.2 ± 8.6	28.4 ± 8.2	0.8 ± 0.4	37.6 ± 4.2	22.5 ± 3.4	15.0 ± 4.1	13.8 ± 6.8	13.2 ± 6.3	0.9 ± 0.8	3.2 ± 1.0	2.6 ± 0.8	0.6 ± 0.3
15	29.8 ± 7.5	28.2 ± 6.2	1.6 ± 1.4	37.2 ± 5.6	22.5 ± 1.3	16.5 ± 5.8	16.5 ± 1.1	16.0 ± 1.0	0.5 ± 0.3	2.7 ± 0.5	2.4 ± 0.6	0.3 ± 0.1
20	52.8 ± 18.4	49.4 ± 16.7	3.5 ± 1.7	46.4 ± 10.5	40.3 ± 8.5	6.1 ± 2.1	35.1 ± 9.4	33.3 ± 8.7	1.1 ± 1.1	7.9 ± 3.5	7.5 ± 3.2	0.5 ± 0.3
25	42.8 ± 13.5	39.6 ± 12.2	3.2 ± 1.8	40.6 ± 10.9	36.0 ± 8.8	4.6 ± 2.3	24.0 ± 7.3	22.0 ± 5.4	2.1 ± 2.0	6.2 ± 3.5	5.6 ± 3.1	0.6 ± 0.5
30	47.7 ± 3.6	43.6 ± 5.0	3.2 ± 0.4	38.9 ± 2.9	34.2 ± 4.6	9.1 ± 1.8	27.3 ± 3.9	23.8 ± 4.4	2.1 ± 1.0	3.0 ± 1.3	3.6 ± 1.7	0.4 ± 0.3
30 (ctrl)	8.8 ± 3.3	5.1 ± 1.3	0.6 ± 0.5	13.3 ± 3.5	9.3 ± 3.1	2.9 ± 1.4	2.6 ± 0.9	3.1 ± 1.0	0.1 ± 0.0	1.6 ± 0.2	1.4 ± 0.2	0.9 ± 0.3

Table 12.1. Formation of aggregates between leukocytes and platelets and/or PEV in whole blood over time in response to 100μM TRAP

Percentage of GPIbα+ve leukocytes as a whole, in the PEV gate and in the platelet gate. Data are represented as Mean +/- SEM.

	GPIbα Fluorescence Intensity												
	CD16-ve Monocytes			CD16+ve Monocytes			Neutrophils			Lymphocytes			Plts
Time (min)	Whole population	PEV gate	Plt gate	Whole population	PEV gate	Plt gate	Whole population	PEV gate	Plt gate	Whole population	PEV gate	Plt gate	
0	2.8 ± 0.9	48.2 ± 10.6	269.0 ± 182.1	2.9 ± 1.0	48.9 ± 6.0	542.3 ± 258.9	5.1 ± 0.5	54.0 ± 11.6	1602 ± 365.5	1.6 ± 0.5	76.9 ± 13.11	1039± 380.1	493.4 ± 189.2
10	13.2 ± 6.4	49.0 ± 3.1	648.7 ± 584.4	15.2 ± 2.5	45.5 ± 7.7	4387 ± 422.0	8.1 ± 1.5	40.1 ± 5.9	2437 ± 839.0	2.3 ± 1.1	33.3 ± 6.9	1832± 181.3	
15	10.7 ± 6.8	61.4 ± 20.2	578.3 ± 289.4	14.2 ± 3.4	65.6 ± 17.9	4346 ± 571.7	8.0 ± 0.7	60.3 ± 19.2	3756 ± 1160	1.8 ± 0.4	49.8 ± 18.8	1832 ± 63.8	
20	41.5 ± 21.7	66.7 ± 17.2	539.7 ± 287.6	35.1 ± 12.9	63.2 ± 16.2	2761 ± 820.0	15.1 ± 3.7	63.2 ± 16.3	2373 ± 767.8	3.6 ± 1.8	48.6 ± 13.5	1280 ± 326.9	
25	25.4 ± 12.2	60.8 ± 11.1	571.7 ± 323.5	27.6 ± 10.7	60.5 ± 6.9	2644 ± 1301	10.2 ± 2.3	52.1 ± 10.5	3366 ± 1131	3.0 ± 1.5	42.1 ± 9.9	1311 ± 423.5	
30	28.8 ± 4.2	68.7 ± 16.5	484.3 ± 142.7	17.5 ± 3.1	86.8 ± 11.6	1839 ± 628.6	10.9 ± 0.8	59.9 ± 4.1	2704 ± 510.7	2.6 ± 0.6	49.7 ± 5.0	1417 ± 320.9	
30 (ctrl)	7.4 ± 2.7	65.9 ± 13.6	693.0 ± 261.8	6.8 ± 1.4	132.8 ± 47.4	1216 ± 755.3	5.9 ± 0.5	60.1 ± 14.2	1576 ± 198.2	1.7 ± 0.4	50.6 ± 8.4	1134 ± 447.6	

Table 12.2. Formation of aggregates between leukocytes and platelets and/or PEV in whole blood over time in response to 100μM TRAP

Median GPIbα expression on leukocytes as a whole, in the PEV gate and in the platelet gate. Data are represented as Mean +/- SEM.

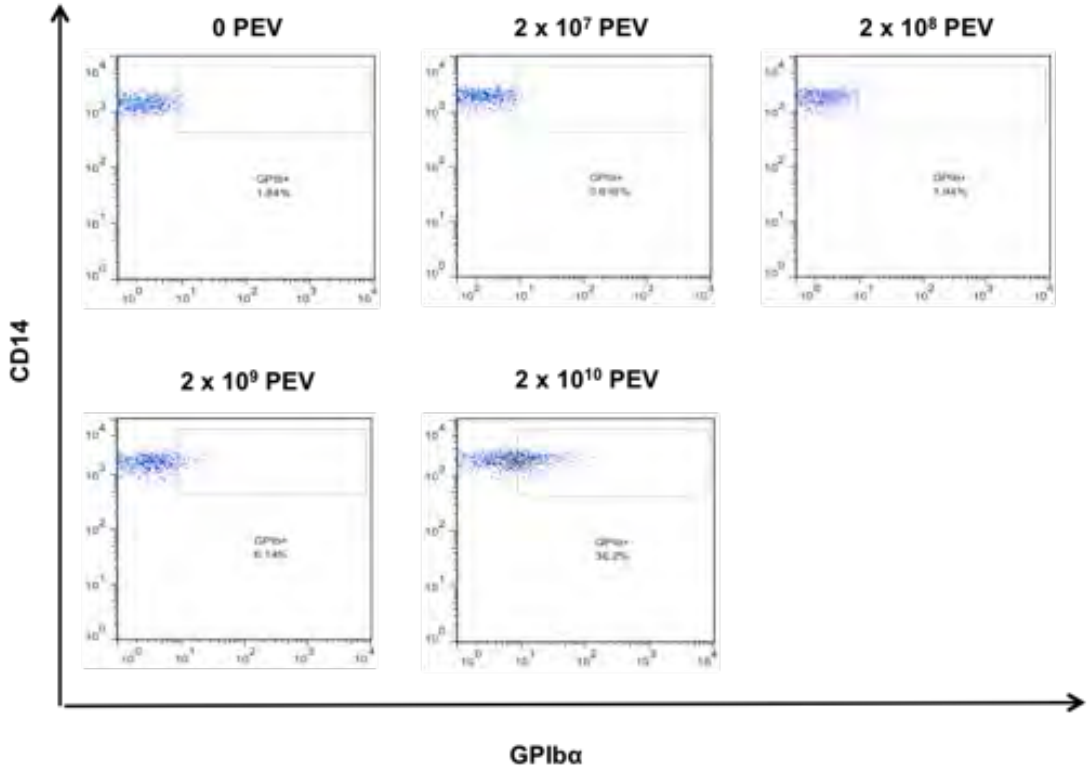

Figure 12.1. Formation of aggregates between CD16-ve Monocytes in blood and exogenously provided PEV over a PEV concentration gradient

Representative FACS dotplots demonstrating percentage of CD16-ve monocytes positive for GPIbα over PEV concentration gradient. Gate of positive events was set by isotype sample (not shown).

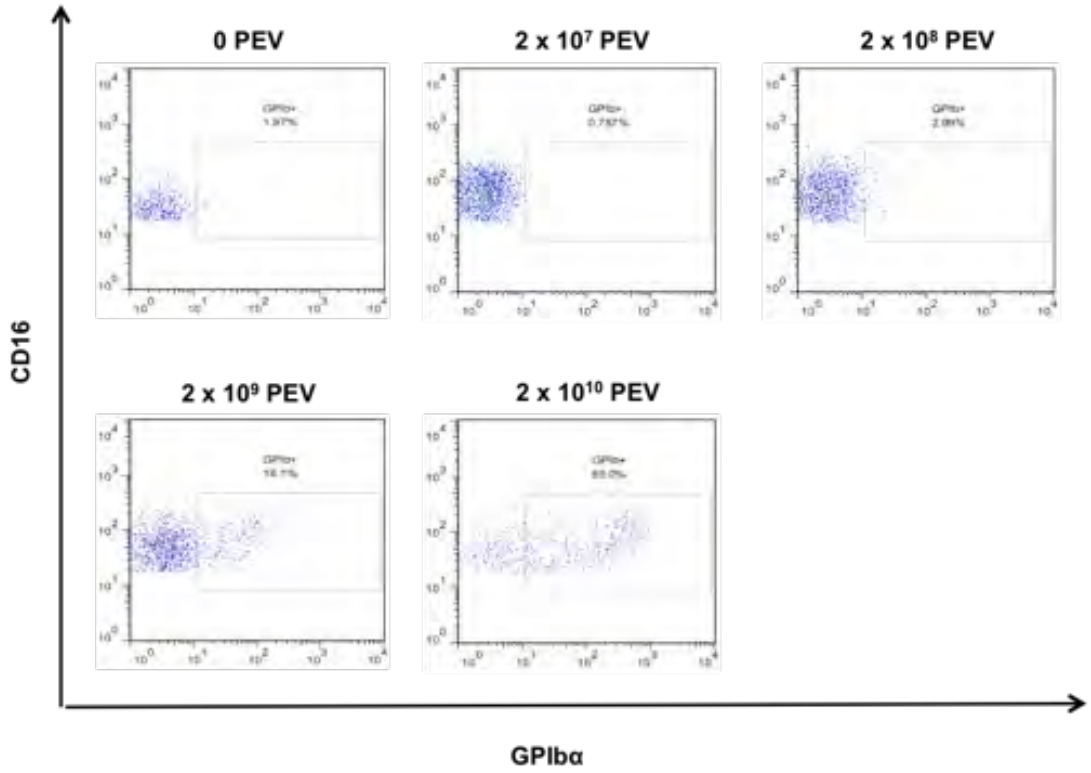

Figure 12.2. Formation of aggregates between CD16+ve Monocytes in blood and exogenously provided PEV over a PEV concentration gradient

Representative FACS dotplots demonstrating percentage of CD16+ve monocytes positive for GPIbα over PEV concentration gradient. Gate of positive events was set by isotype sample (not shown).

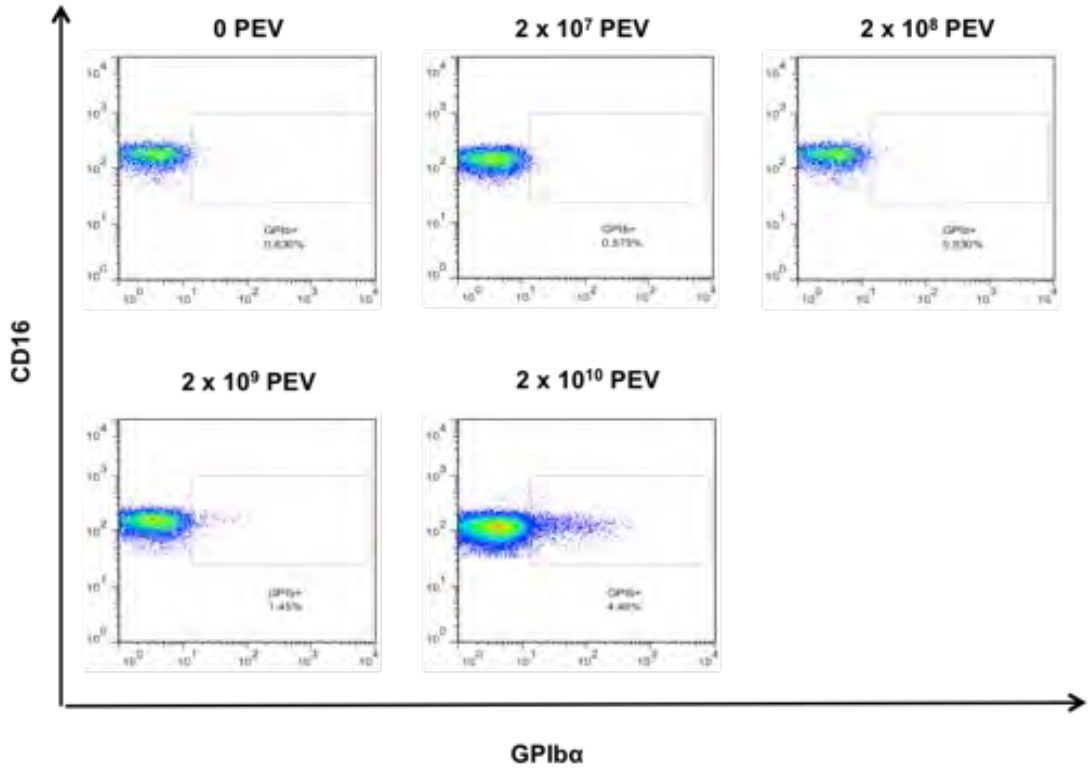

Figure 12.3. Formation of aggregates between Neutrophils in blood and exogenously provided PEV over a PEV concentration gradient

Representative FACS dotplots demonstrating percentage of Neutrophils positive for GPIbα over PEV concentration gradient. Gate of positive events was set by isotype sample (not shown).

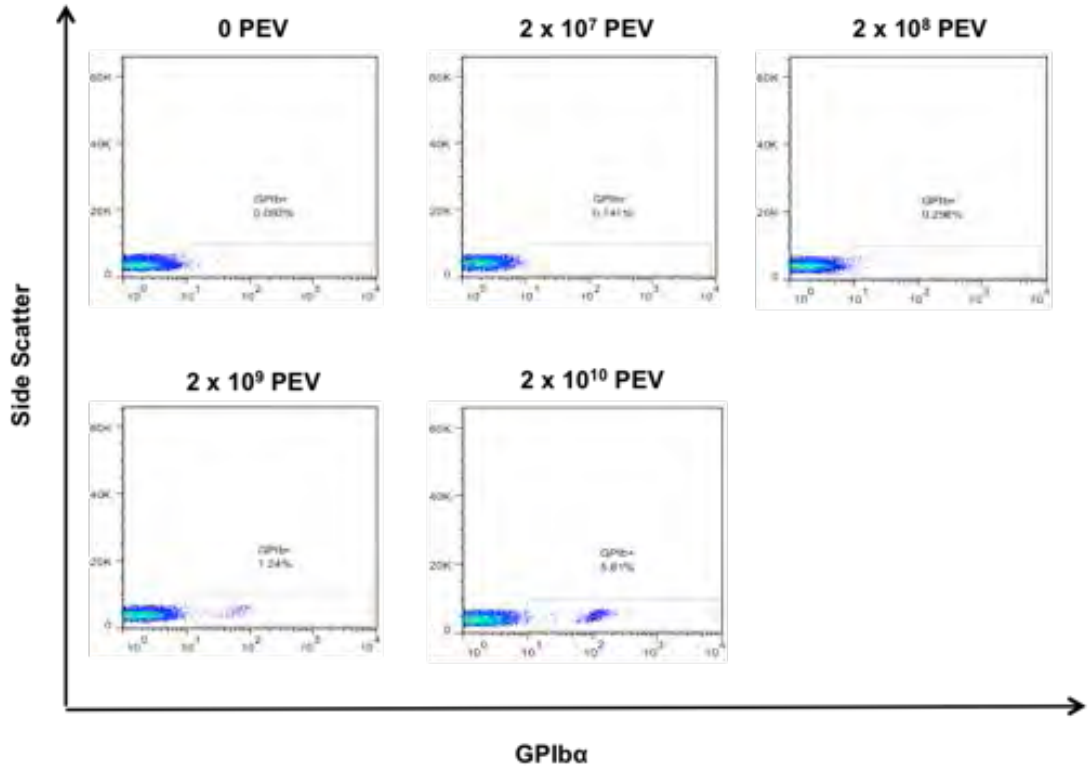

Figure 12.4. Formation of aggregates between Lymphoocytes in blood and exogenously provided PEV over a PEV concentration gradient

Representative FACS dotplots demonstrating percentage of Lymphocytes positive for GPIbα over PEV concentration gradient. Gate of positive events was set by isotype sample (not shown).

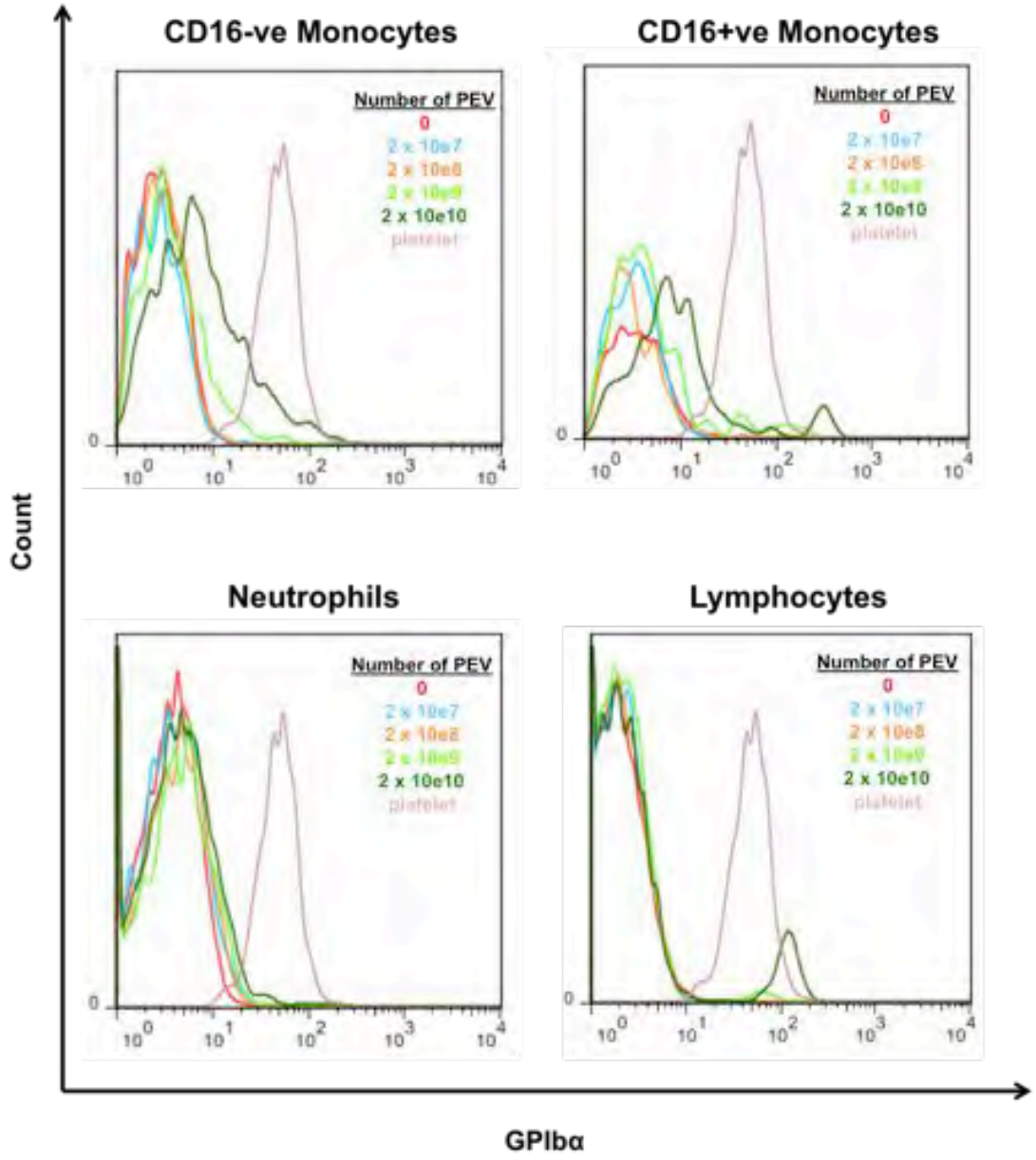

Figure 12.5. GPIbα expression on leukocyte subsets in whole blood over a PEV concentration gradient

Representative FACS overlay histograms demonstrating GPIbα expression on leukocyte subsets over a PEV concentration gradient. The GPIbα expression trace of resting platelets is also shown.

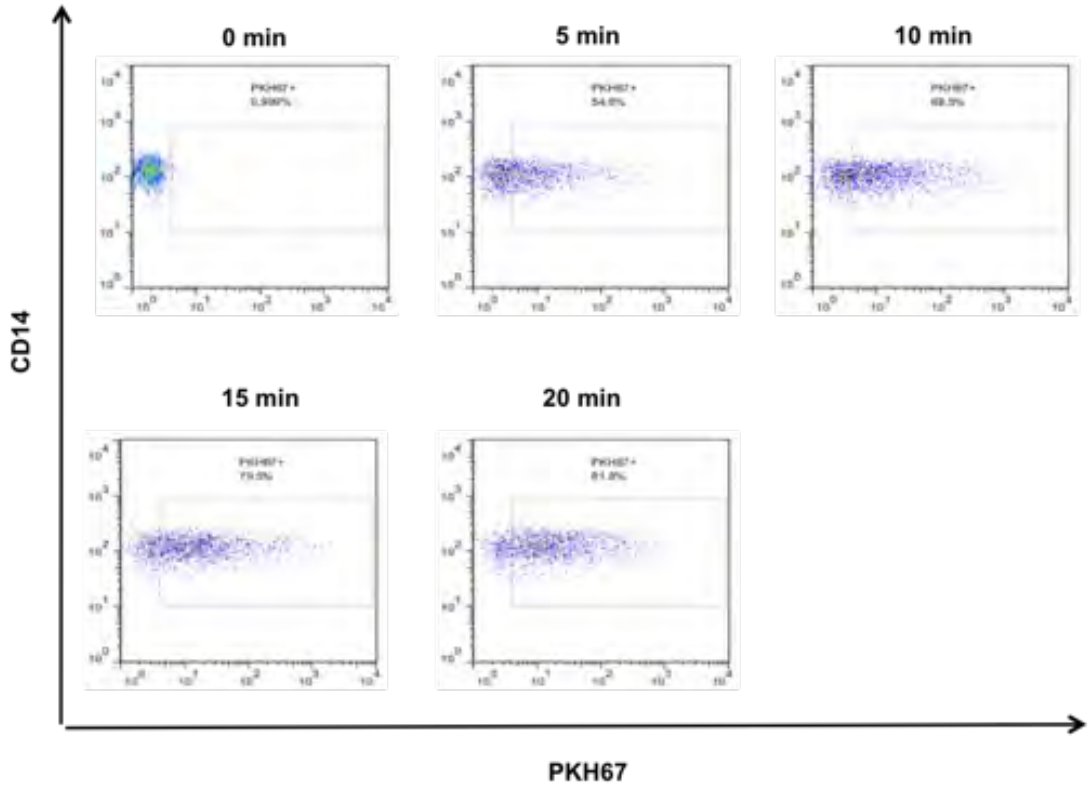

Figure 12.6. Formation of aggregates between CD16-ve monocytes in blood and added PEV over time

Representative FACS dotplots demonstrating percentage of PKH67+ve CD16-ve monocytes over time.

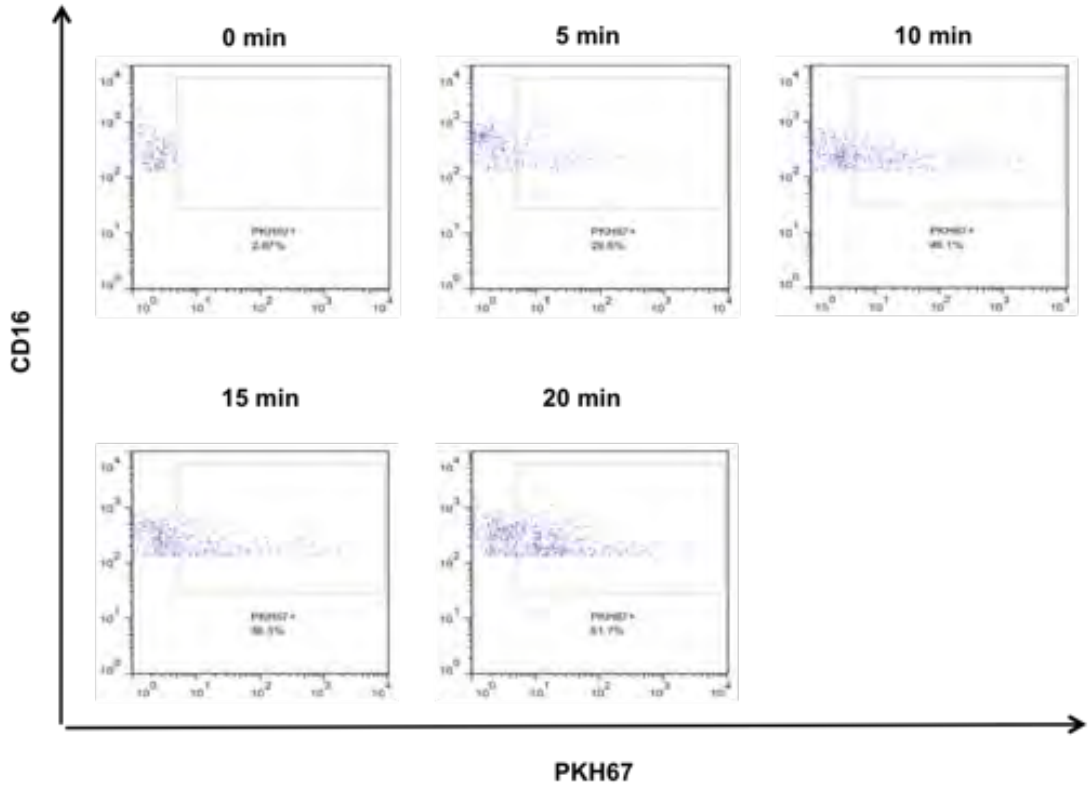

Figure 12.7. Formation of aggregates between CD16+ve monocytes in blood and added PEV over time

Representative FACS dotplots demonstrating percentage of PKH67+ve CD16+ve monocytes over time.

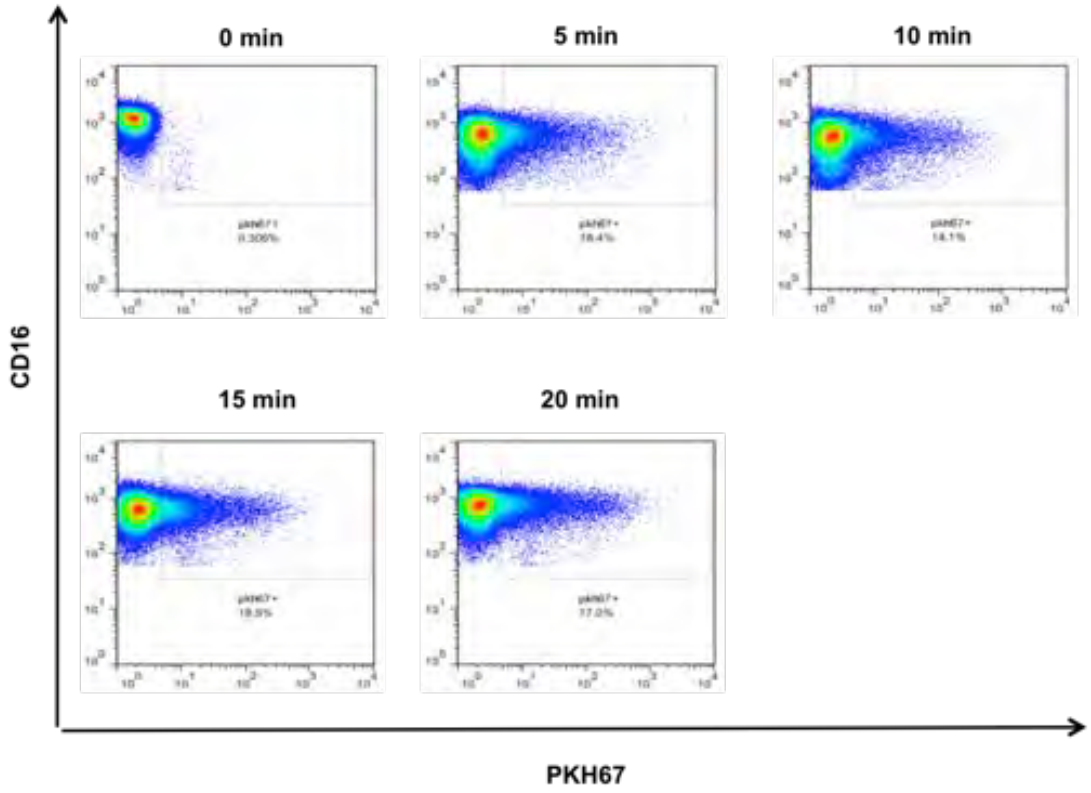

Figure 12.8. Formation of aggregates between Neutrophils in blood and added PEV over time

Representative FACS dotplots demonstrating percentage of PKH67+ve Neutrophils over time.

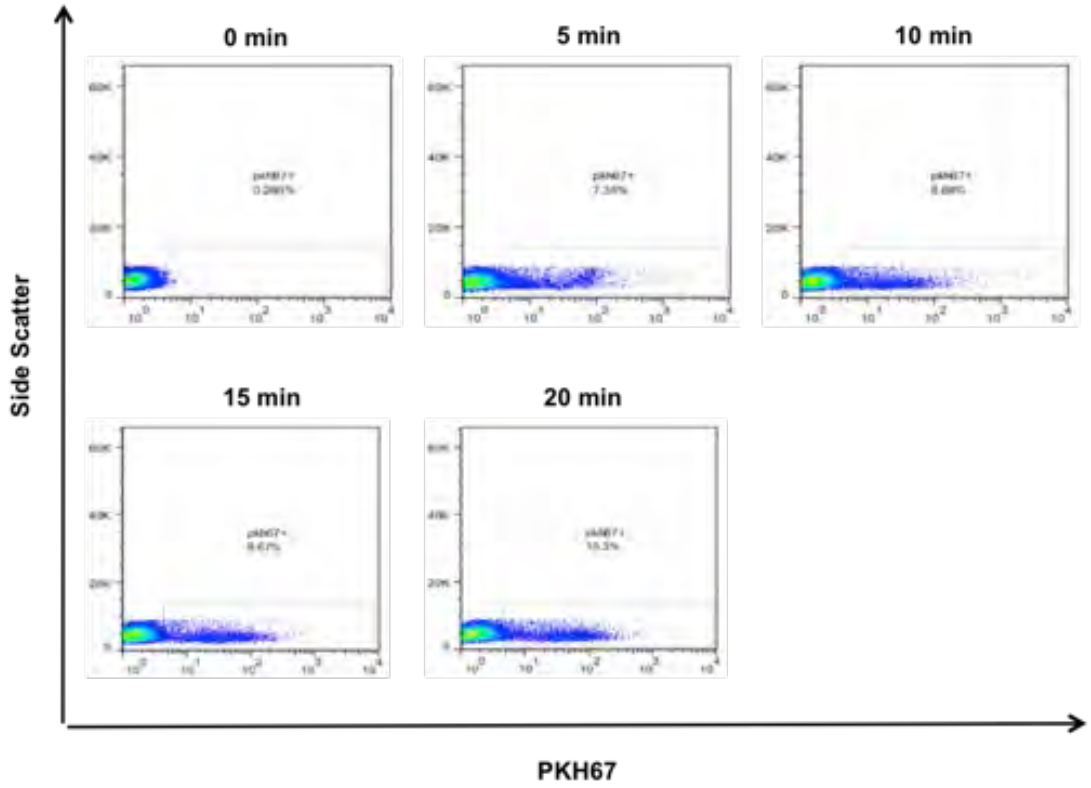

Figure 12.9. Formation of aggregates between Lymphocytes in blood and added PEV over time

Representative FACS dotplots demonstrating percentage of PKH67+ve Lymphocytes over time.

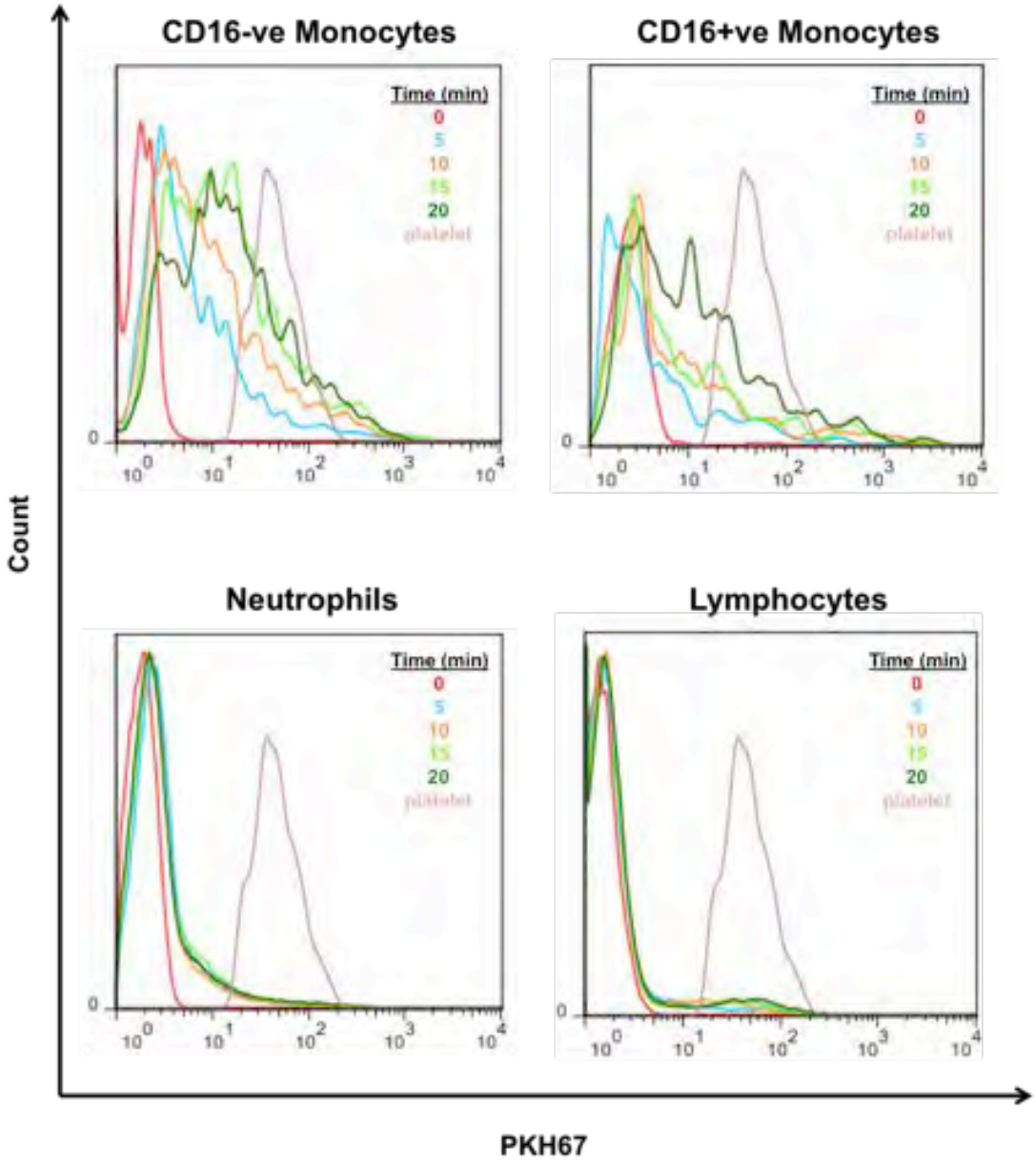

Figure 12.10. PKH67 expression on leukocyte subsets in whole blood in response to incubation with PEV over time

Representative FACS overlay histograms demonstrating GPIbα expression on leukocyte subsets over a PEV concentration gradient. The GPIbα expression trace of resting platelets is also shown.

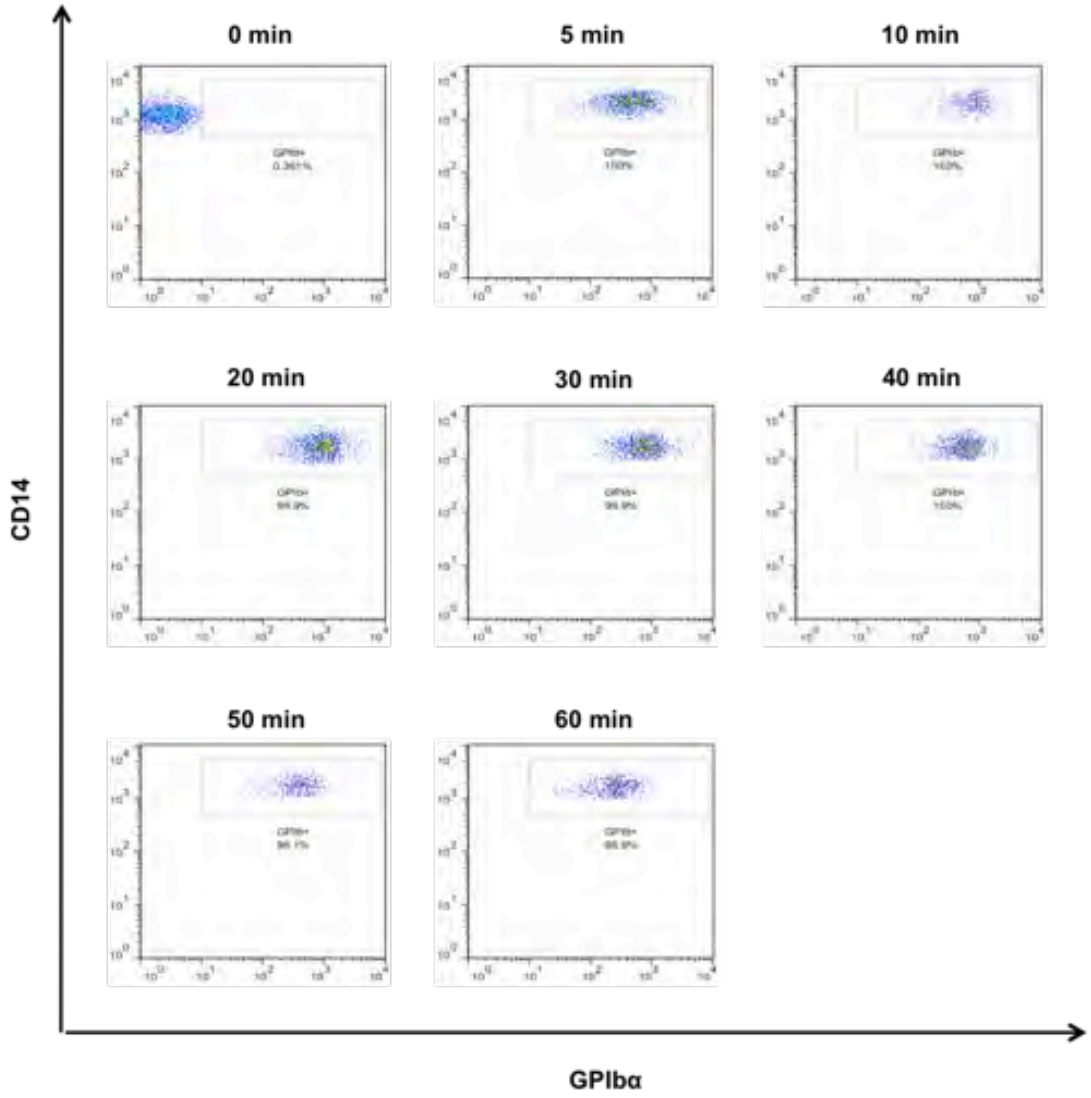

Figure 12.11. Formation of aggregates between washed CD16-ve monocytes and washed PEV over time

Representative FACS dotplots demonstrating percentage of GPIbα+ve CD16-ve monocytes over time.

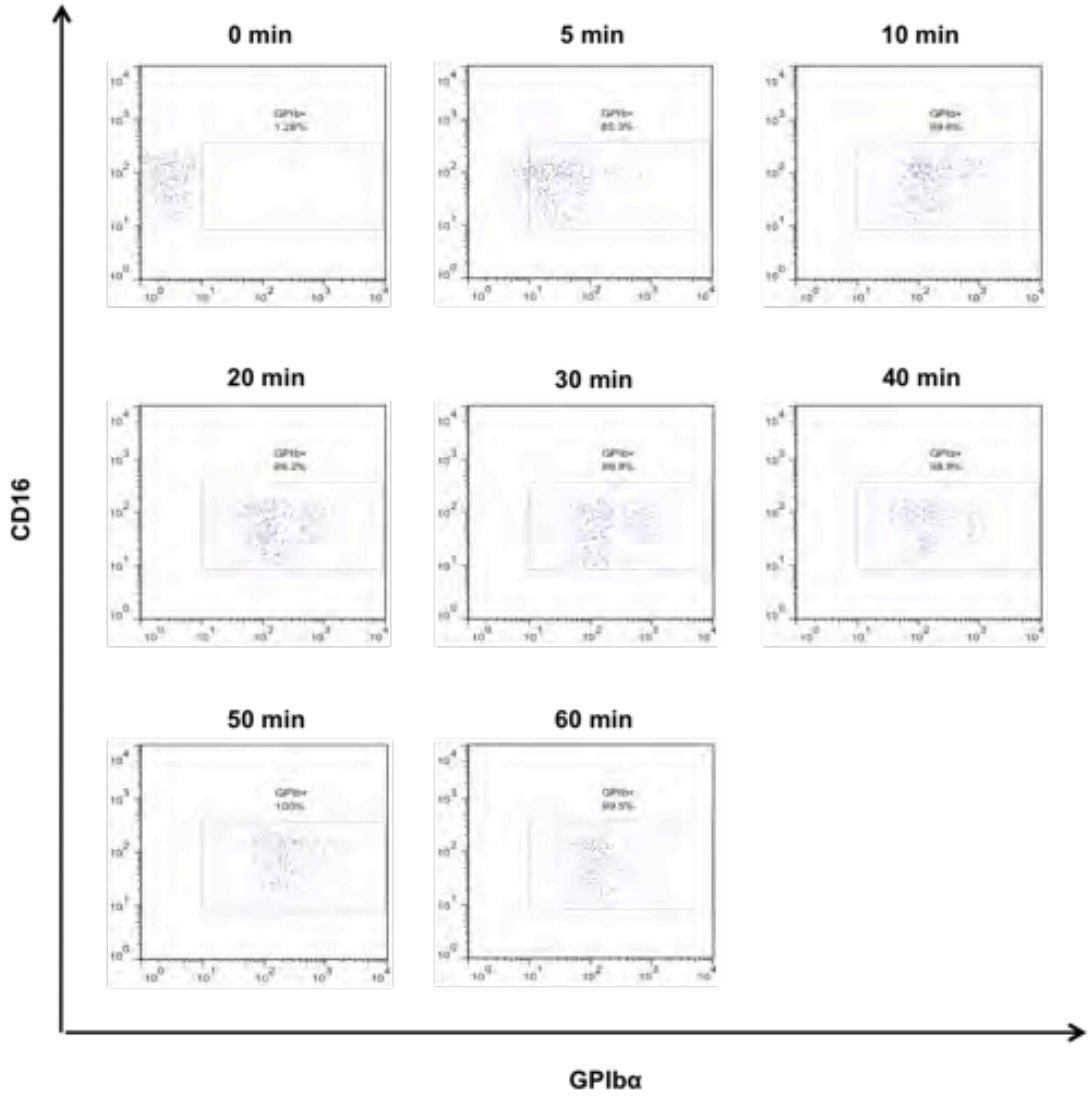

Figure 12.12. Formation of aggregates between washed CD16+ve monocytes and washed PEV over time

Representative FACS dotplots demonstrating percentage of GPIbα+ve CD16+ve monocytes over time.

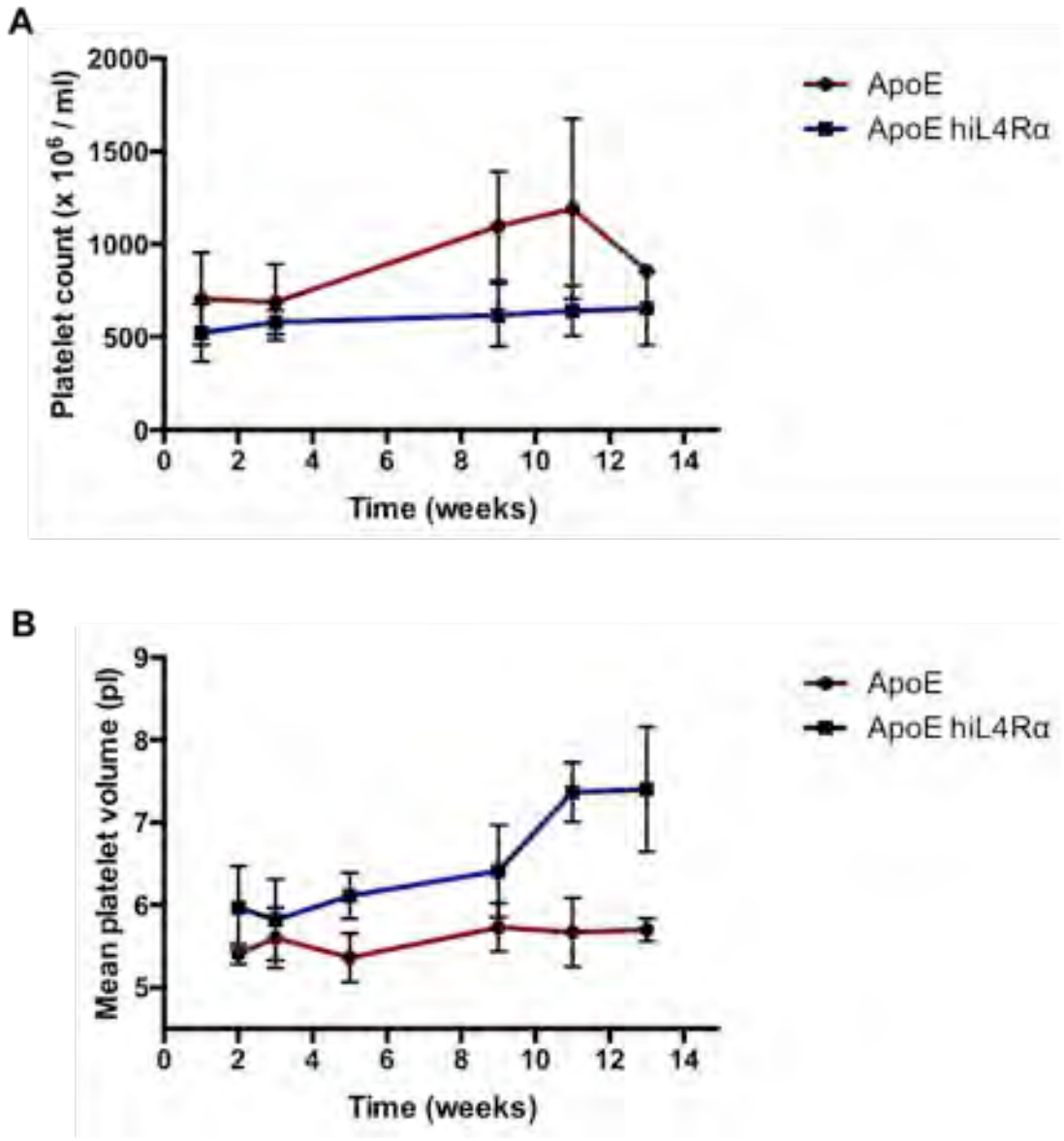

Figure 12.13. Circulating platelets on a high fat diet

(A) Platelet counts and (B) mean platelet volume in the ApoE and ApoE KO-hiL4Rα/GPIbα-Tg over the course of 14 weeks on the high fat diet. Data are shown as Mean +/- SEM of 8-10 mice. Data were analyzed by two-way ANOVA test.

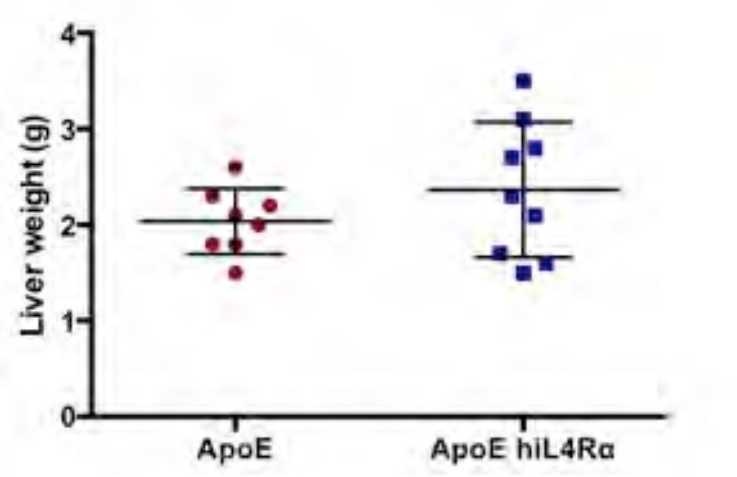

Figure 12.14. Weight of livers in response to a high fat diet

The weight of the livers of the ApoE and ApoE KO-hiL4Rα/GPIbα-Tg mouse upon 14 weeks on the high fat diet. Data are shown as Mean +/- SEM. Data were analyzed by t-test.